UNIVERSITAT POLITÈCNICA DE CATALUNYA BARCELONATECH

Structural and functional effects of natural phenolic compounds on rhodopsin mutants associated with retinitis pigmentosa

by

María Guadalupe Herrera Hernández

UNIVERSITAT POLITÈCNICA
DE CATALUNYA
BARCELONATECH

Structural and functional effects of natural phenolic compounds on rhodopsin mutants associated with retinitis pigmentosa

A thesis submitted in fulfilment of the requirements for the degree of

International Doctor of Philosophy

by

María Guadalupe Herrera Hernández

at the

Universitat Politècnica de Catalunya

under the direction of

Prof. Dr. Pere Garriga Solé

Terrassa, 2017

This thesis was financially supported by:

Ref beca: 218117

Grup de Biotecnologia Molecular i Industrial

ABSTRACT

Dietary polyphenols represent a group of secondary metabolites which widely occur in fruits, vegetables, wine, tea, extra virgin olive oil, chocolate and other cocoa products. These compounds exhibit many biologically-relevant functions, such as protection against oxidative stress, and can potentially have beneficial effects in the treatment of pathological conditions, such as age-related and degenerative diseases. Polyphenols may offer an indirect protection by activating endogenous defense systems and by modulating cellular signaling processes. Studies have reported the interaction of certain phenolic compounds with estrogen and adenosine receptors. In this regard, an important group of receptors, the G protein-coupled receptors G protein-coupled receptors superfamily, are the largest family of signal transduction molecules involved in most physiological processes. These receptors are widely studied because of their potential use as pharmacological targets in drug development. In fact, they are the most important targets for drug discovery representing ~40% of all drugs currently in the market.

Rhodopsin, the prototypic member of the G protein-coupled receptors superfamily, is the major protein found in the disks membrane of the outer segments of retinal rod photoreceptor cells and the first whose crystal structure was solved. Some mutations in rhodopsin are associated with retinitis pigmentosa, a group of inherited visual diseases that causes progressive retinal degeneration leading to blindness. Some of the proposed strategies, to fight this condition, are based on pharmacological rescue, in which small molecules known as chemical or pharmacological chaperones bind to and stabilize misfolded opsins. Polyphenols have been proposed as useful agents against retinal toxicity but no clear direct evidence of the effect of these compounds at the visual phototransduction system level has been presented so far.

Given the interest in finding new ligands that can compensate the deleterious effects caused by retinitis pigmentosa mutations, the aim of the current work was to evaluate the effect of polyphenols on the structure and function of the visual pigment rhodopsin and on the G90V, Y102H and I307N retinitis pigmentosa mutants and to study the binding preferences of such polyphenols to rhodopsin and 9-*cis*-rhodopsin.

It was found that upon the addition of quercetin, resveratrol and epigallocatechin gallate to COS-1 cell cultures expressing opsin, the expression of the wild-type and mutant opsins studied here decreased. However, no differences were observed in the physical and functional properties of immunopurified pigments regenerated with 11-*cis*-retinal when treated with quercetin and resveratrol at 1 μM and 10 μM. In contrast, molecular docking complementary analysis, conducted on pigments harboring 9-*cis*-retinal, indicated that these polyphenol compounds could bind to rhodopsin and could presumably act as allosteric ligands.

The results obtained by carefully analyzing the spectral and biochemical properties of rhodopsins heterologously expressed in cell cultures showed that quercetin improved the percentage and rate of regeneration of opsin regenerated with 9-*cis*-retinal when compared to the sample regenerated with 11-*cis*-retinal. Moreover, quercetin enhanced the structural compaction around the Schiff base in the retinal binding pocket, preventing the chemical reagent hydroxylamine from entering to hydrolyze the linkage. Moreover, functional studies on wild-type rhodopsin and the G90V mutant regenerated with 9-*cis*-retinal treated with 1 μM quercetin, presented a sigmoidal kinetics clearly representative of cooperative binding. Furthermore, the presence of quercetin in the final sample after immunopurification was demonstrated by HPCL-MS analysis.

The results were further validated by means of molecular modeling approaches which suggested that the potential ligand binding sites are different when the orthosteric ligand is 11-*cis*-retinal or 9-*cis*-retinal. In addition, docking studies revealed that quercetin bound to a site involving the extracellular loop 2 in 9-*cis*-rhodopsin, a site not found on 11-*cis*-rhodopsin.

In summary, the results reported demonstrate, by using complementary molecular biology and analytical methods and *in silico* computational studies, that some polyphenol compounds, and particularly quercetin, can act as allosteric modulators of 9-*cis*-rhodopsin. This effect is particularly significant in the case of the G90V mutation associated with the retinal degenerative disease retinitis pigmentosa, where the deleterious properties of the mutation were partially compensated, and opens a novel possibility of using such compounds in the treatment of visual neurodegeneration such as that associated with retinitis pigmentosa.

ABBREVIATIONS, ACRONYMS AND SYMBOLS

11CR	11-cis-retinal
9CR	9-cis-retinal
ABCA4	ATP-binding cassette transporter
Abs	absorbance
ABTS	2,2'-Azino-bis(3-ethylbenzothiazoline-6-sulfonic acid)
Amax	absorption maximum
APS	ammonium persulfate
ATP	adenosine-5'-triphosphate
BSA	bovine serum albumin
C	cytosine
cDNA	complementary DNA
cmp	counts per minute
CRBP	cellular retinol-binding protein-1
CSNB	congenital stationary night blindness
C3G	cyanidin-3-glucoside
DAPI	4',6-diamidino-2-phenylindole
DM	n-dodecyl β-D-matoside
DMEM	Dulbecco's modified eagle's medium
dmp	disintegrations per minute
DMSO	dimethyl sulfoxide
DNA	deoxyribonucleic acid
ds	double stranded
DTT	dithiothreitol
E	extracellular
EDTA	ethylenediaminetetraacetic acid
EGCG	epigallocatechin gallate
ER	endoplasmic reticulum
FBS	fetal bovine serum
G	guanine
G90V 11CR	G90V mutant regenerated with 11CR without 1 μM quercetin treatment
G90V 11CR-Q	G90V mutant regenerated with 11CR with 1 μM quercetin treatment
G90V 9CR	G90V mutant regenerated with 9CR without 1 μM quercetin treatment
G90V 9CR-Q	G90V mutant regenerated with 9CR with 1 μM quercetin treatment
GPCRs	G protein-coupled receptors

Gt	transducin
HRP	horseradish peroxidase
IF	immunofluorescence
IRBP	interphotoreceptor retinoid-binding protein
isoRho	9-*cis*-rhodopsin
kDa	kilodalton
λmax	wavelength maximum
LRAT	lecithin:retinol acetyltransferase
Meta II	metarhodopsin II
Methanol	MetOH
min	minutes
MOPS	3-morpholinopropane-1sulfonic acid
NADPH	nicotinamide adenine dinucleotide phosphate
ON	overnight
PAGE	polyacrylamide gel electrophoresis
PBS	phosphate buffered saline
PCR	polymerase chain reaction
PE	phosphatidylethanolamine
PEI	polyethyleimine
PSB	protonated Schiff base
Q	quercetin
qRT-PCR	quantitative real-time-RT-PCR
R	resveratrol
RDH	all-*trans*-retinol dehydrogenase
Rho	rhodopsin
RNA	ribonucleic acid
ROS	rod outer segment
RP	retinitis pigmentosa
RPE	retinal pigment epithelium
RPE65	retinal pigment epithelium-specific 65kDa protein
rpm	revolutions per minute
SB	Schiff base
SDS	sodium dodecyl sulfate
SN	supernatant
SP	sodium phosphate

SR	solubilized ROS rhodopsin
t1/2	half-time
TBS	tris buffered saline
TEAC	trolox equivalent antioxidant capacity
TEMED	N,N,N',N'-tetramethylethane-1,2-diamine
TM	transmembrane
Trolox	6-hydroxy-2,5,7,8-tetramethylchroman-2-carboxylic acid
TTBS	tween tris buffered saline
UV-Vis	ultraviolet-visible
W/O	without
WT	wild-type
WT 11CR	wild type regenerated with 11CR without 1 μM quercetin treatment
WT 11CR-Q	wild type regenerated with 11CR with 1 μM quercetin treatment
WT 9CR	wild type regenerated with 9CR without 1 μM quercetin treatment
WT 9CR-Q	wild type regenerated with CR with 1 μM quercetin treatment

TABLE OF CONTENTS

LIST OF FIGURES

LIST OF TABLES

1. INTRODUCTION

1.1 G protein-coupled receptors (GPCRs)

In order to transmit extracellular signals, cells evolved transmembrane receptor proteins that connect the extracellular environment with the interior of the cell. Within these groups of proteins, GPCRs constitute the largest class of membrane receptors, with approximately 800 different members in humans (Hofmann et al., 2009). About 2% of the genes in the mammalian genome encode these receptor types.

GPCRs superfamily is the largest family of signal transduction molecules involved in most relevant physiological processes. They respond to a broad spectrum of chemical entities, ranging from protons and calcium ions to small organic molecules (including odorants and neurotransmitters), peptides and glycoproteins. In addition, the photoreceptor rhodopsin (Rho) is specifically sensitive to photons of the light physical stimulus. Many GPCRs are members of closely related subfamilies that respond to the same hormone or neurotransmitter. However, they have different physiologic functions based on the cells in which they are expressed and the different signaling pathways that they exploit (Kobayashi, 2016). This receptor family is being widely studied due to the potential use of its members as pharmacological targets in drug discovery. Currently, one of the most active areas of interest in GPCRs signaling is “biased agonism”, a phenomenon that occurs when a given ligand is able to preferentially activate one (or some) of the possible signaling pathways (Franco et al., 2016; Pupo et al., 2016). This approach has received close attention recently also for its potential use in the development of new biosensors (Hillger et al., 2015).

1.1.1 GPCRs structure

GPCRs have a variable length with an average between 450 and 600 amino acids which constitute a single polypeptide chain. They share a common structural architecture of seven hydrophobic transmembrane (7TM) helical segments, forming a helical bundle, connected by three extracellular hydrophilic loops (e1, e2 and e3) and three intracellular loops (c1, c2 and c3) (Figure 1.1). A fourth loop is formed when the C-terminal segment binds to the membrane by means of lipid anchoring of palmitoylated cysteines to the lipid bilayer. The N-terminal region of GPCRs is at the extracellular side, and the C-terminal tail is located at the intracellular side. The N-terminal segment and the extracellular loops are responsible for recognizing a vast variety of ligands and modulating ligand binding to the receptor. The 7TM bundle region forms the structural core, binding ligands and transducing extracellular signals to the intracellular domain through conformational changes. The intracellular loops interact with cytosolic G-proteins, arrestins, GPCRs kinases and other downstream signaling effectors (Zhang et al., 2015).

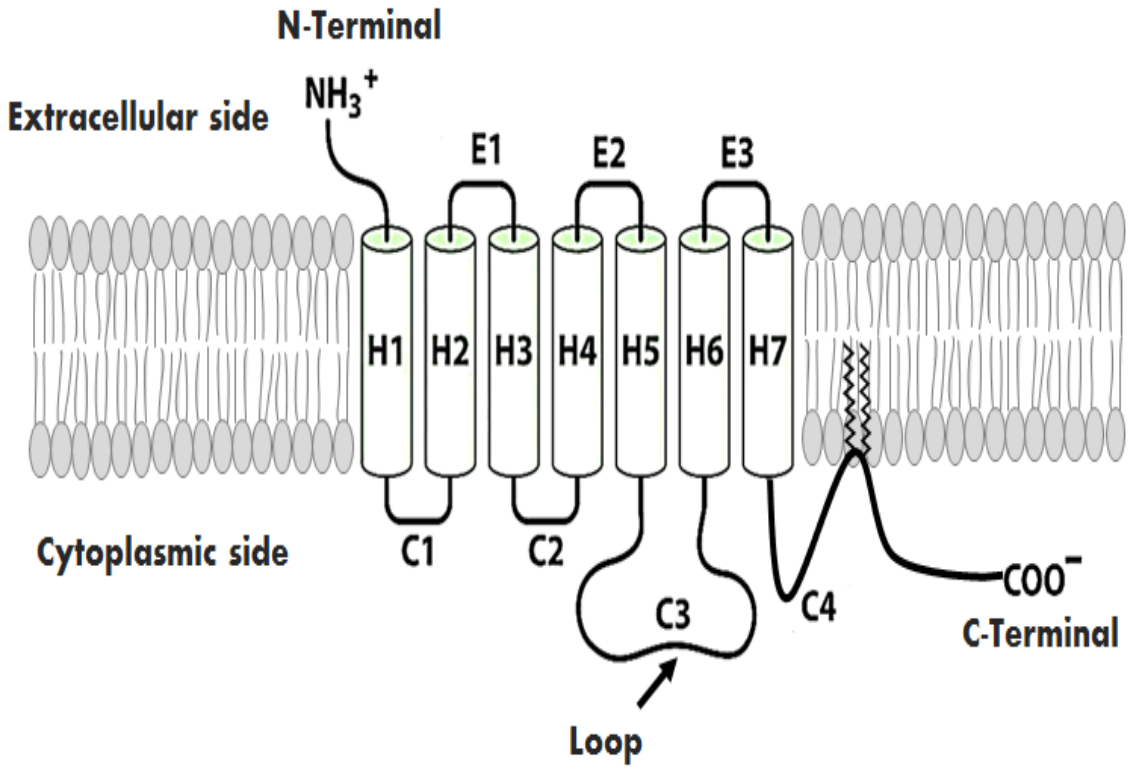

Figure 1.1 Schematic representation of GPCRs general secondary structure showing the 7TM helices and the cytoplasmic and extracellular loops. The N-terminus is oriented to the extracellular domain and the C-terminus to the cytoplasmic domain.

1.1.2 GPCRs classification

Despite having a common 7TM motif and a great conservation in their three-dimensional structure, GPCRs exhibit a high functional and sequence diversity. This makes it difficult to develop a comprehensive classification system based on amino acid sequence. In humans, GPCRs are classified, according to PSI GPCR network, in five major groups or classes based on their sequence and functional similarity. This classification includes Class A containing the Rho-like receptors, Class B with the secretin-like receptors, Class C with the glutamate receptors, class D with the adhesion receptors and Class F with the frizzled/smoothened receptors family (Alexander et al., 2013; Fredriksson et al., 2003; Stevens et al., 2013). Figure 1.2 shows the phylogenetic tree constructed from the sequence similarity in the 7TM motif among the different members.

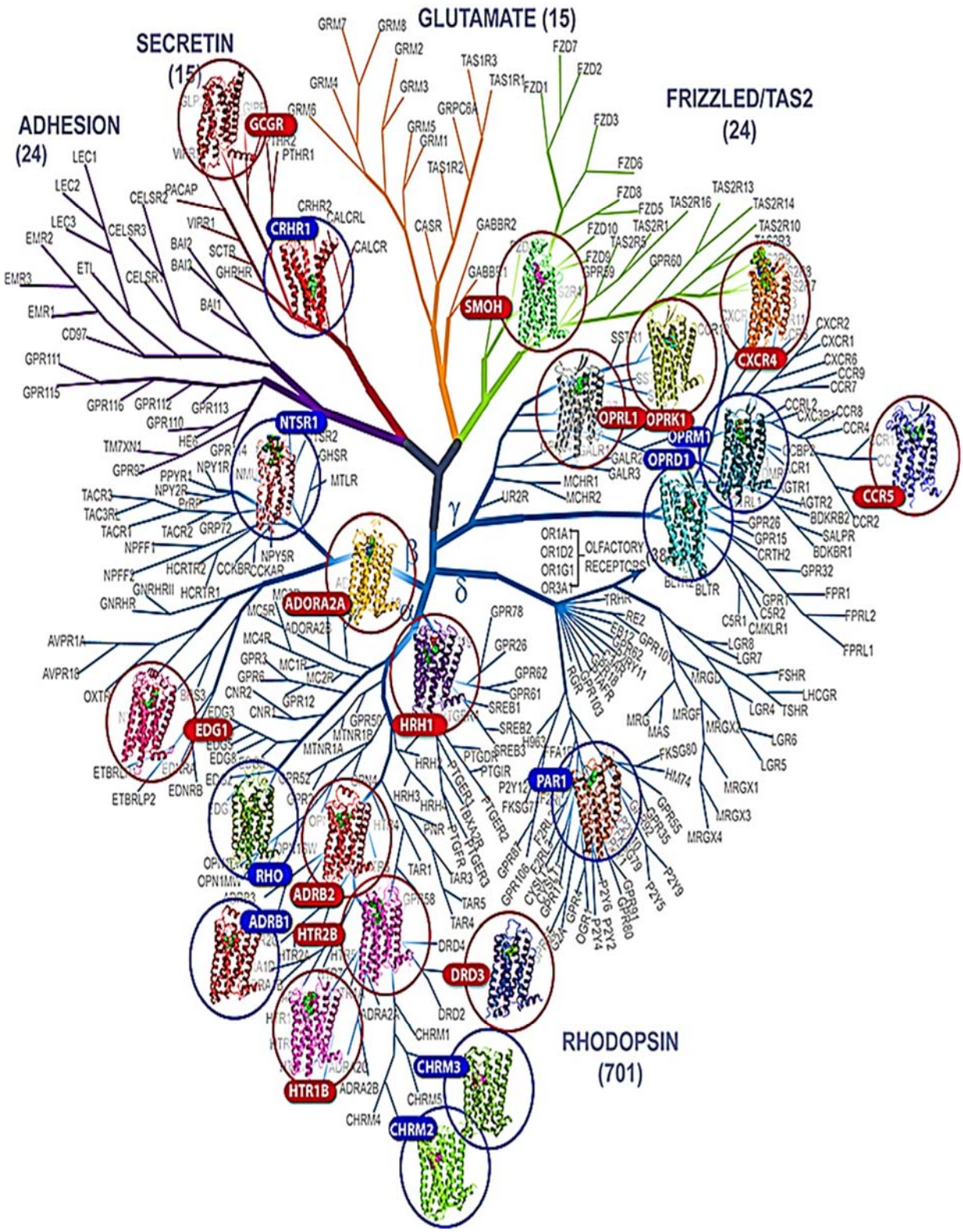

Figure 1.2 Phylogenetic tree of the GPCRs showing their classification. The number of receptors in each group is shown between brackets and the solved structures are shown in circles (from GPCR network-The Scripps Research Institute).
http://www.scripps.edu/news/press/images/cherezov_vadim/gpcr_xfel3.jpg

The Rho-like family binds a wide range of diverse ligands in the 7TM region and usually has a small extracellular domain (Figure 1.3). Secretin-like family members detect peptide hormones and have a relatively large extracellular N-terminus with a conserved structural fold stabilized by cysteine bonds. Members of the glutamate family have a large extracellular N-terminal ligand-binding region in the “Venus flytrap” fold for ligand binding with a conserved disulfide linkage to form a dimer. The adhesion and frizzled families contain GPCR-like transmembrane-spanning regions fused together with one or several functional N-terminal domains (Culhane et al., 2015).

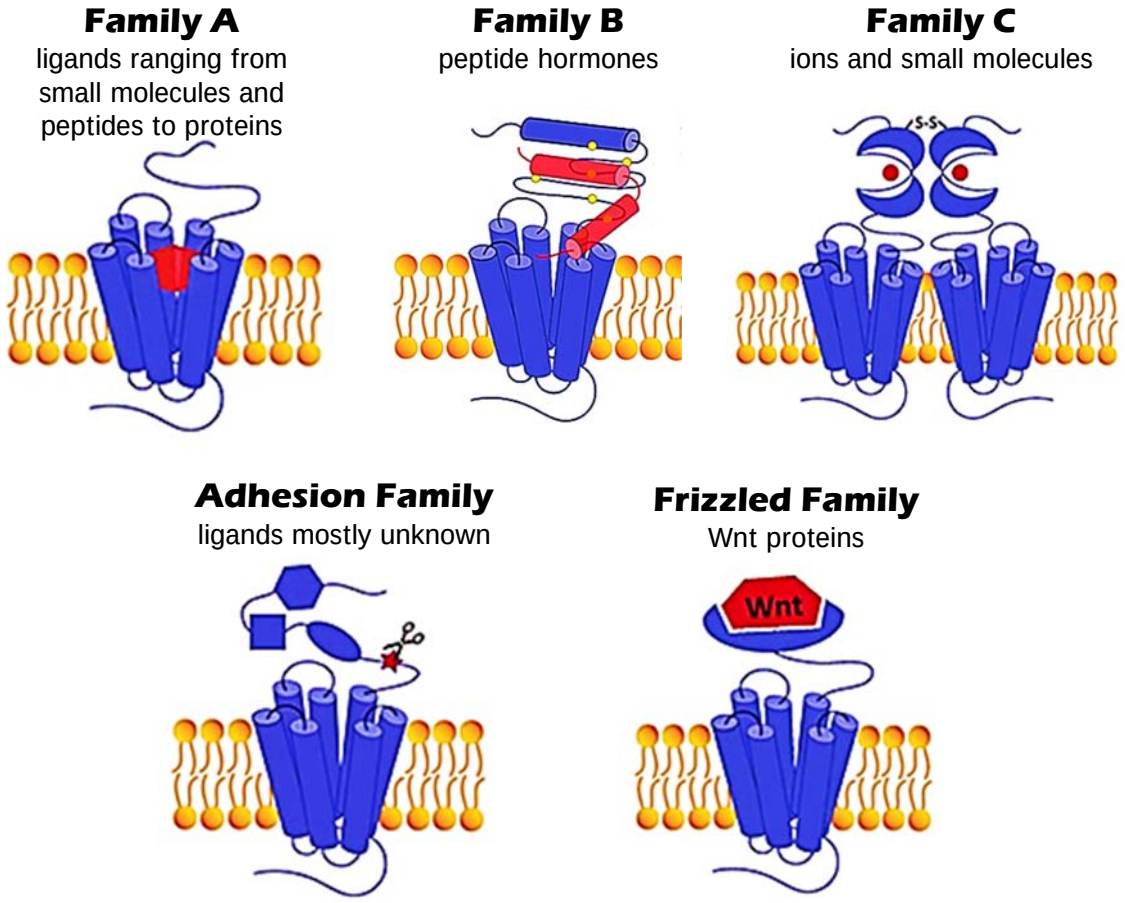

Figure 1.3 Comparison of GPCRs families.
Ligands are shown in red. Scissors in the adhesion family indicate the autoproteolysis-inducing domain (from Culhane et al., 2015)

The Rho-like family has the largest number of receptors accounting for nearly 90% of all GPCRs (Fredriksson et al., 2003; Hiller et al., 2013; Zalewska et al., 2014). In this thesis, the Rho was used as a study model for GPCRs in order to get new insights into the effect of polyphenols on receptor structure and function in connection to the molecular mechanism of the visual degenerative disease retinitis pigmentosa (RP) associated with Rho mutations.

1.2 GPCRs as drug targets

GPCRs represent ~40% of all drugs currently in the market (Pupo et al., 2016), including 25% of the 100 top-selling drugs with world market profits in the range of >$100.000 million each year (Cvijic et al., 2015; Rask-Andersen et al., 2011). In addition, major research projects involving GPCRs are widely distributed throughout the pharmaceutical industry (Guo et al., 2014). The Human Genome Project has identified about 400 GPCR that are considered as potential drug targets, but currently marketed drugs target only about 30 of them, less than a 10%. They have identified 210 natural ligands for some receptors, but many others are still unknown. A great interest in the pharmaceutical industry is focused in gaining deep knowledge on the physiological roles of these receptors, in order to be used as targets for the development of new drugs (Franco et al., 2016; Martí-Solano et al., 2016)

In recent years, the conformational flexibility of proteins and receptors has been exploited to identify ligands that modulate pharmacological function by actions at topographically distinct binding sites other than the defined regulatory site of the endogenous ligand (Lindsley et al., 2016). In this regard, the main function of GPCRs is to recognize specific ligands from the variety of molecules present in the extracellular space and transmit information through the plasma membrane. When the ligand interacts with the receptor on the outside of the cell membrane, a conformational change occurs at the cytosolic domain. These changes in remote areas of the actual ligand-binding site are known as allosteric changes. The role of GPCRs as proteins able to interact with extracellular ligands has made of them good candidates as targets for drug design (Khoury et al., 2014; Sato et al., 2016)

1.2.1 GPCRs signaling and ligands: potentials for new therapeutics

GPCRs activation was first described as a two-stage model, where there is an equilibrium between two conformations, the active sate (e.g., G protein-coupled: the “on” state) and the inactive state (e.g., G protein-uncoupled: the “off” state). In the absence of ligands, the receptor activity is in the basal level, but any extracellular stimulus, such as hormones, neurotransmitters, peptides, and amino acids may alter the equilibrium between the inactive and the active states (Zhang et al., 2015). Considering this model, the properties of ligands were classified as agonists, antagonists and inverse agonists, according to their ability to stabilize the “on” state of the receptors. Those allowing full activation of the G protein are agonists, those reducing the basal spontaneous coupling to G proteins are termed inverse agonists, whereas those inhibiting receptor activation by competing with agonists for the receptor, without changing the equilibrium, are the “neutral” antagonists (Khoury et al., 2014) (Figure 1.4). In GPCRs, ligands bind to their main site, called the orthosteric site. However, accumulating evidence also indicates that such ligands, alone or in combination with others; such as those acting outside the orthosteric site (e.g.,

allosteric modulators), have the ability to selectively engage subsets of signaling responses as compared to the natural endogenous ligands. Binding locations outside the orthosteric area are called allosteric sites (Khoury et al., 2014; Lane et al., 2013)..

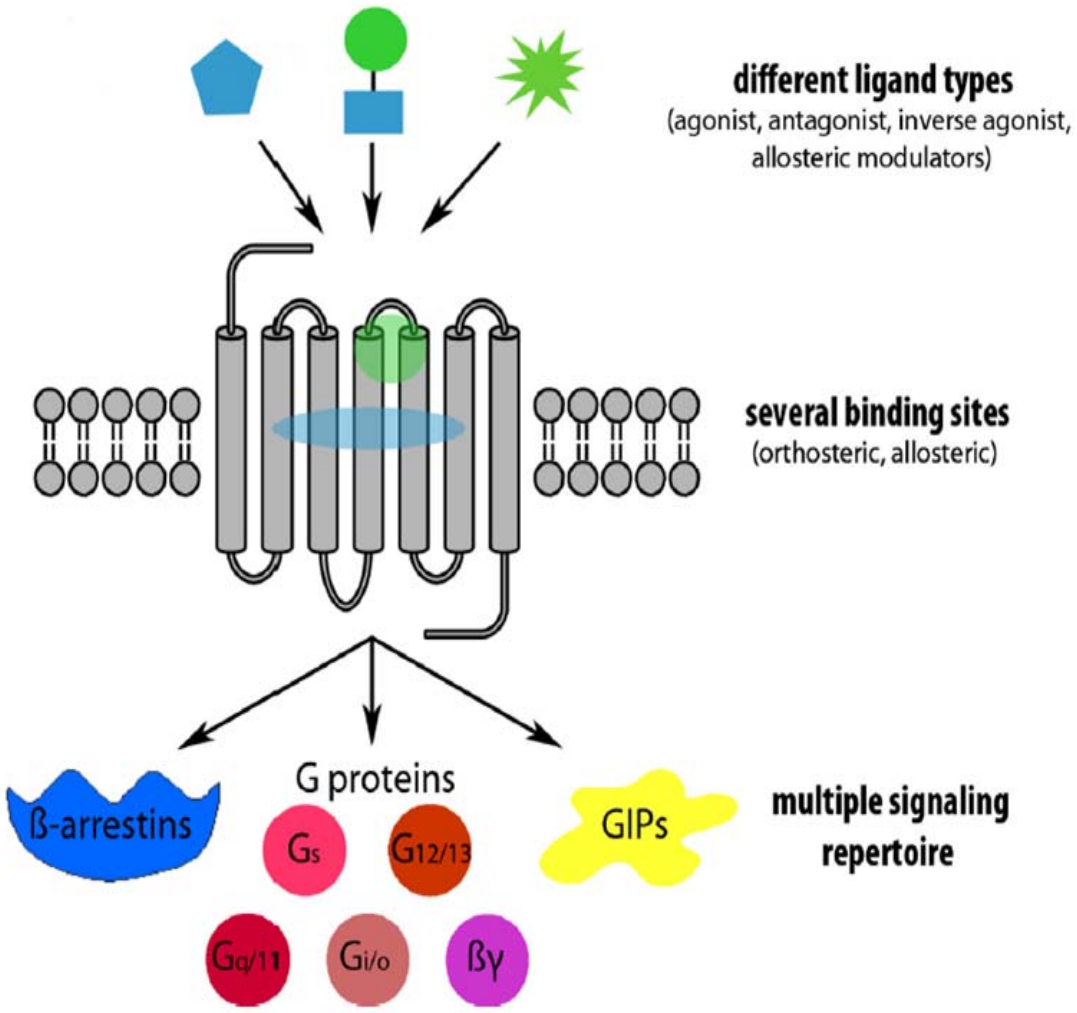

Figure 1.4 Different ligand types and binding sites for GPCRs.
The GPCRs respond to a broad spectrum of chemical entities (orthosteric (blue ellipsoid) or/and allosteric (green circle) ligands), and trigger multiple signal-switching mechanisms, not only G-protein activation but also binding of β-arrestin proteins and other GPCR-interacting proteins (GIPs) which results in a highly complex signaling network (from (Bermudez & Wolber, 2015)).

1.2.2. Regulation of GPCRs by allosteric ligands

As mentioned above, GPCRs also respond to a variety of endogenous allosteric modulators (Figure 1.5) which include ions, ligands, lipids, small and large molecules (e.g., antibodies) and/or protein complexes (e.g., receptor dimers and receptor-effector complexes). This kind of modulators regulate receptor function by binding to alternative regions, i.e. allosteric binding sites, instead of the conventional orthosteric binding site but still allowing orthosteric ligands to bind. As

such, allosteric ligands can modulate both orthosteric ligand affinity and efficacy (Lane et al., 2013).

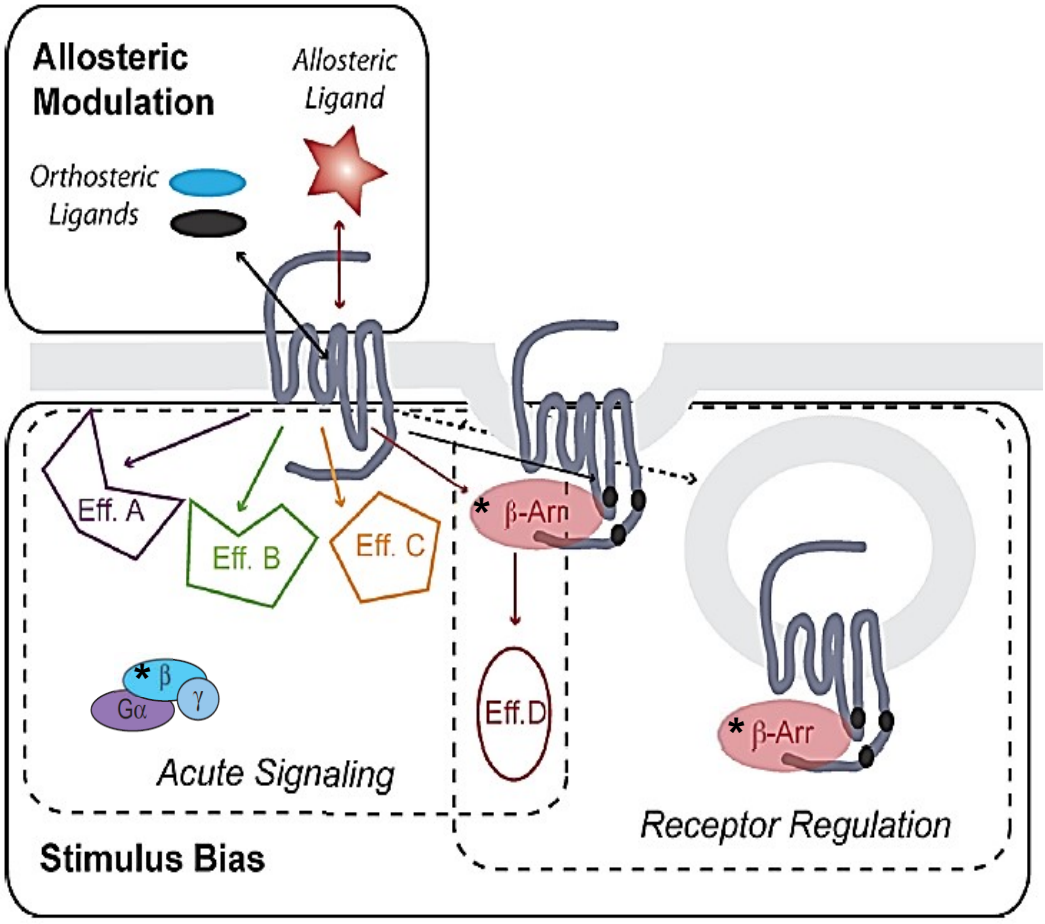

Figure 1.5 Biasing GPCRs signaling by allosteric ligands.
Ligand-directed signaling can occur through the binding of either orthosteric or allosteric ligands to the receptor. This leads to the activation of multiple signaling pathways that are balanced between the G-proteins, β-arrestins, and/or other signaling effectors. * Regulatory proteins (From Lane et al., 2013).

In both cases, orthosteric and allosteric ligands acting at the same GPCR can engage in acute signaling and trigger regulatory pathways by interacting with distinct effector proteins (Eff A, Eff B, and Eff C) and regulatory proteins such as β-arrestin (β-arr, Eff.D) or G protein (Figure 1.5). Both orthosteric and allosteric ligands may select different subsets of these signaling and regulatory pathways by stabilizing distinct receptor conformations, a phenomenon termed functional selectivity or stimulus bias. The subset of these pathways and processes engaged by a ligand-receptor complex will underlie the specific physiological effect of the ligand (Katritch et al., 2012; Lane et al., 2013).

1.2.3 Discovery of novel GPCR ligands for therapeutic applications

In recent years, there has been increasing interest in ligands that bind to the allosteric sites of GPCRs because allosteric ligands can potentially be more selective than orthosteric ligands. This is because their binding to less conserved regions makes them promising therapeutic drug candidates with less adverse effects and lower overdose risk (Zhang et al., 2015). *In silico* methods such as virtual screening and *de novo* design can guide the search for novel ligands in the drug development process. Virtual screening is a powerful technique for the identification of potential ligands as starting points for medicinal chemistry and has been successfully applied to a wide range of different pharmacological targets (Lavecchia & Di Giovanni, 2013; Murgueitio et al., 2012).

Molecular docking is the most commonly used computational screening method for the discovery of new GPCR ligands (Shoichet & Kobilka, 2012). It is used as a standard computational tool in structure-based drug design that aims at a prediction of experimental binding modes and affinities of small molecules within the binding site of a protein target. Other computational techniques applied in the field of GPCR research are: homology modeling and molecular dynamics simulations. The performance of the broad variety of *in silico* methods currently used for drug design, varies significantly with the target protein, available data, and available resources (Bermudez & Wolber, 2015). Nowadays, increased computational power enables docking screens of large chemical libraries to identify molecules that complement GPCR binding sites, and this may provide novel possibilities of ligand identification with suitable tailored pharmacological properties.

1.3 Rhodopsin (Rho) as a model of GPCR: structure and function

1.3.1 Rho structure

Rho is the major protein found in the disk membranes of the rod outer segment (ROS) of retinal rod photoreceptor cells (Rho represents >90% of total membrane protein with a 5mM concentration within ROS) of the vertebrate retina and is responsible for scotopic vision (Nickell et al., 2007). The retina is a neuronal tissue composed of several cell types but rods constitute about 80% of cells in human, mouse, and bovine retina (Figure 1.6). The visual pigment Rho is composed of two elements: an apoprotein, opsin, and the chromophore 11-*cis*-retinal (11CR) (Bourne & Meng, 2000)

Rho was the first GPCR whose crystal structure was solved at atomic resolution (Palczewski et al., 2000). It is considered the prototypic member of the GPCR superfamily, however, this visual pigment presents specific and unique structural features. Rho mediates dim light vision by converting photons into chemical signals that can trigger the biological processes enabling the

brain to sense the light stimulus (Hubbard & Kropf, 1958). 11CR is a vitamin A derivative that has been conserved throughout evolution because of its highly specialized role in vision, which includes a very fast response, and a high quantum yield, for its photon-triggered isomerization.

The retinal ligand is covalently bound to opsin through a protonated Schiff Base (PSB) linkage to Lys-296 in the seventh transmembrane helix. Upon light absorption, 11CR changes its configuration to all-*trans*-retinal triggering a conformational change in the receptor that results in the formation of the active metarhodopsin II (Meta II) photointermediate through a series of short-lived photointermediaries. Meta II binds and activates Gt eventually decaying to free opsin and all-*trans*-retinal.

The photoactivated intermediates of Rho have been shown to be altered by several parameters such as ionic strength, pH, glycerol, and temperature (Figure 1.7). As a result, these intermediates can be trapped at low temperature and their lifetime can be determined (Palczewski, 2006).

In order to unravel the structural features of the retinal binding site, and the details of the opsin-ligand recognition process, other retinal isomers such as 7-*cis*-retinal, 9-*cis*-retinal (9CR), 13-*cis*-retinal and all-*trans*-retinal have also been investigated for their binding ability (Harbison et al., 1984). 9CR is often used as an exogenous analog to study the structure and function of visual pigments (Hubbard & Kropf, 1958; Nakamichi & Okada, 2007).

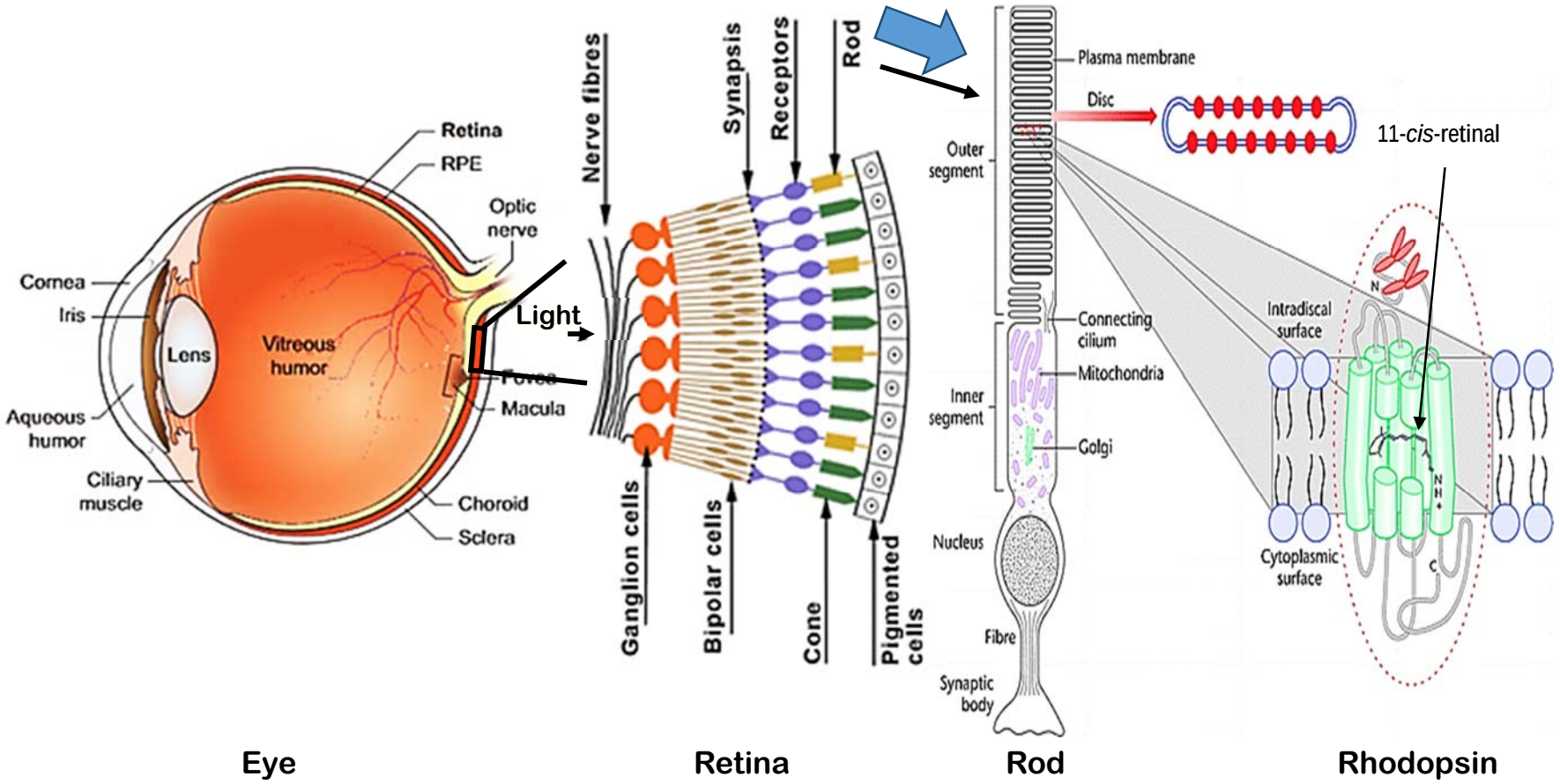

Figure 1.6 Schematic representation of the retina, rod cells and Rho location in the eye.
In the eye, the retina is the essential component and serves the primary purpose of photoreception. The retina is uniquely structured for perception, integration, and transmission of visual information. It is a highly organized, multilayered complex of photosensitive neurons which includes photoreceptors, containing the rod and cone photoreceptor cells; driving neurons, including bipolar and ganglion cells; and the synaptic regions. Light absorption is mediated by visual pigments contained in the rod and cone cells. Rods are responsible for vison under dim-light illumination. These highly specialized cells have the visual pigment Rho which has two components, the 11CR chromophore and the opsin apoprotein.

1.3.2 Rho function

1.3.2.1. Visual signal transduction

The photoreceptors (rods and cones) are the primary sensory neurons that sense light and convert light energy into nerve impulses in a process called visual phototransduction. Light absorption is mediated by visual pigments.

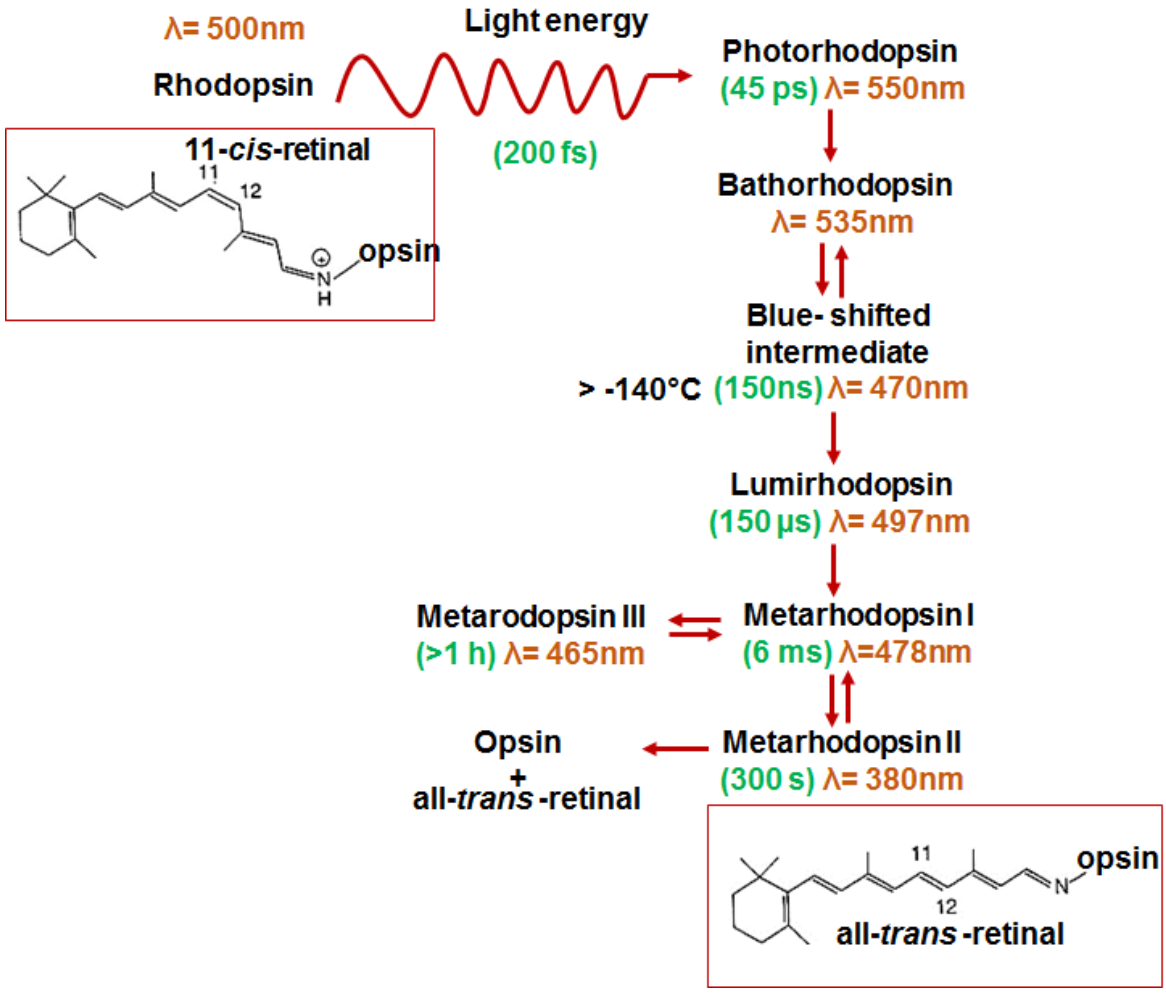

Figure 1.7 Rho photointermediates after photoactivation.
Upon the absorption of a photon, Rho passes through several photointermediates till reaching the active form Metar II and decaying to opsin and free all-*trans*-retinal. (Palczewski, 2006)

Signal transduction in the visual system involves two main processes: first, the activation of Rho by absorption of a photon of light, leading to a conformational change, and second, regeneration of Rho into the original dark inactive state, a the fundamental process regulating light adaptation (Kalt et al., 2010; Zhong et al., 2012).

The visual signal, responsible for light perception in the brain, starts with a photon absorption by the Rho chromophore, 11CR, causing its isomerization to the all-*trans* configuration. Complete isomerization to all-*trans*-retinal causes the molecule to straighten, making its adjustment to the opsin protein energetically less favorable. This form of higher energy, called Meta II, activates the signal transduction process through binding to, and activating Gt. This, in turn, activates a phosphodiesterase that hydrolyzes cGMP, leading to the closure of ion channels in the membrane and subsequent cell hyperpolarization (Figure 1.8) (Garriga & Manyosa, 2002; Kalt et al., 2010; Ridge et al., 2003). The difference potential in the outer segment in rods or cones is transferred through the synaptic terminal to second order neurons in the inner retina via modulation of neurotransmitter release towards the synaptic terminals of bipolar, amacrine, horizontal and ganglion cells (Travis et al., 2007).

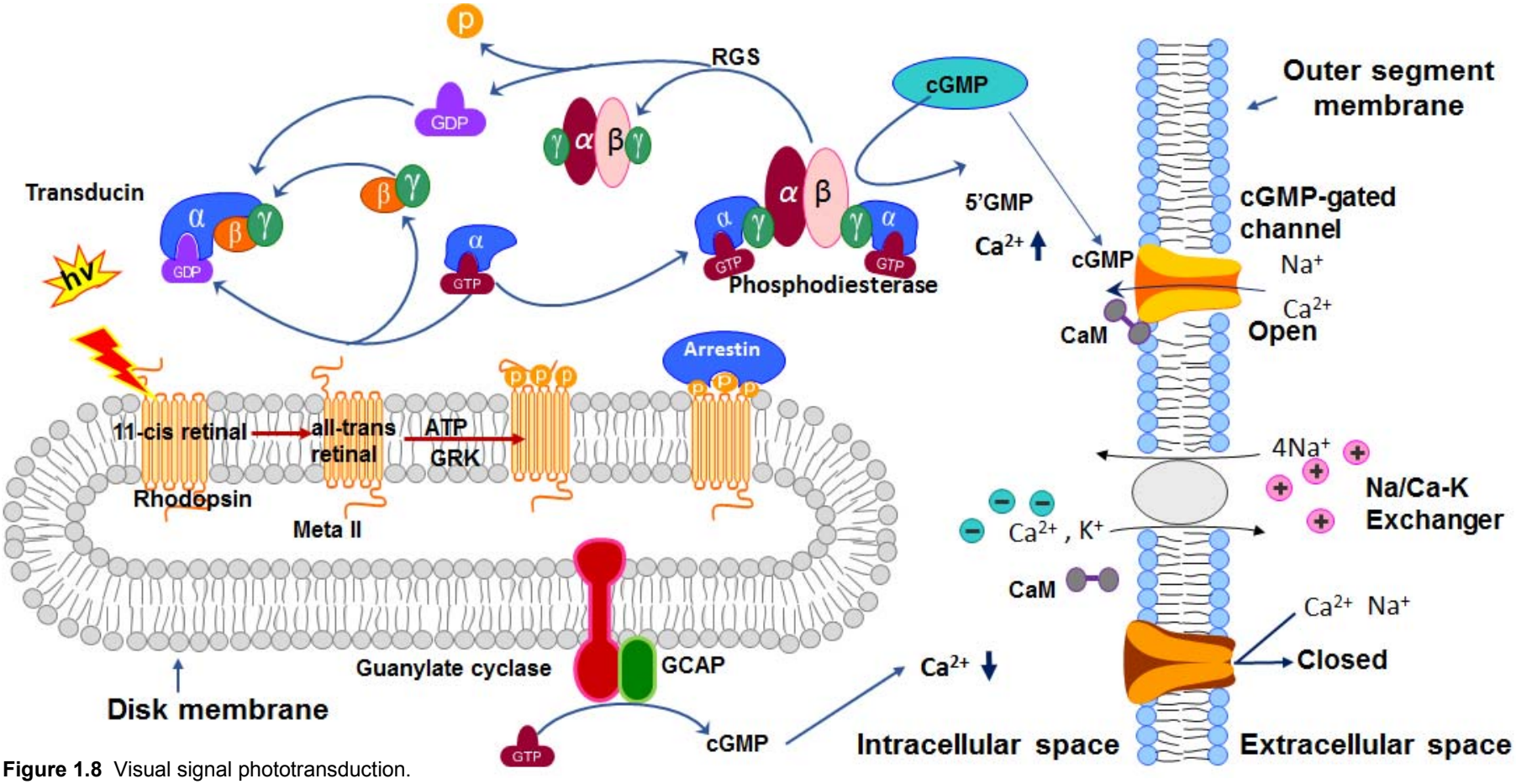

Figure 1.8 Visual signal phototransduction.

Upon striking the retina, light activates Rho by causing the isomerization of covalently attached 11CR to all-*trans*-retinal. Activated Rho (Meta II) interacts with Gt, the heterotrimeric G-protein composed of α, β and γ subunits. Gt activation involves the exchange of guanosine diphosphate (GDP) for guanosine triphosphate (GTP),and dissociation of Gt α-subunit, containing GTP, from the βγ-subunit complex. Gtα-GTP activates cyclic guanosine monophosphate (cGMP) phosphodiesterase (PDE), promoting the hydrolysis of cGMP and its conversion to 5'-GMP. The consequent reduction in the cytoplasmic concentration of cGMP leads to the closure of cyclic nucleotide gated channels, blockage of the inward flux of Na^+ and Ca^{2+} and final hyperpolarization of the cell. The decrease in intracellular Ca^{2+} concentration also activates the otherwise inhibited guanylate cyclase-activating protein (GCAP) which leads to the activation of guanylate cyclase and subsequent re-synthesis of cGMP, ensuing the continuity of the cycle. The modified membrane potential is transmitted as a neural signal to the brain. The inactivation of Rho is mediated by Rho kinase (RK) phosphorylation, inducing Gt α-subunit to uncouple, promoting the binding of arrestin, leading to a decrease in PDE activity, followed by an increase in the cGMP levels and the opening of cGMP-gated Ca^{2+} channels. A final step involving the recycling of opsin, will enable a fresh 11CR to reconstitute Rho (Herrera-Hernández, 2015).

1.3.2.1 The retinoid visual cycle

After Rho activation, a constant supply of 11CR is required. This constant supply is obtained by the metabolic pathway referred to as the retinoid visual cycle, by which all-*trans*-retinal is re-isomerized back to 11CR (Kiser et al., 2014) through a complex enzymatic pathway that is split between processes in photoreceptor cells and the retinal pigment epithelium (RPE) (Figure 1.9).

As part of the phototransduction cascade, Rho releases all-*trans*-retinal, which is cleared by an ATP-binding cassette transporter (ABCA4) (Sun & Nathans, 2001; Weng et al., 1999) and all-*trans*-retinol dehydrogenase (RDH). ABCA4 transports all-*trans*-retinal from the intradiscal space to the cytoplasmic space across photoreceptor disc membranes (Molday, 2007).

The ABCA4 functions as an ATP-dependent flippase for N-retinylidine-phosphatidylethanolamine (N-retinylidine-PE) (Beharry et al., 2004; Sun et al., 1999). This requires the reaction of all-*trans*-retinal with PE. After hydrolysis, N-retinylidine-PE is released to the cytosol of the photoreceptors as all-*trans*-retinal. The reduction of all-*trans*-retinal to all-*trans*-retinol is done by RDH, using NADPH as a reducing factor, mainly by RDH8 expressed in photoreceptor ROS (Maeda et al., 2007; Parker & Crouch, 2010) whose activity is a limiting step in the cycle (Crouch et al., 1996; Saari, 2000). All-*trans*-retinol is taken up from the photoreceptors to the extracellular space, also called the interphotoreceptor matrix, where micromolar concentrations of an interphotoreceptor retinoid-binding protein (IRBP) (Adler & Edwards, 2000; Adler & Evans, 1985; Edwards & Adler, 1994) are secreted by photoreceptors. Endogenous retinoid ligands for IRBP include all-*trans*-retinol, 11CR and 11-*cis*-retinol (Adler & Spencer, 1991; Lin et al., 1989). These ligands are protected from oxidation and isomerization when bound to IRBP (Crouch et al., 1992; Pepperberg et al., 1993). Cellular retinol-binding protein-1 (CRBP) in the RPE has 100-fold higher affinity for all-*trans*-retinol than IRBP and promotes its uptake. All-*trans*-retinol is taken up from blood in the choroidal circulation through the basal membranes of RPE cells. All.*trans*-retinol is converted to all-*trans*-retinylester by the enzyme lecithin:retinol acetyltransferase (LRAT) and subsequently isomerized to 11-*cis*-retinol by a isomerohydrolase, a retinal pigment epithelium-specific 65kDa protein (RPE65) (Jin et al., 2005; Moiseyev et al., 2005). 11-*cis*-Retinol is oxidized to 11CR by 11CR dehydrogenase, and this retinoid is transported back to the rod photoreceptor where it recombines with opsin in disk membranes to regenerate Rho (McBee et al., 2001)

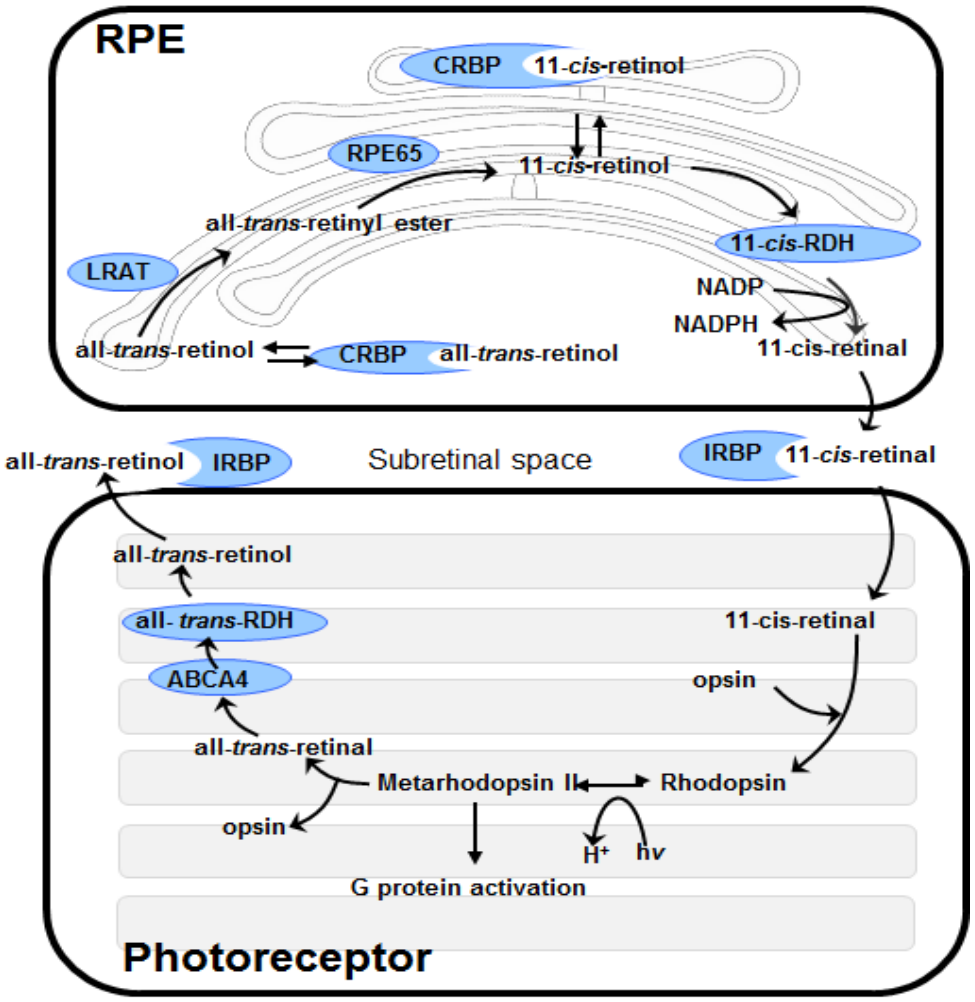

Figure 1.9 Retinoid visual cycle.
After photoisomerization of 11CR to all-*trans*-retinal, the chromophore dissociates from opsin. All-*trans*-retinal is metabolized into all-*trans*-retinol and transported to de RPE where it is re-isomerized to 11-*cis*-retinal and then redelivered to the photoreceptor. ABCA4 moves all-*trans*-retinal through the membrane of the photoreceptor disc into the cytoplasm of the outer segment. RDH catalyzes the reduction of all-*trans*-retinal to all-*trans*-retinol, which is transported by means of IRBP through the subretinal space into the pigment epithelium cell. CRBP promotes all-trans-retinol uptake into de RPE. Then this is esterified by means of LRAT. RPE65 transforms it into 11-*cis*-retinol and finally, by means of 11CR RDH, it is transformed into 11CR. Later is transported by IRBP to the photoreceptor to reconstitute Rho (Herrera-Hernández, 2015).

1.4 Rho mutations and retinal diseases

The integrity and function of photoreceptors are crucial for the complex process of vision. Mutations that affect photoreceptor function, or any other factor that may disrupt the phototransduction process, can lead to vision dysfunction and vision loss (Toledo et al., 2011). In addition, defects in other retinal cells types, specifically the RPE, can also lead to photoreceptor dysfunction and retinal degeneration (Veleri et al., 2015).

Naturally-occurring mutations in the opsin gene mainly consist of individual aminoacid replacement and are associated with retinal diseases. Most of these mutations are the cause of RP, a group of hereditary degenerative diseases of the retina (Farrar et al., 2002) that cause blindness through death of photoreceptor cells (Travis, 1998). Only a small number of mutations have been associated with a retinal disease characterized by a mild phenotype, congenital stationary night blindness (CSNB), which seems to affect the amino acid residues that cluster around the SB and are presumably associated with changes in the conformational stability and protonation state of the SB nitrogen (Ramon et al., 2003)

1.4.1 Retinitis pigmentosa (RP)

RP is a heterogeneous group of hereditary retinal degenerative disorders in which progressive loss of rod cells and then cone cells, with atrophy of RPE affecting the ocular fundus, leading to night blindness, tunnel vision, and eventually to blindness (Figure 1.10).

Night blindness clinical signs include poor adaptation to darkness and dimly lit places. The reduction of peripheral vision requires those affected to turn his head to see what is around them. This is known as tunnel vision, because the visual field is narrowing and becoming more distant and diffuse. This reduction often causes serious visual impairments and can significantly affect the personal mobility of the affected individuals

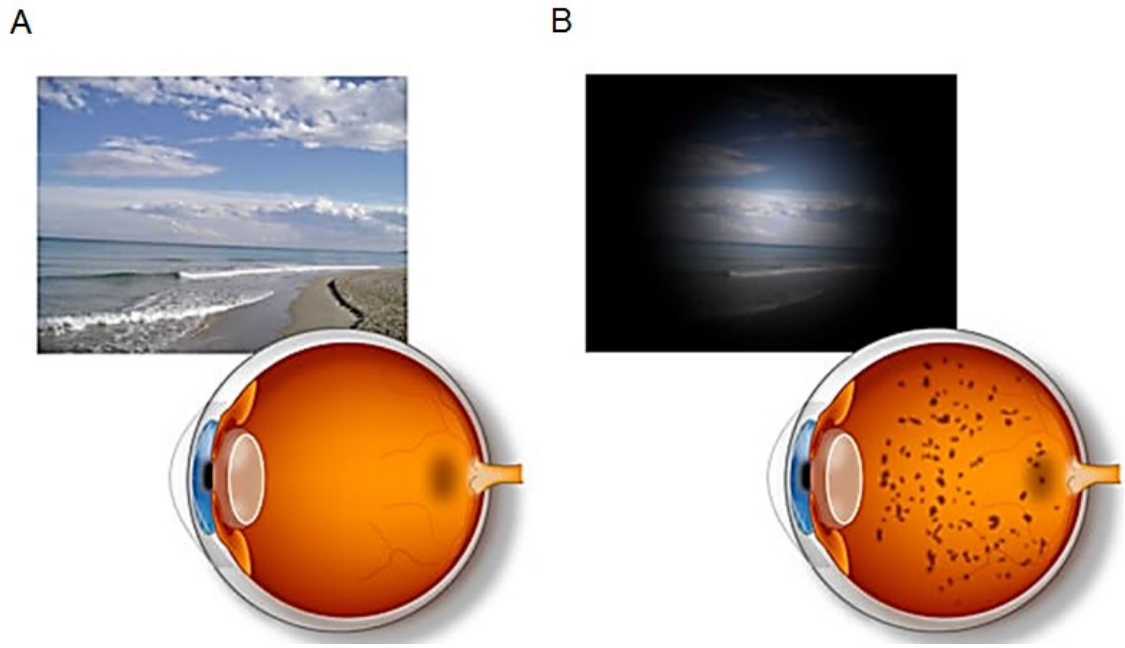

Figure 1.10 Example of a healthy retina and retina with RP disease.
A. Representation of a healthy retina and the visual field. **B**. Representation of an RP retina. Intraretinal pigmentary deposits are clearly visible in the RP retina and the corresponding associated tunnel vision. From http://retinosis.umh.es/retinosis.html.

More than 150 mutations have been found to date in the opsin gene associated with RP, most of them inherited as an autosomal dominant trait. These mutations are found in all three domains of Rho: the intradiscal, transmembrane and cytoplasmic domains (Berson, 1993). Many of the mutations found in the transmembrane and intradiscal domains of Rho cause misfolding of the mutated proteins thereby preventing binding of 11CR (Liu et al., 1996) The proper folding conformation of Rho allows efficient binding of the ligand by maintaining the correct set of interactions due to the appropriate structure of the retinal binding pocket. One of the molecular consequences in RP mutated Rho is the altered conformation of the protein with the formation of an abnormal disulfide bond between Cys-185 and Cys-187 that would irreversible lock the protein in its misfolded conformation (Figure 1.11)

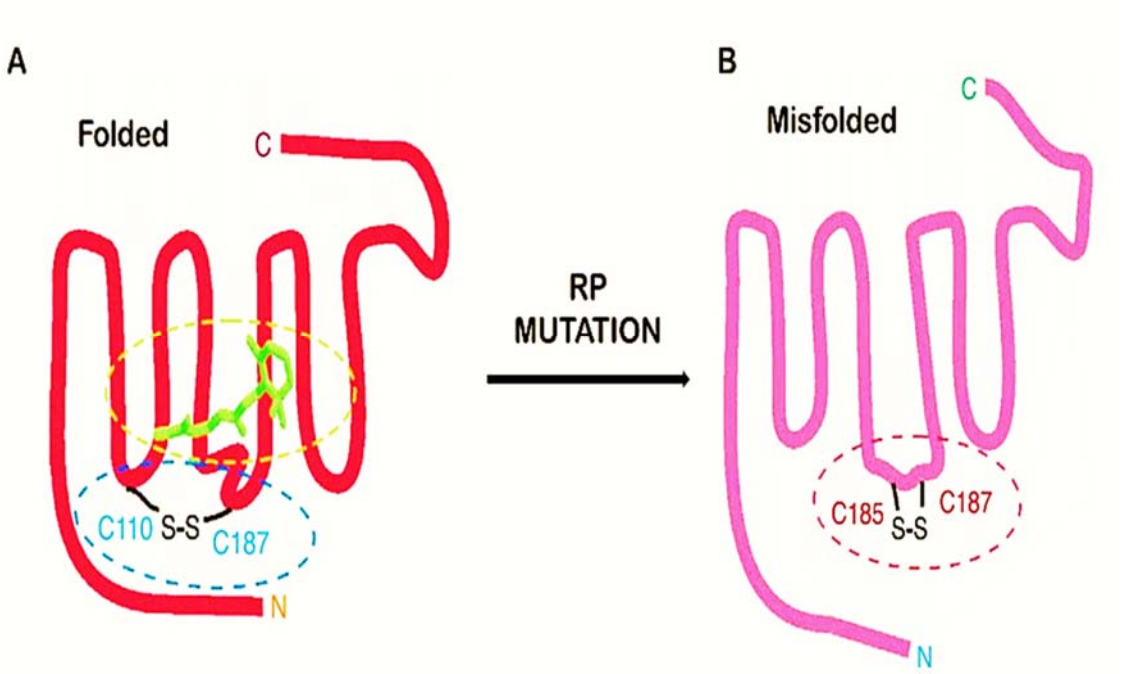

Figure 1.11 Representation of a misfolded conformation due to mutations associated with RP.
A. The disulfide linkage in correctly folded Rho is between Cys-110 and Cys-187. **B**. In misfolded Rho an abnormal disulfide bond can be formed between Cys-185 and Cys-187.

Rho mutants associated with RP are grouped into different classes which are shown in Figure 1.12 and in Table 1.1.

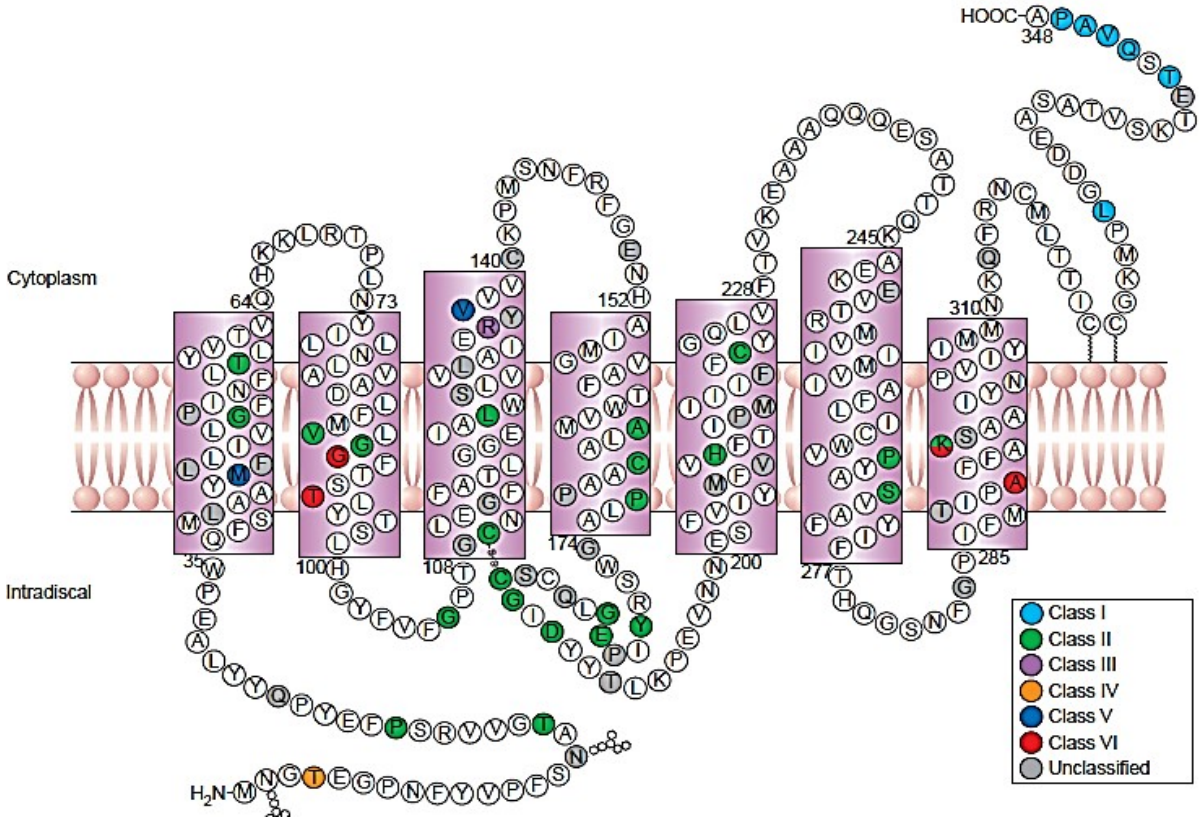

Figure 1.12 Secondary structure of Rho showing the location of the point mutations. Mutation listed in Table 1. Taken from Mendes et al., 2005.

Table 1.1 Classification of Rho mutants

Classification	Behavior	Site of point mutation	Misfolds
Class I	Fold normally but are not transported to the outer segment	L328, T342, Q344, V345, A346, P347	No
Class II	Are retained in the endoplasmic reticulum (ER) and cannot easily reconstituted with 11CR	T17, P23, G51, T58, V87, G89, G106, C110, L125, A164, C167, P171, Y178, E181, G182, C187, G188, D190, H211, C222, P267, S270, K296	Yes
Class III	Affect endocytosis	R135	No
Class IV	Do not necessarily alter folding but affect Rho stability and posttranslational modification	T4	No
Class V	Mutations show increased activation rate for Gt	M44, V137	No
Class VI	Show constitutive activation of opsin in the absence of chromophore and in the dark	G90, T94, A292	No
Unclassified	No observed biochemical or cellular defects or not studied in detail	N15, Q28, L40, F45, L46, P53, G109, G114, S127, L131, Y136, C140, E150, P170, G174, P180, Q184, S186, T193, M207, V209, P215, M216, F220, E249, G284, T289, S297, E341	

1.5 Rho ligand binding domain

One of the specific characteristics of Rho is its ligand, 11CR, intrinsically linked in the inactive state of the receptor by a PSB to Lys296. The binding site for the retinal is in the 7TM domain whereas the extracellular domain is partially involved in ligand binding for many other GPCRs. This is certainly a limitation when the crystal structure of Rho is used as a template for other GPCRs. However, the structure of Rho can still be very useful as a model for studies of lipophilic drug-receptor interaction in the transmembrane domains (Zhang et al., 2015).

Complete knowledge of the structural ligand binding cavity of a GPCR allows the design of novel agonists and antagonists. In this regard, new avenues for the design of ligands were opened by the resolution of the crystal structure of Rho (Palczewski et al., 2000). In the broad family of GPCRs, ligands usually bind to the extracellular portion of the receptor, and can interact with the 7TM domain, the three extracellular loops and/or the N-terminal domain. A significant number of GPCRs binding sites have been mapped, for their corresponding ligands, with a combination of mutagenesis, together with other biochemical techniques, and molecular modeling approaches relying on sequence homology (Bosch et al., 2005). Thus, a large number of small molecules capable of binding to receptors have been characterized. These ligands range from small catecholamines such as serotonin and dopamine, to large and small peptides, hormones, chemokines and proteins. From the standpoint of drug discovery, small molecules have main binding sites where most of candidates drugs would bind (Becker et al., 2003).

1.6 Rho interaction with small molecules

In numerous studies, attempts have been made in order to find novel ligands that could potentially compensate the mutational effects in Rho. Binding interactions between mutated Rho models and potential ligands have been predicted with the help of molecular docking using ligands that act either as agonists or as antagonists (Kanwal et al., 2012).

A class of agonists proposed for Rho are cyanidin compounds (Matsumoto et al., 2003). Cyanidins belong to the group of anthocyanins (C6-C3-C6 structure) which belong to the group of flavonoids and fall within the large family of polyphenols (Figure 1.13). Among them, dietary polyphenols, and especially flavonoids, have been widely studied for their strong antioxidant properties and other effects on cell function regulation (Hartman et al., 2006). This family of compounds has been investigated for its potential benefits against cancer, as well as in cardioprotection, neuroprotection, urinary tract health, and antiaging effects (Stevenson & Hurst, 2007)

,

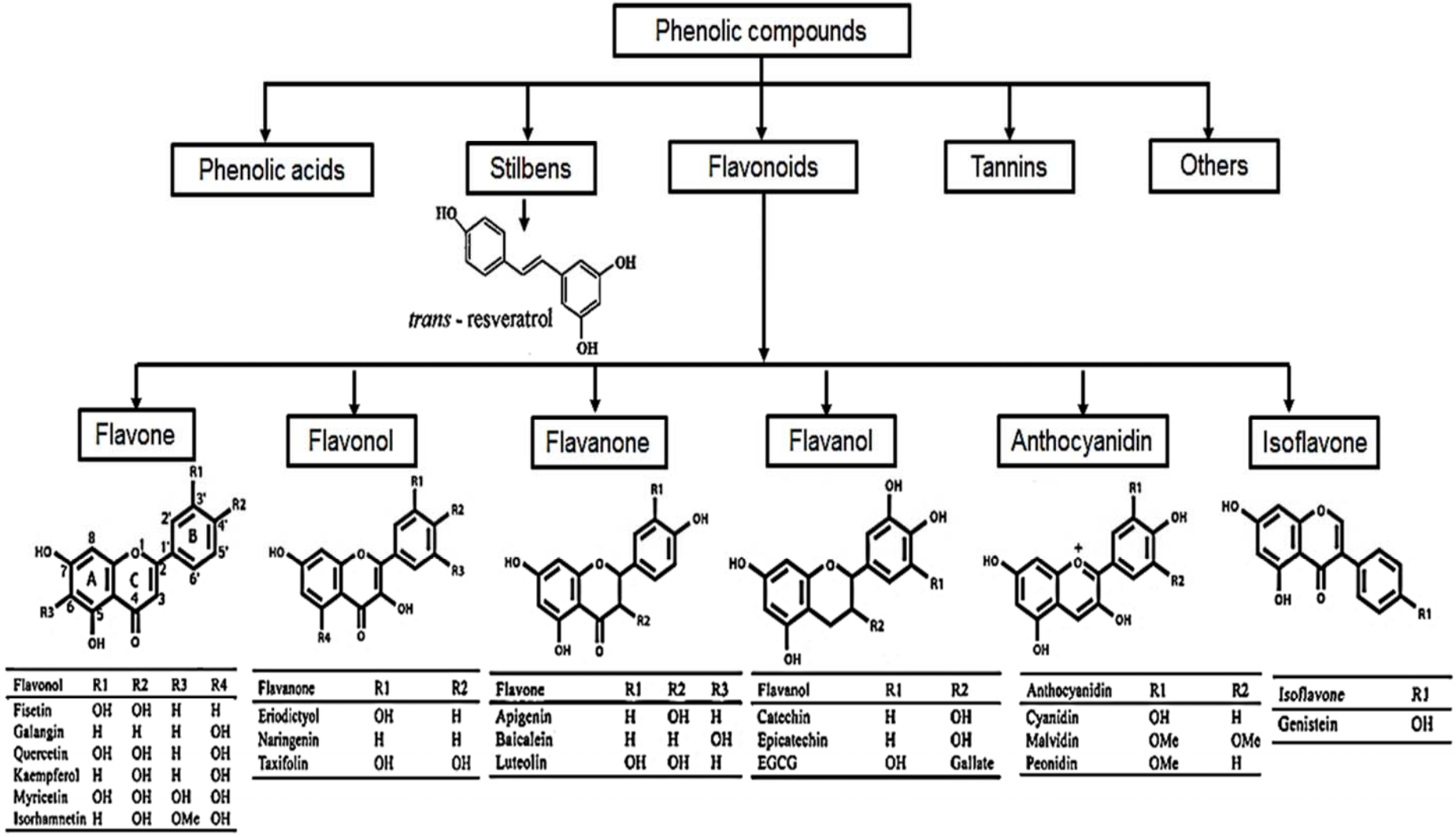

Flavonol	R1	R2	R3	R4
Fisetin	OH	OH	H	H
Galangin	H	H	H	OH
Quercetin	OH	OH	H	OH
Kaempferol	H	OH	H	OH
Myricetin	OH	OH	OH	OH
Isorhamnetin	H	OH	OMe	OH

Flavanone	R1	R2
Eriodictyol	OH	H
Naringenin	H	H
Taxifolin	OH	OH

Flavone	R1	R2	R3
Apigenin	H	OH	H
Baicalein	H	H	OH
Luteolin	OH	OH	H

Flavanol	R1	R2
Catechin	H	OH
Epicatechin	H	OH
EGCG	OH	Gallate

Anthocyanidin	R1	R2
Cyanidin	OH	H
Malvidin	OMe	OMe
Peonidin	OMe	H

Isoflavone	R1
Genistein	OH

Figure 1.13 Classification of dietary polyphenols.

Dietary polyphenols are the most abundant antioxidants in human diets. With over 8000 structural variants, these are secondary metabolites of plants and denote many substances with aromatic ring(s) bearing one or more hydroxyl moieties. They are subdivided into groups (Figure 1.13) characterized by the number of phenolic rings and by the structural elements that link these rings (Crozier et al., 2009; Tsao, 2010): (1) phenolic acids with the subclasses derived from hydroxybenzoic acids, such as gallic acid; and from hydroxycinnamic acid, such as caffeic acid, ferulic acid, and coumaric acid; (2) the large flavonoid subclass, which includes flavonols, flavones, isoflavones, flavanones, anthocyanidins, and flavanols; (3) stilbenes; and (4) lignans and polymeric lignins.

Flavonoids are the most abundant polyphenol class, and recent research suggests that flavonoids may be involved in two major aspects of the different processes involved in vision physiology and eye health. On the one side, flavonoids may function in visual signal transduction, in ways that are as yet not well understood. On the other side, flavonoids may also function in their well-established role as antioxidants, which is particularly important in the eye, where oxidative stress is significant and its damage is involved in a number of vision pathologies, including macular degeneration (Rhone & Basu, 2008).

Cyanidin 3-glucoside (C3G) is an anthocyanin, belonging to the group of flavonoids, which has been evaluated for its role at different stages in the visual signal transduction process. Matsumoto et al. (Matsumoto et al., 2003) reported that specific blackcurrant anthocyanins stimulated regeneration of Rho. Kinetic analysis revealed that the Km for the formation of Rho was reduced by the presence of cyanidin glycosides, although it was not possible to determine the specific reaction affected. They also reported insignificant effects of these compounds on phosphodiesterase activity by means of cGMP-testing at different stages of the activation process, in light and in darkness.

C3G has also been reported to directly interact with the dark and illuminated forms of Rho (Tirupula et al., 2009; Yanamala et al., 2009). Such interaction of C3G and Rho, purified from bovine retinas, was determined by nuclear magnetic resonance (Tirupula et al., 2009). C3G was also found to increase the rate of Rho regeneration with 11CR. It was also suggested that anthocyanins could either inhibit or activate GMP-cyclic phosphodiesterase. Furthermore, computational docking experiments, using pH-dependent forms of C3G, suggested coupling of the cytoplasmic side of Rho with the C3G chalcone that was proposed to show higher binding affinity for this receptor domain. The pH of the extracellular medium of the photoreceptor is increased by exposure to light, and the vertebrate retina experiences diurnal changes of pH; such as being more alkaline during the day. Differences in the pH of the photoreceptor cells make the study of the pH-dependent differential effects of anthocyanins particularly interesting (Stevenson & Hurst, 2007).

Other studies described C3G interaction of the flavanone eriodictyol with opsin *in vitro*, affecting opsin signaling activity and also inducing G-protein activation in cone cells. In these studies, it was suggested that eriodictyol could act in a similar way to a retinoid and could potentially modulate physiological changes in photoreceptor function (Johnson et al., 2009). Significant beneficial effects of Q on eye health have also been proposed (Kalt et al., 2010).

In addition, the *in vitro* antioxidant effects of flavonoids, and other phenolic compounds, have recently been studied using models and ocular cell types that are relevant to vision processes and pathologies. Cultured RPE cells have been employed to investigate how flavonoids cause oxidative damage and metabolic responses to oxidative stress *in vitro* (Table 1.2). In a previous study, a number of flavonoids were tested for their effect on the survival of immortalized human RPE cells after an oxidative stress treatment by the addition of either tert-butyl peroxide or hydrogen peroxide (Hanneken et al., 2006). The effective flavonoids included fisetin, luteolin, Q, eriodictyol, baicalein, galangin and epigallocatechin-gallate (EGCG), and the synthetic flavonoids, 3,6-dihydroxy flavonol and 3,7 dihydroxy flavonol. Flavonoids acted through an intracellular route to block the accumulation of reactive oxygen species. Many of these flavonoids induced the expression of Nrf2 and the phase-2 gene product heme-oxygenase 1 in human RPE cells. Similar flavonoid antioxidant studies have been conducted in retinal ganglion cells (Maher & Hanneken, 2005).

Moreover, cellular models have been used to evaluate the antioxidant effect of flavonoids. *In vivo* models, using rats and mice, have also been used in order to assess the protective effect of flavonoids against light-induced retinal degeneration. In addition to flavonoids, other compounds of the polyphenols family, such as resveratrol (R), have been evaluated for their protective effect against light-induced damage, and in animal models of RP (Table 1.2).

Table 1.2 Phenolic compounds potentially active against retinal damage.

Adapted from Herrera-Hernández et al., 2015.

COMPOUND	CONDITION	EFFECT	REFERENCES
EGCG	UV-B light-induced retinal damage	Regulates autophagy in RPE cells	(Li et al., 2013)
Valproic acid	Preserving sight in glaucoma patients	Prevents retinal ganglion cells death. Stimulates brain-derived neurotrophic factor (BDNF) up-regulation in Müller glial cells.	(Kimura et al., 2015)
Lutein	Light-induced retinal damage	Attenuated light-induced visual impairment by protecting the photoreceptors cells DNA. Attenuates the thinning of the photoreceptor cell layer owing to apoptosis. Reduce oxidative stress in the retina.	(Sasaki et al., 2012)
Q	Oxidative stress model. Assay *in vitro* in human RPE cells	Significant dose-dependent reduction of caveolin-1 mRNA. Down-regulation of caveolin-1 may be important for the RPE to prevent apoptotic cell death in response to cellular stress	(Hanneken et al., 2006; Kook et al., 2008)
Luteolin	Oxidative stress model. Assay *in vitro* in human RPE cells	Protects RPE cells from oxidative-stress–induced death with a high degree of potency and low toxicity	(Hanneken et al., 2006)
Eriodictyol	Oxidative stress model. Assay *in vitro* in human RPE cells	Protection through its effects on Nrf2 activation and phase 2 gene expression and enhance multiple cellular defenses to oxidative injury	(Hanneken et al., 2006; Johnson et al., 2009)
Fesitin	Oxidative stress model. Assay *in vitro* in human RPE cells	Protects RPE cells from oxidative-stress–induced death with a high degree of potency and low toxicity	(Hanneken et al., 2006)
R	Oxidative stress model. Assay *in vitro* in human RPE cells.	Prevents programmed cell death of human RPE cells induced by oxidative stress and the proliferation of RPE cells via inhibition of the mitogen activated protein kinase (MAPK)/ERK (MEK) and extracellular signal-regulated kinase (ERK 1/2)	(King et al., 2005)
	Antibody-induced apoptosis of retinal cells *in vitro*	Protection of retinal cells from apoptosis by R occurred through multiple early molecular events, such as reduction of intracellular calcium levels, down-regulation of pro apoptotic protein Bax, up-regulation of Sirtuin-1 (SIRT-1) a regulator of aging and Ku70 protein activities, and inhibition of caspase-3 activity	(Anekonda & Adamus, 2008)
	Light-induced retinal degeneration	Suppresses the thinning of the outer nuclear layer thickness and the activity of the activator protein 1, a heterodimeric protein responsible for the regulation of cell proliferation and apoptosis. Activates SIRT-1.	(Kubota et al., 2010)
	Cells treated with benzo(e)pyrene (B(e)P), a toxic component of cigarette smoke.	Can reverse the apoptosis and oxidant production generated by B(e)P. These inhibitors may be beneficial against retinal diseases associated with the loss of RPE cells	(Mansoor et al., 2010)
Hesperidin	Against the toxic effects of systemic cisplatin	Prevents the effects caused by cisplatin, increasing of thiobarbituric acid reactive substances levels and decreasing glutathione levels and antioxidant enzyme activity of catalase, superoxide dismutase and glutathione peroxidase	(Polat et al., 2015)

2. OBJECTIVES

Novel methodological approaches have been developed on RP mutants in order to elucidate the molecular mechanism of the disease as a necessary first step before suitable therapeutic approaches can be developed. Some of the proposed treatments have been based on pharmacological rescue, in which small molecules known as chemical or pharmalogical chaperones bind and stabilize misfolded opsins acting as allosteric modulators. The use of natural products, like polyphenolic compounds, alone or in combination with other molecules, like retinal analogs, can be a powerful strategy to counteract the effects of mutations associated with retinal degeneration in RP.

2.1 Main objective

In view of this lack of scientific evidence on the potential benefits of these kind of natural products on visual health, the global objective of this research is to evaluate the effect of polyphenolic compounds on the structure and function of the visual pigment Rho and mutants associated with the retinal degenerative disease RP.

2.2 Specific Objectives

In line with the main goal, the specific objectives of this thesis are:

1. To characterize selected polyphenols by UV-Vis and fluorescence spectroscopy in the same conditions as recombinant purified Rho will be studied.
2. To clone, express and immunopurify WT Rho and RP mutants and to characterize the purified proteins by means of spectroscopic and biochemical methods.
3. To determine the structure and stability properties of ROS Rho, WT and mutants associated with RP by different assays including chromophore regeneration, thermal and chemical stability, Meta II decay, photobleaching and acidification, in the absence and in the presence of the polyphenolic compounds studied.
4. To determine the effect of the polyphenols studied on the chemical and thermal stability of WT Rho and the selected RP mutants.
5. To evaluate the effect of the selected polyphenols on the ability of ROS Rho, WT and RP mutants, to activate Gt.
6. To investigate the binding preferences of polyphenolic compounds to Rho by means of computational-aided modeling (*in silico*) studies.

3. MATERIALS AND METHODS

3.1 Materials

3.1.1 General laboratory equipment

Autoclave DARLAB K-400
Balance Precisa QUALITY
Benchtop centrifuge Beckman Coulter, Allegra X-15R.
Biological safety cabinet laminar flow type II, NuAire
CO_2 Water-Jacketed Incubator, NuAire
Double distilled water system, Millipore
Electrophoresis system, BioRad Mini-PROTEAN-2.
Fiber optic illuminator Doland-Jenner MI-150
Fluorescence microscope, NIKON/Eclipse Ti-S
Gel documentation system; Chemidoc XRS, BioRad
Horizontal shaker MAGNA-AS-15
Hybrid liquid coolant system Reserator XT, Zalman connected to the spectrofluorimeter
Ice machine, BAR-LINE
Incubator Certomat^{R} BS-T, Satorius stedim biotech
Incubator, SANYO
Inverted microscope Olymus CK30
Liquid nitrogen container, Air Liquid
Liquid scintillation counter Tri Carb 2100TR, Perkin-Elmer
Long-life mercury light source, Nikon intensilight
Microtubes centrifuge, Biocen
Millipore vacuum pump XF54 230 50
Multiwell plate reader, Tecan/Infinite M200
Orbital shaker, OVAN OS10-E
Personal thermal cycler MJ Mini^{TM}, BioRad
pH meter Hanna Instruments; Model pH213
Refrigerated centrifuge, ALRESA
Refrigerated centrifuge, Kubota 6500
Safelight filter KODAK 2
Spectrofluorimeter Photon Technologies QM-1
Temperature controller dual cell peltier accessory connected to the spectrophotometer
Transfer chamber for western blot, BioRad
Ultracentrifuge Beckman Coulter, Optima LE-80K
UV-Visible spectrophotometer Varian, Cary 100 Bio
Vortex shaker, Heildoph REAX Top

Water bath Tectron 3000543

Water bath Bath-100, DARLAB

3.1.2 Chemicals and other materials

11CR, National Eye Institute, National Institutes of Health (USA)

9CR, Sigma, Spain

Acrylamide/Bisacrylamide mix, BioRad, USA

Alamar blue, Invitrogen-Thermo scientific, Spain

Biodegradable scintillation fluid, GE healthcare life sciences, Spain

Cellulose membrane and manifold for radioactivity assay, Millipore, France

Chlorogenic acid ≥ 95 %, Sigma, Spain

Cyanogen bromide (CNBr)-activated Sheparose 4B beads, Sigma, Spain

Dark adapted bovine retinas, W L Lawson Company, NE, USA.

DMEM-F12, Lab clinics, Spain

dpnI, Agilent technologies, CA,USA

Dulbecco's modified eagle medium (DMEM), Sigma, Spain

EGCG ≥ 95 %, Sigma, Spain

Ellagic acid ≥ 96 %, Sigma, Spain

Fetal bovine serum (FBS), Sigma, Spain

$GTP\gamma S^{35}$ (250 µCi), Perkin Elmer, Spain

Hesperetin ≥ 95 %, Sigma, Spain

Hesperidin ≥ 80 %, Sigma, Spain

Hydroxilamine, Sigma, Spain

L-glutamine, Sigma, Spain

mAb rho-1D4 antibody, Cell Essentials, Boston, USA

n-dodecyl-β-D-maltoside (DM), Anatrace Inc., Maumee, OH, USA

Naringenin ≥ 95 %, Sigma, Spain

Naringin ≥ 95 % (HPLC), Sigma, Spain

Nitrocellulose membrane 0.45µm , BioRad, USA

Nonamer-peptide H-TETSQVAPA-OH, Unitat de Tècniques Separtatives i Sìntesi de Pèptids, Universitat de Barcelona, Barcelona, Spain

Oligonucleotides, Sigma, Spain

Opti-MEM, Fisher scientific, France

Penicillin-streptomycin, Sigma, Spain

Pfu ultra II fushion hsDNA polymerase, Agilent technologies, CA,USA

Phenylmethanesulfonyl fluoride (PMSF) , Sigma, Spain

Polyethyleneimine (PEI), Polysciences Inc. (USA)

Protease inhibitor cocktail, Sigma, Spain

Q ≥ 95% (HPLC), Sigma, Spain

R ≥ 99% (HPLC), Sigma, Spain

Rutin hydrate ≥ 94% (HPLC), Sigma, Spain

SuperSignal West Pico chemiluminescent substrate, Thermo scientific, Spain

SuperSignal West Pico stable peroxide solution, Thermo scientific, Spain

Tris-HCL 0.5mM pH 6.8, BioRad, USA

Tris-HCL 1.5mM pH 8.8, BioRad, USA

All other chemicals and reagents were purchased from Sigma, Spain

3.1.3 Biologic Materials

3.1.3.1 pMT4 plasmid vector

pMT4 is a 6.2 kbp ampicillin resistance vector containing the bovine opsin gene (**Annex A**) between EcoRI and NotI restriction sites (Figure 3.1)

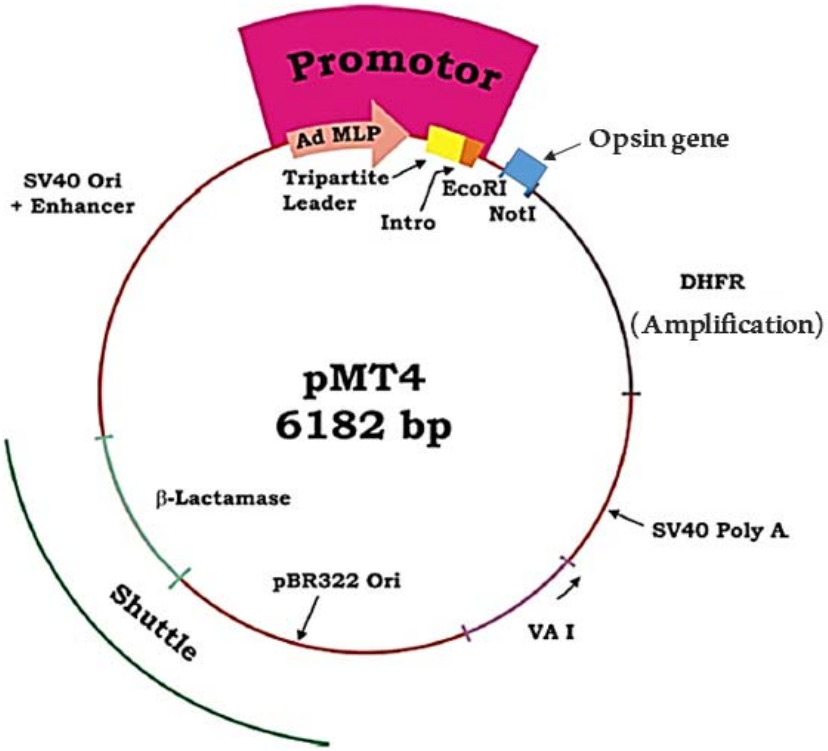

Figure 3.1 pMT4 plasmid vector.
The β-lactamase confers the antibiotic resistance to the bacteria carrying this vector, allowing artificial selection to the transformed cells on an ampicillin supplemented media.

3.1.3.2 DH5α *E. Coli* cells

DH5α cells are an E. coli strain widely used in molecular biology to clone recombinant DNA. Herein, these cells are utilized to obtain large amounts of the opsin gene for subsequent transfection into eukaryotic cells. Before usage, these cells need to be pretreated to facilitate the absorption and incorporation of the vector. For this purpose, $CaCl_2$ was used to permeabilize the cell membrane under thermal shock in a procedure described in **Annex D.**

3.1.3.3 Eukaryotic cell lines

The cell lines employed during the development of this work were:

COS-1: African green monkey kidney cells. They are obtained from the transformation of CV-1 cells (monkey cells permissive for the development of lytic virus SV40) with SV40 DNA mutated in the origin of replication. COS-1 cells are generally used for transient transfections producing thousands and hundreds of thousands of copies of proteins in a time frame of 72h after transfection. These cells were used to express recombinant Rho.

HEK 293S GnTI^{-}: Human embryonic kidney cells transformed with adenovirus 5 DNA. They lack N-acetylglucosaminyltransferase I (GnTI^{-}) activity, and consequently are unable to synthesize complex N-glycans, yielding homogenously glycosilated proteins. Herein, these cells are used for the production of WT and Rho mutants for electrophoretic and immunofluorescence assays.

3.1.4 Preparation of polyphenol samples

To evaluate the effect of phenolic compounds on Rho, recombinant Rho WT and mutants, the following experimental strategy shown below was followed. The compound initially selected to start this research was the flavonoid Q due to its proposed beneficial effect on eye health and its presence in the retina. Furthermore, this compouns is recognized by the Food and Drug Administration (USA) as safe. The compounds and concentrations used are shown in Table 3.1.

To quickly assess if the compounds mentioned have an effect on recombinant WT and mutant expression levels, Western blot was chosen to detect possible changes in the electrophoretic pattern. Western blot was chosen instead of SDS-PAGE because it requires lower amount of protein for the assay.

Table 3.1 Phenolic compounds

Phenolic compound	Concentration
Q	1, 2.5, 5, 10, 15 and 50μM

Naringenin	1, 2.5, 5, 10, 15 and 50μM
Hesperetin	1, 2.5, 5, 10, 15 and 50μM
Chorogenic acid	1, 2.5, 5, 10, 15 and 50μM
R	1, 2.5, 5, 10, 15 and 50μM
Rutin	1, 2.5, 5, 10, 15 and 50μM
EGCG	1, 2.5, 5, 10, 15 and 50μM
Ellagic acid	1, 2.5, 5, 10, 15 and 50μM

3.2 METHODS

3.2.1 Obtaining recombinant DNA

3.2.1.1 Transformation of DH5α competent cells

1μg DNA was mixed with 50 μl of *E. Coli* competent cells, prepared as described in annex B, and incubated on ice for 30 min. After heat-shock treatment at 42°C for 45s, the cells were immediately placed back on ice for 5 more min. Then, 500 μl of sterile 2YT media (composition described in **Annex G**) was added to the transformed cells and shaked at 37°C, 230 rpm for 1 h. Finally, 100 μl of cells were plated on LB agar (go to annex G for recipe) plate supplemented with ampicillin (100μg/mL). The plate was incubated inverted overnight (ON) at 37°C.

3.2.1.2 Small-scale plasmid DNA purification (Miniprep)

A single colony from the transformed plate was inoculated into 6 ml of LB broth containing 100 μg/ml of ampicillin at 37°C, and shaked at 230 rpm ON. The mini-culture was centrifuged at 4000 rpm for 20 min and the supernatant (SN) discarded. DNA was purified using QIAprep spin Miniprep kit (Qiagen plasmid purification kits, La Jolla, CA) and the protocol is detailed in annex C. Concentration and purity of the obtained DNA were determined by UV-vis spectroscopy.

The concentration of purified DNA was calculated using:

$$\text{Concentration of DNA } \left(\frac{\mu g}{ml}\right) = A_{260nm} \times 50 \times DF$$

DF, dilution factor

1 OD_{260nm} of dsDNA = 50 µg/ml.

DNA purity (Kim et al., 2005) was determined by analyzing the following parameters :

A_{260}/A_{280} <1.8, contamination by proteins.

1.8 ≤ A_{260}/A_{280} ≤ 2, pure DNA

A_{260}/A_{280} >2, contamination by RNA

3.2.1.3 Large-scale plasmid DNA purification (Maxiprep)

Large scale DNA purification for transient transfection was carried out from a 500 µl mini culture, prepared as indicated in **3.2.1.2**, in 1 L of LB media containing 100µg/ml ampicillin. For optimal growth conditions, the culture was split into two 500-ml flasks and incubated at 37°C 230 rpm ON. Cells were harvested at 4000 rpm, at 4°C, for 30 min. The SN was discarded and the DNA was purified following the protocol of PureLink™ HiPure Plasmid filter Purification kit from Invitrogen, described in annex D. DNA concentration and purity were determined as described in **3.2.1.2.**

3.2.1.4 Site directed mutagenesis for mutants construction

Quick-change mutagenesis protocol (Stratagene) was employed to introduce point mutations into the opsin gene and the procedure was conducted according to the following protocol.

i Mutagenic primer design. Mutagenic primers are short oligonucleotides containing the desired mutation. The primers should be 25 bp to 45 bp with a melting temperature (Tm) ≥78°C. The GC content of the primers should be 40-60%, the desired mutation located in the middle of the primer and they should terminate with 1 or 2 C or G bases. The mutated primers for the forward and backward strands were done using a DNA codon table.

To calculate theTm, the next formula was used:

$$\mathrm{Tm} = 81.5 + 0.41\,(\%\mathrm{GC}) - 675/\mathrm{N} - \%\mathrm{mismatch}$$

Where :

Tm=oligonucleotide melting temperature

% GC= percentage of GC in the oligonucleotide

N=length (number of bases)

%mismatch = percentage of changes made in sequence from the original sequence.

The primers were provided by Sigma Aldrich in lyophilized form, and were prepared at a concentration of 125 ng/µl with sterile milliQ water

ii Polymerase chain reaction (PCR). The mutated opsin genes were synthesized using a thermal cycler by PCR. The reaction mixture for synthesizing and amplifying the mutated plasmid is shown in Table 3.2.

Table 3.2 Reaction mixture for the construction of mutated plasmid

Reagents	Volume (µl)
Double-distilled water	41
Forward primer (125 ng/µl)	1
Reverse primer (125 ng/µl)	1
pMT4 PLASMID (100 ng/ µl)	1
dNTP MIX (100 Mm)	1
10X reaction buffer	5
PfuTurbo DNA polymerase (2.5 U/ µl)	1

The mixture was prepared in a microfuge tube and was subjected to the conditions described in Table 3.3.

Table 3.3 Thermocycler conditions for construction and amplification of plasmids containing mutation in the opsin gene.

Step	Temperature	Time
Initial denaturation	95 °C	30 s
Amplification (18 cycles)	95 °C	30 s
	60 °C	60 s
	68 °C	7 min
Final extension	68 °C	7 min

iii DpnI digestion. In order to digest the template plasmid, 1 µl of the DpnI restriction enzyme was added and mixed well by pipetting the solution up and down several times and the mixture was incubated at 37°C for 2 h. After this time, 10 µl of the resulting DNA sample were taken and analyzed by 1% agarose gel electrophoresis. The remaining sample was placed in an Eppendorf tube, and 100 µl of cold ethanol and 5 µl of 3 M sodium acetate (pH 5.5) were added. The mixture was kept 30 min at -80 °C and subsequently centrifuged for 15 min at 14000 rpm. The SN was discarded and the tube was left open to allow the complete drying of the plasmid and eventually dissolved in water.

iv Transformation. *E. Coli* DH5α cells were transformed according to the protocol described in section **3.2.1.1**. pMT4 plasmid from the growing colonies was purified by following the experimental conditions described in section **3.2.1.2** .

v DNA sequencing. The mutation introduced into the opsin gene was confirmed by DNA sequencing. The primers for DNA sequencing were designed from the sequence and they must be located 50pb upstream the mutation site. The DNA sequencing was carried out by STAB VIDA company in Caparica, Portugal.

3.2.2 Protein expression

Protein expression refers to the synthesis, modification and regulation of proteins in living organisms. In protein research, the term can apply to either the object of study or the laboratory techniques required to manufacture proteins. Proteins produced from recombinant DNA are called recombinant proteins. Traditional strategies for recombinant protein expression involve transfecting cells with a DNA vector containing the gene for the desired protein, and then culturing the cells to promote correct transcription and translation of the protein. Typically, the cells are then lysed to extract the expressed protein for subsequent purification. Both prokaryotic and eukaryotic protein expression systems are widely used.

3.2.2.1 Thawing frozen cells

The cells used in this study were recovered from liquid nitrogen storage container by thawing the cryotubes at 37°C in a water bath. Then, the cryotubes were cleaned using 70% ethanol and cells were transferred aseptically into a cell culture plate containing the specific culture medium of the cell line (see **Annex I** for more details). The thawed cells were incubated at 37°C and 5% CO_2 incubator and the media was replaced after 12 h.

3.2.2.2 Cell subculturing

COS-1 and HEK GnTI^{-} cells were routinely cultured in their respective cell culture media. When the cells achieved 90% confluence, the medium was removed using a suction pump under a pre-UV-sterilized laminar flow hood, washed with sterile PBS in order to remove the dead cells and residual medium. In the case of COS-1 cells, the mono-layer of adherent cells was treated with 5ml of trypsin solution (as described in **Annex G**), incubated at 37°C for 10 min, and immediately after cells detachment carefully by pipetting, 5ml of media were added in order to inactivate trypsin. Cells were subsequently split from 1 to 4 plates containing 20 ml of media. Trypsin was not needed for HEK-293S GnTI^{-} cells due to their weak adherence on plate. Plates were incubated in a 37°C humid incubator with 5% CO_2.

3.2.2.3 Cryopreservation of cells

For long term storage, cells were frozen in liquid nitrogen. For this purpose, detached cells from the plates were harvested by centrifugation at 2500 rpm, at 4ºC for 5 min. Then, after discarding the SN, cells were resuspended (1 ml/plate) in freezing media (see composition in **Annex G**. Finally, cells were aliquoted in 1 ml labeled cryotubes and kept at 4°C for 2 h followed by 5 h at -20°C and ON at-80°C. Next day vials were transferred into a liquid nitrogen container.

3.2.2.4 Transient transfection of pMT4

Transfection process allows the introduction of a vector into eukaryotic cells for protein expression. Opsins were expressed after transient transfection of COS-1 or HEK-293S GnTI^{-} cells by using polyethylenimine (PEI). PEI condenses DNA into positively charged particles (polymer-DNA complex) binding to anionic cell surface residues and enters the cell via endocytosis (Figure 3.2). Once inside the cell, PEI protonation results in an influx of counter-ions and a lowering of the osmotic potential in the vesicle. Consequently, osmotic swelling results and bursts the vesicle, releasing the polymer-DNA complex into the cytoplasm (Longo et al., 2013).

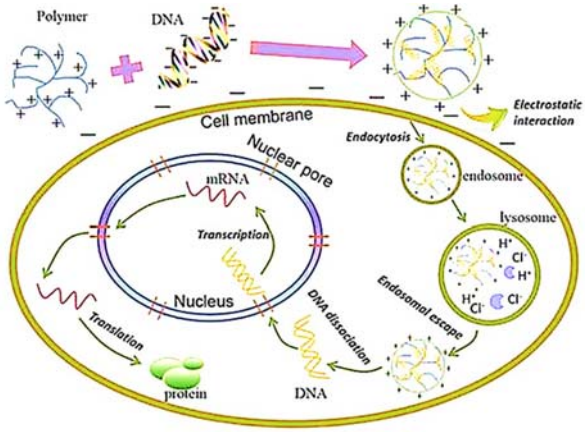

Figure 3.2 . Schematic representation of chemical transfection using PEI.

For PEI preparation; 30 mg of powder were dissolved in distilled water and the pH was adjusted to 6.0 (the solution becomes clear as the pH is adjusted). After PEI was completely dissolved, the final concentration was adjusted to 1mg/ml and filtered through a 0.22 µM filtering unit. The prepared PEI was aliquoted and stored at -20°C until use and maintained at 4°C after thawing.

Two types of plates, either 6-well plates or 150x20mm dishes, were used depending upon the type of experiment to be performed. In both cases, cells were grown as described in section **3.2.2.2** until a confluence about 80% was reached. Transfection was performed following the procedure shown in Figure 3.3.

In order to study the effect of the selected phenolic compounds on the expression of recombinant opsins, the culture medium was supplemented with the required amount of the stock solution of the given compound (20 mM), to achieve the desired final concentration. In any case, care was taken that the final concentration of 0.25% of DMSO (v/v) was never exceeded to avoid cell toxicity.

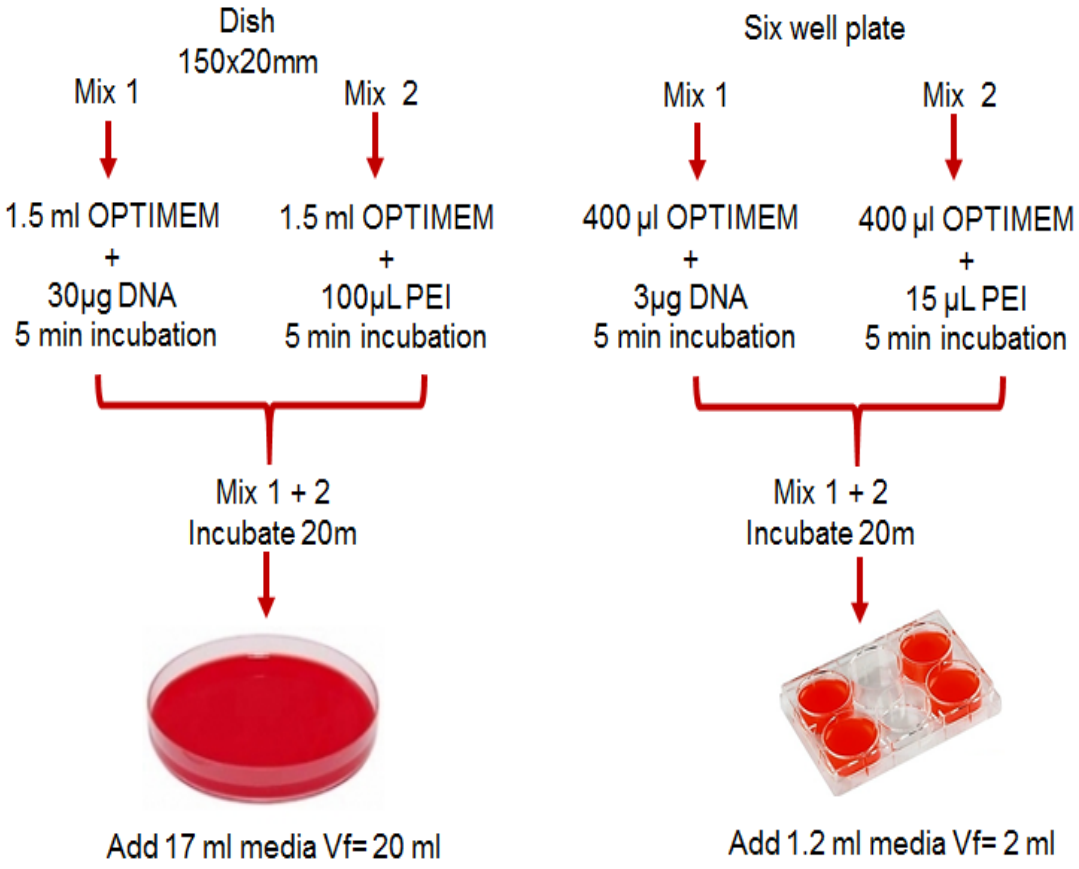

Figure 3.3 Transfection procedure for the expression of recombinant opsins.
For transfection in presence of polyphenolic compounds the quantity necessary to reach the desired concentration was added to the medium from the stock solution of each compound

3.2.2.5 Cell viability

It was important to determine the cell viability in the presence of the compounds that we wanted to study to rule out toxic effects on the cells. AlamarBlue reagent, containing resazurin as the active compound, was used following the manufacturer's recommendations for this test.

Resazurin is used as an oxidation-reduction (REDOX) indicator that undergoes colorimetric change in response to cellular metabolic reduction. The reduced form resorufin is pink and highly fluorescent, and the color change from blue to pink is proportional to the number of living cells. Through detecting the level of oxidation during respiration, alamarBlue acts as a direct indicator to quantitatively measure cell viability and cytotoxicity (Figure 3.4).

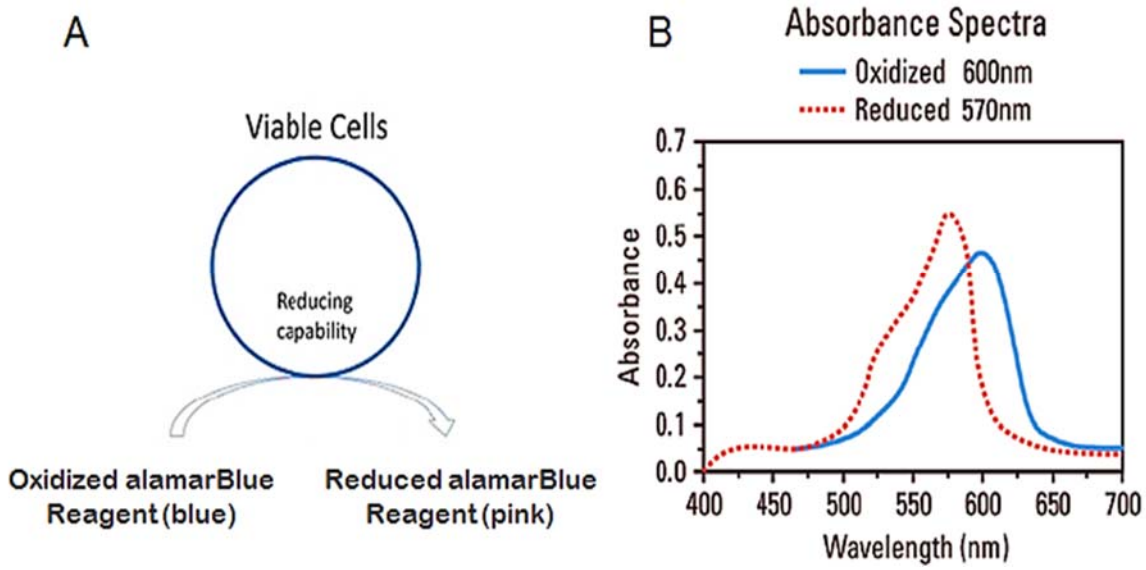

Figure 3.4 A. Representative schematic of alamarBlue cell viability reagent undergoing reduction within the cells. B. Absorbance spectra of alamarBlue reagent in oxidized and reduced states. From www.thermoscientific.com/pierce.

One plate of COS-1 cells was trypsinized and resuspended in cell culture medium. The resuspended cells were adjusted at a density of $1x10^5$ cells using a Neubauer chamber to count them. 100 µl per well of resuspended cells were placed into a 96-well plate and incubated in a 37°C humid incubator with 5% CO_2. 24 h later, the cell culture medium was removed and the cells were exposed to 300 µl of culture medium containing the corresponding concentration of compound (1, 10, 50 and 100 µM) under the same conditions described in section **3.2.2.4.** Furthermore, one sample containing transfection solution was prepared to evaluate their toxicity together with two different controls, 1) cell culture medium without cells to determine the absorbance of the negative control; 2) an untreated cell control prepared by adding the same solvent used to dissolve the compound (DMSO). After 48 h of incubation, 200 µl of medium were

removed and 10 µl of alamarBlue reagent was added. The absorbance at 570nm was measured after 4h of incubation at 37°C using 600 nm as reference wavelength in a microplate reader. To calculate the % reduction of alamarBlue reagent the next formula was used:

$$\%\text{Reduction of alamarBlue reagent} = \frac{(E_{oxi}600 \text{ x } A_{570}) - (E_{oxi}570 \text{ x } A_{600})}{(\text{Ered}570 \text{ x } C_{600}) - (E_{red}600 \text{ x } C_{570})} \text{ x } 100$$

Where,

$E_{oxi}570$ =E of oxidized alamarBlue reagent at 570nm = 80586 M^{-1} cm^{-1}

$E_{oxi}600$ =E of oxidized alamarBlue reagent at 600nm = 117216 M^{-1} cm^{-1}

A_{570} = Abs of test wells at 570nm

A_{600} = Abs of test wells at 600nm

$E_{red}570$ =E of reduced alamarBlue reagent at 570= 155677 M^{-1} cm^{-1}

$E_{red}600$ =E of reduced alamarBlue reagent at 570= 14652 M^{-1} cm^{-1}

C_{570} = Abs of negative control well at 570nm

C_{600}= Abs of negative control well at 600nm

3.2.2.6 Protein subcellular localization

In eukaryotes, numerous complex sub-cellular structures exist. The majority of these are delineated by membranes. Many proteins are trafficked to be able to carry out their correct physiological function. As previously mentioned, Rho is a membrane protein that must be inserted into the lipid bilayer to be functional. Immunofluorescence (IF) microscopy is a broadly applicable method to assess the cellular localization of proteins of interest. This technique uses the specificity of antibodies, an unlabeled primary antibody that specifically binds to the target protein and a fluorophore-conjugated secondary antibody that recognizes this primary antibody.

Briefly, a low density of HEK-293S GnTI^{-} cells was seeded in six-well plates containing sterile coverslips and incubated for 24 h at 37ºC, 5% CO_2. Next day, the old medium was removed and the cells were transfected as described in section **3.2.2.4**. 24 h after transfection, the solution was removed and the cells were washed twice with 3 ml PBS. Then, cells were incubated in 1 ml of a mixture containing 37% formaldehyde and 15% methanol in water at 37°C for 20 min in order to fix and to permeabilize the transfected cells onto the coverslips. After this time, the formaldehyde solution was removed and the cells were washed three times with 2ml of TTBS buffer for 10 min in an orbital shaker. After washing, cells were blocked with 5% skim milk in TBS stirring for 30 min. Cells were washed again three times with 2ml of TTBS for 10 min with shaking. Rho-1D4 antibody (dilution 1: 2000 in TBS) was added and the cells were incubated for 1 h by shaking and

washed three times (2ml TTBS buffer for 10 min). Subsequently, the goat anti-mouse secondary antibody tagged with FITC (1:200 dilution in TBS) was added and cells were incubated for 1 h and washed as described. Coverslips containing the cells were mounted on a glass slide with the help of *Vectashield Mounting Medium* containing DAPI (Vector Labs, RU) which stains the nucleus. Images were collected using a fluorescence microscopy system, Nikon eclipse Ti equipped with a DS-QiMc camera.

3.2.3 Purification of native bovine rhodopsin and heterologously expressed recombinant Rho mutants

Purification of proteins used in this study was performed by immunoaffinity chromatography using sepharose coupled to the Rho-1D4 antibody according to the manufacturer instructions ((GE Healthcare) see **Annex E** for more details)**.** Once Rho-1D4 was bound to sepharose, the binding capacity was determined.

3.2.3.1 Capacity binding of 1D4-coupled Sepharose

This experiment was carried out to determine the efficiency of Rho binding by the sepharose-Rho-1D4 resin. All manipulations were performed in total darkness (or dim red light) and keeping the samples on ice at all times to avoid protein aggregation.

ROS membranes extracted from bovine retina using a sucrose gradient ((kindly provided by Dr. Sundaramoorthy Srinivasan), were solubilized in n-dodecyl-β-D-maltoside (DM) detergent. DM is a mild detergent. DM can dissolve membranes and as a result membrane proteins are transferred into detergent micelles, preserving membrane protein functionality.

Briefly, 50 µl of ROS were placed in an Eppendorf tube with 400 µL of PBS and 50 µl of 10% DM (w/v in MilliQ water). The mixture was stirred for 1 h at 4°C and subsequently centrifuged for 30 min at 7000 rpm and 4°C. Rho initial concentration was determined from the SN (solubilized ROS) by UV-vis spectroscopy and the Lambert-Beer law (initial protein). Then,100 µl of sepharose-Rho 1D4 were added into the SN and incubated for 3 h, at 4°C by gently nutating. Finally, the sample was spun down for 5 min at 2500 rpm and 4°C and the concentration of unbound Rho was determined by using the Lambert-Beer law in (unbound protein).

The binding capacity was measured by subtracting the initial protein to the unbound protein.

$$\text{Capacity binding } \mu g/\mu l = (\mu g \text{ initial protein} - \mu g \text{ unbound protein})/100\ \mu l(\text{Sepharose} - \text{Rho 1D4})$$

3.2.3.2 Rho purification

ROS membranes were solubilized as explained in the previous section and the sepharose-Rho-1D4 beads were added. After the centrifugation, the SN containing the unbound Rho was collected and stored at -20°C for future purifications. The sepharose-Rho1D4 beads were washed 4 times with 1 ml of elution buffer. The bound Rho was eluted in 100 µl of elution buffer containing 100 µM 9-mer peptide (H-TETSQVAPA-OH). After 2 h incubation at 4ºC, the beads were centrifuged and the SN was collected for further experiments. The amount of purified Rho was measured from the collected SN by UV-vis spectroscopy. The sepharose beads were kept at 4ºC for further use after their regeneration (see **Annex F** for details).

3.2.3.3 Regeneration and purification of recombinant proteins

COS-1 cells are not photoreceptor cells, so they do not have the chromophore to form rhodopsin and retinal needs to be exogenously added.

Preparation of retinal. Both 11CR and 9CR were obtained in solid form and dissolved in ethanol. Both retinal molecules are light-sensitive changing the conformation to all-trans-retinal when illuminated, therefore they should be kept with aluminum foil and work under dim red light or in complete darkness.

Retinal was prepared by taking a small amount of retinal and dissolving it in 200 µl of spectroscopic grade absolute ethanol and subsequently stored at -80ºC. A 1:2000 dilution was prepared and the concentration was determined by UV-vis spectroscopy. The values of molar extinction coefficient (ε) and λ are shown on Table 3.4 (Garwin & Saari, 2000).

Table 3.4 *λ of maximum (λmax)* absorbance and ε of 9CR and 11CR.

Retinal	**λ_{max} (nm)**	**ε ($M^{-1}cm^{-1}$)**
9-cis retinal	373	36068
11-cis-retinal	376.5	24935

Regeneration of the transfected opsin. After 48 h of transfection (see section **3.2.2.4** for transfection details), cells were mechanically harvested using a scraper and centrifuged at 4000 rpm for 20 min at 4°C. SN containing the medium was discarded and the cells were washed by resuspending the pellet with PBS (1 mL per plate) and centrifuged under the same conditions. The washing step was performed in duplicate. Once washed, the cells were resuspended in PBS (1ml per plate) and either 10 µM of 11CR or 20 µM of the 9CR analog were added. Cells were incubated ON at 4ºC in an orbital shaker.

Purification of recombinant proteins. Regenerated cells were subsequently solubilized adding 1 ml 10% DM, 10 µl of 100 mM PMSF (prepared in methanol) and 10 µl protease inhibitors (Sigma). The mixture was stirred 1 h at 4°C and subsequently ultracentrifuged 35 min at 35000 rpm and 4°C in a Ti50 rotor. The SN was transferred into a falcon tube containing 100 µl of sepharose-Rho-1D4 and incubated 3 h, at 4°C in a orbital shaker. After 2 or 3 hours, the sepharose-1D4 beads were washed in the same way than in section **3.2.3.2.**

3.2.4 Gel electrophoresis of proteins

3.2.4.1 SDS-PAGE

Sodium dodecyl sulfate polyacrylamide gel electrophoresis (SDS-PAGE) is a type of electrophoresis in which samples are denatured by the presence of reducing agents such as DTT or beta-mercaptoethanol, to break the disulfide bridges, and the water chaotropic agent SDS. This detergent denatures and coats the protein with negative charge allowing the separation of proteins depending only on their length and mass-to-charge ratio. Most of these gels are made of polyacrylamide, as a result of the chemical polymerization of a mixture of acrylamide and bisacrylamide.

For electrophoresis, a Bio-Rad Mini-PROTEAN 2 gel running apparatus was used. A vertical gel was prepared consisting on a separating gel with a degree of crosslinking of 12%, and a stacking gel with low degree of crosslinking (5%) according to details shown in Table 3.5.

Casting frames (clamping two glass plates in the casting frames) were set on the casting stands. The separating gel was prepared in a separate small beaker mixing the solution gently. The appropriate amount of separating gel solution was pipetted into the gap between the glass plates. Isopropanol was added to avoid oxidation of the mixture, facilitating correct solidification and flattening of the gel surface.

After a few minutes, the isopropanol was discarded and the stacking gel prepared and pipetted into the glass plates until overflow. Immediately after, a well-forming comb was inserted. After gel solidification, the glass plates were taken out of the casting frame and set in an electrode assembly. The electrophoresis running buffer was poured into the inner chamber and kept pouring after overflow until the buffer surface reaches the required level in the outer chamber, and the comb was removed carefully to allow sample loading.

To prepare the samples, concentrations of the solubilized or purified proteins were normalized to equal amount of protein and mixed with protein loading buffer 4X (**Annex G** for composition). The prepared samples and 6 µl of the protein molecular weight marker were loaded into the corresponding wells and the gel was run at 100V for 2 h. The gel was stained ON using Generon

quick Coomassie stain. The stained gels were distained with water until the protein bands could be visualized. .

Table 3.5 Reagents concentration for SDS-PAGE.

Separating gel

Reagents	***Stock***	***Concentration in the gel***	***Volume ml***
Distilled water	- - -	- - -	1.25
Tris-HCL	1.5M pH 8.8	0.75 M	5
Acrylamide/Bisacrylamide	37.5%/0.8%	12%/0.5%	3.2
SDS	10%	0.1%	0.1
APS	10%	0.1	0.1
TEMED	100%	0.05%	0.05

Stacking gel

Reagents	***Stock***	***Concentration in the gel***	***Volume ml***
Distilled water	- - -	- - -	2.9
Tris-HCL	0.5M pH 6.8	0.75 M	1.25
Acrylamide/Bisacrylamide	37.5%/0.8%	5%/0.13%	0.67
SDS	10%	0.1%	0.05
APS	10%	0.1%	0.05
TEMED	100%	0.1%	0.05

3.2.4.2 Western blot

Western blot is a technique that allows specific detection of proteins previously separated by an electrophoretic gel through the use of specific antibodies. Proteins are detected by a primary

antibody which is recognized by a horseradish peroxidase (HRP) conjugated secondary antibody. This HRP will react to a specific substrate and generate a detectable product.

After separating the proteins using SDS-PAGE, the proteins from the gel were transferred onto a nitrocellulose membrane using the *Trans-Blot* SD Semi-Dry Transfer Cell (Bio-Rad). Before the transference, the nitrocellulose membrane, filter paper and gel were placed in transfer buffer (see composition in **Annex G**) separately for 10 min. The transfer sandwich was formed as follows: filter paper, membrane, gel and filter paper (avoiding the formation of bubbles between the gel and the membrane) and placed in the transfer apparatus. The transference was carried out for 30 min at 15 V. Then, the membrane was blocked with 5% skim milk in TBS (see **Annex G** for composition) stirring ON. Next day, the membrane was washed 3 times for 10 min with TTBS (see **Annex G** for composition). Later, the membrane was incubated for 1 h with the primary antibody Rho-1D4 (1:10000 in TBS buffer) and washed 3 times for 10 min with TTBS buffer. Subsequently, the blot was incubated with goat anti-mouse secondary IgG antibody (1:5000 in TBS buffer) for 1 h and after this time it was washed 3 times for 10 min in TTBS buffer. The blots were developed using substrate SuperSignal Wester Pico Chemiluminescent Substrate (Luminol/H_2O_2 1:1) (Thermo fisher scientific, France) by exposure to X-ray paper.

3.2.5 Ultraviolet-visible (UV-vis) spectroscopy

UV-vis spectroscopy plays an important role in analytical chemistry and has widespread application in chemistry, physics and life sciences. This technique covers only a small part of the electromagnetic spectrum, which includes such other forms of radiation as radio, infrared (IR), cosmic, and X rays. UV and visible absorption spectroscopy measures the attenuation of a beam of light after it passes through a sample or after reflection from a sample surface at a single λ or over an extended spectral range. When a sample is exposed to light energy that matches the energy difference between a possible electronic transition within the molecule, a fraction of the light energy would be absorbed by the molecule and the electrons would be promoted to the higher energy state orbital. A spectrometer records the degree of absorption by a sample at different λ and the resulting plot of absorbance (Abs) versus wavelength (λ) is known as a spectrum.

This technique is commonly used to determine the concentration of an absorbing molecule in solution using Lambert-Beer law:

$$A = \varepsilon \, \mathrm{x} \, c \, \mathrm{x} \, l$$

where

A= absorbance

ε= the molar absorptivity with units of L mol^{-1} cm^{-1}

l = the path length of the sample- that is, the path length of the cuvette in which the sample is contained in cm.

c= concentration of the chromophore in solution expressed in mol L^{-1}

3.2.5.1 Measurement conditions

For spectroscopic characterization of Rho mutants, a Varian Cary 100 bio spectrophotometer (Varian, Australia) was used. Temperature was controlled by a peltier accessory equipped with a water-jacketed cuvette holder connected to a circulating water bath. All the spectra were recorded in the 250 nm-650 nm range with a bandwidth of 2nm, a response time of 0.5s and a scan speed of 400nm/min. The cuvettes used for these experiments are made of quartz with black wall and teflon cap to prevent evaporation of the sample.

Given the photosensitivity of Rho, all spectroscopic experiments were carried out under dim red light using a red filter (Kodak safelight No.2). Rho absorbs light at 500 nm and the concentration of the sample can be determined by sing the absorbance value at this λ and ε= 40600 $M^{-1}cm^{-1}$.

The assay is non-destructive as the protein in most cases is not consumed and can be recovered. Secondary, tertiary and quaternary structures all affect absorbance; therefore, factors such as pH, ionic strength among others, can alter the absorbance spectrum.

3.2.5.2 Photobleaching and acidification

Samples were illuminated with a 150-watt Dolan-Jenner MI-150 power source equipped with an optic fiber guide and using a 495nm cut-off filter for 90 s to ensure complete photoconversion to 380nm absorbing species. Acidification was carried out, immediately after photobleaching, by the addition of 2N H_2S0_4 which yields a pH ~2.0 and the absorption spectrum was subsequently recorded. The reprotonated Schiff base caused by acidification shifts the $A_{\lambda max}$ to 440nm.

3.2.5.3 Thermal stability

Thermal stability of Rho was studied by monitoring the decrease of A_{max} of the visible spectral band as a function of time at 48°C. Spectra were recorded every 5 min and half-life times were determined by fitting the experimental data to single exponential curves.

3.2.5.4 Chemical stability

A solution of 1M hydroxylamine hydrochloride (adjusted to pH 7) was added to dark-adapted samples in a spectroscopic cuvette (final concentration of 50mM), and successive spectra were

recorded every 5min to monitor the decrease of $A_{\lambda max}$ and formation of retinaloxime. The reactions were carried out in the dark at 20°C. The initial velocity was obtained by a linear regression fitting the first data points.

3.2.5.5 Regeneration experiments

For the regeneration experiments, 2.5-fold molar excess of 11CR (stock solution in ethanol) was added over dark adapted samples in the spectroscopic cuvette and thoroughly mixed. Immediately after, the sample was illuminated with a yellow cut-off filter (>495 nm) to avoid photobleaching of the free retinal, and successive spectra were registered every 5min at 20°C in the dark until no further increase in $A_{\lambda max}$ was observed.

3.2.6 Fluorescence spectroscopy

Fluorescence spectroscopy is one of the most powerful methods to study protein folding, dynamics, assembly, an interaction, as well as membrane structure. This is because almost all proteins have natural fluorophores such as tyrosine and tryptophan residues, which allow the study of changes in protein conformation (Munishkina & Fink, 2007).

3.2.6.1 Measurements conditions

Fluorescence characterization was performed on a QuantaMaster 4 spectrofluorimeter (Proton Technology International) equipped with a cuvette holder peltier accessory TLC 50, for temperature control. Emission spectra of proteins and phenolic compound were recorded in the 320nm-600 nm range when exciting at λ=280 nm and 295 nm, and in the 350 nm-600 nm range when exciting at λ=320 nm and 337 nm. Low excitation light intensities were used, by setting the excitation slits at 0.5 nm, to prevent Rho photobleaching

3.2.6.2 Meta II decay measurements

Initially, the Trp fluorescence of a dark-adapted sample was recorded at 20°C until a steady base line was obtained. After that, the sample was illuminated for 30s with a 150-watt Dolan-Jenner MI-150 power source using a cut-off filter (>495 nm) and the fluorescence intensity was monitored until it reached a plateau. All fluorescence spectra were carried out by exciting the samples for 2s at 295 nm, using a slit bandwidth of 0.5 nm, and blocking the excitation beam for 28 s with a beam shutter to avoid photobleaching of the sample. Trp emission was monitored at 330 nm with a slit bandwidth of 10 nm.

3.2.7 Transducin (Gt) activation

In order to study the ability of Rho to bind and activate Gt, the uptake of [S^{35}] $GTP_{\gamma}S$ by Gt was followed with time. To this aim, Gt was first isolated from bovine retina (Fukada et al., 1994).

3.2.7.1 Isolation of Gt from bovine retina

Briefly, 100 dark adapted frozen bovine retinas unwrapped from the original package, were thawed ON at 4ºC. Next day, retina were transferred into a glass beaker and left on ice for 1h under direct light exposure. After this time, they were mixed with 150 ml of 47% sucrose (containing 2 mM DTT and 0.1 mM PMSF added immediately before use) and the retinas were broken by pressure using a 60 ml syringe (without needle) until the sample was homogenous (a homogenizer grinder was also employed to disaggregate some difficult retinas). The homogenized sample was centrifuged at 42000 g, 4°C for 20 min. The SN and the orange pellet attached to the walls were carefully taken and transferred into another glass beaker and diluted 1:1 with buffer A (composition described in annex G). The residual pellet obtained at the bottom of the tube was discarded. The diluted sample was passed three times by syringe (using a 23G needle) and centrifuged at 30000 g for 20 min at 4°C. SN was discarded and the pellet was resuspended with buffer A up to 50 ml and passed 3 times by syringe and a 23G needle. The sample was divided and layered on top of polyethylene tubes containing a sucrose density gradient (from bottom to top: 1.2 mM / 1mM / 0.78 mM all them prepared in buffer A) and centrifuged at 42000 g for 30 min at 4°C, without break.

The orange layer was taken out carefully and diluted (1:2) with buffer A to remove the sucrose and passed three times through a syringe using a 23G needle and centrifuged at 42000 g for 20 min at 4°C. The SN was discarded and the pellet was resuspended with buffer C (100 ml) (composition described in **Annex G**) and passed again 3 times through syringe with 23G needle and centrifuged at 42000 g for 20 min at 4°C. The pellet was resuspended with 100 ml of buffer D (composition described in **Annex G**) and passed again 3 times through syringe and centrifuged at 42000 g for 20 min at 4°C (this process was done twice). Finally, the pellet was resuspended in 50 ml of buffer D containing 100 µM of GTP and after 30 min incubation at 4°C, the sample was spun down at 163000 g for 45 min at 4°C. The SN was collected into a 50 ml falcon tube and filtrated using a syringe and 0.22 µm syringe driven filter to remove traces of membrane. Later, Gt sample was concentrated with amicon tubes of 10 kDa cut-off down to 8 ml**.** The concentrate was placed into a dialysis membrane and dialyzed using 250 ml buffer E (composition described in **Annex G**) (to remove the excess of GTP, to concentrate the SN by osmotic pressure and to exchange the buffer to 50% glycerol). Buffer E (composition described in **Annex G**) was replaced twice at intervals of 8 h. The harvested Gt was stored at 4°C. The concentration and quality of the purified Gt were analyzed using SDS-PAGE with bovine serum albumin (BSA) as standard.

3.2.7.2 Gt activation assay

Gt activation was monitored with a radionucleotide filter binding assay by measuring the uptake of GTPγ^{35}S by Gt upon binding to photoactivated Rho. For this purpose, a mixture (140 µl) containing the reagents and concentrations shown in Table 3.6 was prepared.

Table 3.6 Mixture of reagents used for the Gt activation assay.

Compound	Concentration
Sample (Rho, WT or mutant)	10 nM
Gt buffer(composition in annex I)	1 X
DTT	2.5 mM
DM	0.0012%
Gt	500 nM
[S^{35}]GTPγS	5 µM

The assay was initiated by the addition of Rho in dark state. After different incubation times (every 4 minutes), either in the dark (at 0, 4 and 8 min) or after illumination for 90s (at 12, 16, 20, 24 and 28 min),15 µl of the mixture were placed onto a well of a 96-well cellulose membrane plate, and filtrated. The plate was fixed to a manifold filtering system unit. Immediately after, the membrane was washed ten times with 300 µl of Gt buffer and let it dry at room temperature. Finally, the filter was cut and placed in a vial containing 4mL of scintillation liquid, vortexed and bound GTPγ^{35}S was measured by means of a Tri Carb 2100TR liquid scintillation counter. The activity measured as cpm was converted to pmol using the next formula:

$$Bound\ GTP\gamma S^{35}\ (pmol) = \frac{dpm}{2.22\ x10^{12}\ x\ radioactivity\ of\ ligand}$$

where,
dmp= cpm / counter efficiency (55%)
Radioactivity of the ligand = 1250 Ci/mMol
1Ci= 2.22 *x* 10^{12} dpm

3.2.8 Antioxidant capacity of polyphenol compounds

3.2.8.1 Trolox equivalent antioxidant capacity (TEAC) assay

ABTS radical cation ($ABTS^{\bullet+}$) solution (7 mM) was produced by reacting ABTS with 2.45 mM potassium persulphate and allowing the mixture to stand in the dark at room temperature for 12-16 h before use. $ABTS^{\bullet+}$ radical was diluted with PBS buffer to give an Abs of about 0.700 ± 0.020 at 734 nm. For antioxidant capacity measurements, 10 µL of sample was mixed with 990 µL of the radical solution and Abs was monitored at 734 nm for 6 min. The decrease in absorption at this λ at min 6, was used to calculate the TEAC value(van den Berg et al., 1999). All experiments were in triplicate. A calibration curve was prepared with different concentrations of Trolox diluted in ethanol. By measuring ΔAbs over 6 min for Trolox and the sample, Abs values were corrected for the solvent as follows:

$$\Delta Abs_{Trolox\ or\ sample} = (Abs_{t=0\ Trolox\ or\ sample} - Abs_{t=6\ min\ Trolox\ or\ sample}) - \Delta\ Abs_{solvent\ (0\text{-}6min)}.$$

Where
Abs = Absorbance at 734 nm.

Results were expressed in terms of µM Trolox equivalent

3.2.9 Rho expression studies in COS-1 cells with quantitative real-time RT-PCR (qRT-PCR)

qRT-PCR is an excellent tool for basic research, molecular medicine and biotechnology. It has become the method of choice widely used to quantify gene expression changes. The amount of an expressed gene can be measured by the number of copies of a RNA transcript of that gene present in a sample. In order to robustly detect and quantify gene expression from small amounts of RNA, amplification of the gene transcript is necessary. In real-time PCR, the fluorescence is measured during each cycle, which greatly increases the dynamic range of the reaction, since the amount of florescence is proportional to the amount of PCR product. Prior to PCR, RNA first needs to be transcribed into cDNA using a reverse transcriptase.

qRT-PCR assays are easy to perform, capable of high throughput, and can combine high sensitivity with reliable specificity. The whole process includes three stages: RNA purification, reverse transcription and PCR.

3.2.9.1 Purification of total RNA

The RNA isolation was done using the RNeasy Mini Kit Qiagen, following the manufacturing directions. Briefly, 24 h after transfection, a maximum of $3x10^6$ COS-1 cells were harvested (using

trypsin and PBS). 350 µl of Buffer RLT (supplied in the kit) containing β-mercaptoethanol (10 µl per 1 ml of RLT) were added to harvested cells, and homogenized in vortex for 1 min. Immediately after, 350 µl of 70% ethanol were added and mixed well pipetting. The mixture (up to 700 µl, including any precipitate) was placed into an RNeasy Mini spin column placed in a 2ml collection tube, the lid was closed and the sample was centrifuged for 15s at 10000 rpm (re- use the collector tube). 350 µl of buffer RW1 were placed into the RNeasy column and centrifuged for 15 s at 10 000 rmp (the flow-through was discarded). DNase I incubation mix (10 µl DNase I, prepared following the manufacturing directions, + 70 µl RDD were mixed by gently inverting the tube) was added directly to RNeasy column membrane, and placed on a benchtop (20°C-30°C) for 15 min. After the incubation, 350 µl Buffer RW1 were added to the RNeasy column and centrifuged for 15 s at 10000 rpm (the flow-through was discarded). 500 µl of RPE buffer (prepared according to the manufacturer's instructions) were added to the column and centrifuged for 2 min at 10000 rpm, and also centrifuged at full speed for 1 min to dry the membrane. The RNeasy spin column was placed in a new 1.5 ml collection tube and 30 µl-50µl of RNase-free water were added directly to the spin column membrane and centrifuged for 1 min at 10000rpm to elute the RNA.

3.2.9.2 Quantification of RNA and its quality

The concentration of RNA was determined by measuring the absorbance at 260 nm in a spectrophotometer. To ensure significance, A_{260} readings were greater than 0.15. An absorbance of one unit at 260 nm corresponds to 40 µg of RNA per ml. This relationship is valid only for measurements at neutral pH. The ratio of the readings at 260 nm and 280 nm (A_{260}/A_{280}) provides an estimate of the purity of the RNA with respect to contaminants that absorb in the UV spectrum, such as proteins. Pure RNA has an A_{260}/A_{280} ratio of 1.9-2.1.

In order to determine the RNA concentration, the A260nm of a diluted sample (1/100 in RNase-free water) was measured by UV-vis spectroscopy and used in the next formula:

$$Concentration\ of\ RNA\ sample = 40\mu\frac{g}{ml}\ x\ A_{260}\ x\ dilution\ factor$$

3.2.9.3 RNA Integrity

The assessment of RNA integrity is a critical first step in obtaining meaningful gene expression data. Working with low-quality RNA may strongly compromise the experimental results. Using intact RNA is a key element for the successful application of qRT-PCR (Fleige & Pfaffl, 2006). The integrity and size distribution of total purified RNA should be checked by denaturing agarose gel electrophoresis. The respective ribosomal RNAs should appear as sharp bands. The apparent

ratio of 28S rRNA to 18S RNA should be approximately 2:1. If the ribosomal band or peaks of a specific sample are not sharp, but appear as a smear towards smaller size RNAs, it is likely that the sample suffered major degradation either before or during RNA purification.

A formaldehyde agarose gel was prepared with 1.5 g of agarose, 10 ml of 10X formaldehyde gel buffer (Table 3.7) and 90 ml of RNase-free water.

Table 3.7 Composition of 10X formaldehyde gel buffer

Compound	Final Concentration
MOPS	200 mM
Sodium acetate	50 mM
EDTA	10 mM
pH to 7.0 with NaOH	

The RNA sample was prepared adding 1 volume of 5X RNA loading buffer (see composition in Table 3.8) to 4 volumes of RNA sample and mix. Then the mixture was incubated for 5 min at 65°C, chilled on ice, and loaded onto the gel.

Table 3.8 RNA loading buffer composition

Compound	Volume/reaction
Saturated aqueous bromophenol blue solution	10 µl
EDTA 500 mM, pH 8.0	80 µl
Formaldehyde 37% (12.3M)	720 µl
Glycerol 100%	2 ml
Formamide	3.084 ml
10X formaldehyde buffer	4 mL
RNase-free water fill up to 10 ml	

3.2.9.4 Reverse transcription, synthesis of cDNA

The synthesis of cDNA was carried out using the QIAGEN Kit QuantiNova Reverse Transcription, for cDNA synthesis with integrated removal of genomic DNA.

A genomic DNA removal reaction was prepared on ice according to Table 3.9.

Table 3.9 Genomic DNA removal reaction components

Component	Volume/reaction
G DNA removal mix	2 µl
Template RNA, 5 µg	variable
Internal control RNA	1 µl
RNase-Free water	variable
Total reaction volume	15 µl

The mixture was incubated for 2 min at 45°C. Then place immediately on ice. After that, freshly prepared reverse-transcription master mix (table 3.10) was added, incubated for 3 min at 25°C, then 10 min at 45°C and finally 5 min at 85°C.

Table 3.10 Reverse-transcription reaction components

Component	Volume/reaction
Reverse transcription enzyme	1 µl
Reverse transcription MIx	4 µl
Template RNA (entire genomic DNA elimination reaction)	15 µl
Total reaction volume	20 µl

The reaction was placed on ice and it was carried out directly with real-time PCR.

3.2.9.5 Real-Time PCR

QuantiNova SYBR Green PCR Kit was used to carry out the real-time PCR following the protocol and recommendations described by the manufacturer. The primers used in this assay also were designed accordingly to the manufacturer recommendations.

A reaction mix was prepared according to Table 3.11. The cDNA template from the reverse transcription was diluted 1:10 and 1 µl was added to the reaction mix.

Table 3.11 qRT-PCR reaction mix.

Compound	Volume/reaction
2x SYBR Green PCR master mix	10 µl
Primer A (10 µM)	1.4 µl
Primer B (10 µM)	1.4 µl
RNase-free water	6.2 µl
cDNA template	1 µl

The mixture was placed in a LightCycler capillary and the real-time cycler was programed according to table 3.12.

Table 3.12 Cycling conditions

Step	Time	Temperature	Ramp rate
PCR Initial heat activation	2 min	95°C	Maximal
2-step cycling			
Denaturation	15 s	95°C	Maximal
Combined annealing/extension	45 s	60°C	Maximal
Number of cycles	45		
Melting curve analysis			

After real-time cycler, the specificity of PCR products was checked by agarose gel electrophoresis.

3.2.10 Quercetin (Q) identification by HPLC-ESI-MS/MS

For Q extraction, 200 µl of 80% ethanol acidified with 0.1% formic acid was added to the sample. The mixture was vortexed for 1min and then sonicated for 5 min on ice. After centrifugation at 4000rpm for 20 min at 4°C, the SN was collected and evaporated to dryness under a steam of nitrogen gas. The sample was redissolved in 200 µl of (0.1% formic acid). After filtration with 4mm 0.45 µm PTFE syringe filters, 20 µl of the resulting filtrate was injected into the HPLC-MS/MS.

For the HPLC-ESI-MS/MS analysis, an Agilent Technologies 1100 HPLC equipped with autosampler and column oven (30°C) and coupled to an API 4000 triple-quadrupole mass spectrometer with a TurboIon spray source used in negative mode was used to identify Q. Chromatographic separation was achieved on a Luna C18 (50 x 2.0 mm, 5 µm) from Phenomenex column and a precolumn C18 (4x3 mm i.d.). The mobile phase was water (A) and acetonitrile (B) with 0.1% formic acid in both solvents. An increasing linear gradient (v/v) of B was used as follows: at time =0, 5% of B, from 5% to 18% B in 10 min, from 18% to 100% B in 13 min, 100% B for 1 min and from 100% to 5% of B in 15 min, followed by a 5 min re-equilibration step at a constant flow rate of 0.4 ml min^{-1}. The TurboIon spray source settings were as follows: capillary voltage, -4000V; nebulizer gas (N2), 10 (arbitrary units), curtain gas (N2), 12 (arbitrary units) drying gas (N2) heated to 400°C and introduced at a flow rate of 8000 cm^3 min^{-1}. Full-scan data were acquired by scanning from m/z 100 to 800 in profile mode using a cycle time of 1s.

3.2.11 Computer-aided modeling *in silico.*

This work was carried out at the Laboratory of Molecular Engineering of UPC and was performed by Dra. Cecylia Severin Lupala and Prof. Juan Jesús Pérez.

These assays use computational methodologies based on established chemical and biophysical knowledge and their application in the drug discovery process. The process can be carried out by comparison of the structural features of a set of diverse ligans or by studying the structure of the ligand (drug)-receptor (target) complex with the aim to postulate ligand refinements (Kapetanovic, 2008; Terstappen & Reggiani, 2001)

3.2.11.1. Protein-ligand docking.

Molecular docking approaches are focused to computationally simulate the target-ligand recognition process. Using this technique our goal was to study the binding preferences of diverse polyphenols to opsin and the ligand bound Rho-11CR and Rho-9CR. For this purpose, the crystallographic structures 3CAP (opsin), 1GZM (Rho-11CR and 2PED (Rho-9CR) were obtained from the protein data bank. These structures were prepared (optimization of hydrogen bonds, protonation states, and other relevant parameters) using the protein preparation wizard tool of the Schrodinger software.

The structures of the polyphenols used in the present study were downloaded from the PubChem website and prepared (generating energy minimized 3D structures, sampling diverse ring conformation, stereoisomers, and other relevant factors) using LigPrep tool also from Schrodinger.

Prior to molecular docking studies, all three receptors were examined in order to identify energetically favorable sites for ligands to bind. For this purpose, we used the Schrodinger's site recognition software SiteMap, which locates binding sites which size, functionality, and extent of solvent exposure are suitable for occupancy by hydrophobic groups or by ligand hydrogen-bond donors, acceptors, or metal-binding functionalities. The sites are assessed for their inclination to ligand binding, and then accurately ranked in order to eliminate those not likely to be suitable for ligand occupancy.

4. RESULTS AND DISCUSSION

4.1 Effect of phenolic compounds on the Rho GPCR

4.1.1 Spectroscopic characterization of Q at different conditions of buffer, pH and concentration of DM.

As mentioned in the materials and methods section, the compound that was selected as the study model was Q, which is one of the most often studied dietary flavonoid compounds ubiquitously present in various vegetables as well as in tea and red wine (D'Andrea, 2015). The flavonoids are the large subclass of the polyphenol family. Epidemiological research has suggested that the consumption of foods and beverages rich in flavonoids correlates with lower risk of various diseases (Graf et al., 2005). Nowadays, this family of compounds is being investigated for its potential benefits against cancer, as well as in cardioprotection, neuroprotection, urinary tract health, and antiaging effects (Croft, 2016; Tsao, 2010).

The first task at hand was to select the solvent to prepare the Q stock solution taking into account that this compound is sparingly soluble in aqueous media. Methanol (MetOH) and dimethyl sulfoxide (DMSO) were used. A solution of Q in each solvent was prepared and was spectrophotometrically characterized (Figure 4.1). The compound solubility was better in DMSO. This was expected since DMSO has a higher dielectric constant compared to methanol, 47 and 33 respectively, which makes DMSO a better solvent for the compound.

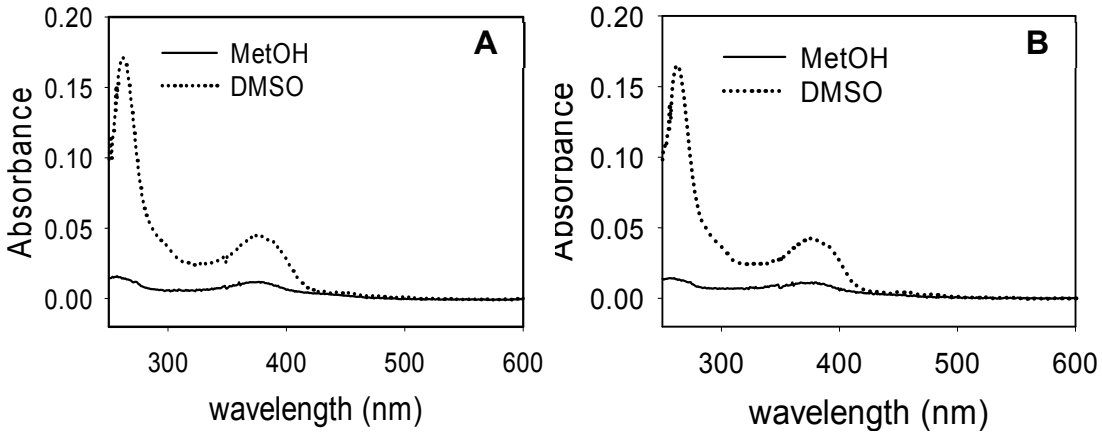

Figure 4.1 UV-vis spectra of 1 μM Q in dimethyl sulfoxide (DMSO) and methanol (MetOH).
A, Q dissolved in MetOH (solid line) and DMSO (dotted line) at 1 μM, the UV-vis spectrum was recorded immediately after its preparation. **B**, UV-vis spectra of Q dissolved in MetOH (solid line) and DMSO (dotted line) at 1 μM 90 min after its preparation.

Many flavonoids are structurally derived from the parent compound with a tricyclic (C6-C3-C6) skeleton (Tsuchiya, 2010) (Figure 4.2 A). The UV-vis spectrum of flavonoids is characterized by the presence of two main absorbance bands that are attributed to different parts of the conjugated

aromatic rings (Figure 4.2 A). The first band (Band I) located in the 300nm-380nm region, represents the absorption due to ring B, comprising the cinnamoyl system; and the second band (Band II) at 240nm-280nm corresponds to the absorption due to ring A, mainly representing the benzoyl system (Naseem et al., 2010). The number of hydroxyl groups modifies the absorption maximum of band I.

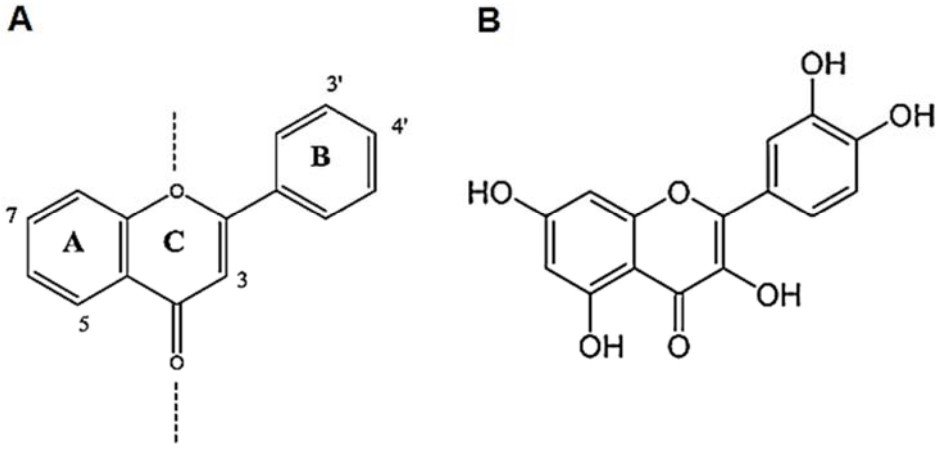

Figure 4.2 Chemical structure of flavonoids. **A**, General structure of flavonoids. **B**, Q structure.

The Q UV-vis spectrum shows the two characteristic absorbance peaks at 260nm and 375nm (Figure 4.1). Spectra were measured with time to discard any changes, but after 90 min no change was observed in the UV-vis spectrum of Q.

Given the existing knowledge of the flavonoid-dependence to environmental factors, such as solvent, pH, buffer and copigmentation to get the equilibrium, Q was characterized at pH values of 4, 6, 7.4 and 8 and different buffers in the presence of DM detergent micelles by Abs spectroscopy (Figure 4.3).

Figure 4.3 shows the Q absorption spectra in different buffers where some differences were observed. At pH 8 a red shift of 8 nm (from 375 to 383) was detected. In addition, a new band appeared at 316nm. In the case of pH 7, the appearance of a small shoulder at 316 nm could be detected.

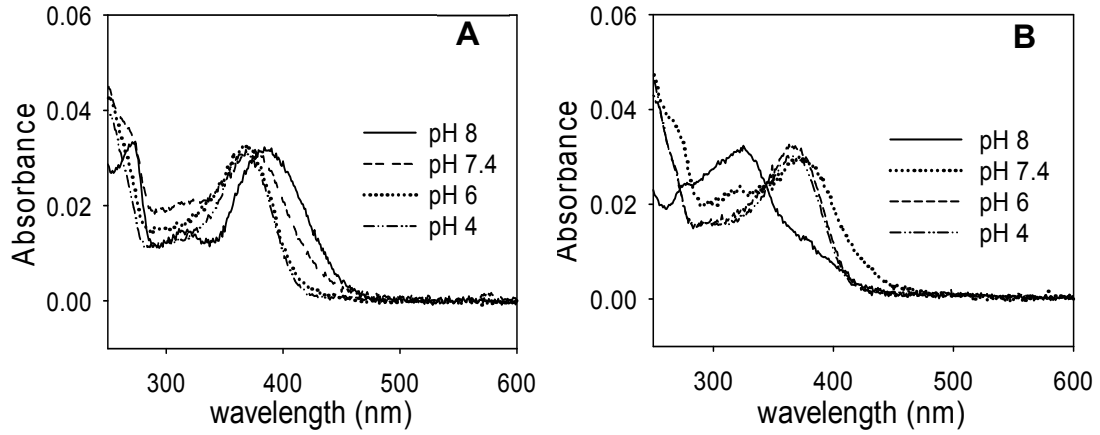

Figure 4.3 UV-vis spectra of 1µM Q at different pH and buffer.
From a stock solution of 20mM Q, dissolved in DMSO, a dilution to 100 µM was prepared in the same solvent. 1 µL of Q 100 µM was mixed with 99 µL of buffer at 50 mM and 0.05% DM detergent. UV-vis spectrua of 1 µM Q at pH 8 (Tris-HCl), pH 7.4 (HEPES-NaOH), pH 6 (SP) and pH 4 (sodium acetate-acetic acid). **A**, spectra recorded immediately after its preparation. **B**, spectra after 90 min of its preparation.

For buffers at pH 6 and pH 4, a shift of 8 nm was also noticed but in this case, on the contrary to the case of pH 8, it was a blue shift. According to previous work (Day et al., 2000), the conjugation of the hydroxyl group at position 3 of Q causes a Band I shift of around 12-17 nm, whereas a shorter shift (3-5nm) occurred when conjugation was at position 4', and no spectral modification was produced for substitutions at 7 and 3'. Spectra were measured with time until 90 min, and the biggest change was observed at pH 8. In view of the potential effect of time on the spectral behavior of the Q solution, spectra of Q, in the different buffer solutions, were recorded over time (Figure 4.4).

No important changes were observed at pH 7.4, 6 and 4 buffers, the only difference being that it took some time for the compound to equilibrate in the buffer solution. However, significant changes were observed in Q at pH 8 where Band I (383 nm) underwent a large decrease with time and the concomitant appearance of a new band at 330 nm could be observed.

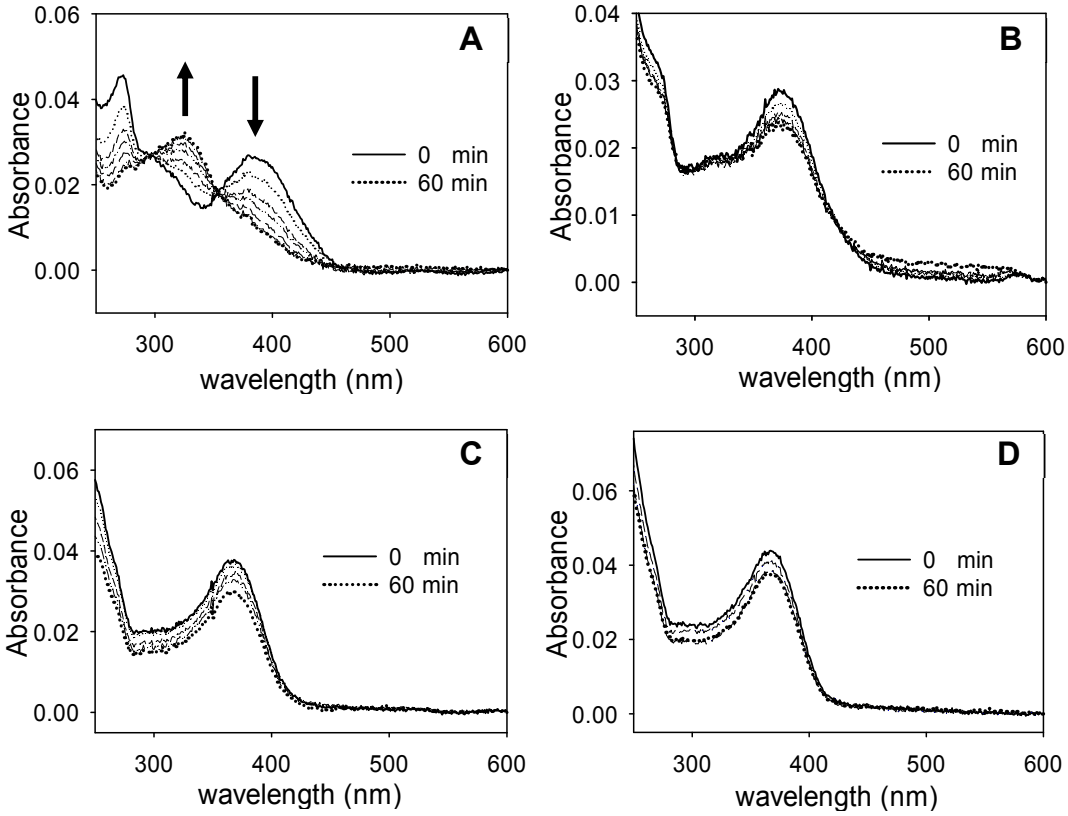

Figure 4.4 Stability of 1 µM Q over time at different pH and buffer.
Spectra show the time that it takes for 1 µM Q to equilibrate in the different buffers and pHs, and 0.05% DM. In all buffers, Q solution reached equilibrium after 1 h. **A**, pH 8 (Tris-HCl). **B**, pH 7.4 (HEPES-NaOH). **C**, pH 6 (SP). **D**, pH 4 (sodium acetate-acetic acid).

The behavior of Q has been widely studied in different media including organic, aqueous, hydro-alcoholic or physiological media (Jurasekova et al., 2014; Naseem et al., 2010; G. Xu et al., 2007; Zhou et al., 2007). One of the main chemical changes is that it can undergo a series of oxidation reactions in which the two -OH groups in ring B are readily oxidized (Volikakis & Efstathiou, 2000; G.-R. Xu & Kim, 2006) and the stabilities of the intermediate species resulting from this oxidation are substantially different depending on the environment. In this case, the simultaneous appearance of a new peak at 330 nm with increased absorbance would indicate that a quinone has been formed (Metodiewa et al., 1999; Zhou et al., 2007).

In addition to the experiments conducted at different pH, the behavior of Q by varying the detergent concentration was also evaluated (Figure 4.5). This effect was tested because the proteins are purified in this detergent and the concentration differs depending on the assay employed.

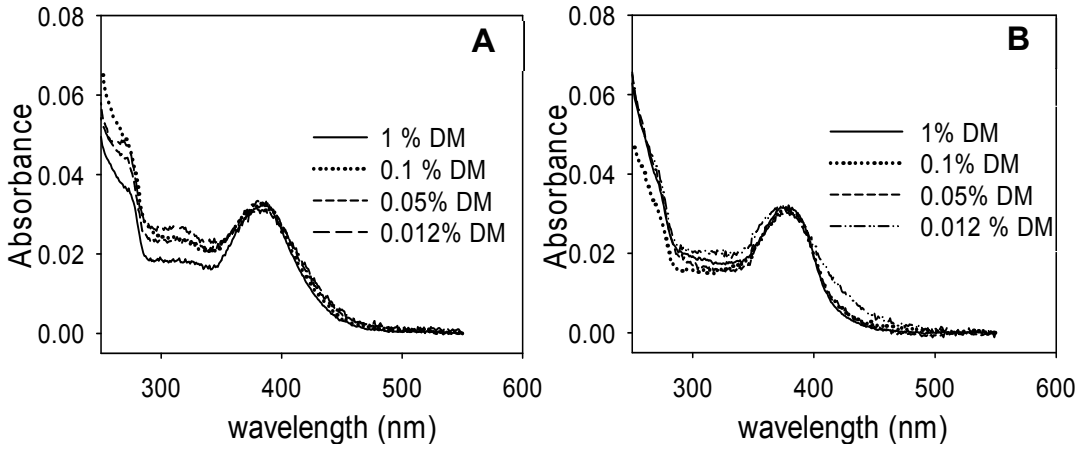

Figure 4.5 Effect of DM detergent on the stability of 1 µM Q.
UV-vis spectra of Q at 1%, 0.1%, 0.05% and 0.012 % in **A**, buffer Tris-HCl pH 8 and **B**, buffer HEPES-NaOH pH 7.4.

No differences in Q spectra at pH 6 and pH 4, by varying the DM detergent concentration, were observed. Similarly, no changes were observed at pH 7.4. Only pH 8 caused an increase in the 330 nm band. This behavior is consistent with previous studies indicating that the hydrogen donating ability of Q may be due to the fact that the 3'- and 4' hydroxyl, in presence of in SDS micelles, would be masked, and hence its activity reduced, and its B ring would be oriented towards the inside of the micellar surface (Liu & Guo, 2006).

In addition, other tests were carried out in order to have the complete characterization of Q under the same experimental conditions used for Rho work (Figure 4.6). Such experiments include the effect on Q of temperature, illumination, acidification, among others, so that when performing the experiments of Rho-Q interactions we can be sure that the changes observed are a consequence of such interaction and we can rule out spectral changes arising from the effects of the experimental conditions on Q Abs properties.

No major differences under the conditions evaluated were observed. Q was not affected by illumination. In the case of the thermal stability, at pH 7.4, a similar effect found for buffer at pH8 could be observed, that is the appearance of a new band at 330 nm. This behavior was not seen at pH 6, but in this sample, an increase in Band II was observed.

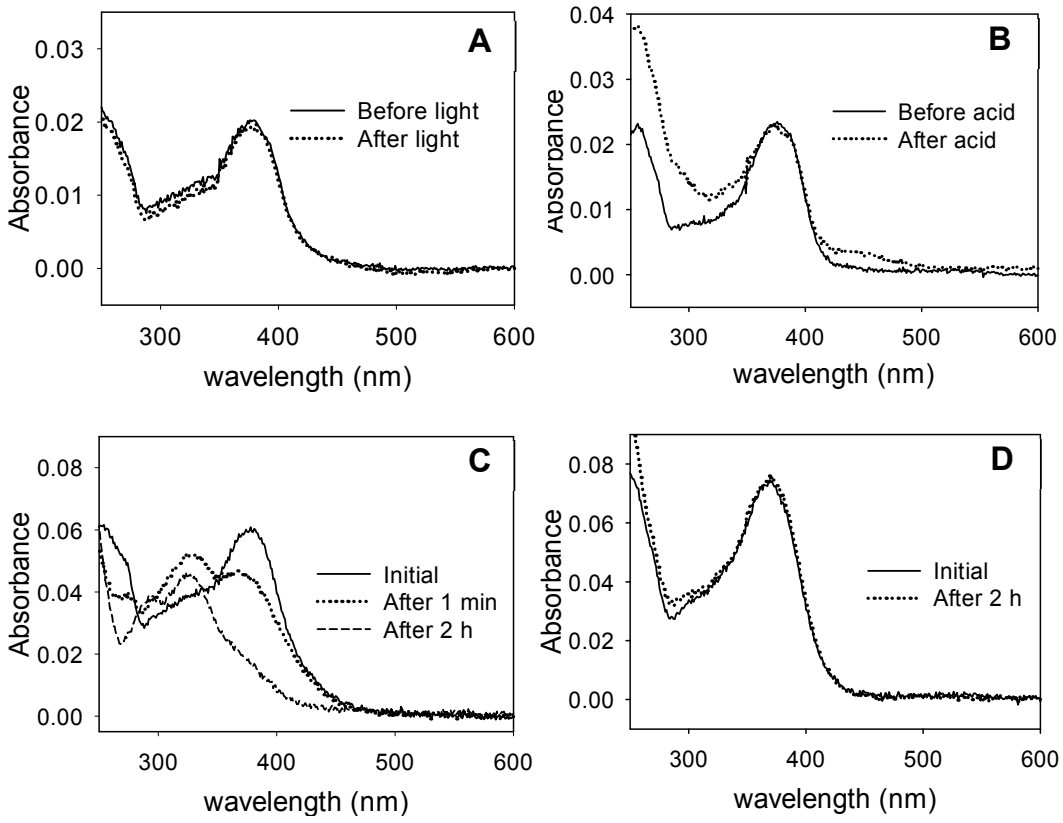

Figure 4.6 Characterization of Q at conditions of temperature, illumination and acidification.
A. Absorption spectra of 1 µM Q in HEPES pH 7.5 and 0.05% DM, before (solid line) and after (dotted line) illumination. Q was illuminated for 30 s and its UV-vis spectrum was immediately recorded at 20°C. **B**. Abs spectra of 1 µM Q in sodium phosphate (SP) pH 6 and 0.05% DM, before (solid line) and after (dotted line) the addition of 2 µL of H_2SO_4 2N. The spectra after acidification were recorded 20 min after acid addition. **C**. Thermal stability of 5 µM Q in HEPES pH 7.5 and 0.05% DM. The initial spectrum was taken at 20°C, the temperature was increased to 55 °C and successive spectra were recorded every 10 min until no spectral change was observed**. D**. Thermal stability of 5 µM Q in SP pH6 and 0.05% DM. The initial spectrum was taken at 20 °C, the temperature was increased to 55 °C and successive spectra were recorded every 10 min until no spectral change was observed.

4.1.2. Q effect on solubilized ROS Rho (SR)

4.1.2.1 Photobleaching and acidification of SR

After Q characterization, a series of experiments to evaluate the effect of Q on Rho were conducted. For the beginning of this part of the research, we decided to use SR rather than the purified protein in order to optimize the working methodology and to avoid wasting purified protein given the high cost (and time) involved in the protein purification process. Once the best conditions for the experimental protocols were established, we set out to work with immunopurified Rho.

For these experiments two different pHs 7.4 and 6 were chosen. In the case of pH 7.4, two buffers were used, HEPES and PBS. For pH 6 buffer the reagent used was SP. The first step was to

solubilize ROS Rho using the buffers mentioned above according to the methodology described under Materials and Methods.

The SR samples in DM in different buffers were analyzed at room temperature using a UV-vis spectrophotometer in which the absorbance spectra were recorded from 250nm to 650nm (Figure 4.7). The measured spectra showed two main bands, one at 280 nm characteristic of the opsin apoprotein and another one at 500nm caused by the interaction of the 11CR chromophore with the protein.

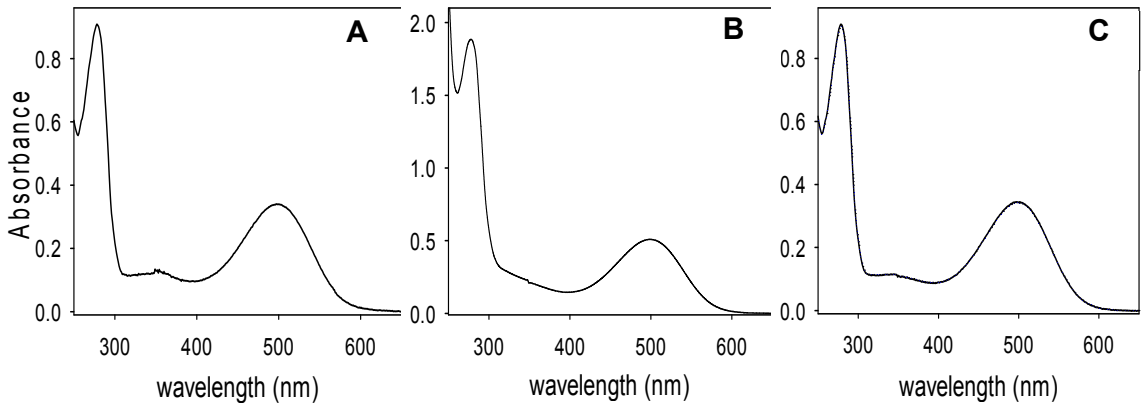

Figure 4.7 SR at different pH and buffer
A. PBS pH 7.4. **B** HEPES pH 7.4. **C**. SP pH 6. The three samples contain 1% of DM. Spectra recorded at 20 °C.

Rho concentration was determined from the absorbance at 500nm using the Lambert-Beer law. All experiments were performed using these prepared solutions and the final protein concentration used in each assay was 0.37 µM.

Figure 4.8 shows the characteristic dark state, photobleaching and acidification spectra of Rho. One of the important features of Rho, relevant to its function, is the formation of the active conformation (Meta II) upon illumination. Photoactivation of Rho can be monitored by following the blue-shift of the 500 nm chromophoric band in the visible region to 380 nm. This shift reflects SB nitrogen deprotonation in the Meta II conformation (Palczewski, 2006).

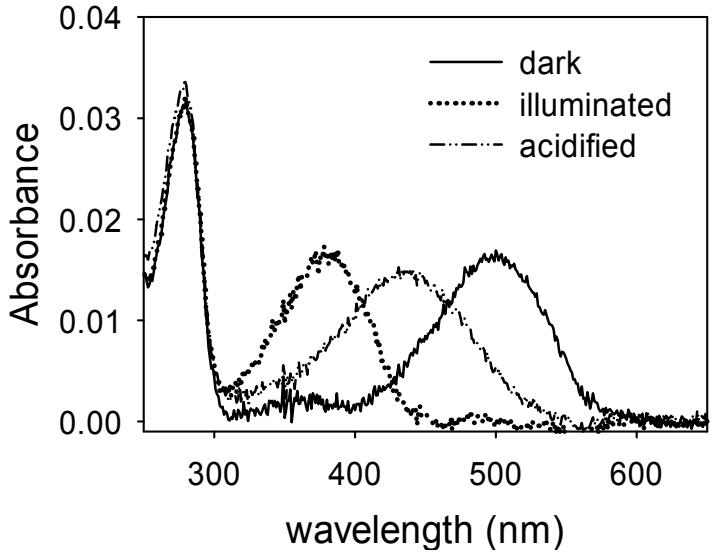

Figure 4.8 Dark state, photobleaching and acidification behavior of SR in HEPES pH 7.4.

Upon acidification, the spectral band at 380 nm shifts to 440 nm. The acid denaturation of the protein causes this shift, characteristic of a PSB linkage between 11CR and the opsin apoprotein. The SR in different buffers showed the same spectroscopic pattern shown in figure 4.8.

To ensure complete Rho photoconversion upon illumination, it is useful to calculate a difference spectrum between the dark and the illuminated states (Figure 4.9). With this spectrum we can verify that the absorbance corresponds to the same initial absorbance. In our case, for a concentration of 0.37 μM which is being used in the experiments corresponds to an A_{500nm} of 0.015.

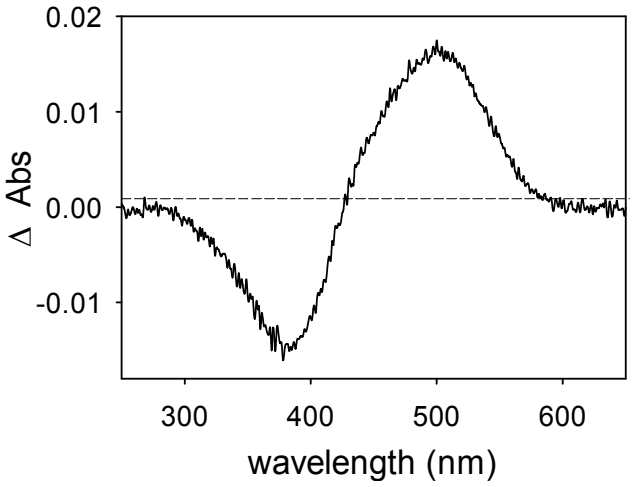

Figure 4.9 Difference spectra of dark minus light state of SR in HEPES pH 7.4.

4.1.2.2 Photobleaching and acidification of SR in the presence of Q

As the Q stock was dissolved in DMSO, control tests were also performed where the effect of this solvent on Rho spectra was assessed (Figure 4.10). The presence of DMSO did not affect the photobleaching pattern. By contrast, in the acidification experiment, an increase of about 15% in the band of 280 nm was observed. Conformational changes in proteins induced by high concentrations of DMSO have been reported (Batista et al., 2013; Jackson & Mantsch, 1991). DMSO concentrations below 10% have been recommended to avoid such effects, and in our case the DMSO concentration was below 1% in all experiments.

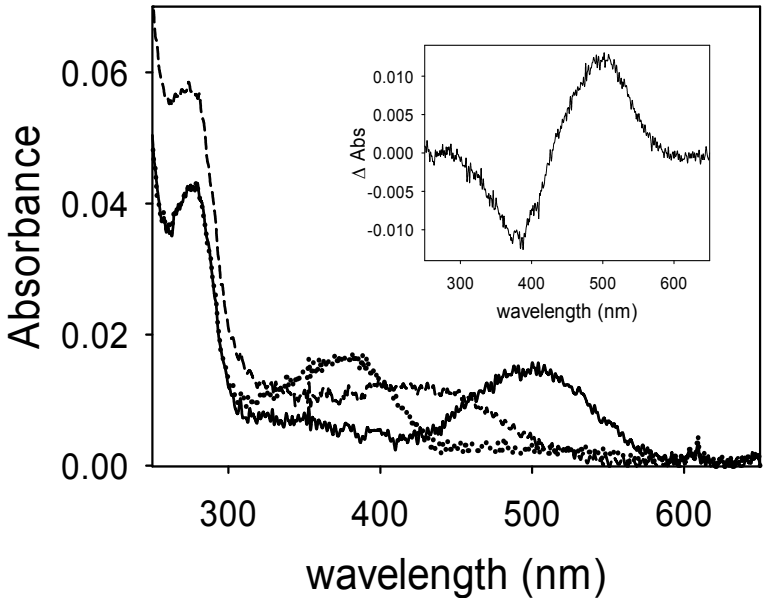

Figure 4.10 UV-vis spectrum of SR in DMSO.
Dark state (solid line), photobleaching (dotted line) and acidification (dashed line) behavior of SR, in HEPES buffer pH 7.4 in the presence of 1% of DMSO. The inset shows the dark minus light difference spectrum.

The SR sample, in PBS pH 7.4, showed differences upon illumination and acidification. It could be noted that when the Q spectrum reaches an equilibrium in the presence of SR, it shows an increase in the Abs at 330 nm with the consequent decrease at 375 nm suggesting quinone formation due to the oxidation of the hydroxyl groups of ring B (Figure 4.11). This behavior was not observed when Q stability alone, at pH 7.4, was evaluated. This would mean that the presence of SR could be accelerating its oxidation. An increase in Abs at 280 nm was also noticed, probably due to the effect of Q on ring B oxidation.

On the other side, SR does not apparently completely photobleach upon illumination, and there is about 50% absorbance remaining in the visible region at around 470 nm which could be

assigned to the photointermediate metarhodopsin III that has an A_{max} at 465 nm. A remarkable increase in the band of 280 nm is also observed which suggests the join effect of Q on ring A, and the additional effect of DMSO under the acidification experimental conditions.

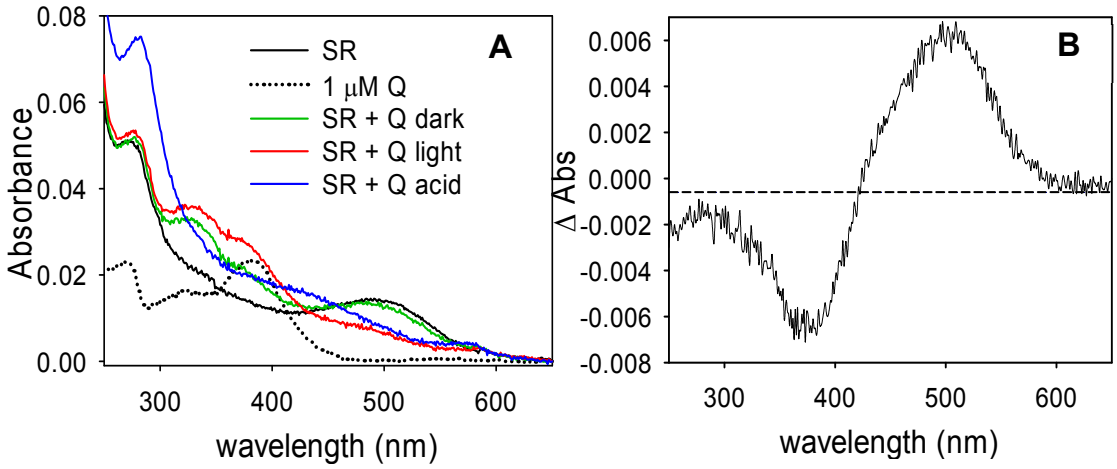

Figure 4.11 . Photobleaching and acidification behavior of SR in the presence of 1 μM Q.
A. UV-vis spectrua of SR in the presence of 1μM Q after photobleaching and acidification,in PBS pH 7.4 and 1% DM.. **B** Difference spectrum of the dark state of SR with 1 μM Q (SR+Q) minus the spectrum recorded after its illumination. Spectra were recorded at 20°C.

4.1.2.3 Thermal stability of SR in the dark

The thermal stability of the SR samples was determined by measuring the decrease in the Abs visible maximum at various intervals at 48°C. Rho can be photobleached in the dark by increasing the temperature that would force chromophore isomerization. Such thermally-induced retinal isomerization consists of two steps. First, thermal isomerization of 11CR in the binding site of Rho yields all-*trans*-retinal bound to opsin, followed by hydrolysis of the deprotonated SB yielding free all-*trans*-retinal and opsin (Liu et al., 2013).

The thermal decay was followed by the decrease in the 500 nm absorbing band and the concomitant increase in 380 nm band with time (Figure 4.12). The normalized Abs values at the absorption maximum were plotted against the incubation time. Curves were fit to an exponential decay equation and the half-life time ($t_{1/2}$) values were obtained.

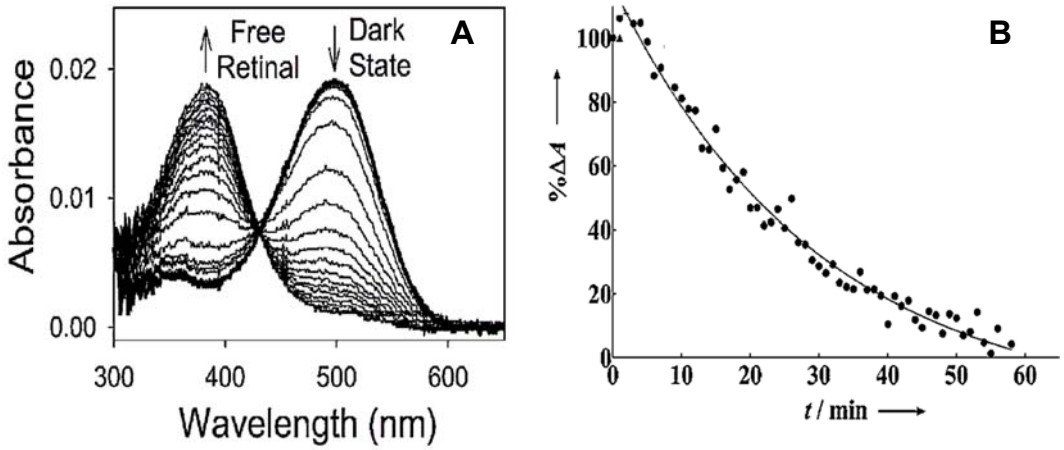

Figure 4.12 An example of loss of Rho absorbance by thermal decay.
A. Shows the loss of the 500nm absorbing species and increase in the 380nm absorbing species. **B.** Spectral data are curve fitted to obtain $t_{1/2}$.

Figure 4.13 shows the $t_{1/2}$ of the samples in the different buffer conditions. No significant differences in SR thermal stability, among the three buffer conditions in which ROS was solubilized, could be observed.

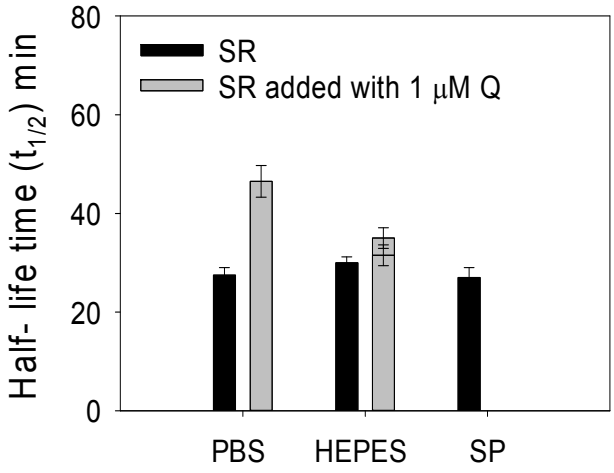

Figure 4.13 Thermal stability of SR in different buffer solutions.
The immunopurified Rho in the different buffers containing 0.05% DM, were incubated at 48°C. The normalized Abs values at λ_{max} were plotted as a function of incubation time and the $t_{1/2}$ was calculated.

In contrast, an increase in thermal stability was observed when Q was added to SR, especially in PBS pH 7.4 with an increase in stability of 65%. The fact that Q increases the thermal stability of SR is of great interest, especially in the case of some Rho mutants in which thermal stability is greatly diminished. However, this effect could not only be attributed to Q, since SR contain other

membrane proteins and lipids. Therefore, this effect should be confirmed on purified Rho samples.

4.1.2.4 Measurement of Meta II decay by fluorescence spectroscopy

In the dark state, Trp265 fluorescence is quenched by the β-ionone ring of the retinal and, upon illumination, retinal is released from the protein binding pocket thereby resulting in an increase in Trp265 fluorescence emission which can be followed at 330 nm using an excitation wavelength of 295 nm. The fluorescence changes were monitored continuously over time (Farrens & Khorana, 1995) (Figure 4.14). To determine the $t_{1/2}$ values for retinal release, experimental data was analyzed using a mono-exponential rise to maxima fit.

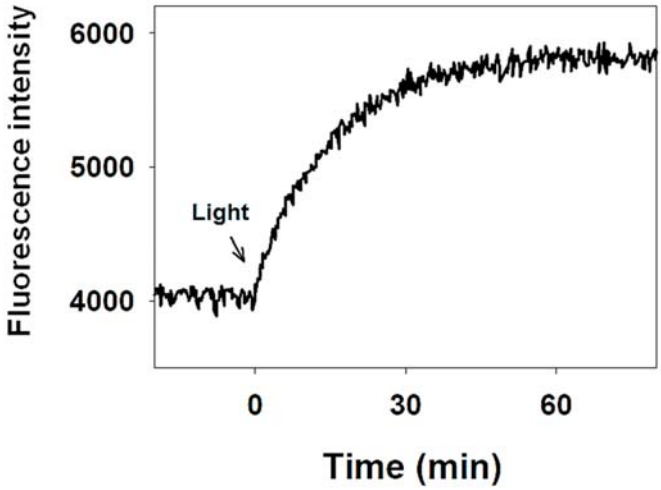

Figure 4.14 Typical fluorescence curve of retinal release during Meta II decay experiments.
The curve shows the kinetics profile for the fluorescence increase (330 nm) as the retinal leaves the binding pocket which parallels the Meta II decay process under our experimental conditions.

Slight differences were observed regarding to Meta II decay in the conditions evaluated in the different buffers (Figure 4.15). At pH 7.4, the Meta II hydrolysis appeared to be slightly faster in HEPES (8.5±0.7min) compared to PBS (9.5±0.9min). However, this difference was not statistically significant. In the case of the SP buffer pH 6, the velocity was found to be significantly slower compared to the other buffers. This pH-dependence of Meta II hydrolysis was already reported in other previous studies (Janz et al., 2003).

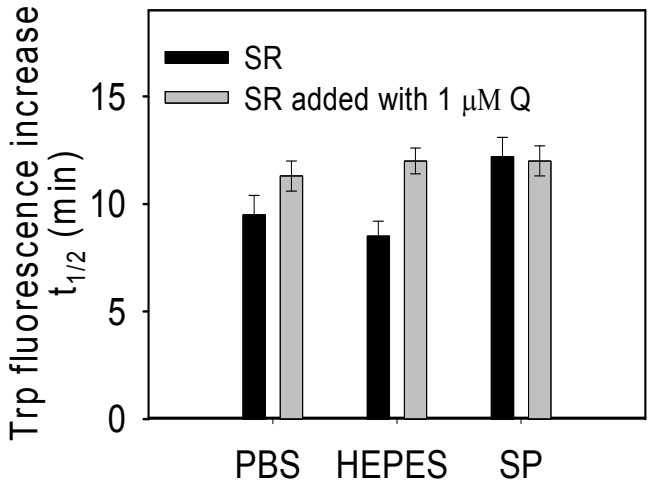

Figure 4.15 Meta II decay of SR in different buffers and pHs in the presence of 1 μM Q.
The immunopurified Rho samples, in the different buffers containing 0.05% DM + 1μM Q, were incubated at 20°C. The samples were measured until obtaining a steady base line, and they were subsequently photobleached and the Trp fluorescence was monitored over time The $t_{1/2}$ of the fluorescence increase was fit to a single exponential function.

In contrast, the presence of Q decreased the velocity of Meta II hydrolysis in HEPES pH 7.4, whereas no significant differences were observed in PBS pH 7.4 and SP pH 6.

4.1.2.5 Regeneration of SR

After Rho has been activated by light, it undergoes a series of inactivating reactions, passing through several intermediate forms before being regenerated to the original state, Rho, and being able to bind a fresh 11CR molecule (Lamb & Pugh, 2006). In specific cases where opsin fails to reunite with the chromophore to regenerate Rho, the persistent activation of G protein by opsin destabilizes and eventually damages the rod cells leading to retinal degeneration (Deretic et al., 2005; Frederick et al., 2001) Hence, the importance of the Rho regeneration process.

In a chromophore regeneration experiment, 11CR is added to ROS Rho in the dark state and the sample is immediately illuminated with a yellow cut-off filter (λ >495 nm) to avoid photobleaching of the free retinal, and successive spectra are taken over time until no further increase in A_{max} is detected (Figure 4.16 A)). The percent of regeneration was calculated considering the increase at 500 nm and plotted against time (Figure 4.16 B)).

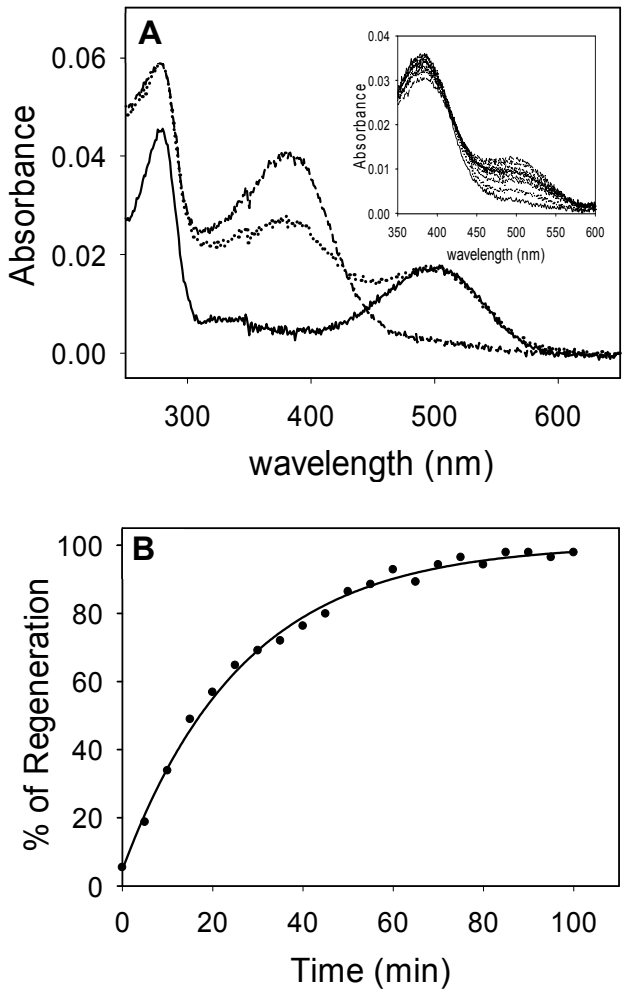

Figure 4.16 An example of the Rho regeneration process.
A. Rho dark state (solid line), Rho dark state + 11CR (dotted line), and Rho dark state + 11CR illuminated (dashed line). The inset shows the increase at 500 nm over time due to the regeneration process. **B**. Plot of % of regeneration.

The percentage of SR regeneration in different buffers is shown in Figure 4.17. SR in PBS showed the highest % of regeneration (97.5±1.4) followed by HEPES (90.5±6.2) and SP (85.5±6.0). The presence of Q significantly decreased the percentage of regeneration, about 20% for PBS pH 7.4 and SP pH 6. In the case of the HEPES buffer pH 7.4 only a 12 % decrease was observed.

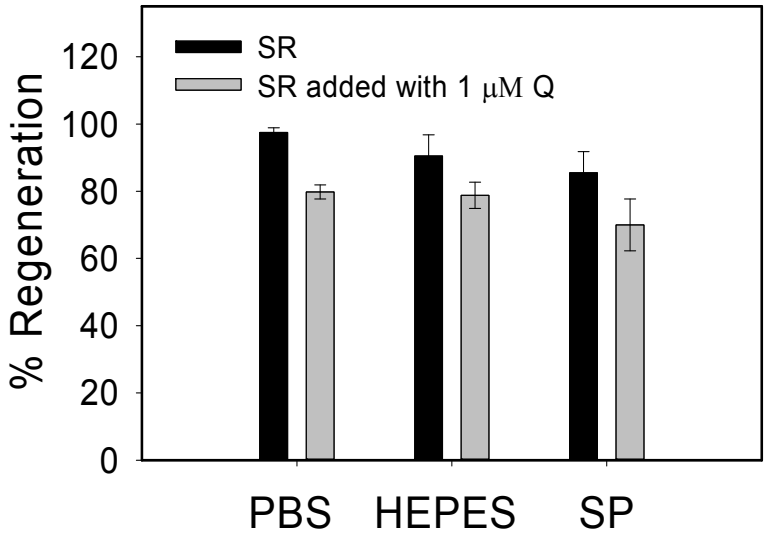

Figure 4.17 Regeneration (%) of SR in different pH and buffers and in the presence of 1μM Q.

2.5 fold of 11CR was added to the immunopurified Rho, in the different buffers containing 0.05% DM + 1μM Q, This sample was illuminated with light of > 495 nm to avoid photobleaching of the free retinal, and successive spectra were registered every 5 min at 20°C in the dark until no further increase in A_{max} was detected. The regeneration % was determined from the Abs increase at 500nm with time.

As already mentioned above, the Q effects observed on SR should be corroborated with purified Rho because in the case of SR some other membrane proteins and lipids could be present in the sample.

4.1.3 Q effect on purified Rho

4.1.3.1 Binding capacity of 1D4 antibody-sepharose beads and Rho purification

In order to carry out Rho immunopurification, it was first necessary to couple the 1D4 antibody to CNBr-activated sepharose beads. Upon coupling of the antibody, the sepharose-1D4 beads binding capacity was determined. After ROS solubilization, its spectrum was recorded (Figure 4.18) and 100 μl of beads were added to the ROS sample.

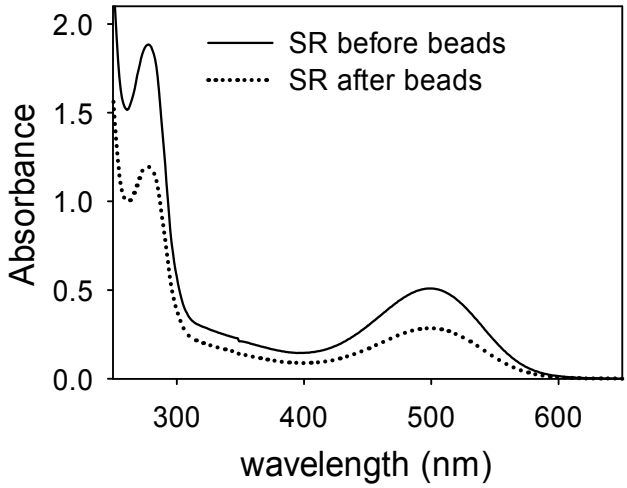

Figure 4.18 UV-vis spectra of SR before and after addition of sepharose-1D4 beads.

After the incubation time, the SN spectrum was again recorded and the binding capacity was calculated to be 1.1 µg Rho/µL beads. This result indicated a successful antibody-sepharose coupling process.

Once the Rho1D4 antibody-sepharose beads capacity binding was verified, Rho purification was carried out under different buffer and pH conditions (Figure 4.19).

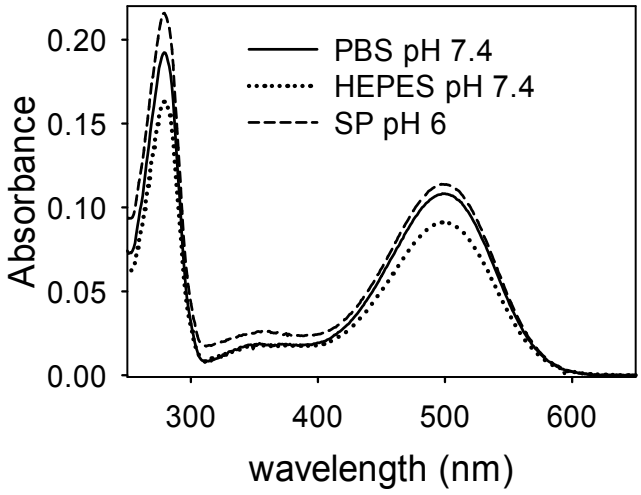

Figure 4.19 Rho purified at different buffer and pH.
UV-vis spectra in PBS pH 7.4, 0.05% DM, HEPES pH 7.4, 0.05% DM and SP and 0.05% DM. Spectra were recorded at 20°C.

Purified Rho under different conditions showed a A_{280nm}/A_{500nm} ratio of 1.8.This ratio is one of the criteria that indicates the purity of the Rho protein (Hubbard, 1954; McConnell et al., 1981; Salesse et al., 1984). Very pure Rho should have a ratio ranging within 1.6-1.8 (Heitzmann, 1972),

although ratios in the middle range (2.5-3.5) for ROS Rho purified on sucrose density gradients have been reported. Further purification of Rho would bring the ratio down to less than 2 (McConnell et al., 1981). These considerations are in agreement with the results obtained for our samples.

4.1.3.2 Photobleaching and acidification of purified Rho in the presence of Q

In purified Rho samples at different buffers, a similar effect of Q on illumination and acidification behavior was observed. For Rho in PBS the same effect was observed as in SR, an increase in the Q band at 330 nm (Figure 4.20).

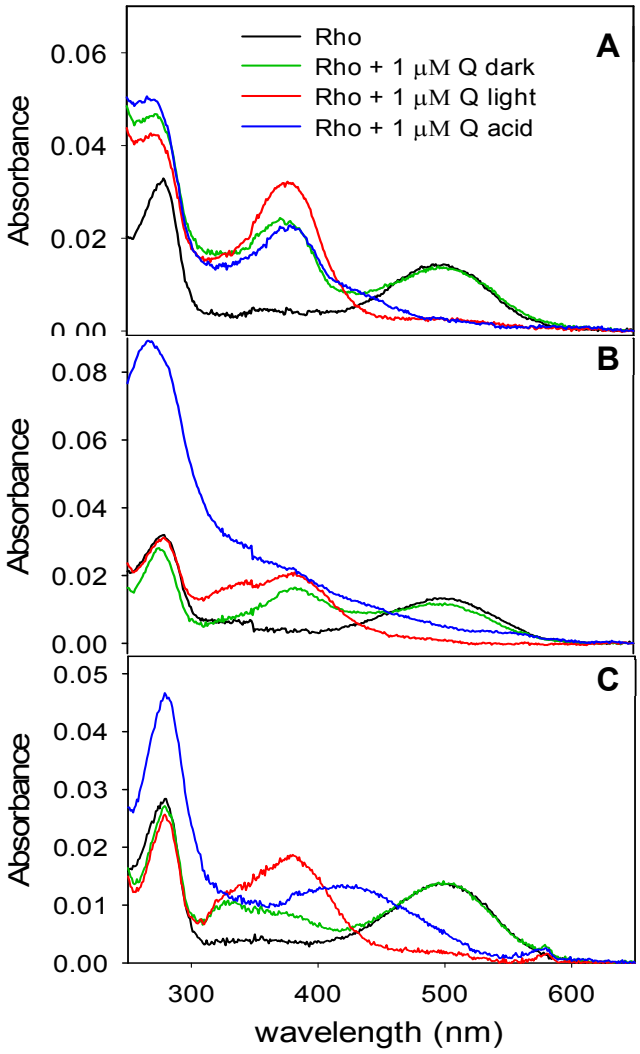

Figure 4.20 . Photobleaching and acidification behavior of Rho purified in different buffers in the presence of 1 μM Q.
UV-vis spectra of Rho in the presence of 1 μM Q before after photobleaching and acidification. Spectra were recorded at 20°C, 0.05% of DM in different buffers. **A** SP 50 Mm pH 6. **B**. HEPES 50 Mm pH 7.4. **C**. PBS, pH 7.4.

An increase in the Abs at 280 nm, after acidification of the Q-containing sample, was also noticed. This increase could be due to the effect of the acid on the ring A of Q or because the protein is losing its structure by the combined effect of acid and DMSO.

In the case of HEPES pH 7.4, the band at 280 nm was greatly affected by acidification suggesting so that in this buffer the presence of acid and DMSO in the Q-containing sample considerably affects the protein structure (Batista et al., 2013).

Less change could be observed in the Q-containing sample measured in SP buffer. Furthermore, a blue shift of 5 nm in the band at 375nm, induced by the Rho presence, was also noticed which suggested Q 4' hydroxyl group conjugation. After acidification, Q band I showed a red shift and reverted to its original position at 375nm. Unlike in the cases of HEPES and PBS, the increase in the 280 nm band observed in SP buffer. suggests that this effect may be rather due to ring A of Q.

4.1.3.3 Thermal stability, Meta II decay and regeneration of purified Rho in the presence of Q

A slight decrease in thermal stability due to Q was noticed in Rho purified in PBS and HEPES pH 7.4. In SP buffer pH 6 there were no significant differences. Comparing the three conditions, Rho presents a greater thermal stability in PBS buffer. Regarding to Meta II decay, no important differences were observed. Only in the case of SP buffer the presence of Q appears to slightly decrease the hydrolysis rate of Meta II (Figure 4.21).

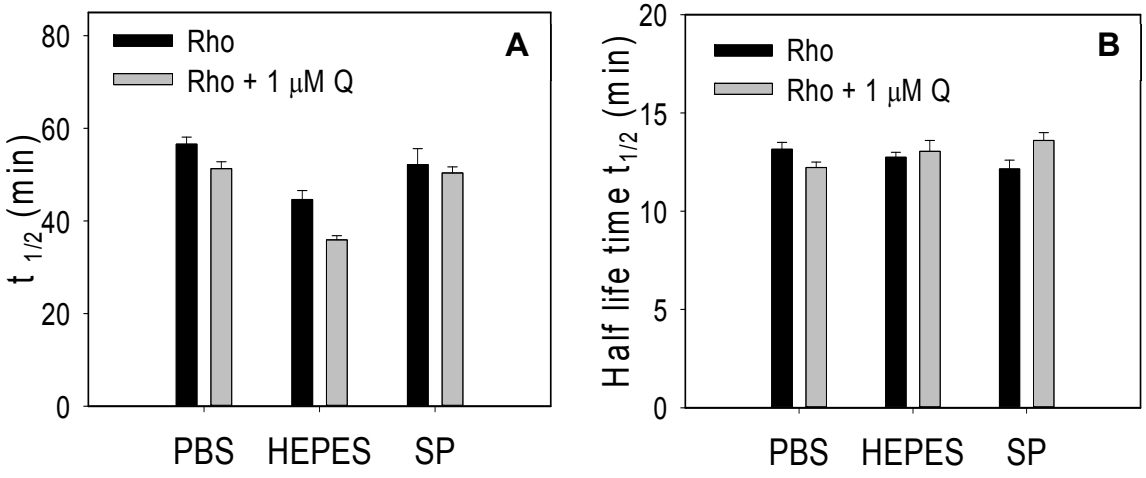

Figure 4.21 Thermal stability and Meta II decay of Rho in different pH and buffer with Q.
A. Rho in the different buffers conteining 0.05% DM and 1 μM Q, were incubate at 48°C, the normalized absorbance values at λ_{max} were ploted as a function of incubation time and the $t_{1/2}$ was calculated. **B**. Samples were incubated at 20°C in the dark until a steady base line was obatined, and were subsequently photobleached and the Trp fluorescence was monitored over time The $t_{1/2}$ of the fluorescence increase was fit to a single-exponential function.

The following regeneration pattern was observed in the different buffers: SP pH 6>PBS pH 7.4 > HEPES pH 7.4. In all treatments, the presence of Q decreased the regeneration by about 10% (Figure 4.22).

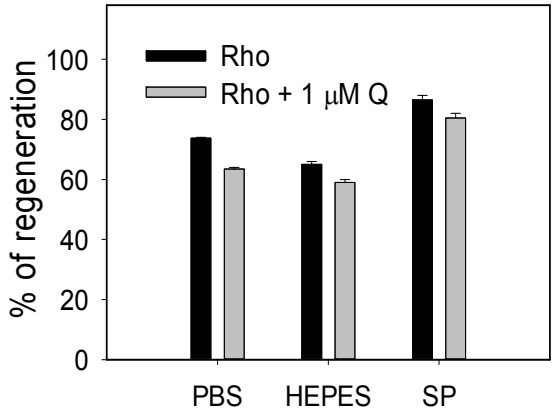

Figure 4.22 Rho regeneration at different pH and buffer in the presence of Q.
2.5 fold of 11CR was added to the immunopurified Rho, in the different buffers containing 0.05% DM + 1μM Q, This sample was illuminated with light of > 495 nm to avoid photobleaching of the free retinal, and successive spectra were registered every 5 min at 20°C in the dark until no further increase in A_{max} was detected. The regeneration % was determined from the Abs increase at 500nm with time.

Although in the experiments carried out until now no important changes could be observed, we proceeded to evaluate Q and other phenolic compounds on recombinant Rho in order to try to find some possible effect under these novel conditions.

Based on the results obtained so far, PBS buffer 7.4 was selected for the following experiments

4.1.4 UV-vis spectra of polyphenol compounds

The characterization of other phenolic compounds belonging to the class of flavonoids, as well as ellagic and chorogenic phenolic acids, and the stilbene R, were also carried out. Like in the case of Q, stability tests were performed on these compounds in PBS buffer pH 7.4 The spectroscopic pattern of each compound is shown in Figure 4.23.

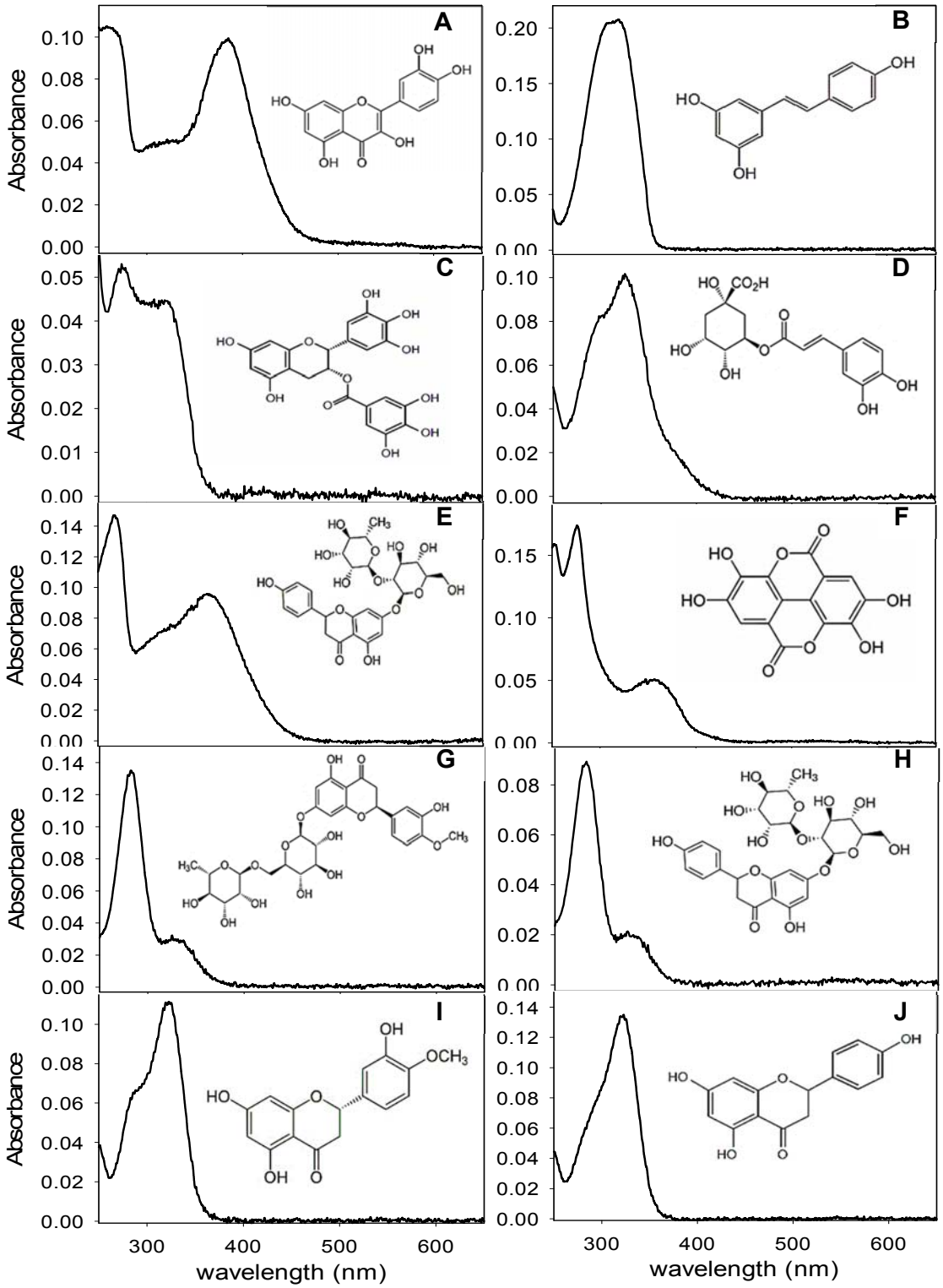

Figure 4.23 Spectroscopic pattern of phenolic compounds studied at 5 µM.
A polyphenol sample of 500 µM in DMSO was prepared from a polyphenol stock solution of 20mM. dissolved in the same solvent. 1 µL of this dilution was mixed with 99 µL of PBS buffer and 0.05% of DM detergent. The UV-vis spectrum of each phenolic compound was recorded at 20°C. **A.** Q; **B**, R; **C**. EGCG; **D.**.Chlorogenic acid; **E**. Rutin; **F**. Ellagic acid;.**G**. Hesperidin; **H**. Naringin; **I.** Hesperetin; **J.** Naringenin.

4.1.5 Effect of polyphenol compounds on opsin electrophoretic pattern

Once the compounds were spectroscopically characterized, experiments were continued on cell cultures. The effect of phenolic compounds at different concentrations during opsin expression was evaluated according to the experimental protocol described in section **3.2.2.4**. The first compound evaluated was Q and the Western blot is shown in Figure 4.24.

In these experiments, before performing the membrane solubilization in the different treatments, all the samples were adjusted to the same optical density to ensure the same amount of cells. After solubilization and before electrophoresis, the samples were adjusted to equal concentrations of protein by measuring their Abs at 280 nm. This was done to ensure that the possible differences found, were due to the compounds and not to differences in the handling of the samples. In addition, a sample of purified Rho was used as a reference control.

Four concentrations of Q, as well a DMSO control (because the compounds are dissolved in this solvent), were evaluated (Figure 4.24). The first lane corresponds to ROS Rho with its two characteristics bands main bands, a very intense one that would correspond to the monomer (40000 Da) and a less intense one corresponding to the dimer (66 000 Da).

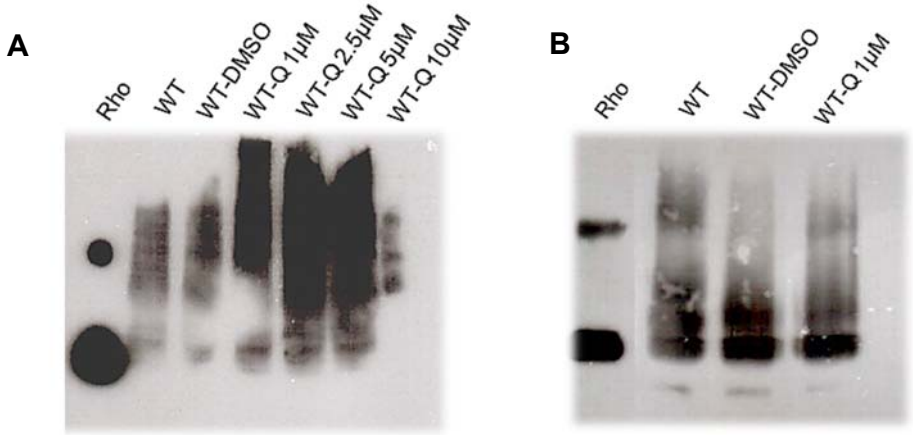

Figure 4.24 Effect of different Q concentrations on the Rho electrophoretic pattern. Frist (A) and second (B) repetition

In all the other samples a pronounced smear was observed. This smear is characteristic of protein expressed in COS-1 cells because these cells glycosylate Rho differently than photoreceptor cells do (Oprian et al., 1987). The smear was more intense in treatments with 1, 2.5 and 5 µM of Q, but not for the treatment of 10 µM (where a lower amount of protein could be detected). In this Western blot is difficult to identify the bands corresponding to Rho (Figure 4.24 A), so the experiment was repeated at less concentration (Figure 4.24 B) and in this case the bands

corresponding to the Rho monomer and dimer can be better appreciated. The main observation is that the presence of 1 μM Q does not affect the electrophoretic pattern of the protein.

Considering that a concentration of 10 μM Q produced intensity marked effect on the electrophoretic pattern, an experiment was performed at a higher concentration with other compounds (15 μM) (Figure 4.25). The electrophoretic pattern is similar in all cases except in the case of the EGCG that shows a significant decrease in the protein content.

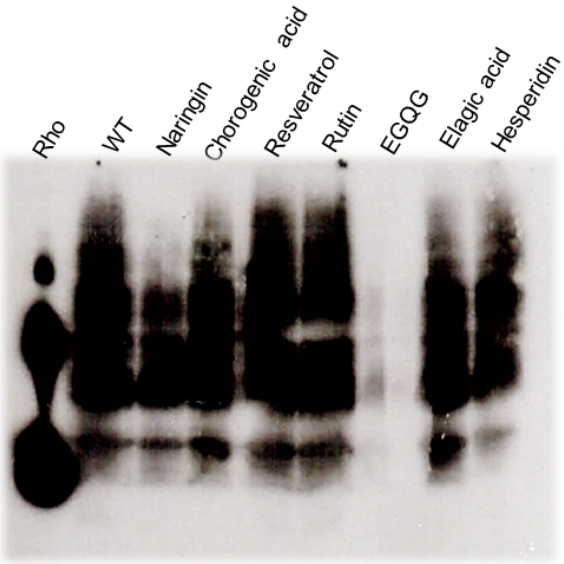

Figure 4.25 Effect of several phenolic compounds (at 15 μM) on the Rho electrophoretic pattern.

Given the fact of the smeary pattern caused by the use of COS-1 cells and which do not allow a good appreciation of possible differences between treatments, we decided to use HEK-293S GnTI^{-} cells which do not have N-acetylglucosaminyltransferase I (GnTI^{-}) enzyme activity and are therefore unable to synthesize N-glycans, making glycosylation more homogeneous (Chang et al., 2007). Using these cells, the experiment was again performed (Figure 4.26 A) showing a similar behavior and confirming the lower amount of protein in the EGCG sample. In this latter case, a noticeable change in color of the collected cells could be also noticed (Figure 4.26 B). The brown color could be the result of some oxidative process of EGCG (Hou et al., 2005).

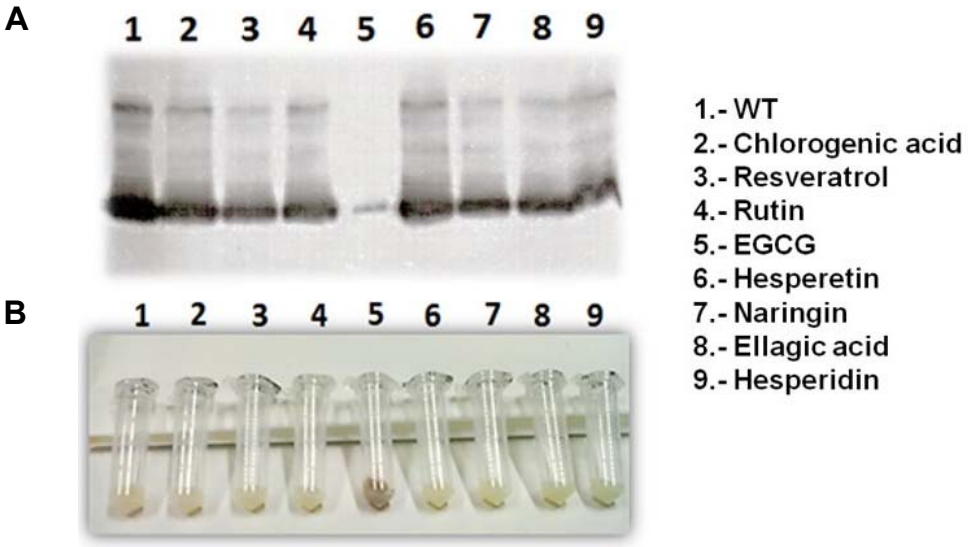

Figure 4.26 Effect of several phenolic compounds (at 15 μM) on the Rho electrophoretic pattern. HEK 293S GnTI^{-} cells were used. **A**. Western blot. **B**. Cells collected for the Western blot.

Subsequently, the compounds naringenin, hesperetin and Q were tested at different concentrations. As shown in Figure 4.27A, only one band was visible in the Western blot which may correspond to Rho monomer. The purification of these samples was carried out to perform SDS-PAGE gel (Figure 4.27 B) in which only a slight decrease of the bands was noted for the treatment with 1 μM hesperetin.

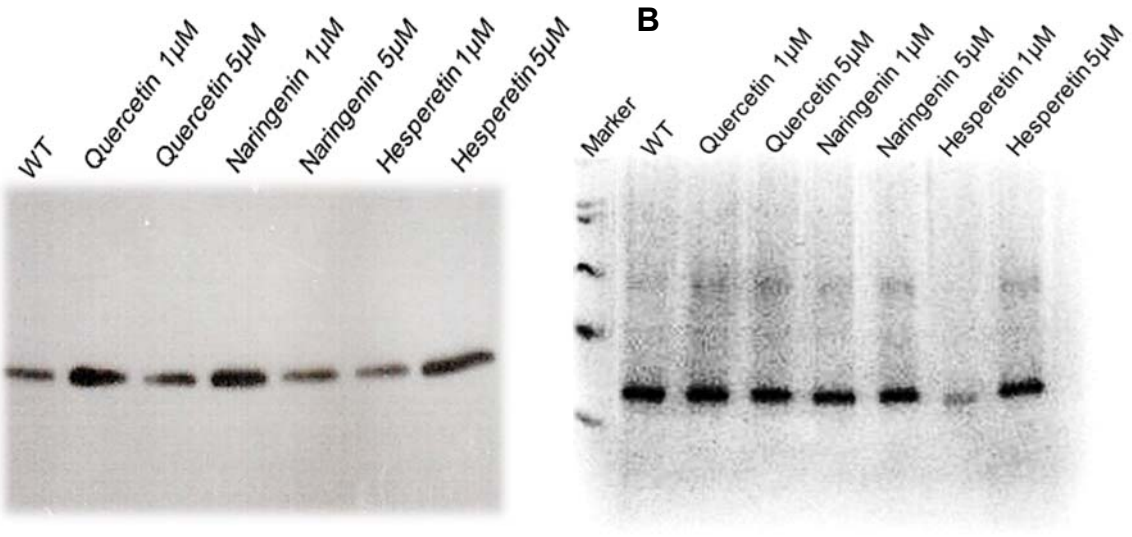

Figure 4.27 Western blot (**A**) and SDS-PAGE gel (**B**) showing the effect of Q, naringenin and hesperetin on Rho electrophoretic pattern.

In another test, Q, R and EGCG were evaluated at concentrations of 10 μM and 50 μM. there is A decrease in the intensity of the Rho monomeric band was detected at concentrations of 50 μM (Figure 4.28). In the case of EGCG, a band below 40000 Da was observed and in the treatments with R, several lower bands could also be noticed.

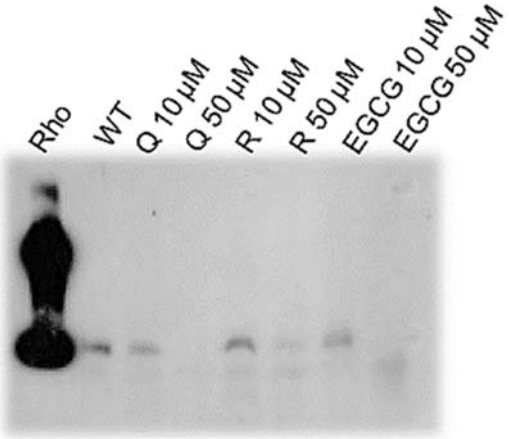

Figure 4.28 Q, R and EGCG effects on Rho electrophoretic pattern.

Continuing the tests at concentrations of 50 μM, Q, R and EGCG were again evaluated in addition to rutin and chlorogenic acid (Figure 4.29). We could clearly confirm the effect observed in the previous experiment where Q, R and EGCG appeared to have more effect on Rho expression in cell cultures. For these treatments, again a change in color was observed in the cells for both EGCG and Q.

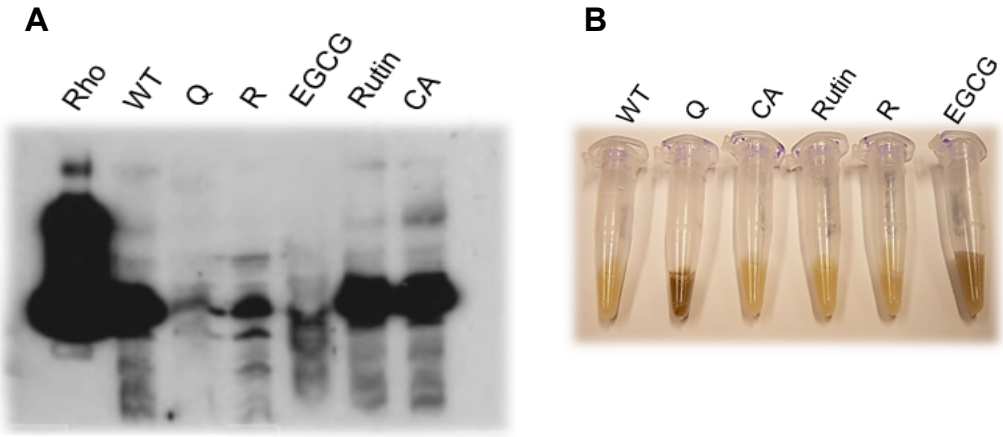

Figure 4.29 Effect of 50 μM of Q, R, EGCG, rutin and chlorogenic acid on the Rho electrophoretic pattern. HEK 293S GnTI^{-} cells were used. **A**. Western blot. **B**. Cells collected for the Western blot.

Based on these results, we decided to focus on Q, R and EGCC for further evaluating their effects on the physical and functional properties of recombinant Rho and mutants associated with degenerative diseases of the retina.

4.1.6 Cytotoxic effect of phenolic compounds

From the results obtained by Western blot, in which a decrease in the intensity of the bands of Rho electrophoretic profile indicating a decrease of protein amount, we decided to evaluate the cytotoxic effect of these compounds on the cells. This is due to the fact that the lower amount of protein detected could be a result of the compounds on cell viability.

The results of the potential cytotoxic effect of Q, R an EGCG, on COS-1 cells, are shown at different concentrations (Table 4.1). It can be seen that OPTIMEM, the transfection solution, reduces cell viability by 4% and the solvent control (also present in the transfection solution) by 6%.

Table 4.1 Cytotoxicity of phenolic compounds.

Treatment	% Cell viability
OPTIMEM	95.8 ± 1.3
DMSO	94.0 ± 1.5
Q1μM	93.2 ± 4.6
Q10 μM	91.7 ± 3.0
Q 50 μM	91.6 ± 3.5
Q100 μM	92.1 ± 2.6
EGCG 1 μM	85.4 ± 4.2
EGCG 10 μM	88.1 ± 2.2
EGCG 50 μM	91.2 ± 4.0
EGCG 100 μM	90.6 ± 1.0
RES 1 μM	89.5 ± 1.8
RES 10 μM	87.8 ± 2.1
RES 50 μM	87.7 ± 1.4
RES 100μM	85.9 ± 2.2

Of the three compounds under study, the one with the lowest cytotoxic effect was Q, which shows no difference in its effect at concentrations ranging from 1 μM to 100 μM. EGCG shows a tendency to increase cytotoxicity at lower concentrations since the 1 μM concentration showed the greatest reduction in cell viability (85%). Compared with the other treatments, the one with the highest cytotoxicity was R. In this case the percentages of viability obtained in the different concentrations indicate an opposite effect to the EGCG since for this compound a slight increase in its toxicity is observed as the concentration increases.

The percentages of viability obtained in this test indicate only a minor effect of these compounds on cell viability. The effect of the compounds is very low, if we consider that around 6% of the observed effect is due to the transfection solution.

4.1.7 Antioxidant capacity of phenolic compounds

TEAC assay

In addition to the cytotoxicity studies performed on the phenolic compounds selected, the antioxidant capacity of different concentrations of Q, R and EGCG was determined. The antioxidant properties of these compounds as well as their health benefits have been extensively studied. The purpose of carrying out this assay is to have complementary information and shed new light into any potential linkage between the antioxidant properties and the effects observed in the Western blot analysis.

To determine the antioxidant capacity, a Trolox calibration curve was first made (Figure 4.30).

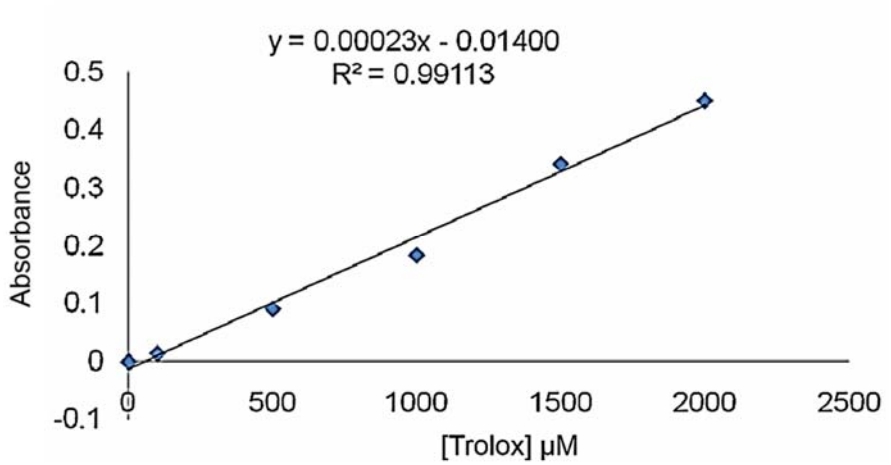

Figure 4.30 Standard curve of Trolox.
The calibration curve was prepared with different concentrations of Trolox diluted in ethanol. The dilutions prepared were subject to the experimental assay to obtain the ΔAbs which was plotted against the concentration.

Solutions of Q, R and EGCG were prepared in DMSO at concentrations of 1 µM, 10 µM and 50 µM. The different concentrations were tested according to the conditions described in section **3.2.8.1**. The antioxidant capacity of the compounds is shown in Figure 4.31.

For the three compounds analyzed here, the antioxidant capacities, up to a concentration of 50 µM, were found to be concentration dependent. This effect is not always observed since at certain concentrations some compounds, instead of exerting an antioxidant action, act as prooxidants. At 1 µM, R had the lowest antioxidant capacity and EGCG the highest. This same behavior was observed at 10µM for these compounds. A completely different behavior could be observed at 50 µM, the antioxidant capacity of Q and R increased more than double, with Q being higher. For EGCG its antioxidant capacity remained the same as for the 10 µM concentration.

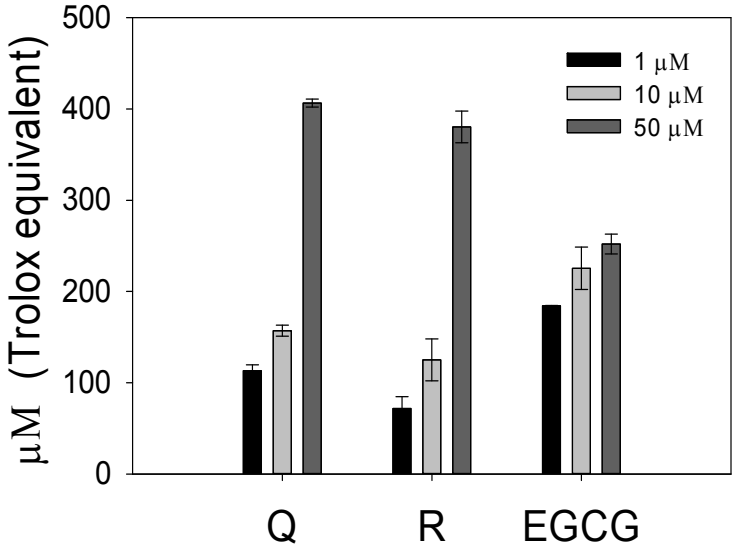

Figure 4.31 Antioxidant capacity of Q, R and EGCG, at 1 µM, 10 µM and 50 µM.

The results obtained for the high antioxidant capacity of EGCG at low concentrations could be correlated with the fact that in the Western blot the first effect observed in the decrease of the amount of Rho was precisely in the EGCG case. Such an effect, at the same concentration, was not observed for R or Q. In the case of Q and R, a similar effect could only be detected at the higher concentration of 50 µM.

.

4.2 Biochemical and functional characterization of the immunopurified wild tpe (WT) and mutant Rho associated with RP

Recombinant DNA techniques have been widely used to perform systematic structure-function studies of bovine Rho by specific amino acid replacements. Many of these amino acid substitutions that have been studied to date have been performed in order to elucidate the molecular mechanisms that accompany certain retinal degenerative diseases such as RP.

The mutant G90V was first reported when it was identified in a Swiss family of three generations which showed a typical phenotype of an autosomal dominant form of RP, with marked fundus changes developing in later stages of life (Neidhardt et al., 2006). Subsequent to its discovery, studies of this mutant have been continued using heterologously expression systems and immunopurification strategies in order to deepen our knowledge on the structural details underlying the molecular mechanisms of the disease (Dong et al., 2015; Toledo et al., 2011). This is always a necessary step for new therapies to be developed.

In the case of mutants Y102H and I307N these were developed in chemically mutagenized mice with the goal to study the disease (Budzynski et al., 2010). The interest in these mutations comes from the fact that there is no need to overexpress the protein since the mutation is already integrated in the mouse genome. This avoids concerns associated with overexpression that can cause retinal degeneration *per se*. It was found that these mutants have phenotypic similarity to human B1 type Rho mutations. Patients with class B mutations display a slower disease progression, and maybe subdivided into class B1 and B2 (Cideciyan et al., 1998). Rod degeneration is focal in class B1 and these mutations exhibit impaired deactivation of phototrasduction after exposure to high intensity light flashes (Cideciyan et al., 2005). That is why these mutations can be important tools in examining mechanisms underlying induced RP and for testing therapeutic strategies.

Prior to the studies of the possible interaction of compounds selected in the previous section with Rho and RP mutants, it was first necessary to characterize these recombinant proteins. For WT and G90V mutant, the corresponding DNA plasmids were already available in the research group and had been obtained by means of site-directed mutagenesis. The other two mutations, Y102H and I307N were newly designed and the corresponding mutated genes were obtained. The primers designed to introduce these mutations were the following:

Y102H:

5’-CCTCTCTCCATGGGCACTTCGTCTTTGGG-3’
5’-CCCAAAGACGAAGTGCCCATGGAGAGAGG-3’

I307N:

5´-CCCGGTCATCTACAACATGATGAACAAGCAGTTCC-3’
5’-GGAACTGCTTGTTCATCATGTTGTAGATGACCGGG-3’

After the mutagenesis process, the mutated plasmids were sequenced in order to confirm the successful introduction of the mutations (Figure 4.32).

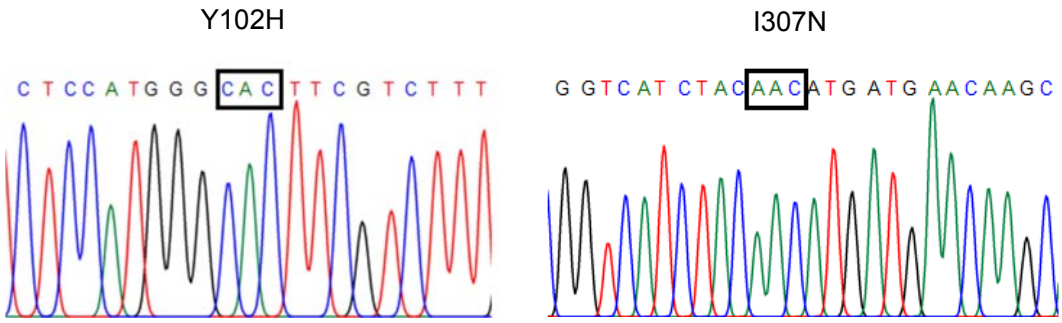

Figure 4.32 DNA sequencing confirmed the presence of the mutations (the mutated codons are boxed).

Once the mutations were inserted, the plasmid was obtained on a large scale by Maxiprep and subsequently the concentration and purity were determined by UV-vis spectroscopy (Figure 4.33). The concentration was determined from the A_{260} and the A_{260}/A_{280} ratio was used for purify assessment. A DNA purity within the established 1.8-2 range was obtained, and the amount obtained varied between 6 - 6.5 µg/µL

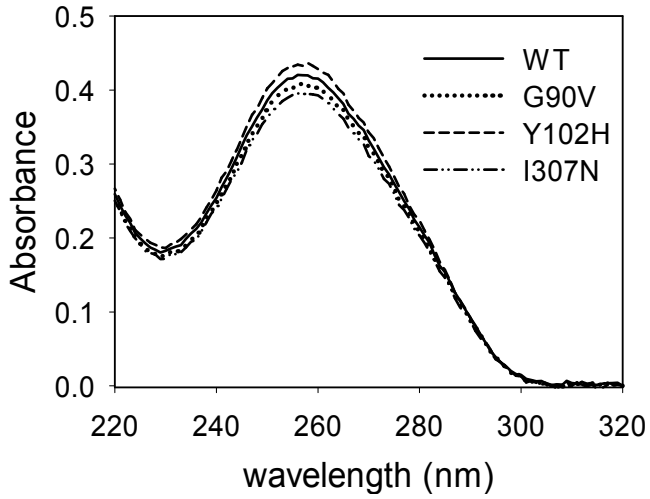

Figure 4.33 UV-vis spectra of purified DNA.

4.2.1 UV-vis spectroscopy

WT and mutants were expressed and immunopurified, and the UV-vis spectra were recorded at 20ºC (Figure 4.34).

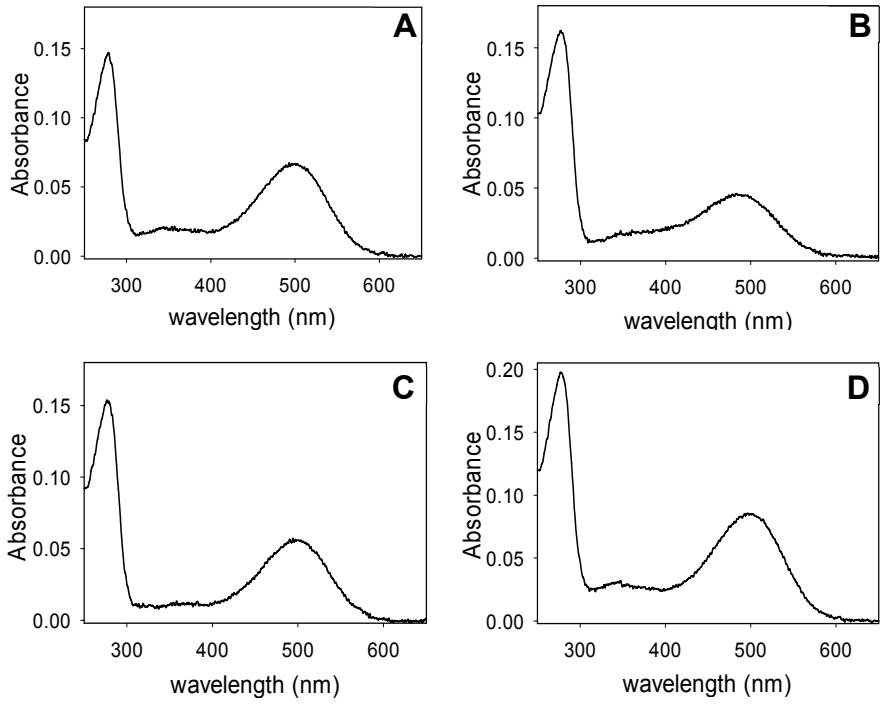

Figure 4.34 Absorption spectra of WT Rho and G90V, Y102H and I307N mutants in the dark state. Samples in PBS pH 7.4 buffer and 0.05% DM. Spectra were recorded at 20°C. **A.** WT. **B**. G90V mutant. **C**. Y102H mutant. **D**. I307N mutant.

The Y102H and I307N mutants showed a spectroscopic behavior similar to WT, with a maximum absorption band in the visible region at 498 nm and 500 nm respectively. In the case of G90V mutant, a blue shift of 10 nm was observed, a behavior that had been previously reported (Dong et al., 2015; Toledo et al., 2011). A summary of the spectral parameters, including the absorbance value of the visible chromophoric band, the molar extinction coefficient (ε) and the spectral $A_{280}/A_{\lambda max}$ ratio is shown in Table 4.2.

Table 4.2 Spectroscopic properties of WT and mutants.

	WT	**G90V**	**Y102H**	**I307N**
λ_{max}	500	490	498	500
Ratio ($A_{280}/A_{\lambda max}$)	2.3 ± 0.20	3.73 ± 0.23	2.7 ± 0.12	2.2 ± 0.04
ε x 10 ^{3}	42.2 ± 2.2	37.8 ± 0.9	37.6 ± 1.3	43.9 ± 0.4

The G90V and Y102H mutants show a slight increase in the ratio which could be due to the fact that the introduction of this mutation causes a small fraction of misfolded protein and/or leads to decreased structural stability. These mutants also have a very similar molar extinction coefficient. On the other hand, the mutant I307N presents a ratio and ε similar to WT.

The purified mutants were also characterized by Western blot and SDS-PAGE. In the Western blot, a sample of purified Rho from ROS (Figure 4.35 A, lane 1) was loaded as a control. ROS Rho was also loaded in the SDS-PAGE gel in addition to the protein ladder molecular marker, as a control (Figure 4.35 B, lanes M and 1).

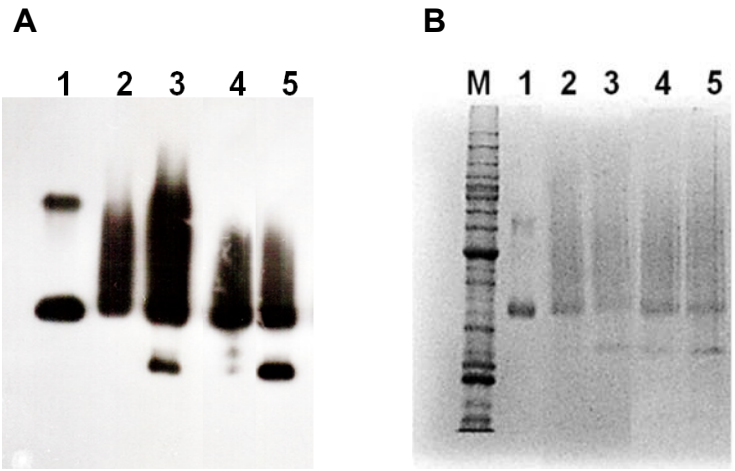

Figure 4.35 Western Blot and SDS-PAGE of purified WT and RP mutants.
A. Westen blot . **B**. SDS-PAGE. M: ladder, 1:Rho, 2: WT, 3:G90V, 4: I307N and 5:Y102H.

A characteristic smear typically observed in Western blots of Rho expressed in COS-1 cells, and usually attributed to heterogeneous glycosylation, can be observed in all the samples, but particularly it appears to be more intense in the case of the G90V mutant (Figure 4.35 A, lane 3). In all cases, the Rho monomeric band is clearly observed, but the corresponding dimer band can only be clearly detected in the case of the ROS Rho control sample and in the case of the G90V mutant sample. In the latter case, however, the presence of the band corresponding to the dimer species is partially occluded by the intense smeary pattern observed for this protein.

For Y102H and G90V, a clear definite band is observed below the Rho monomer band. The presence of a band around 27 kDa which could correspond to a truncated form of Rho has been previously described (Dong et al., 2015; Fernández-Sampedro et al., 2016; Krebs et al., 2010). Alternatively, lower bands at similar position in the gel could be attributed to non-glycosylated species. In the case of the I307N mutant, two less intense bands can be detected below the 40 kDa main opsin band. By means of SDS-PAGE gel, it was possible to confirm the presence of such bands (Figure 4.35B).

The UV-vis spectra of WT and the mutants were recorded in the dark, upon illumination for 30s and after subsequent acidification (Figure 3.36). The main difference observed was in the G90V mutant that did not show a complete conversion of the visible band to 380nm upon illumination. This remaining band (about 40% of the dark visible band) had a similar visible wavelength maximum as the dark pigment, suggesting conversion to a photointermediate with retinal binding pocket similar to the dark pigment, including the presence of a PSB linkage (Ramon et al., 2014).

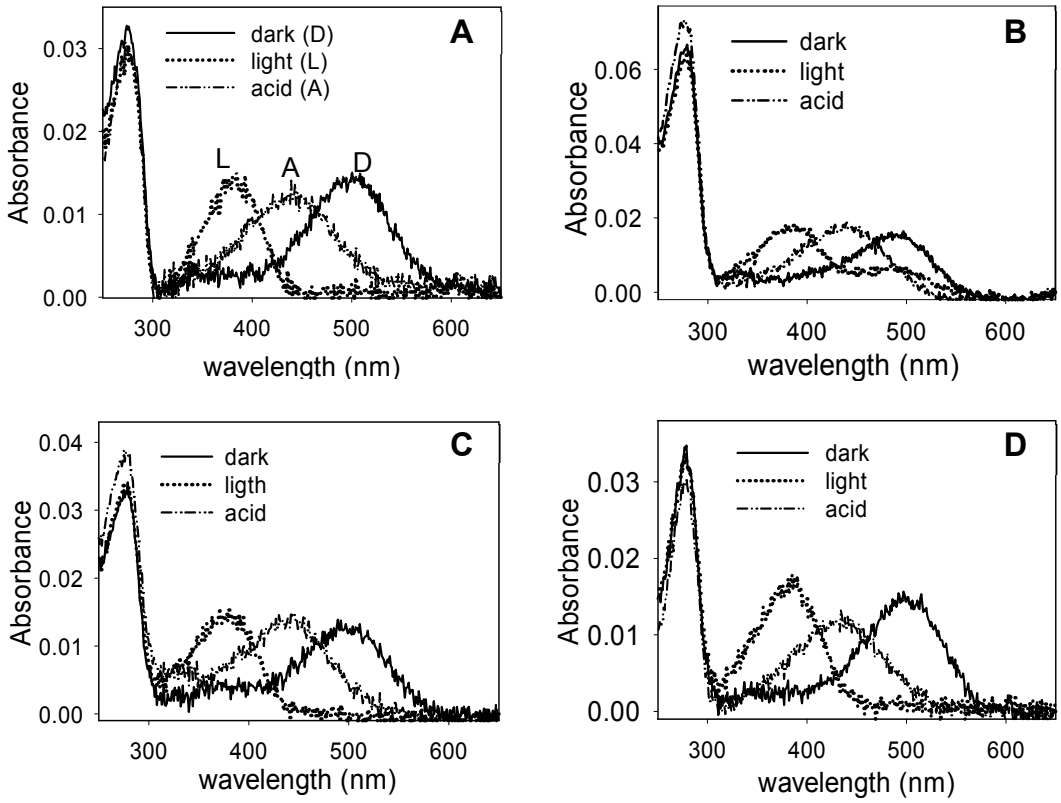

Figure 4.36 UV-vis characterization of the immunopurified WT and RP mutants.
Dark state (solid line), photobleaching (dotted line) and acidification (dashed line). Samples in PBS pH 7.4 buffer and 0.05% DM. Spectra were recorded at 20°C. **A.** WT. **B**. G90V mutan. **C**. Y102H mutant. **D**. I307N mutant.

Acidification of these photoactivated receptors resulted in a similar behavior, showing a band with a maximal absorbance at 440 nm corresponding to the PSB.

4.2.2 Hydroxylamine reactivity and thermal stability

Hydroxylamine is a compound that is used in Rho studies to determine whether a mutation can affect the structural compaction in the SB environment. This reagent can enter the retinal binding site and break the SB linkage. The WT and RP mutants in dark state were treated with hydroxylamine which causes a decrease in the visible maximal absorbance (Figure 4.37).

As it was expected, the SB in Rho is remarkably stable in the presence of hydroxylamine. In contrast, the G90V mutant showed a dramatic decrease in the visible maximal absorbance due to the less compact structure in the SB linkage environment (Dong et al., 2015; Toledo et al., 2011). Also for the mutant Y102H a decrease in A_{max} was observed which was not as marked as in the case of G90V mutant. The I307N showed a similar behavior to that of the WT which indicates that this RP mutant has a better structural compaction, around ths SB, compared to the Y102H and G90V mutants. For a better comparison, the initial velocity was calculated and then normalized. It is noticed that hydroxylamine reactivity is 38.5 times faster for G90V mutant compared to WT, and 4.5 and 1.8 times faster for the case of Y102H and I307N mutants.

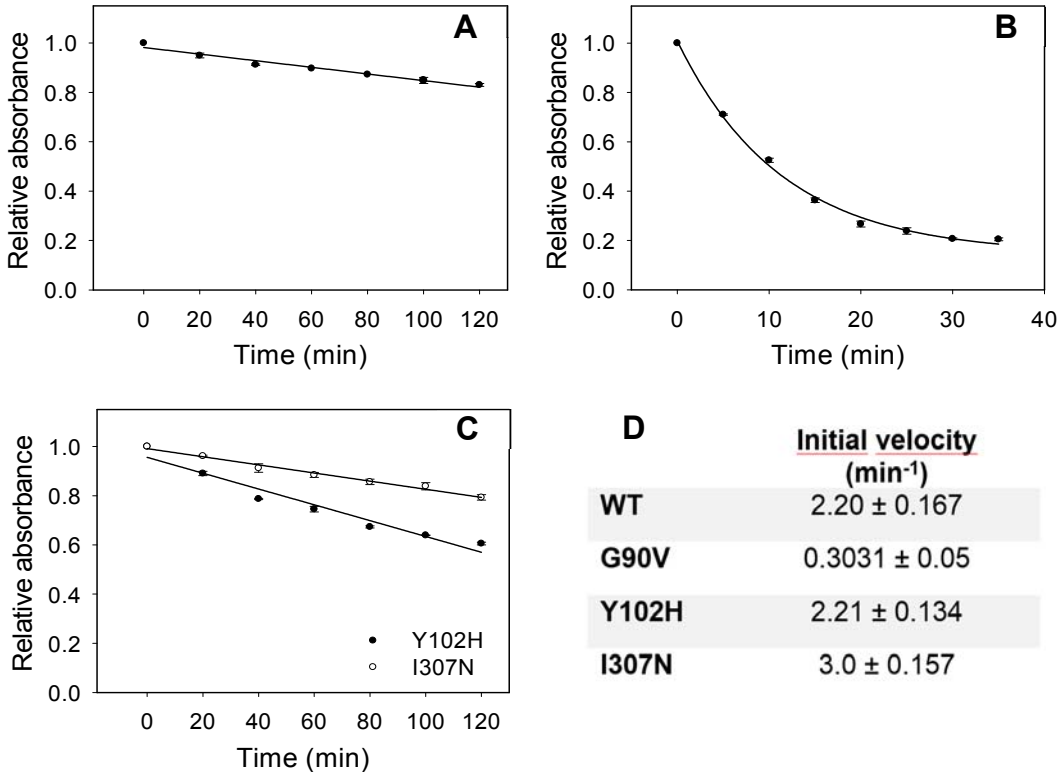

D

	Initial velocity (min^{-1})
WT	2.20 ± 0.167
G90V	0.3031 ± 0.05
Y102H	2.21 ± 0.134
I307N	3.0 ± 0.157

Figure 4.37 Chemical stability of WT and G90V, Y102H and I307N.
Samples purified in PBS pH 7.4 and 0.05% DM were incubated with 50 mM hydroxylamine, pH 7 and the decrease of Abs at λ_{max} was recorded over time at 20°C, and the initial rate was calculated. **A**. WT Rho. **B**.G90V mutant. **C**. Y102H and I307N mutants. **D**. Initial velocity of Abs decrease process.

In the thermal stability monitored at 48°C, the G90V and Y102h mutants were very unstable in dark state (Figure 4.38), showing very fast thermal bleaching kinetics with $t_{1/2}$ of 2min and 3 min respectively. Although less dramatic, I307N receptor was also unstable with a half-life of 23 minutes, four times faster than WT.

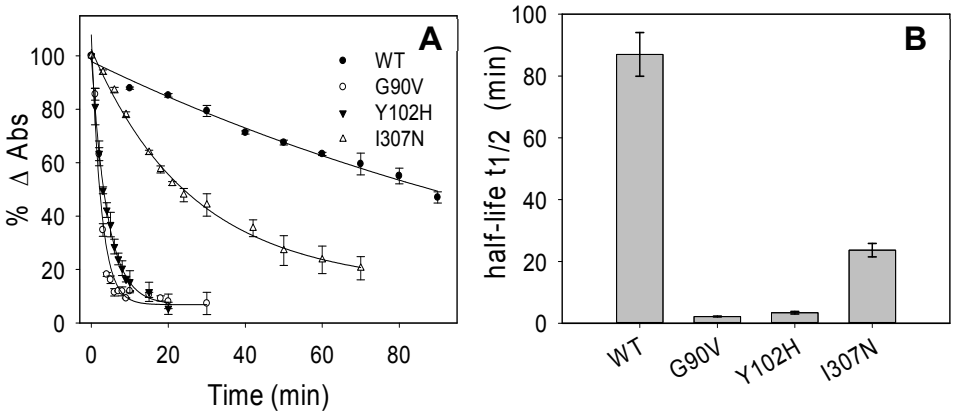

Figure 4.38 Thermal stability of WT and G90V, Y102H and I307N.
Immunopurified WT and mutants in PBS pH 7.4 buffer and 0.05% DM were incubated at 48°C, the normalized Abs values at λ_{max} were plotted as a function of incubation time (**A**) and the $t_{1/2}$ was calculated (**B**).

4.2.3 Meta II decay

The stability of the active state of purified WT and mutants was carried out by means of fluorescence spectroscopy following the Trp fluorescence increase upon illumination, due to its release from the binding pocket. The fluorescence curves are shown in Figure 4.39, as well as the $t_{1/2}$ values derived from each curve. For all mutants, the Meta II stability reflected a slower decay when compared with WT (13 ± 0.20 min) (Figure 4.39). G90V mutant showed the highest difference with a $t_{1/2}$ of 36 ± 1.13. This result agrees with that reported in other studies for this mutant (Toledo et al., 2011).

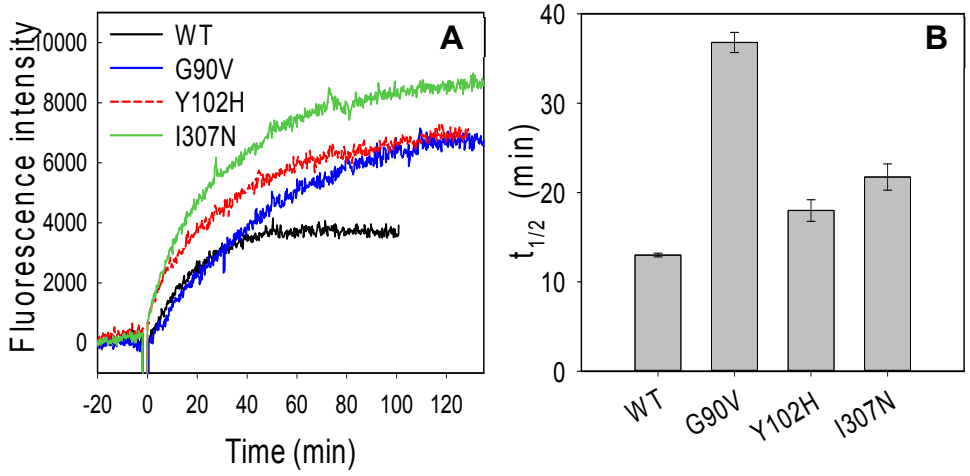

Figure 4.39 Meta II decay of WT and G90V, Y102H and I307N mutants.
A. Fluorescence curve of retinal release. **B**. $t_{1/2}$ values derived from the fluorescence curves.

Y102H and I307N mutants had a $t_{1/2}$ of 18 ± 1.21 min and 21.8 ± 1.50 min. A study carried out by Budzynski et al (2010) showed similar behavior for these mutants, both presented higher MetaII decay values compared to WT (WT= 5.9 min, Y102H=7.5 min and I307N=7.9 min) with a slightly longer time for I307N mutant. These differences were not statistically significant due to the large standard error shown by the experimental values. The difference in the values presented here with those reported in that study could be due to the experimental conditions in which the experiment was carried out, since the buffer used was SP pH 6.7 and the concertation of DM was 0.1%. In our experiment de buffer was PBS pH 7.4 and 0.05% of DM detergent. On this regard, the effect of pH and DM detergent concentration on the stability and function of Rho have been reported(Janz & Farrens, 2003; Ramon et al., 2003). Furthermore, this study was carried out with a mutant with an engineered disulfide bond that is inherently more stable than our case (Budzynski et al., 2010).

4.2.4 Chromophore regeneration

In the experiment of pigment regeneration with 11CR after Rho photobleaching, the percentage and velocity of regeneration were the parameters analyzed (Figure 4.40).

It was found that Y102H and G90V mutants had the lowest percentage of regeneration (61 and 70% respectively) compared to WT. Surprisingly the mutant I307N showed a slightly higher regeneration (97%) than WT. This result agrees with the amount of protein obtained during the purification of these receptors where the highest yield was in I307N mutant, then the WT and with a lower yield the mutants Y102H and G90V.

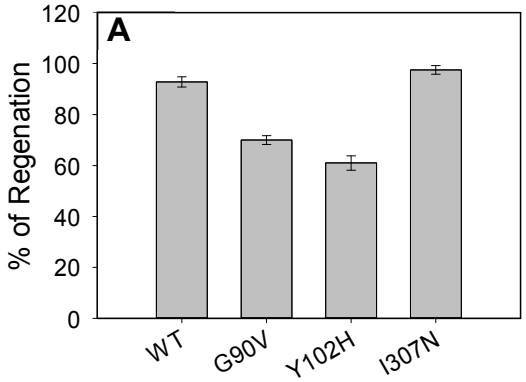

B	Initial velocity (min-1)
WT	2.20 ± 0.167
G90V	0.3031 ± 0.005
Y102H	2.21 ± 0.134
I307N	3.0 ± 0.157

Figure 4.40 Percentage and velocity of regeneration of photoactivated WT and RP mutants.
2.5 fold of 11CR was added to dark adapted immunopurified WT and mutants in PBS pH 7.4 0.05% DM and the percentage of regeneration was determined after pigment illumination with light of > 495 nm to avoid photobleaching of the free retinal. To determine the extent of chromophore regeneration successive spectra were recorded every 5 min at 20°C until no further increase in A_{max} was detected. **A**. Percentage of chromophore regeneration. **B**. Chromophore regeneration rates.

The G90V mutant showed the slowest regeneration rate. In the case of the Y102H mutant, despite presenting the lowest percentage of regeneration, it presents the same regerenration rate as the WT. On the other hand, the I307N had the fastest regeneration rate compared to all other receptors.

4.2.5. Gt activation of purified WT and RP mutant Rho

As already mentioned, the function of Rho is to activate Gt and initiate the visual signal transduction cascade. Gt activation involves the exchange of guanosine diphosphate for guanosine triphosphate which results in the dissociation of the transducin α-subunit from the Gβγ heterodimer. The ability of purified WT and RP mutants to catalyze guanine nucleotide exchange by Gt was assayed using a radioactive filter-binding assay method. Before starting the assay, it was first necessary to isolate Gt. Once purified, the concentration and quality were analyzed by SDS-PAGE with bovine serum albumin (BSA) as a standard (Figure 4.41).

Gt activation was monitored with a radionucleotide filter binding assay by measuring the uptake of GTPγ^{35}S by Gt upon binding to activate Rho. The amount of GTPγ^{35}S bound was determined as described in **3.2.7.2** section.

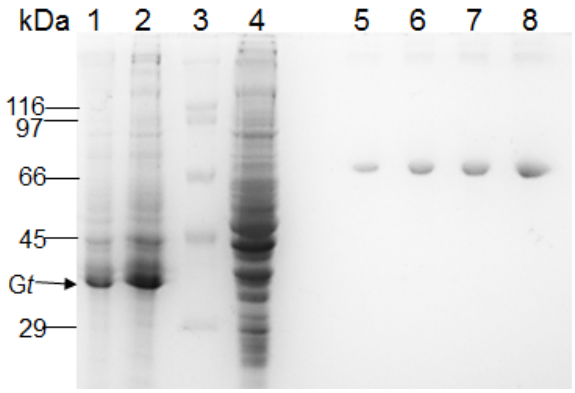

Figure 4.41 SDS-PAGE gel of Gt isolated from bovine retina.
Lane 1, 10µl of purified Gt; lane 2, 20 µl of purified Gt; Lane 3 protein ladder, Lane 4, SN after Gt isolation, Lane 5-8, BSA 1, 2,3 and 5 µg..

The photoactivated mutants Y102H and G90V activated Gt with a similar kinetics to the WT (Figure 4.42). However, the amount of GTPγ^{35}S bound was lower compared to the WT. The I307N mutant showed an altered kinetics but a similar quantity of GTPγ^{35}S bound similar to the WT.

All RP receptors showed lower activation, especially in the case of the mutants G90V and I307N which were twice as slower to activate Gt with respect to the WT.

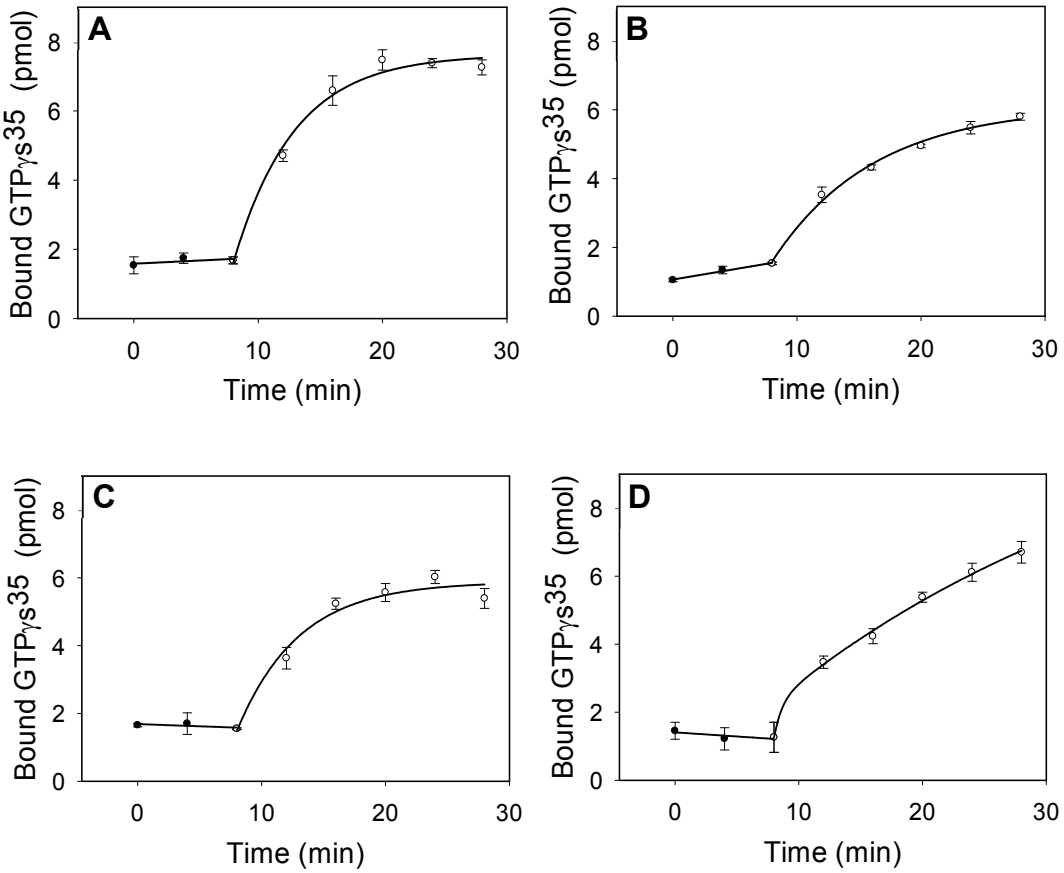

Figure 4.42 Gt activation by WT and G90V, Y102H and I307N mutants.
Gt activity was measured by means of a radionucleotide filter-binding assay in Gt buffer.. The reaction was initiated by the addition of the WT or mutants, and samples were filtrated at different times in the dark and after illumination. **A.** WT. **B**. G90V mutant. **C**. Y102H mutant. **D**. I307N mutant.

4.2.6 Subcellular localization

Rho as a membrane protein, must be localized at their appropriate subcellular compartment (membrane) in order to perform its proper function. Rho synthesis and degradation are highly-regulated processes, and several mutations can affect them by causing misfolding and aggregation. Furthermore, some mutations can impair opsin transport to the outer segment membrane. In this regard, the heterologous expression of rod WT and mutant opsins in cell culture can be used to study protein biogenesis, trafficking, aggregation and degradation.

As reported in previous studies, WT opsin traffic to the membrane is a very efficient process, and most of the synthesized protein can be found in the membrane. We analyzed the location of the RP mutant opsins, and we found that in some cases they showed retention in the ER and also the formation of intracellular inclusions (Figure 4.43), especially for the G90V mutant.

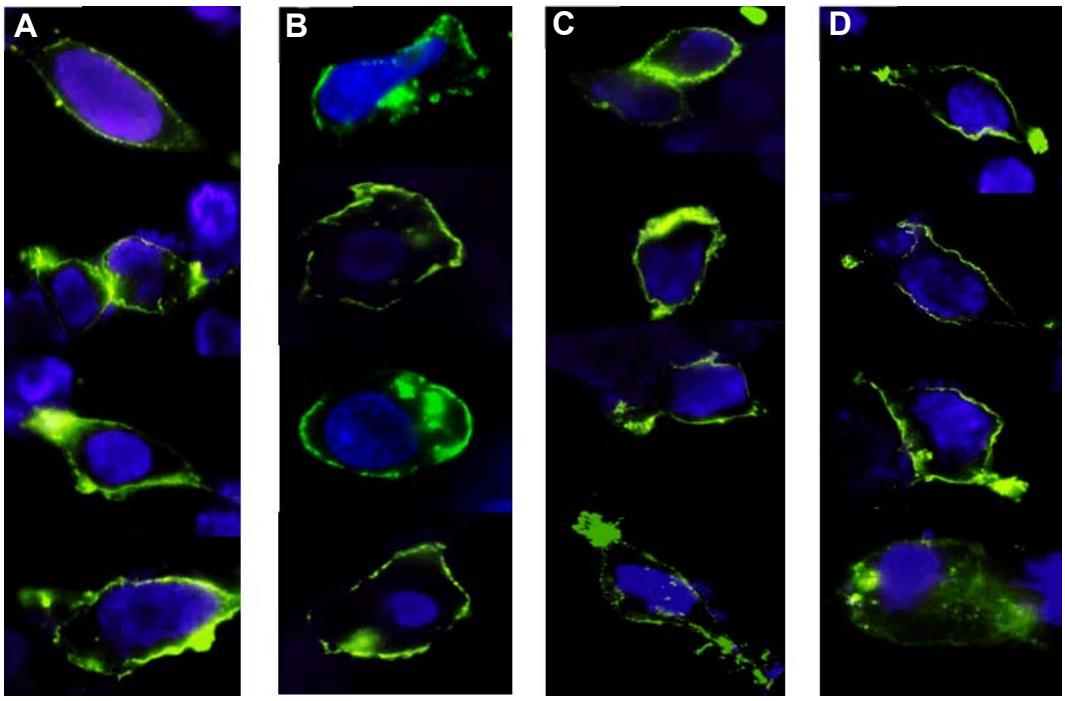

Figure 4.43 Subcellular localization of WT and mutants expressed in HEK 293S GnTI^{-} cells
A. WT Rho. **B**.G90V mutant. **C**. Y102H mutant. **D**.I307N mutant. Cells were immunolocalized 24 h after transfection.

The RP mutants studied here are located in different receptor domains. The Gly90 and Ile307 mutations are found in the transmembrane domain where the helices are closely packed but there is a cavity for retinal binding formed by helices 3,4,5,6 and 7 (Unger et al., 1997). In contrast, Try102 is located at the extracellular domain in E1 loop (Figure 4.42), which is a compact domain that functions as a "retinal plug" including two antiparallel β-sheets in the N- terminus and ECL-II loop. The part of ECL-II that includes Glu 181, penetrates deep into the Rho interior, closer to the chromophore molecule (Palczewski, 2006).

In spite of being found at different domains, the G90V and the Y102H mutants presented a very similar behavior. Both showed a poor performance in the purification process and a higher ratio (A_{280nm}/A_{max}) than the WT indicating a slight problem of protein folding. Likewise, they presented a very similar molar extinction coefficient. Unlike the G90V mutant, Y102H did not present any alteration related to the formation of photointermediaries after illumination and this mutant only showed a slight blue shift of 2 nm instead of the 10-nm blue shift observed for the G90V mutant. In the electrophoretic analysis, in both mutant cases, a prominent band appears below the Rho monomer band that has been reported to correspond to an N-terminal truncated product of opsin. These fragments are recognized by the C-terminal antibody used for Western blot, and having

lost the N-terminus, these fragments would not be glycosylated (Krebs et al., 2010; Tam & Moritz, 2007).

In addition, both mutants showed a great instability in the dark state at high temperature even though the Y102H mutant showed a more compact structure around the SB linkage when compared to the G90V as seen from their hydroxylamine reactivity behavior. Another of the similarities between these two mutants was a somehow lower chromophore regeneration which agrees with the low yield obtained during the purification. It is noteworthy that despite having both lower chromophore regeneration than the WT, the Y102H receptor shows the same regeneration rate than the WT. The same behavior was also noticed in Gt activation where also the Y102H mutant had more similar behavior to that of the WT. This decrease observed in Gt activation correlates well with the results obtained in Meta II decay experiments, where G90V mutant showed a slower rate (about double) but the Y102H mutant showed a $t_{1/2}$ more similar to that of the WT.

In previous studies with the G90V mutant, this behavior has been attributed to an increase in the required space for the valine side chain in comparison to glycine which would be affecting amino acid 113 (Neidhardt et al., 2006) that together with Lys296 are of utmost structural importance in Rho. In dark state Rho, the chromophore is covalently bound by a PSB linkage lo Lys296 at the seventh TM helix. This positive charge is stabilized by an electrostatic interaction with the Glu113 carboxylate side chain that serves as a counterion (Sakmar et al., 1989). If Glu113 is affected, it is likely that the chromophore orientation may be also affected by the amino acid side chain of valine due to the fact that the chromophore is oriented almost parallel to TM 3 involving amino acids 113, 114, 117, 118, and 120. Moreover, the hydrophobic chain in G90V either would not allow a water molecule in the vicinity of Glu 113 and the SB to be accommodated or would decrease the water molecule affinity (Toledo et al., 2011). Such water molecule plays an important role in the deprotonation step of the SB in Meta II (Jastrzebska et al., 2011).

In the case of the Y102H mutant, Tyr102 is a conserved amino acid in the GPCR Rho subfamily (Rakoczy et al., 2011), and for which naturally-occurring mutations at this position had not been reported in humans. The only mutation reported was that by Budzynski et al (2010) in mice to study RP disease. The observed effects caused by this mutation might be related to the fact that Try102 is part of the structural core governing Rho stability. This core includes several clusters, the largest one, in which Tyr102 is found, is located surrounding the conserved disulfide bond between residues Cys110 and Cys187 lining the retinal binding pocket (Iannaccone et al., 2006) (Figure 4.41, amino acid circles in red). 90% of these amino acids were predicted by Floppy Inclusion and Rigid Substructure Topography (FIRST) methodology to be part of the core cause misfolding upon mutation (Rader et al., 2004).

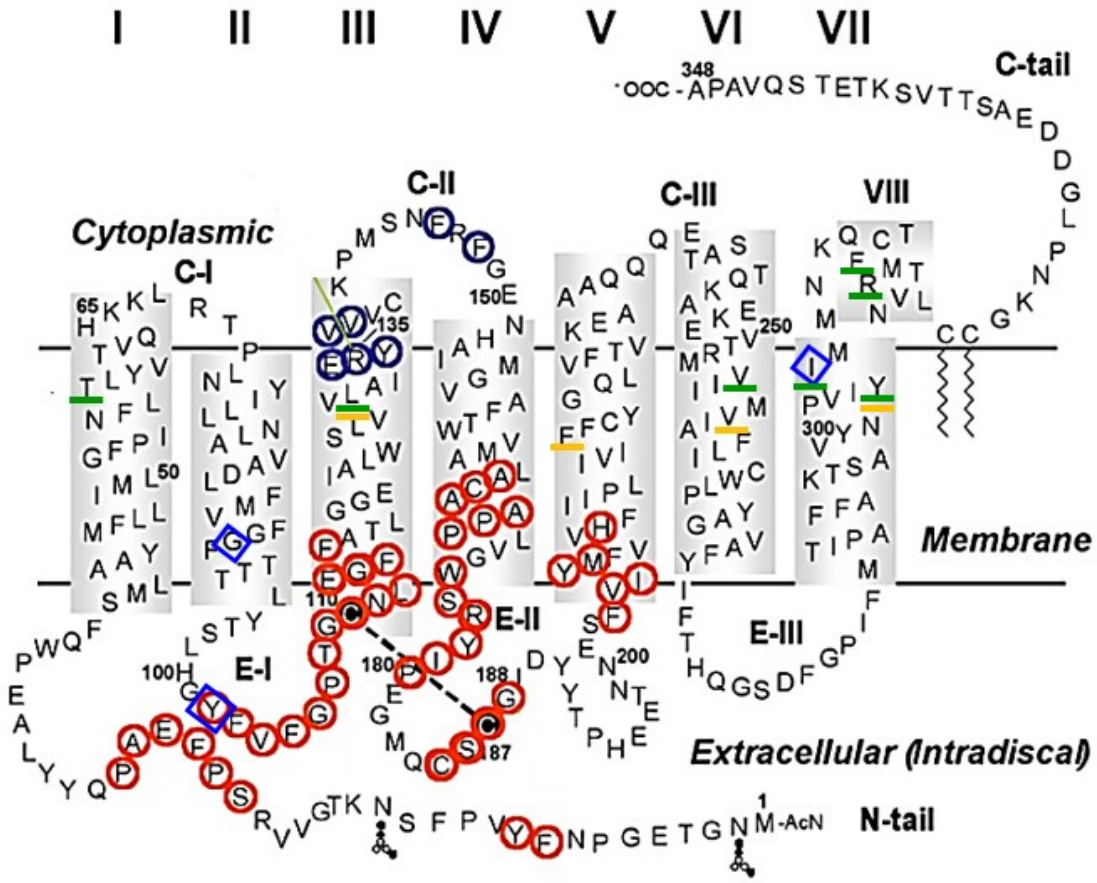

Figure 4.44 Secondary structure model of Rho.
Mutants studied are boxed in blue. Red and blue circles show the two clusters of mutually rigid residues belonging to the core of rhodopsin stability. Amino acids underlined in green are involved in inactive conformation of Rho (L131:V254, T58:Y306, Y306:F313 and I307:R314) Amino acids underlined in orange are involved in Gt activation by the active state of rhodopsin (Y306:L131 and V258:F220) (adapted from Iannaccone et al.,,2006).

The largest core consists of parts of TM helices III-V, and E1 and E2 loops. Specifically, it includes residues 9, 10, 22-27, 102-116, 166-171, 175-180, 185-188, 203-207 and 211. Cys 110 and 187 which form the disulfide bond are also part of this core. Much of this region overlaps with the 11CR binding region which could be related whit the low chromophore regeneration of this mutant.

Ile307 is found in a region further away from the other two mutants, and its thermal stability was not as severely reduced as the other two mutations, accounting for a 80% decrease compared to WT stability. The high percentage and rate of chromophore regeneration together with the slow retinal release in this mutant could be related with the uptake and release of the retinal through the proposed retinal channel. In the Meta II crystal structure, it was noticed that the retinal must go through complex elongation and torsional motions of its polyene chain and of the β–ionone ring during its binding process (Choe et al., 2011). Moreover, the reorganized seven-helical

bundle displays not only the cytoplasmic crevice as a binding site for α-Gt subunit. The reorganization of the TM bundle also provides two openings into the hydrophobic membrane layer namely opening A between TM1 and TM7 and opening B between TM5 and TM6 (Figure 4.45) (Choe et al., 2011; Park et al., 2008; Standfuss et al., 2007).

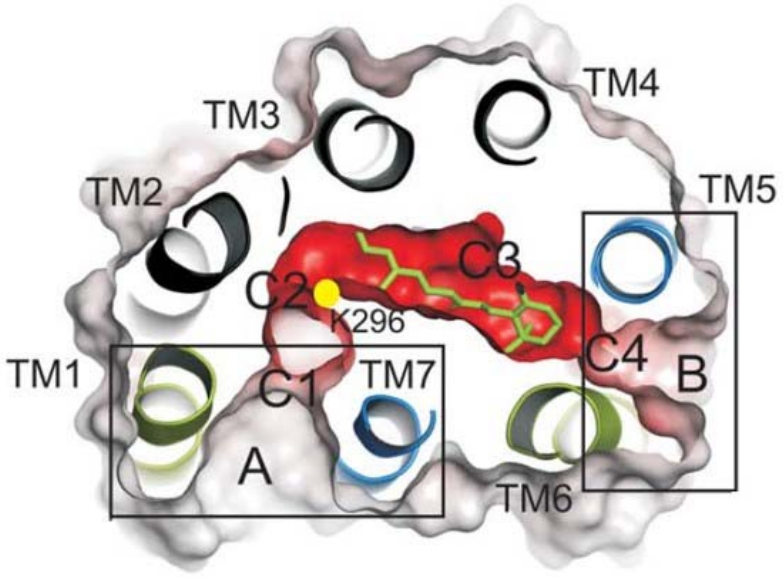

Figure 4.45 Coplanar cut through opsin revealing the channel with openings A and B (from Hildebrand et al., 2012).

A continuous retinal channel through the protein was identified, by means of computational studies, which connects these two nonpolar openings, where the 11CR would be uptaken through opening A and all-*trans*-retinal released through opening B (Hildebrand et al., 2009). It could be possible that the substitution, in TM7, which forms part of opening A, of Ile307 for Asn may improves the entry of 11CR through the channel (Figure 45). However, although studies have been carried out on the effect of channel mutation on uptake and release of the retinal ligand, the mutations did not probe local channel permeability but rather affected global protein dynamics(Piechnick et al., 2012).

Regarding the low Gt activation and its altered kinetics shown by the mutant I307N, recent studies have found that the Ile307 and Try306 play an importer role in the Rho activation pathway (Venkatakrishnan et al., 2016). Upon Rho activation, when retinal isomerises from the 11-*cis* form to the all-*trans* form, due to photon absorption, the β-ionone ring moves up vacating the cavity in the inactive state between TM3, TM5 and TM6 (Tehan et al., 2014). The cytoplasmic side of TM6 moves away from the rest of the TM bundle, exposing several accessible residues which were previously inaccessible. Many of these residues participate in triggering the mechanism for GDP

release in G proteins (Flock et al., 2015). In its inactive state, V254 is engaged in a residue contact with L131, Y306 with T58 and F313 and I307 with R314 (Figure 4.42 underlined in green). Upon activation (Figure 4.42 underlined in orange) V254 breaks the contact with L131 and forms a new contact with Try306 within the highly conserved NPXXY motif of TM7. In the inactive state, Try307 can not engate with L131 because TM7 and TM3 are far apart and require TM6 to move out in order to form a contact. It could be that the mutation at this Ile307 compromises the rearrangement that occurs during the Gt activation in the amino acids Try306 and Ile307 (Venkatakrishnan et al., 2016) and this would be responsible for the altered Gt activation observed in the I307N mutant case.

4.3 Effect of Q, resveratrol (R) and epigallocatechin gallate (EGCG) on WT Rho and the G90V, Y102H and I307N mutants associated with RP

Once the characterization of the mutants was carried out, the effect of the compounds selected in section 4.1, Q, R and EGCG at concentrations of 1 μM, 10 μM and 50 μM were analyzed. During the transfection of WT and mutants into COS-1 cells, these compounds (previously dissolved in DMSO) were added to the cell culture media, yielding the desired concentration of each compound and a maximal DMSO concentration of 0.25%. After 48 h, the cells were harvested and the medium was removed. To completely remove the culture medium and the excess of compounds, the cells were washed twice with 15 mL of PBS. Subsequently, the opsins were regenerated with 11CR ON at 4°, subsequently solubilized in DM and immunopurified.

4.3.1 UV-vis spectroscopic characterization

After immunopurification, the UV-vis spectra of WT and mutants at the different conditions were recorded. Figure 4.46 shows the absorption spectra of WT and mutants obtained after different Q treatments. For both WT and mutants, the protein yield was diminished as the Q concentration increased. The decrease was so drastic at 50 μM that the band at 500 nm was barely detectable.

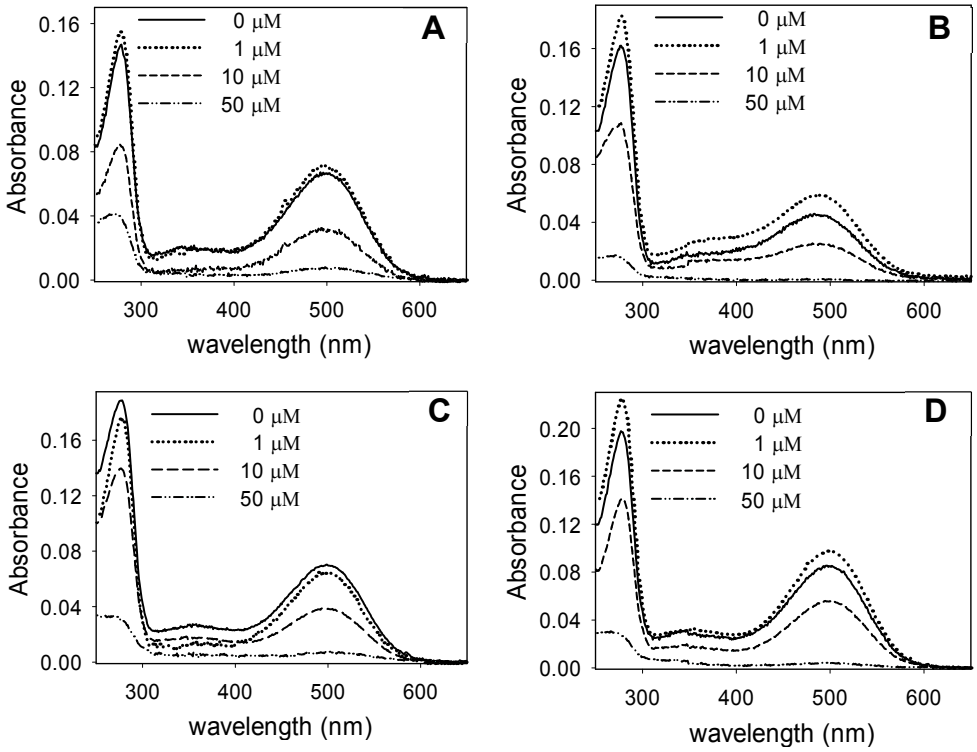

Figure 4.46 Absorption spectra of the immunopurified WT and mutants G90V, Y102H and I307N at different Q treatments.
A. WT Rho. **B**.G90V mutant. **C**. Y102H mutant. **D**.I307N mutant. Samples in PBS pH 7.4 buffer and 0.05% DM. Spectra were recorded at 20°C

Samples treated with R showed the same behavior that those treated with Q (Figure 4.47). As the concentration of R increased the yield of protein was lower. Due the poor protein yield in treatments of Q and R at 50 µM, we decided to exclude this concentration for future experiments. In any event, real-time RT-qPCR experiments were performed to evaluate mRNA levels in order to understand the possible cause of the low protein yield. This assay will be discussed later.

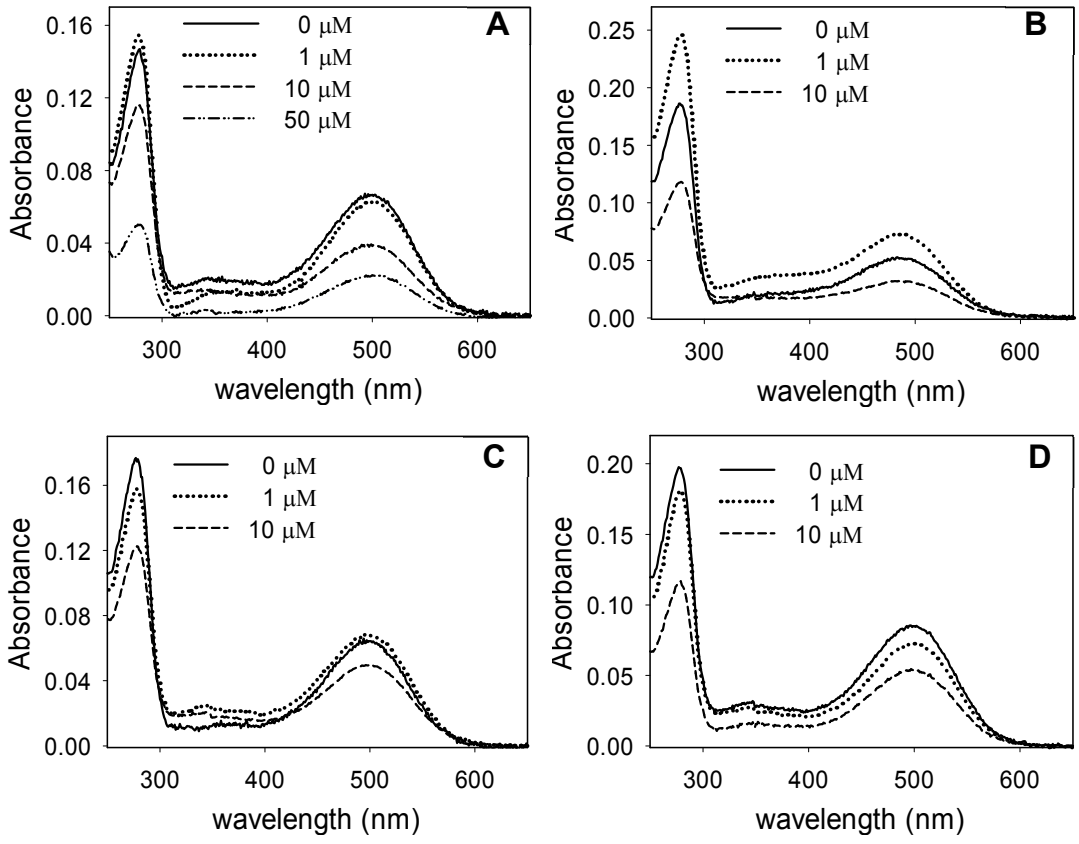

Figure 4.47 Absorption spectra of the immunopurified WT and mutants G90V, Y102H and I307N at different R treatments.
A. WT Rho. **B**. G90V mutant. **C**. Y102H mutant. **D**.I307N mutant. Samples in PBS pH 7.4 and 0.05% DM. Spectra were recorded at 20°C.

For EGCG, its effect on the protein yield was much intense compared to the previous treatments (Figure 4.48), since at 1 µM of EGCG the recovered protein was almost the same than that obtained for the treatments with Q and R at 50 µM. These results are consistent with those obtained in Western blot analyses in section 4.1 in which lower protein content was observed for EGCG-treated samples. For the following tests, the treatments of Q and R were continued only at concentrations of 1µM and 10µM.

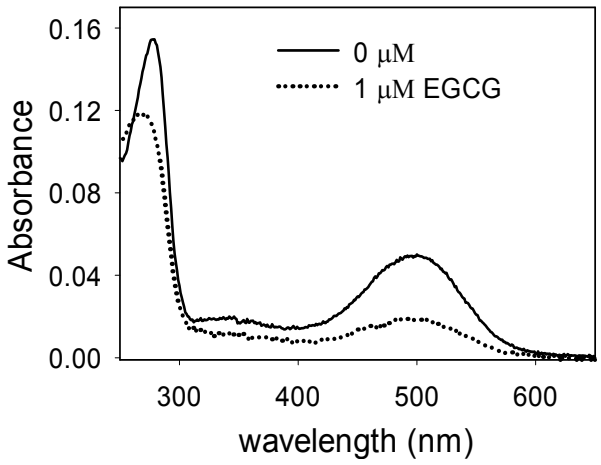

Figure 4.48 Absorption spectra WT and WT expressed in the presence of 1 μM EGCG. Samples in PBS pH 7.4 and 0.05% DM. Spectra were recorded at 20°C.

4.3.2 Photobleaching and acidification

The UV-vis spectra of WT expressed in the presence of Q and R were recorded in the dark, upon illumination for 30 s and after subsequent acidification (Figure 4.49). No differences were observed in the spectroscopic pattern of the WT samples treated with Q and R upon illumination and acidification. In all treatments, the conversion of the 500 nm visible band to 380 nm band corresponding to Meta II was observed. Similarly, after acidification, all samples showed a shift in the band at 380 nm to 440 nm, which is characteristic of PSB linkage between 11CR and opsin.

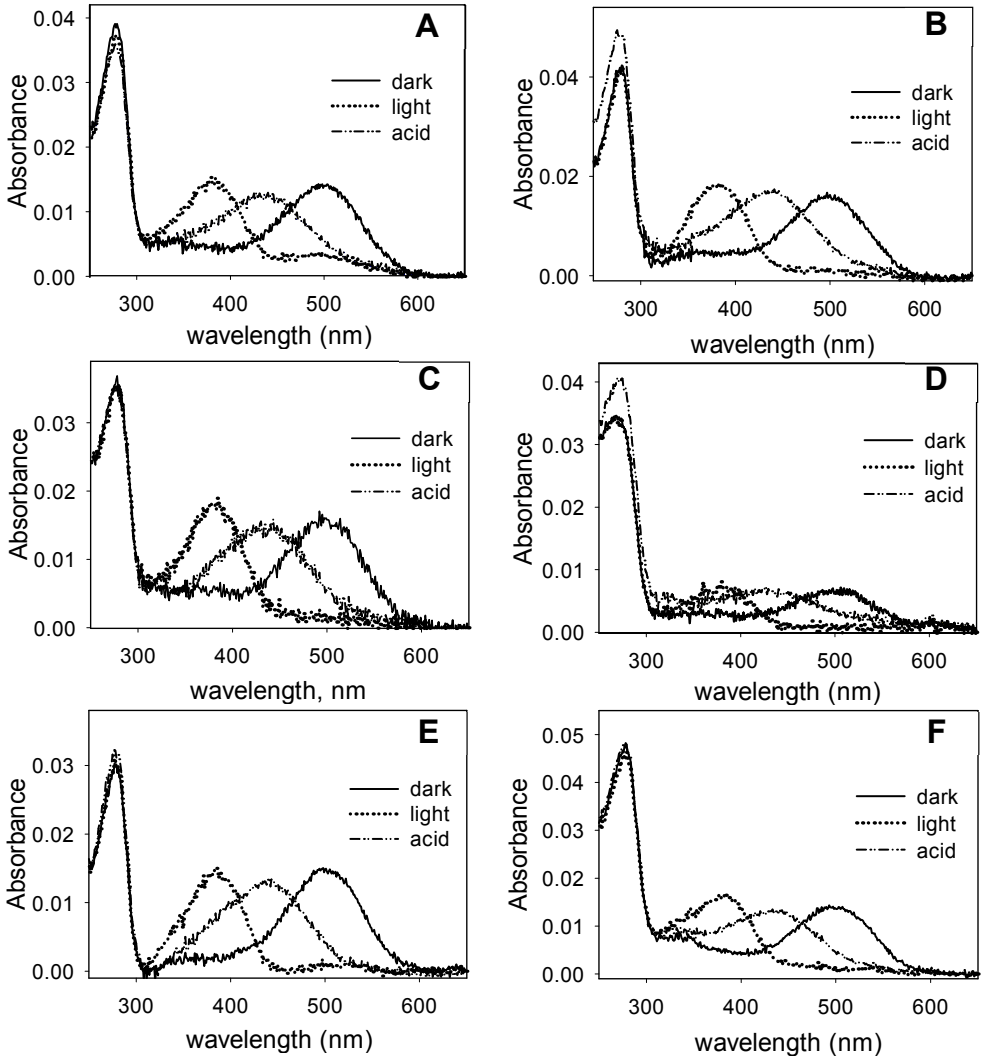

Figure 4.49 UV-vis characterization for the immunopurified WT and WT expressed in the presence of Q and R (1 μM and 10 μM) and 50 μM Q.
A. 0 μM Q. **B**. 1 μM Q. **C**. 10 μM Q. **D**. 50 μM Q. **E**. 1 μM R. **F**. 10 μM R. Samples in PBS pH 7.4 and 0.05% DM. Spectra were recorded at 20°C.

In the case of the G90V mutant, as for WT, no important differences could be observed in the spectroscopic pattern for the treatments with Q and R (Figure 4.50). Only a slight decrease in the remaining band at 490 nm, for G90V, after mutant photoactivation was observed due to the treatments, especially in the case of 1 μM R.

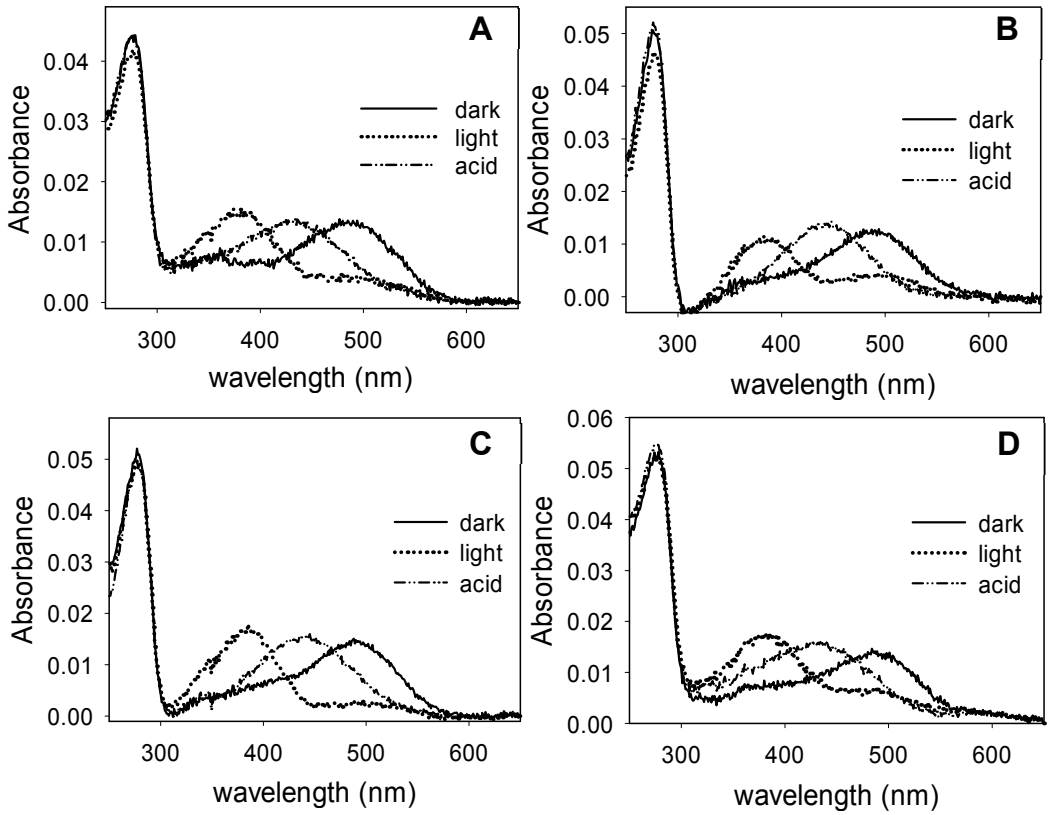

Figure 4.50 UV-vis characterization of the immunopurified G90V mutant expressed in the presence of Q and R.
A. 1 μM Q. **B**. 10 μM Q**. C**.1 μM R. **D**. 10 μM R. Samples in PBS pH 7.4 and 0.05% DM. Spectra were recorded at 20°C.

Neither in the case of the mutants Y102H (Figure 4.51) nor in I307N (Figure 4.52) were differences observed in photobleaching and acidification patterns after Q and R treatments.

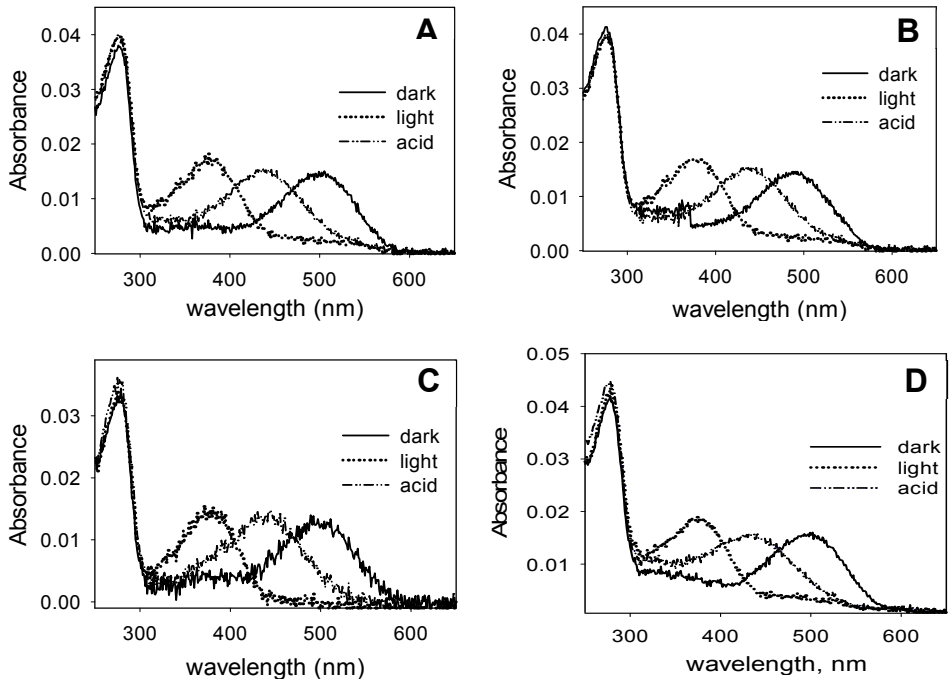

Figure 4.51 UV-vis characterization for the immunopurified Y102H mutant expressed in the presence of Q and R.
A. 1 μM Q. **B**. 10 μM Q**. C**.1 μM R. **D**. 10 μM R. Samples in PBS pH 7.4 and 0.05% DM. Spectra were recorded at 20°C.

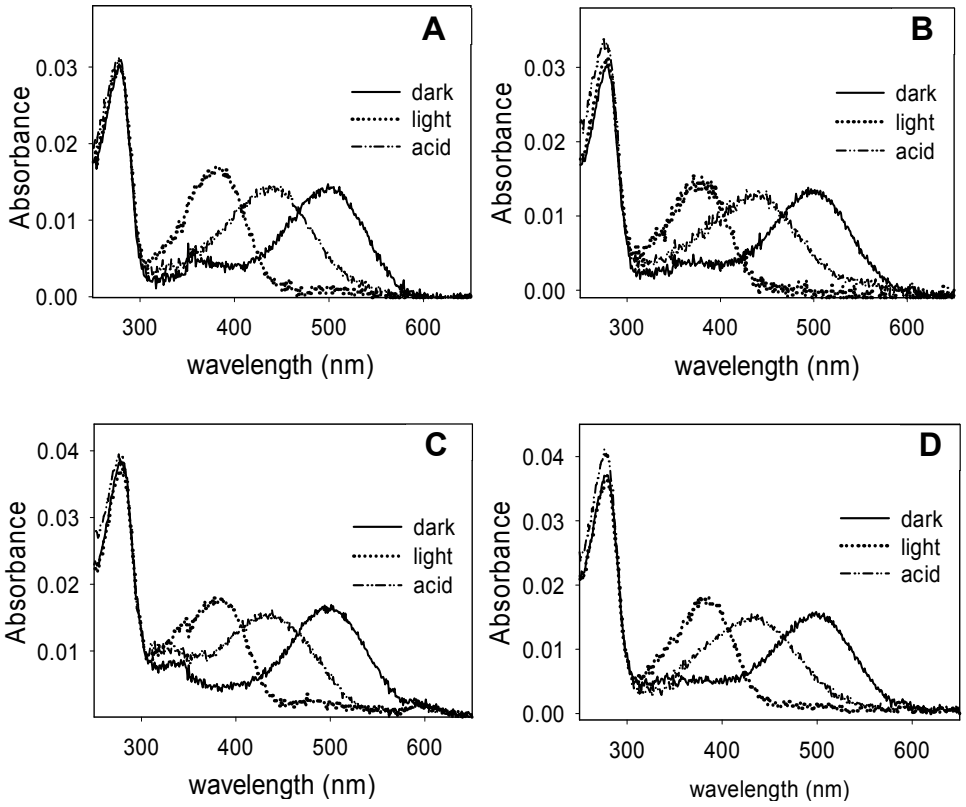

Figure 4.52 UV-vis characterization of the immunopurified I307N mutant expressed in the presence of Q and R (1 μM and 10 μM)
A. 1 μM Q. **B**. 10 μM Q**. C**.1 μM R. **D**. 10 μM R. Samples in PBS pH 7.4 and 0.05% DM. Spectra were recorded at 20°C.

4.3.3 Thermal stability

The thermal stability of WT and mutants was not affected by the treatments with Q and R (Figure 4.53). In the case of the mutant Y102H, 1 μM Q apparently slightly decreased its thermal stability and R at 10 μM slightly increased its stability. However, the differences are not statistically significant.

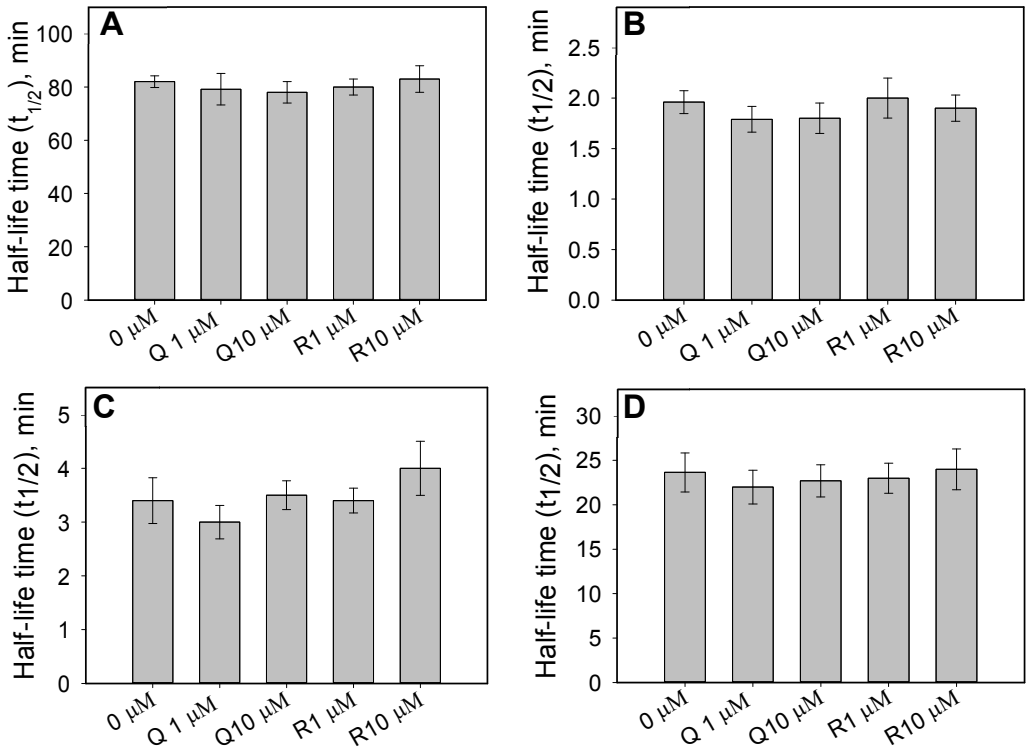

Figure 4.53 Half-life time of the thermal stability of WT and mutants expressed in the presence of Q and R.
A. WT Rho. **B**. G90V mutant. **C**. Y102H mutant. **D**.I307N mutant. Samples purified in PBS pH 7.4 and 0.05% DM, were incubated at 48°C, and the normalized Amax were plotted as a function of incubation time and the $t_{1/2}$ were calculated.

4.3.4 Chemical stability and Meta II decay

Similarly to the thermal stability behavior, the treatments with the compounds had no effect on the structural compaction in the SB environment. Only in the case of the G90V mutant treatments with R 1 and 10 μM there was a somehow increased chemical stability of this mutant (Figure 4.52).

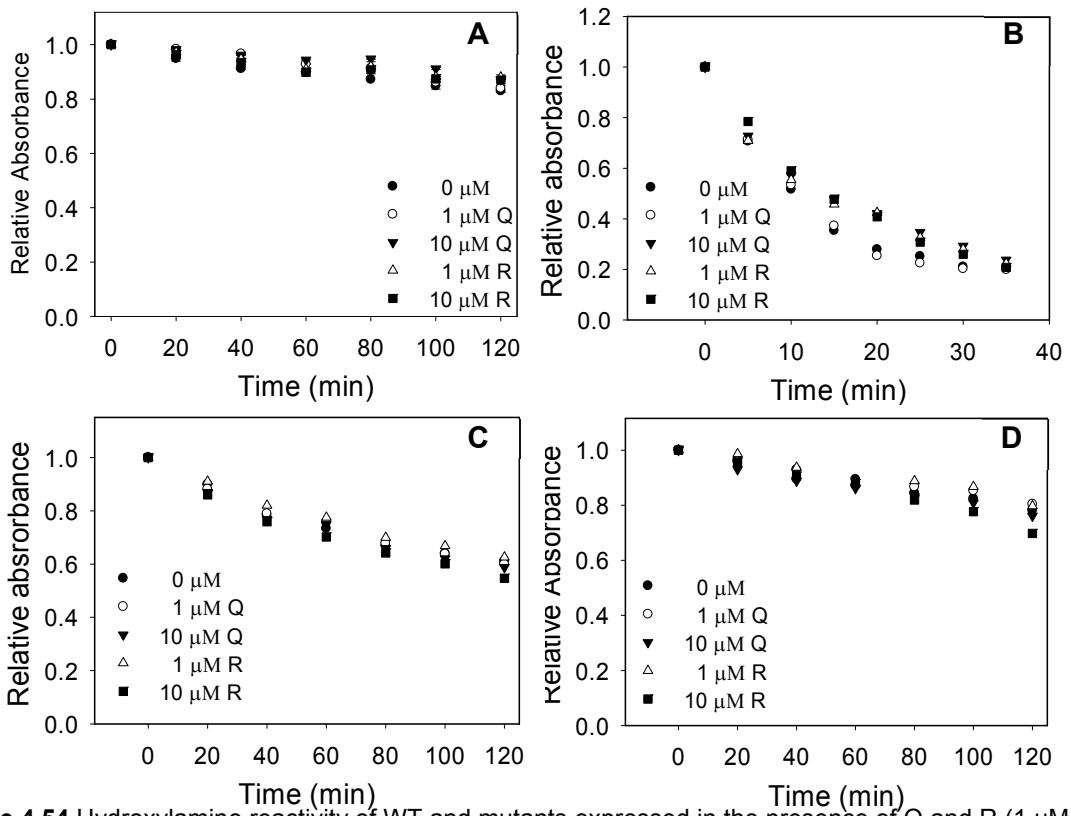

Figure 4.54 Hydroxylamine reactivity of WT and mutants expressed in the presence of Q and R (1 μM and 10 μM).
A. WT Rho. **B**.G90V mutant. **C**. Y102H mutant. **D**.I307N mutant. Samples purified in PBS pH 7.4 and 0.05% DM, were incubated with 50 mM hydroxylamine, pH 7 and the decrease of A_{max} was recorded over time at 20°C.

No significant differences were observed during Meta II hydrolysis and retinal release for the WT and mutants under the different treatments evaluated (Table 4.3).

Table 4.3 Half-life time of retinal release during Meta II hydrolysis of WT and mutants with different treatments of Q and R.

Receptor	**Treatment**				
	0 μM	**1 μM Q**	**10 μM Q**	**1 μM R**	**10 μM R**
WT	13±0.2	13±0.8	13.3±0.5	13.5±0.5	12.5 ±0.6
G90V	36.8 ±1.1	34±1.5	36.0±1.0	35.0±1.5	36.2±1.3
Y102H	18±1.2	17.5±1.0	16.8±1.2	18.5±0.9	17.5±0.7
I307N	21.7±1.4	20.5±1.1	19.5.0±1.5	22.1 ±1.3	21.3±1.0

4.3.5 Chromophore regeneration

In the regeneration assay (Table 4.4), the treatment with 1 μM Q decreased WT regeneration by 25%. None of the treatments had an effect on the percentage of regeneration in the G90V mutant. In the case of the Y102H mutant, R at 10 μM increased its regeneration by 6%. The treatments of 1μM Q, and 1μM and 10 μM R slightly reduced the regeneration for this mutant. Overall the results indicate that the chromophore regeneration is not affected by the compounds studied.

Table 4.4 Chromophore regeneration of WT and mutants at different treatments of Q and R.

Receptor	**Treatment**				
	0 μM	**1 μM Q**	**10 μM Q**	**1 μM Q**	**10 μM Q**
WT	87.5±2.5	65±2.0	89.0±2.0	80.5±3.0	91.0 ±2.5
G90V	71.5 ±1.5	74 ±1.0	70.3±3.0	75.0±1.5	71.0±2.5
Y102H	61±3	61±2.0	60±3.0	63.5±2.0	65.0±3.0
I307N	97±1.5	98.0±1.0	95.0±3.5	94.1 ±2.0	93.0±4.0

4.3.6 Subcellular localization

As mentioned in section 4.2.5, the trafficking of WT opsin to the cell membrane was very efficient in the case of the mutants, no dramatic effects were observed that affect the traffic within the cell. In order to know if the presence of Q and R have any effect on the trafficking of opsins towards the membrane, subcellular localization studies were carried out. As a previous control, an assay was performed to determine if the high concentration of those compounds could be inhibiting the transfection process. For this, an experiment was carried out to monitor the time the cell takes to introduce the plasmid, express the protein and transport it to the membrane. It was observed that opsin is already in the membrane 8 h after transfection (Figure 4.55).

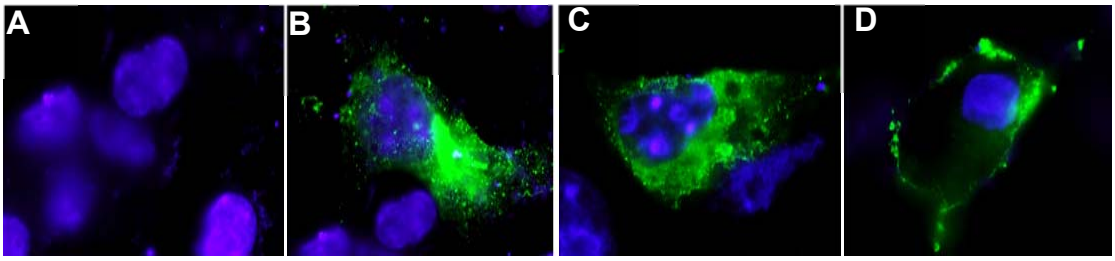

Figure 4.55 Opsin localization in HEK 293S GnTI¯ cells at different transfection times. Localization at 2 h (**A**), 4 h (**B**), 6 h (**C**) and 8 h (**D**) after transfection.

A new experiment was performed with WT by adding 50 μM Q 8 h after transfection. The cells were collected after 48 h, regenerated and the protein immunopurified. Even though Q was added after plasmid insertion, the yield that was obtained after purification continued to be as low as when it was added immediately after transfection (Figure 4.56 A). This result indicates that the lower protein production is not due to Q inhibiting transfection.

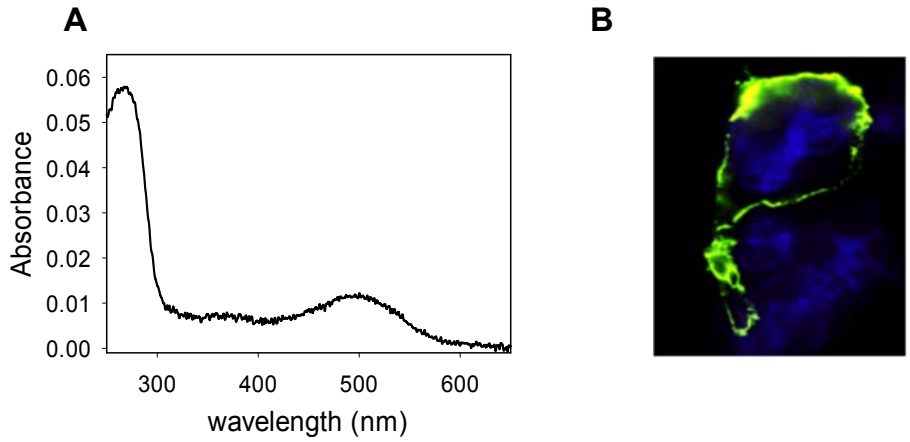

Figure 4.56 UV-vis spectrum of 50 μM WT Rho and opsin subcellular localization
A. UV-vis spectrum of immunopurified WT with 50 μM Q treatment, 8 h after transfection. **B**. Opsin subcellular localization, treatment with 50 μM Q.

In addition, opsin was found on the cell membrane by immunofluorescence analysis (Figure 4.56 B) although the observed amount of transfected cells was much lower compared to WT without treatment.

Table 4.5 shows the images obtained from the immunofluorescence assay of opsin and the mutants subject to Q and R treatments.

Table 4.5 Subcellular localization of opsin and mutated opsins expressed at different concentrations of Q and R.

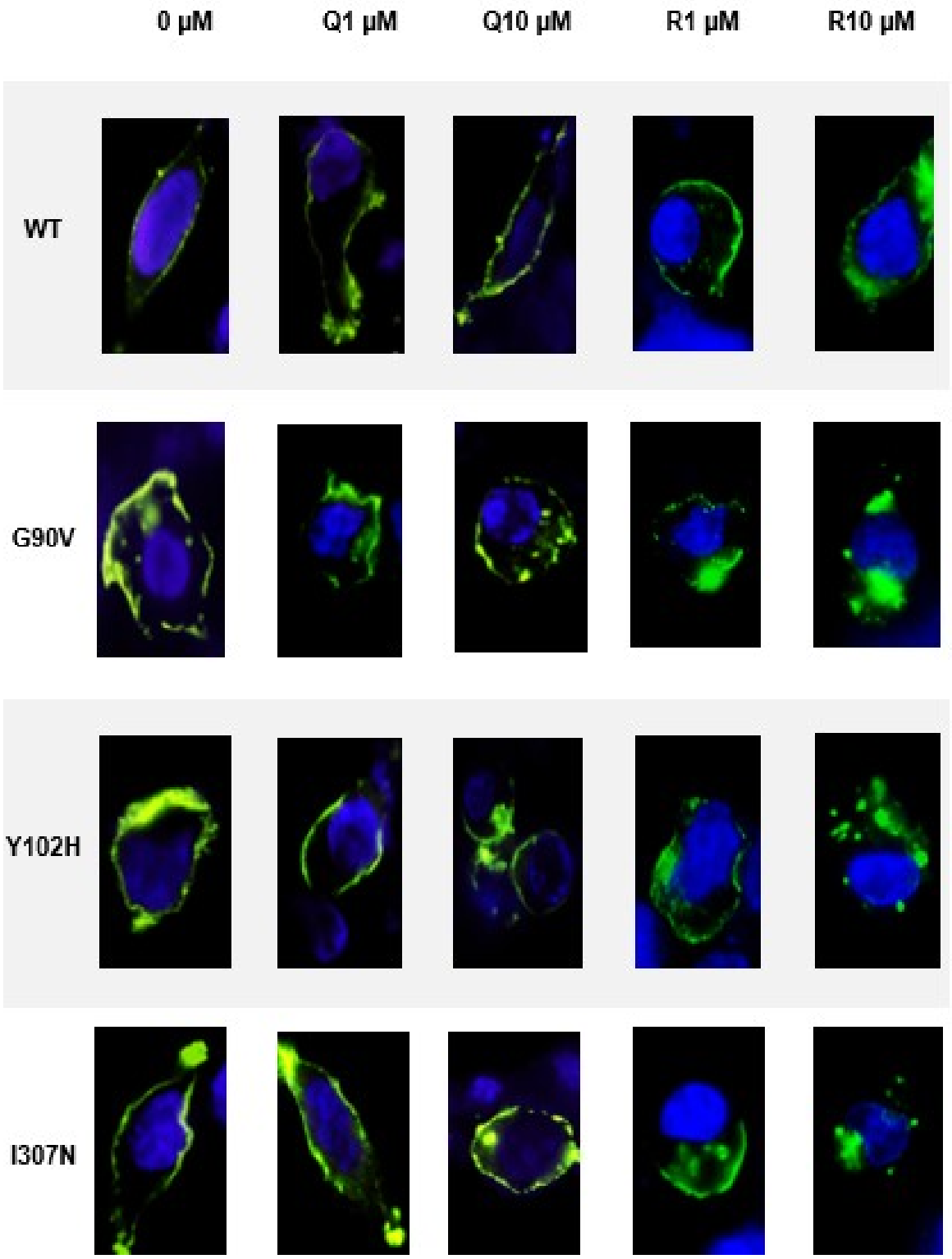

At 1 μM Q, no differences were observed for both WT and mutants. Some inclusion bodies were found at 10 μM Q treatment mainly in the mutants. R was the compound that most affected the trafficking of opsin to the membrane. Inclusion bodies were observed in the WT at 1 μM R as well as for the mutants G90V and I307N in which cases the protein was not able to fully reach the plasma membrane. The most dramatic case was that of the treatment with 10 μM R, where in all mutants the opsin could not be found in the membrane and several inclusion bodies were observed.

4.3.7 SDS-PAGE and Western blot

In order to gain further insight into the causes of the low protein yield obtained during the expression of the receptors in the presence of 50 μM Q, the electrophoretic analysis of these receptors was performed using SDS-PAGE and Western blot. It is well known that chaperones can help stabilizing misfolded proteins. These chaperones aid consists in unfolding the protein for translocation through membranes or for their degradation, and/or aiding them for proper folding and assembly. To determine if these chaperones were present, an elution was performed with 1M NaCl after eluting with the 9-mer peptide in order that the high salt concentration could completely remove any presumably misfolded opsin retained in the sepharose beads.

This process was performed on the WT (Figure 4.57) and mutants G90V (Figure 4.58) and Y102H (Figure 4.59) with and without treatment with 50 μM Q. The protein obtained was analyzed by SDS-PAGE and Western blot.

The UV-vis spectrum of the elution usually performed with buffer and the 9-mer peptide and a second elution with the same buffer but with 1M NaCl added are shown in Figure 4.57 A and B. The absorption spectrum obtained from the 1M NaCl elution showed a largely increased protein band (60%) in the case of the WT treated with 50 μM of Q. This result indicates that after the elution with the 9-mer peptide there was still protein retained in the sepharose beads. However, the band observed shows a displacement of 20 nm being at 260 nm instead of 280 nm. These effects were not observed in WT without treatment.

When performing the SDS-PAGE gel (Figure 4.57 C), no differences were observed in the electrophoretic pattern of the elution with 9-mer peptide compared with the 1M NaCl elution of the untreated WT. However, in the treatment with 50 μM Q, an altered electrophoretic pattern was noticed in the elution carried out with the peptide. For this same sample, the 1M NaCl elution showed the presence of three low molecular weight bands that were not found in the first elution with the 9-mer peptide. These bands correspond to species of apparent molecular weights of 16kDa, 15 kDa and 12 kDa respectively. Western blot analysis (Figure 4.57D) confirmed the altered glycosylation pattern in the WT treated with 50 μM Q showing a great smear in this sample. The low molecular weight bands detected by SDS-PAGE gel in elution with WT NaCl expressed

in the presence of 50 µM Q could correspond to truncated Rho at the N-terminus which could not be detected by Western blot since the 1D4-rho antibody recognizes the C-terminal of Rho.

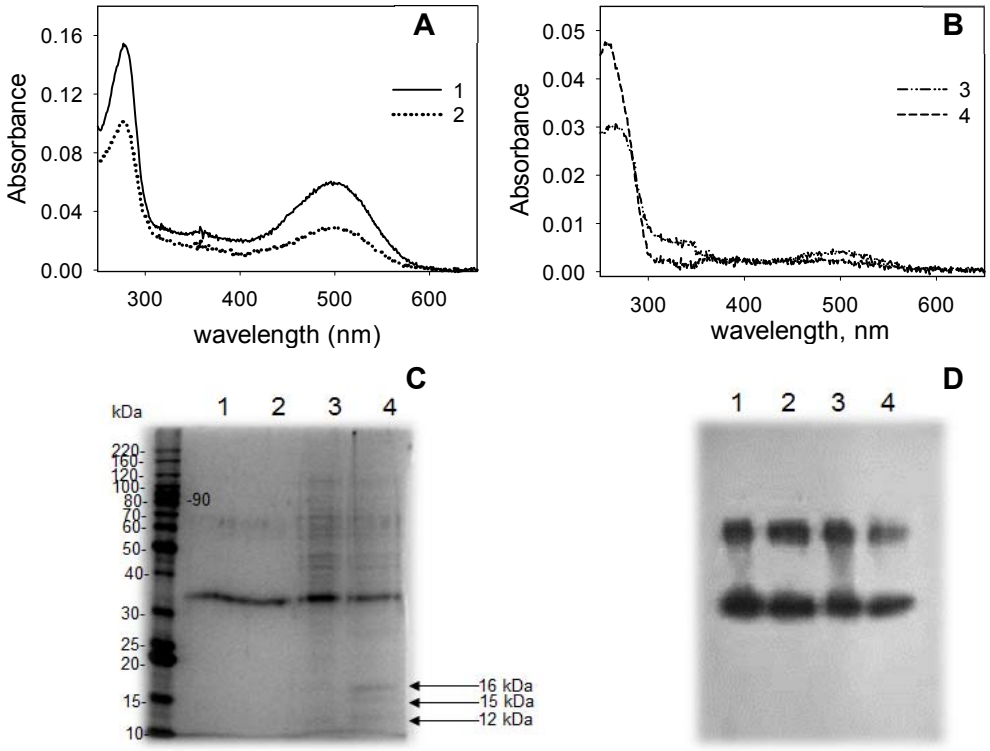

Figure 4.57 Spectroscopic and electrophoretic pattern of WT and WT expressed in presence of 50 µM Q eluted with 9-mer peptide and 1M NaCl.
A. UV-vis spectrum of immunopurified WT eluted with 9-mer peptide in PBS pH 7.4 and 0.05% DM (1) and eluted with 1M NaCl in PBS and 0.05% DM (**2**). **B**. UV-vis spectrum of immunopurified WT expressed in the presence of 50 µM Q eluted with 9-mer peptide in PBS pH 7.4 and 0.05% DM (**3**) and eluted with 1M NaCl in PBS and 0.05% DM (**4**). **C.** SDS-PAGE gel. **D**. Western blot.

In the case of the G90V mutant, the same behavior as the WT was observed (Figure 4.58). For this mutant, the band corresponding to the protein fraction obtained in the elution with NaCl was 5-fold more intense than that of the first elution with the 9-mer peptide. In this case, the low mobility bands could be detected in the Q-treated sample. For this same sample, a band at 120 kDa was observed in the 9-mer pepide elution. Western blot indicated that this band could correspond to a tetrameric form of the G90V mutant.

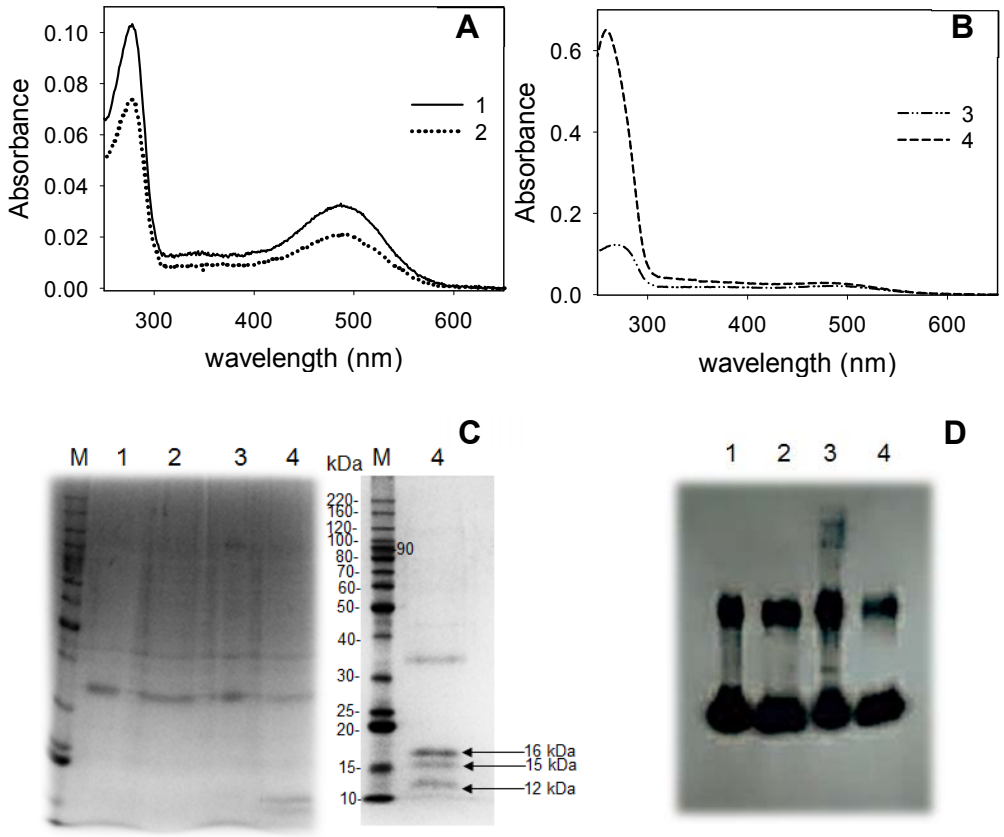

Figure 4.58 Spectroscopic and electrophoretic pattern of G90V and G90V mutant expressed in presence of 50 µM Q eluted with 9-mer peptide and NaCl 1M.
A. UV-vis spectrum of immunopurified G90V mutant eluted with 9-mer peptide in PBS pH 7.4 and 0.05% DM (1) and eluted with 1M NaCl in PBS and 0.05% DM (**2**). B. UV-visible spectrum of immunopurified G90V mutant expressed in the presence of 50 µM Q eluted with 9-mer peptide in PBS pH 7.4 and 0.05% DM (**3**) and eluted with 1M NaCl in PBS and 0.05% DM (**4**). **C.** SDS-PAGE. **D**. Western blot.

Under the same experimental conditions, the Y102H mutant had a similar behavior to that of the WT Rho (Figure 4.59).

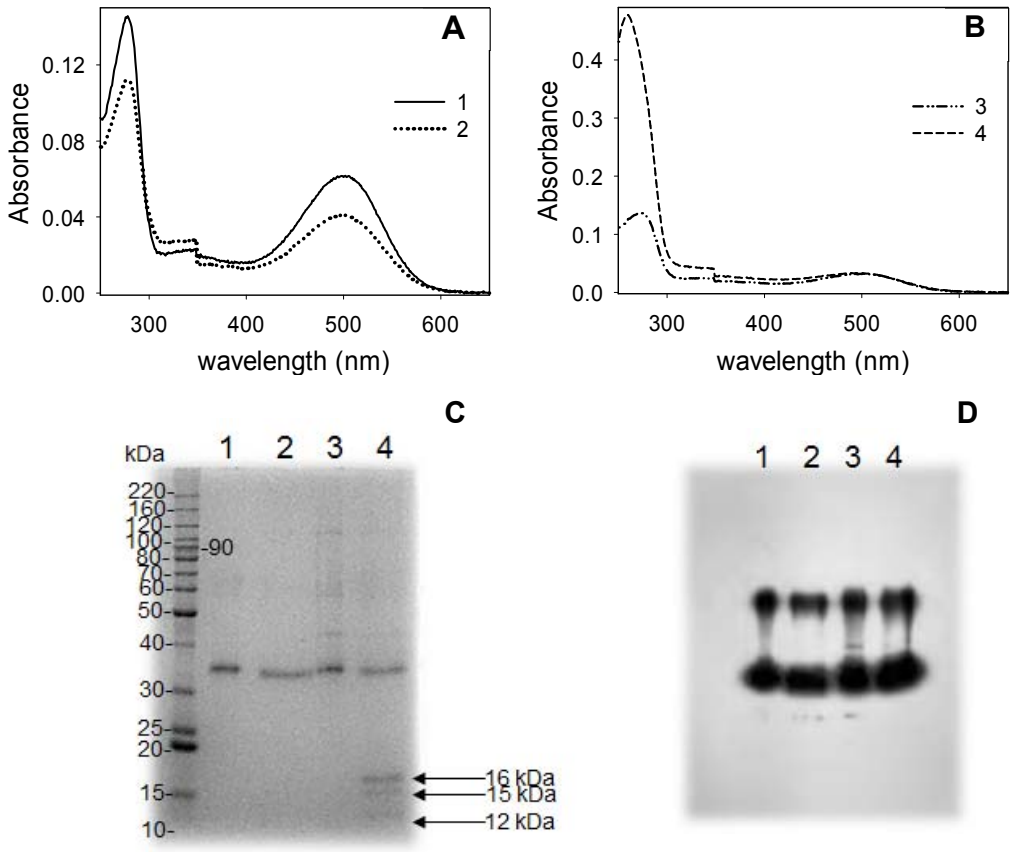

Figure 4.59 Spectroscopic and electrophoretic pattern of Y102H mutant expressed in the presence of 50 μM Q eluted with 9-mer peptide and 1M. NaCl.
A. UV-vis spectrum of immunopurified Y102H mutant eluted with 9-mer peptide in PBS pH 7.4 and 0.05% DM (1) and eluted with 1M NaCl in PBS and 0.05% DM (**2**). B. UV-vis spectrum of immunopurified Y102H mutant expressed in the presence of 50 μM Q eluted with 9-mer peptide in buffer PBS pH 7.4 and 0.05% DM (**3**) and eluted with 1M NaCl in PBS and 0.05% DM (**4**). **C.** SDS-PAGE. **D**. Western blot.

4.3.8 Opsin expression studies in COS-1 cells by means of qRT-PCR

qRT-PCR represents a sensitive and powerful method for the detection of mRNA with a tremendous potential for quantitative applications. Typically, the expression of a target gene is analyzed together with a reference gene to normalize the amount of the PCR template and, thus, to enable the calculation for relative expression of the target gene. Instead of using a standard curve, the target gene expression levels are calculated relative to the reference. In this work, the reference gene was the housekeeping gene β-actin. Opsin expression was evaluated in the case of WT opsin and the G90V and Y102H mutants subject to Q treatments of 1 μM, 10 μM and 50 μM.

4.3.8.1 Isolation and RNA integrity

In qRT-PCR, it is preferable to use high-quality intact RNA as a starting point due to the fact that accuracy of gene expression evaluation is recognized to be influenced by the quantity and quality of the starting RNA. Purity and integrity of RNA are critical elements for the overall success of qRT-PCR analysis. After RNA isolation, its quantity and purity were determined according to section **3.2.9.2**. The amount of total RNA and its purity was determined to be within the established range, the samples were diluted at the same concentration and a denaturing agarose gel was performed to evaluate the integrity of the purified RNA (Figure 4.60). If the analyzed sample showed degradation as was the case of G90V-50μMQ and Y102H and Y102H-50μMQ, a new RNA extraction was carried out ant the analysis was repeated until the obtained RNA was intact.

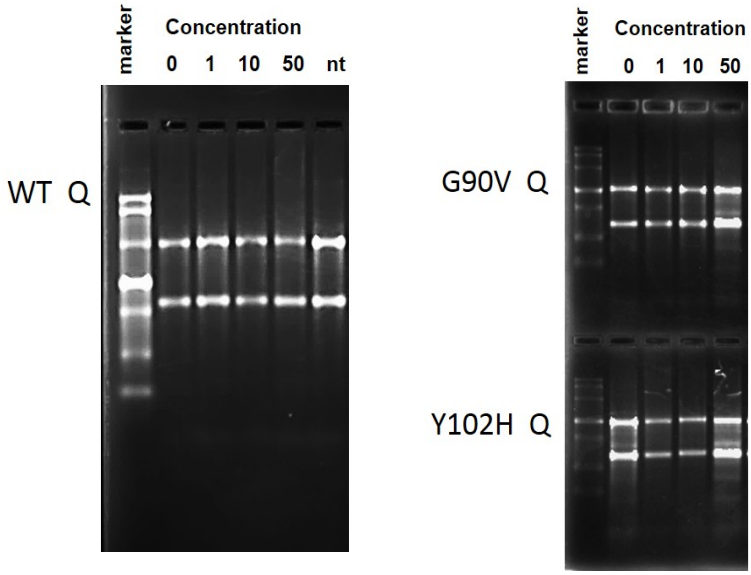

Figure 4.60 Agarose gel of total RNA isolated from the different treatments with Q. Concentration in μM. nt = non-transfected cells.

4.3.8.2 qRT-PCR

Once the RNA quality was confirmed, reverse transcription was performed for cDNA synthesis. To date, internal control genes are most frequently used to normalize de mRNA fraction (Vandesompele et al., 2002). This internal control should not vary in the tissues or cells under investigation, or in response to experimental treatment. In this assay the internal control gene (housekeeping gene) chosen was β-actin. The primers employed for the real-time PCR were the following:

β -Actin:

Forward 5'- CCCCAGGCACCAGGGCGTGAT -3'
Reverse 5'- GGTCATCTTCTCGCGGTTGGCCTTGGGGT -3'

Opsin:

Forward 5′-GTTATCATGGTCATCGC -3’
Reverse 5’-AGACGTCTTGGCAAAGAAA -3’

qRT-PCR was performed in the LightCycler® 2.0 System (Roche) using SYBR green detection. The endpoint used in the real-time PCR quantification, Ct, is defined as the number of cycles required for the fluorescence signal to reach a certain threshold of detection and thus directly correlates with the amount of template (Chey et al., 2010).

The amplification efficiency of both genes was calculated by preparing a dilution series from the cDNA sample. Each dilution series was then amplified in real-time and the Ct values obtained were used to construct standard curves. The amplification efficiency (E) for each target was calculated according to the following equation:

$E = 10^{(-1/S)} - 1$ (S = slope of the standard curve)

The standard curves of opsin and β-actin are shown in Figure 4.61. The amplification efficiencies are comparable since the differences in Ct values of target and reference genes are constant when the amounts of template are varied. The PCR efficiency for the opsin gene was 90% and that for β-actin 93%.

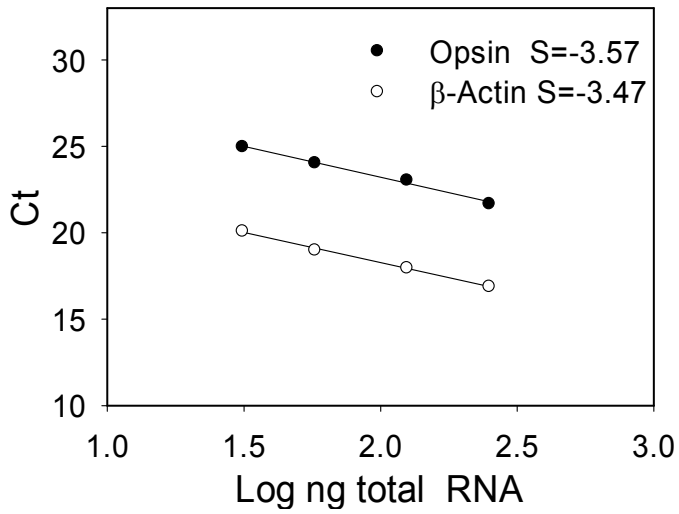

Figure 4.61 Comparison of the amplification efficiencies of opsin and β-Actin genes.

The Ct values of opsin and β-actin of WT and G90V and Y102H mutants at different treatments with Q are shown in Figure 4.62.

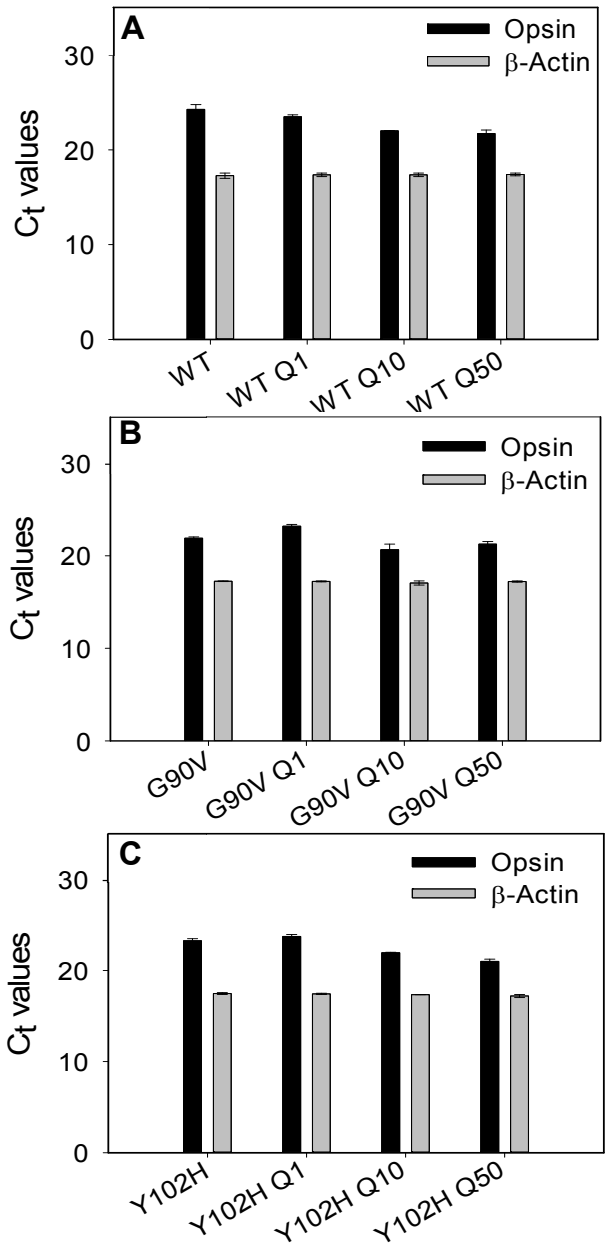

Figure 4.62 Ct values of opsin and β-Actin genes corresponding to different treatments with Q.

It was noticed that the housekeeping gene did not vary in response to the experimental treatment. The average Ct value for the housekeeping gene was 17.3. For the WT, G90V and Y102H mutants significant differences could be detected in Q-treated samples. Gene expression was presented using the $2^{-\Delta\Delta Ct}$ method (Winer et al., 1999) using the following formulas:

Normalized garget gene expression level in sample = $2^{-\Delta\Delta C_T}$

$\Delta\Delta C_T = \Delta C_T$ (sample) - ΔC_T (calibrator) Calibrator = target gene without any treatment

ΔC_T (sample) = C_T target gene – C_T reference gene

ΔC_T (calibrator) = C_T target gene – C_T reference gene

The results showed that the levels of WT opsin expression increased significantly as the concentration of Q increased (Figure 4.63). For mutated G90V opsin, treatment with 1μM Q decreased expression levels by 60% whereas concentrations of 10 μM and 50 μM appeared to increase expression. A similar behavior was observed for the Y102H mutant but the decrease was only 25%.

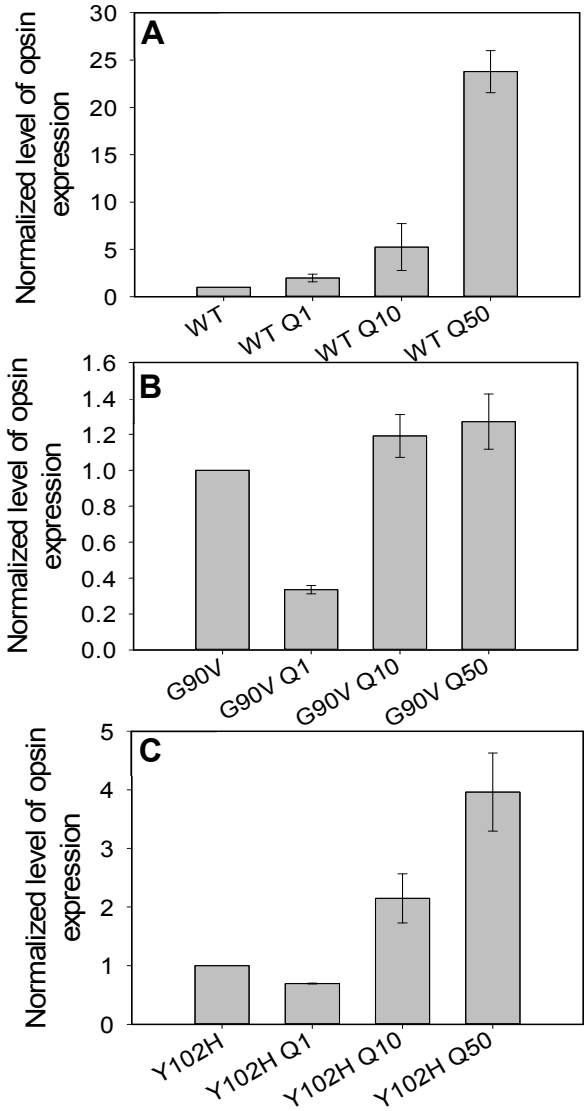

Figure 4.63 Expression of opsin gene and mutated opsins G90V and Y102H at different Q concentrations. **A**. WT. **B**. G90V mutant. **C**. Y102H mutant

The chaperone environment at the cytoplasmic face of the endoplasmic reticulum (ER) plays an important role in the biogenesis of Rho and other GPCRs (Chapple & Cheetham, 2003). In our case, we did not specifically determine the presence of chaperones. For the WT, some bands observed in the SDS-PAGE gel, between 50 kDa and 70 kDa, in the elution with NaCl, could indicate the presence of chaperones, but this was not clearly observed in the mutants case.

When WT opsin is heterologously expressed in cultured mammalian cells, it translocates to the plasma membrane, whereas Rho with misfolding mutations accumulates within the cell. Misfolded opsin does not acquire mature oligosaccharides, indicating that it does not transit through the Golgi apparatus, and also fails to produce a functional receptor. Instead, misfolfed Rho undergoes retro translocation to the ER and degradation by the ubiquitin-proteosome machinery (Saliba et al., 2002). Saturation of the normal proteolytic machinery causes inclusion bodies which were present in nearly all treatments of WT and G90V and Y102H both with Q and R.

Taken together, the results obtained here indicate that the low protein yield eventually obtained for the receptors as the concentration of Q increased, and its poor folding that generated inclusion bodies in the cell, might be due to the fact that the high concentration of Q increased the overexpression of the opsin gene resulting in a highly crowded cytosolic environment enhancing protein aggregation (Hartl & Hayer-Hartl, 2002). The tendency of non-native states to aggregate in the cells is expected to be sharply increased as a result of the high local concentration of nascent chains in polyribosomes and the added effect of macromolecular crowding.

4.4. Binding specificity of retinal analogs influences the allosteric modulation of Q on Rho and G90V mutant associated with RP

As noted in the previous section, no significant effects were detected in the spectroscopic properties of WT and mutants (regenerated with 11CR) at different concentrations of Q and R. The only effect observed was a decrease in protein recovery after purification, at high concentrations of phenolic compounds used, possibly due to mRNA increased production that caused problems in the processing machinery of the cell. 9CR is the most studied analog of retinal that produces isorhodopsin containing a PSB between 9CR and opsin. It undergoes an identical bleaching sequence to that of Rho (regenerated with 11CR) and it is characterized by a blue-shifted A_{max} in the visible band. 9CR is often used as an artificial analog to probe the structure and function of native Rho (Sekharan & Morokuma, 2011).

The pharmaceutical application of 9-cis retinoids to remedy retinal dysfunction caused by delayed or deficient regeneration with 11CR has been investigated over the past decade (Koenekoop et al., 2014; Maeda et al., 2009; Van Hooser et al., 2002). Several properties have been attributed to this retinal analog such as the increase in stability of the RP mutant G90V (Toledo et al., 2011). Hence, these factors increase our interest in carrying out the experiments using the 9CR analog. To this aim, the effect of Q on WT and G90V mutant with its natural chromophore, and its comparison with the opsins regenerated with the 9CR analog, was evaluated.

4.4.1. UV-vis spectroscopic characterization

The UV-vis spectra of WT and G90V mutant Rhos were recorded immediately after immunopurification (Figure 4.64). WT Rho without (WT 11CR) and with treatment of 1 μM Q (WT 11CR-Q) showed a similar spectroscopic pattern with an Amax of 500±1 and 499±2 nm respectively, as well as the ratio (A_{280}/A_{max}) of 2.1±0.2 and 2.2±0.3. In the case of WT isorhodopsin without (WT 9CR) and with treatment (WT 9CR-Q) these also showed a similar spectrum with λmax of 485±3 nm and 486±2 nm and a ratio of 1.86±0.2 and 1.9±0.3 respectively. WT 9CR showed a slight blue shift of 15 nm compared to WT 11CR which may be attributed to the decrease in bond length alternation of the retinal and its interaction with the amino acids in the binding pocket. In the case of G90V mutant without (G90V 11CR) Q treatment, a blue shift of 10 nm was observed, behavior that has already been reported previously (Toledo et al., 2011). In the case of the G90V mutant with 1 μM Q treatment (G90V 11CR-Q), it showed λ_{max} at 488±2 nm and 489±2 nm respectively. A slightly increased ratio was previously reported (Dong et al., 2015; Toledo et al., 2011) that essentially agrees with the results obtained here for G90V 11CR (3.7±0.23). This increase could be due to the introduction of this mutation causes a small fraction of misfolded protein or to the lack of structural stability. In this mutant, the presence of Q reduced its ratio by 15% (3.1±0.2) as well as increased its purification yield.

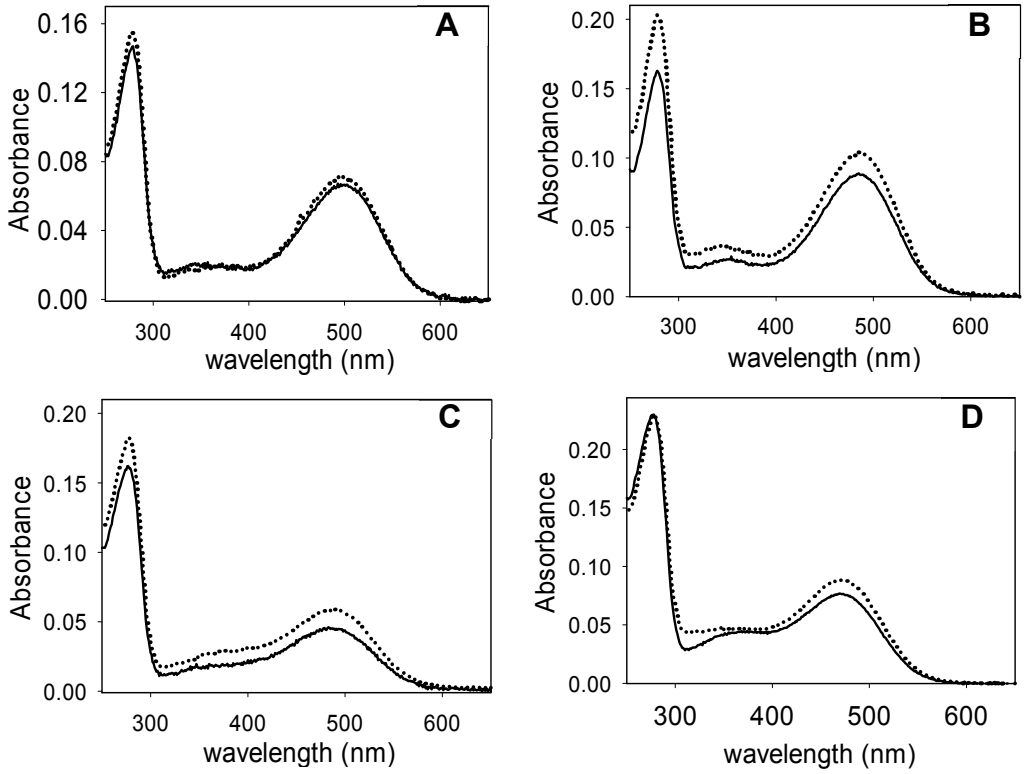

Figure 4.64 Absorption spectra of the immunopurified WT and G90V mutant regenerated with 11-*cis*-retinal (11CR) and 9-*cis*-retinal (9CR).
Solid line represents the receptor without treatment, dotted line represents the receptor with the treatment of 1 µM.Q. Samples in PBS pH 7.4 and 0.05% DM. Spectra were recorded at 20°C. **A.** WT 11CR. **B**. WT 9CR. **C**. G90V 11CR. **D**. G90V 9CR.

G90V 9CR showed a larger blue shift due to the combined effect of the mutation and the 9CR presenting a λmax of 472±3 nm in the case of G90V 9CR and 471±2 for G90V 9CR-Q. In both cases, a higher yield was observed than with 11CR, and the absorbance ratio was more similar to the WT, especially in the case of the G90V 9CR-Q which presented a ratio of 2.5±0.2 whereas in the case of G90V 9CR this ratio was 2.9±0.3.

4.4.2. Photobleaching and acidification

Photobleaching of Rho can be followed by the blue-shift of the 500 nm (A_{max}) chromophoric band in the visible region to 380 nm. This shift is due to the SB nitrogen deprotonation in the Meta II state (Palczewski, 2006). The UV-vis spectra of WT (Figure 4.62) and mutant (Figure 4.65) were recorded in the dark, upon photobleaching for 30s and after subsequent acidification.

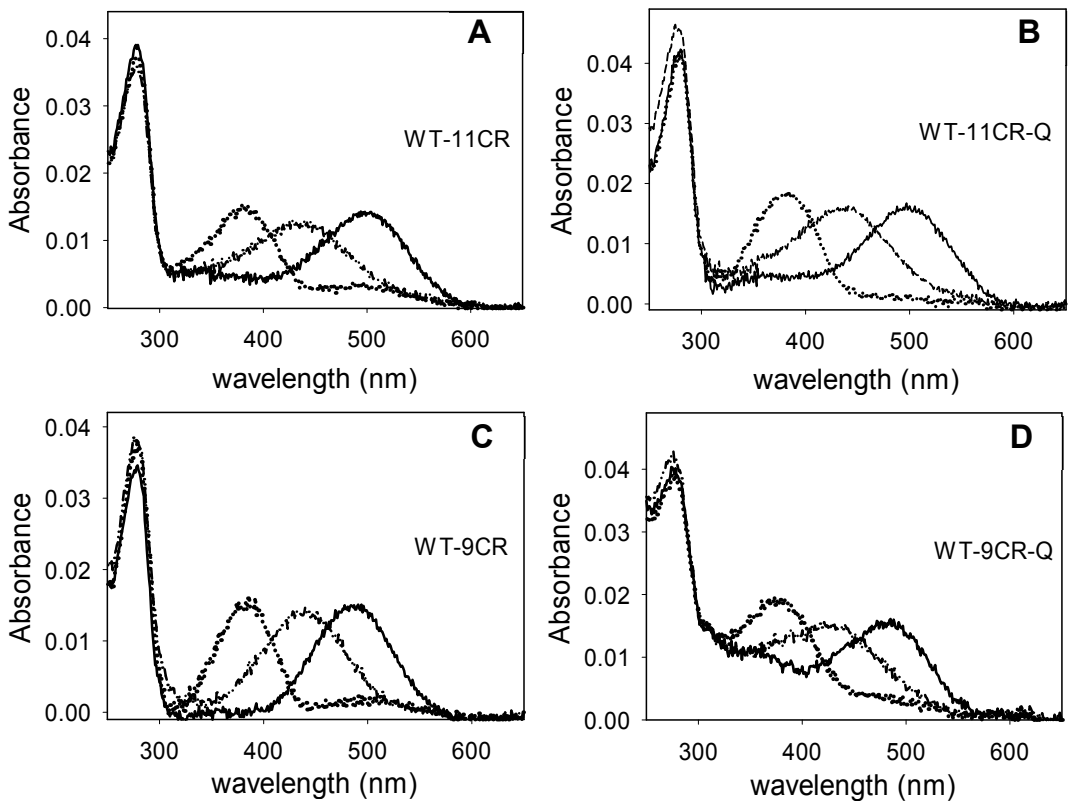

Figure 4.65 UV-vis characterization of WT regenerated with 9CR and 11CR with and without (W/O) 1 µM Q. treatment.
Dark state (solid line), photobleaching (dotted line) and acidification (dashed line). Samples in PBS pH 7.4 and 0.05% DM. Spectra were recorded at 20°C. **A.** WT 11CR. **B**. WT 11CR-Q. **C**. WT 11CR. **D**.WT 9CR-Q.

The largest difference observed was in the case of G90V 11CR (Figure 4.66) which upon illumination did not show a complete conversion of the visible band to the 380 nm species. This remaining band (about 44% of the dark visible band) had a similar visible wavelength maximum as the dark pigment, suggesting conversion to a photointermediate with retinal binding pocket similar to the dark pigment, including the presence of a PSB linkage (Ramon et al., 2014). This effect was diminished by the presence of Q since in G90V 11CR-Q the remaining band upon photobleaching was only about 30%.

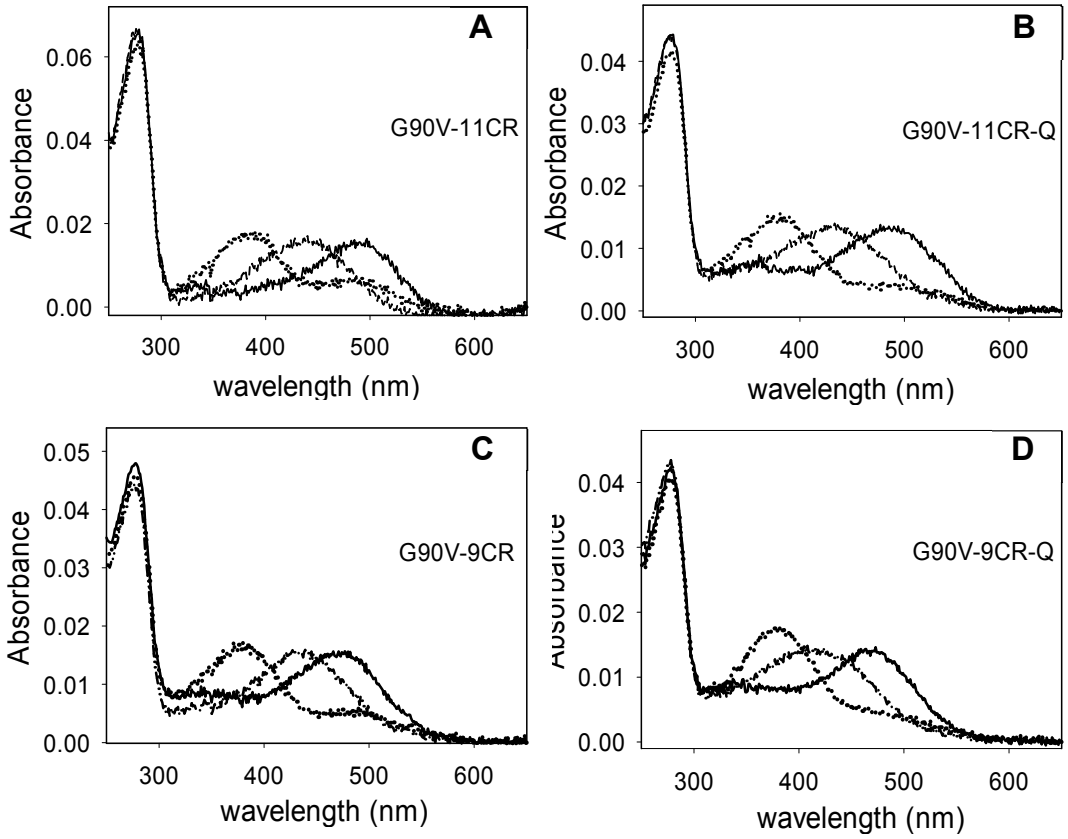

Figure 4.66 UV-vis characterization of G90V mutant regenerated with 9CR and 11CR with and W/O 1 μM Q treatment.
Dark state (solid line), photobleaching (dotted line) and acidification (dashed line). Samples in PBS pH 7.4 and 0.05% DM. Spectra recorded at 20°C. **A.** G90V 11CR. **B**. G90V 11CR-Q. **C**. G90V 11CR. **D**.G90V 9CR-Q.

The change of the natural chromophore to the 9CR analog reduced the effects observed in the remaining Amax band that was only 30% as opposed to 44% for G90V-11CR. In this case, the presence of Q did not affect this measurement.

For all samples, a higher Abs A_{380nm} with regard to the A_{max} was observed after illumination. The acidification of these photoactivated receptors resulted in a distinct behavior, a band with a maximal absorbance at 440 nm corresponding to the PSB except in the case of G90V 9CR-Q which shows an absorbance of 415 nm after acidification. This behavior was previously reported in some Rho mutants (Aguilà et al.; Toledo et al., 2011) but in this case, it is presumably due to the presence of Q. The band obtained by acid denaturation of illuminated G90V 9CR-Q indicated that the SB linkage had undergone partial hydrolysis and this band shows the contributions from both free retinal at 380 nm and PSB-linked species absorbing at about 465 nm.

4.4.3 Thermal stability

In the thermal stability assay, monitored at 48°C, the G90V mutant was very unstable in the dark state compared to the WT, showing faster thermal bleaching with $t_{1/2}$ of ~2 min (Figure 4.64). In the WT, the change of the natural chromophore to the 9CR analog reduced significantly its thermal stability by 30%, an effect that was compensated by Q. In the case of G90V-9CR, it appears that Q can slightly increase the thermal stability of the mutant. Although this effect is not as clear because of the fact that the temperature-induced retinal isomerization and hydrolysis of the deprotonated SB is too fast. The thermal stability of the samples was determined by measuring the samples from 250 nm to 650 nm at various time intervals at the temperature of 48°C. It has been shown that Rho can be activated in the dark by increasing the temperature that would force chromophore isomerization (Liu et al., 2013).

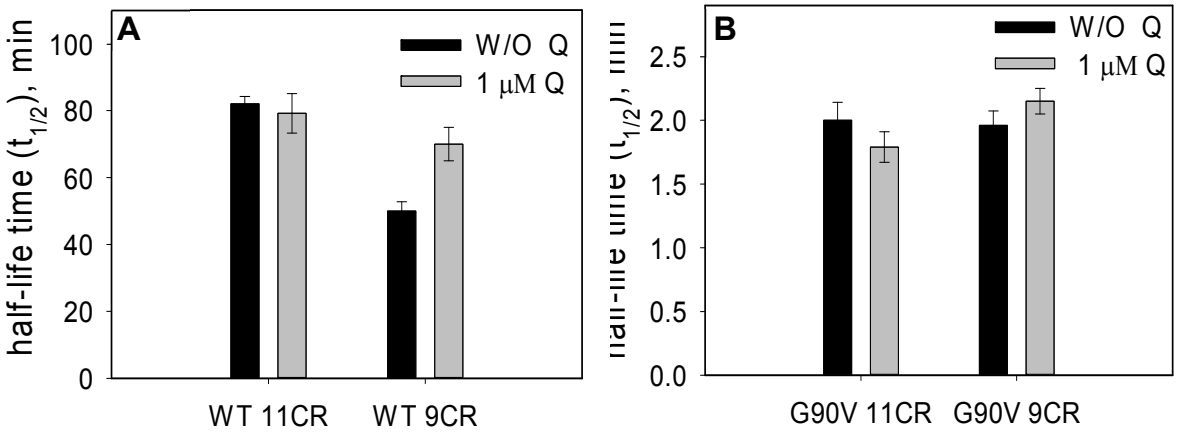

Figure 4.67 Thermal stability of the immunopurified WT and G90V mutant regenerated with 11CR and 9CR.
WT and G90V mutant were regenerated with 11CR or 9CR and immunopurified in PBS pH 7.4 and 0.05% DM, and were incubated at 48 °C. The normalized Abs values at A_{max} were plotted as a function of incubation time and the $t_{1/2}$ was calculated. **A.** WT**. B**. G90V. W/O= without

4.4.4 Chemical stability

WT 11CR is remarkably stable in the presence of hydroxylamine as well as WT 9CR and they showed a linear kinetics for this assay. For the WT 9CR, the presence of Q favors the compaction of the protein preventing hydroxylamine accessibility to the retinal binding site and hydrolysis of the SB linkage. In contrast, G90V 11CR showed a non-linear kinetics and a dramatic decrease due to the less compact structure in the SB linkage environment (Dong et al., 2015; Toledo et al., 2011). In our measurements, Q slightly increased the chemical stability of G90V 11CR-Q. However, for G90V the 9CR analog increased considerably the stability of this mutant and also showed a non-linear kinetics. A similar behavior was previously reported for this mutant (Toledo

et al., 2011). Furthermore, treatment with Q on this mutant receptor further increased the stability of the receptor, which is indicative of a more compact structure of the protein. In addition, it could also be observed that this kinetic behavior was more linear than non-linear, as in the case of WT (Figure 4.68).

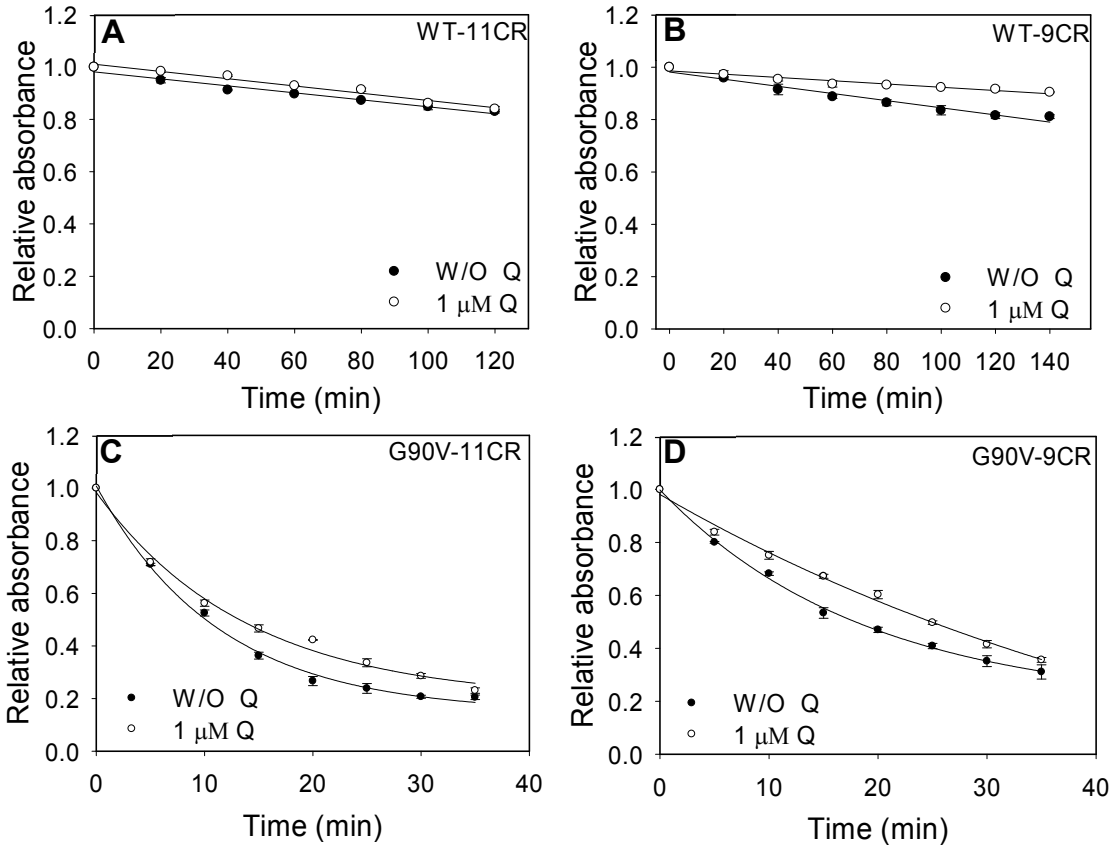

Figure 4.68 Chemical stability of the immunopurified WT and G90V mutant.
Samples immunopurified in PBS pH 7.4 and 0.05% DM after Q treatment, were incubated with 50 mM hydroxylamine, pH 7 and the decrease of A_{max} was recorded over time at 20°C. **A.** WT 11CR with (○) and W/O 1 μM Q (●). **B**. WT 9CR with (○) and W/O 1 μM Q (●). **C**.G90V 11CR with (○) and W/O 1 μM Q (●). D. G90V 9CR with (○) and W/O 1 μM Q (●).

4.4.5. Chromophore regeneration

WT 11CR showed the highest percentage of regeneration which was affected by Q, decreasing the WT 11CR regeneration by 25% (Figure 4.69). In the case of WT 9CR, the regeneration was slightly lower compared to WT regenerated with its natural chromophore 11CR. However, the presence of Q improved the regeneration of WT 9CR which was eventually the same as that of WT 11CR.

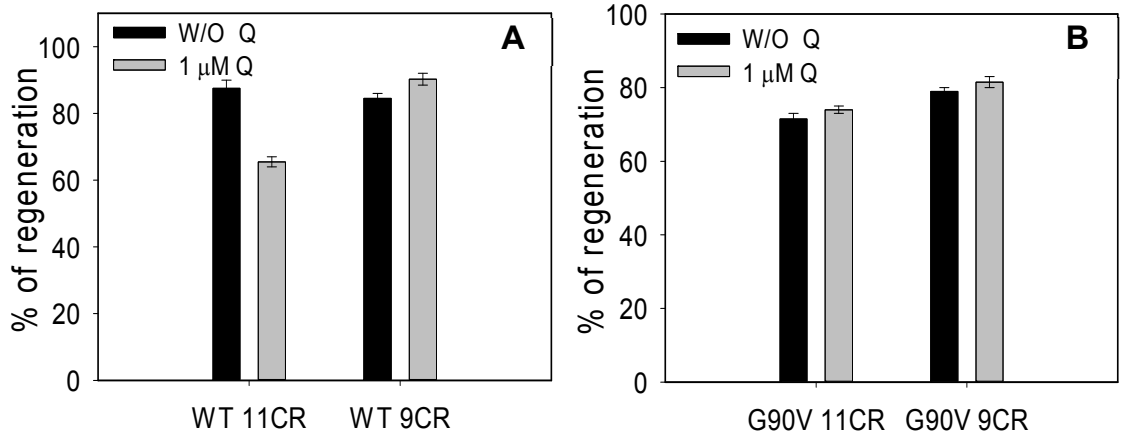

Figure 4.69 Chromophore regeneration of the immunopurified WT and G90V mutant with 1 μM Q. treatment

2.5 fold of 11CR or 9CR was added to the immunopurified WT and the G90V mutant, in the different buffers containing 0.05% DM + 1μM Q, The sample was illuminated with light of > 495 nm to avoid photobleaching of the free retinal, and successive spectra were registered every 5 min at 20°C in the dark until no further increase in A_{max} was detected. The regeneration % was determined from the Abs increase at 500nm with time. **A**. Percentage of chromophore regeneration of WT 11CR and WT 9CR **B**. Percentage of chromophore regeneration of G90V 11CR and G90V 9CR

The G90V mutant presented a lower regeneration compared to that obtained for the WT. For this receptor, the lowest percentage of regeneration was observed when it was regenerated with 11CR. The treatment with 1 μM Q did not affect this percentage. An increase of 8% was observed in this mutant, when using 9CR, upon expression in the presence of Q. This result agrees with the amount of protein obtained during the purification of these receptors where the highest yield was in the G90V 9CR-Q and G90V 9CR cases. This could be attributed to the stronger interaction energy acquired by the C-13 methyl group from Y268 and W265, favoring the entry into the retinal binding site (Srinivasan et al., 2014).

The initial velocities of regeneration (Table 4.6) coincide with the results obtained from the regeneration percentage with the exception of WT 11CR-Q which showed the lowest percentage of regeneration but its velocity was slightly higher than that of WT-11CR-Q.

Table 4.6 Initial velocities of chromophore regeneration.

		Initial velocity (min^{-1})			
WT 11CR	W/O* Q	2.20 ± 0.167	0.30 ±0.005	W/O Q	**G90V 11CR**
	1 μM Q	2.65 ± 0.190	0.44 ± 0.01	1 μM Q	
WT 9CR	W/O Q	3.05 ±0.155	0.56 ± 0.02	W/O Q	**G90V 9CR**
	1 μM Q	4.60 ± 0.250	0.92 ± 0.05	1 μM Q	

During the experiments, a second protein elution was performed to recover as much protein as possible. This second elution was done in PBS pH 6 and used in the regeneration experiments. When it was possible, up to a third elution was carried out in the samples that showed a higher yield, as was the case in the treatments with Q in the receptors regenerated with 9CR. When the absorption spectrum of the third elution of G90V 9CR-Q was recorded, a different spectroscopic pattern was observed and two more bands appeared, one large and marked at 310 nm and a small shoulder at 360 nm. In addition, the band a 280 nm representing the protein fraction showed a red shift of 4 nm (Figure 4.70).

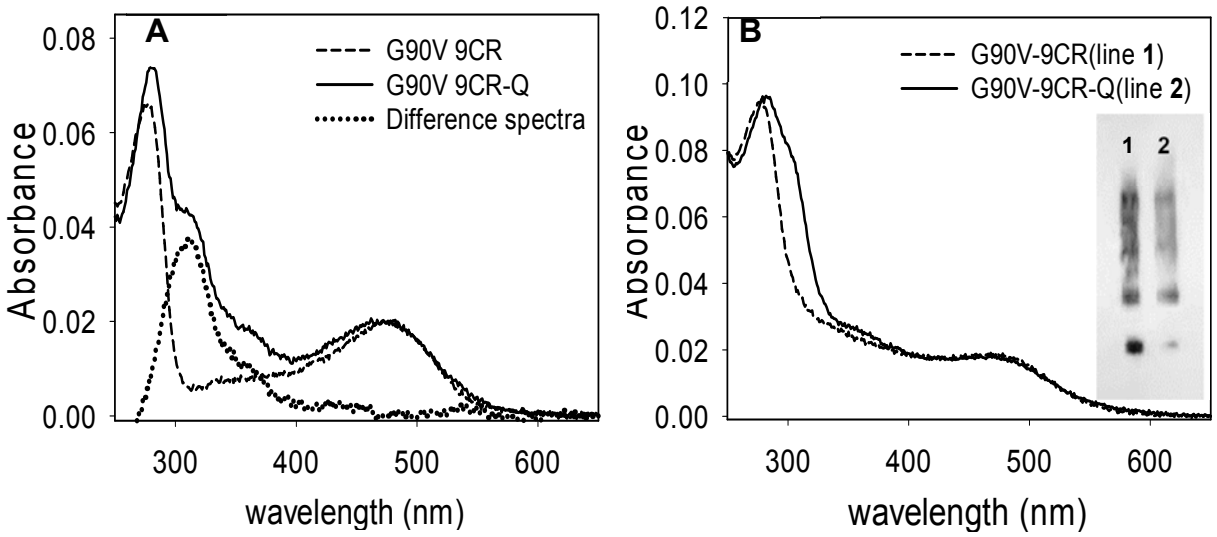

Figure 4.70 Q identification in immunopurified G90V 9CR mutant.

UV-vis spectra of G90V 9CR and G90V 9CR-Q first (**A**) and second (**B**) independent purifications. Inset Western blot of both samples

A new independent experiment was carried out under the same conditions and the same bands were observed but not in the same amount as in the previous one (compare Figures 4.70 A and B). These results indicated that Q could actually be bound to the protein and this interaction had survived the purification process. In order to confirm the Q presence, a HPLC-ESI-MS/MS study was performed that would be later described.

In addition, the Western blot of these samples was performed and the G90V 9CR-Q mutant showed reduced intensity in the band corresponding to truncated protein.

4.4.6 Meta II decay measurement

The stability of the active state of purified WT and mutant was carried out by means of fluorescence spectroscopy. In dark state, Trp265 fluorescence is quenched by the β-ionone ring of the retinal and, upon illumination, retinal is released from the protein binding pocket thereby resulting in an increase in Trp265 fluorescence emission which can be followed at 330 nm at an

excitation wavelength of 295 nm. The fluorescence changes were monitored continuously over time (Farrens & Khorana, 1995). To determine the $t_{1/2}$ values for retinal release, experimental data was analyzed using a mono-exponential rise to maxima fit.

The Meta II hydrolysis was slightly slower for WT 9CR than for WT 11CR. In both cases, the $t_{1/2}$ was not affected by Q. G90V 11CR mutant showed a higher difference compared to the WTs with a $t_{1/2}$ of 36 ± 1.13 which is twice slower. For this mutant, regenerated with its natural chromophore, the presence of Q did not affect the Meta II decay (Figure 4.71).

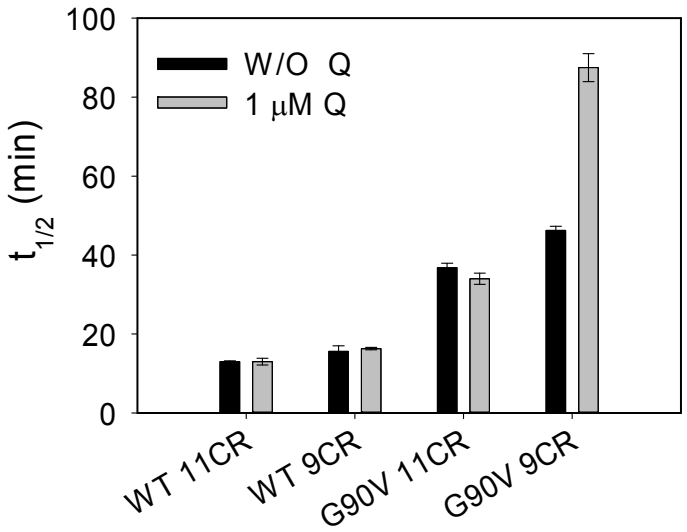

Figure 4.71 Meta II decay of the immunopurified WT and G90V mutant regenerated with 11CR or 9CR with or W/O 1 µM Q treatment
Samples were incubate at 20 °C, and after a steady base line was obtained, they were photobleached and the Trp fluorescence was monitored over the time The fluorescence increase was fit to a single exponential function and the $t_{1/2}$ calculated.

The reverse case was observed when the G90V mutant was regenerated with 9CR analog in which the hydrolysis of the photointermediates Meta II was slower (46 min) compared to the G90V 11CR. Strikingly, in this case the presence of Q almost doubled the hydrolysis rate of Meta II with a $t_{1/2}$ of 88 min.

4.4.7 Gt activation

In this assay, Gt activation by WT and mutant was measured in the dark and after photobleaching. A similar kinetics behavior for WT 11CR and WT 9CR was observed (Figure 4.69). In the case of WT 11CR-Q the activation velocity was slightly faster than in the case of WT 11CR. Surprisingly, the WT 9CR-Q showed a completely different kinetics to the hyperbolic kinetics presented by WT. In this case the kinetics is sigmoidal which clearly would reflect cooperative binding (Figure 4.72).

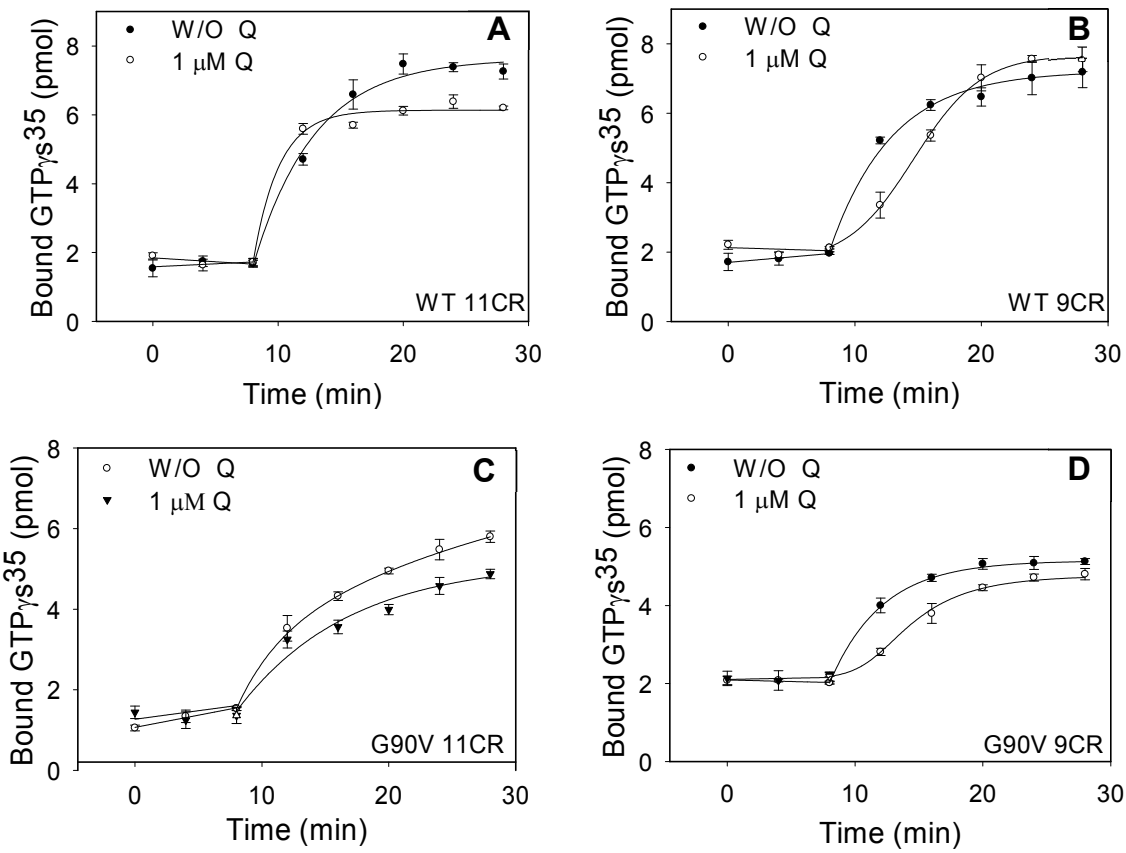

Figure 4.72 Gt activation by WT and G90V mutant regenerated with 11CR or 9CR with or W/O 1 μM Q treatment.
Gt activity was measured by means of a radionucleotide filter-binding assay in Gt buffer. The reaction was initiated by the addition of the WT or mutant, and samples were filtrated at different times in the dark and after illumination. **A.** WT 11CR with (○) and W/O 1 μM Q (●). **B**. WT 9CR with (○) and W/O 1 μM Q (●). **C**.G90V 11CR with (○) and W/O 1 μM Q (●). D. G90V 9CR with (○) and W/O 1 μM Q (●).

G90V 11CR showed a similar kinetics to that of WT 11CR but in this case the rate of Gt activation was slower compared to WT 11CR. The presence of Q during the expression decreased its Gt activation rate. This demeanor observed in the Gt activation for this mutant, correlates very well with the results obtained in the Meta II decay experiments where the all-*trans*-retinal release as consequence of Meta II hydrolysis is slower with respect to WT 11CR. For G90V 9CR-Q the Gt activity was slower compared to the mutant without treatment. In the case of the mutant regenerated with the 9CR analog, the same effect than in the WT 9CR case could be observed. Of all treatments, the G90V 9CR-Q showed the lowest Gt activation and could be correlated with its high $t_{1/2}$ in the Meta II decay assay. These results suggest again that Q is likely bound to the immunopurified receptors.

4.4.8. Q identification by HPLC-ESI-MS/MS

For the mass spectrometry study, Q standard was run at a concentration of 1 ppm (Figure 4.73) and it was found at a retention time of 3.97 min.

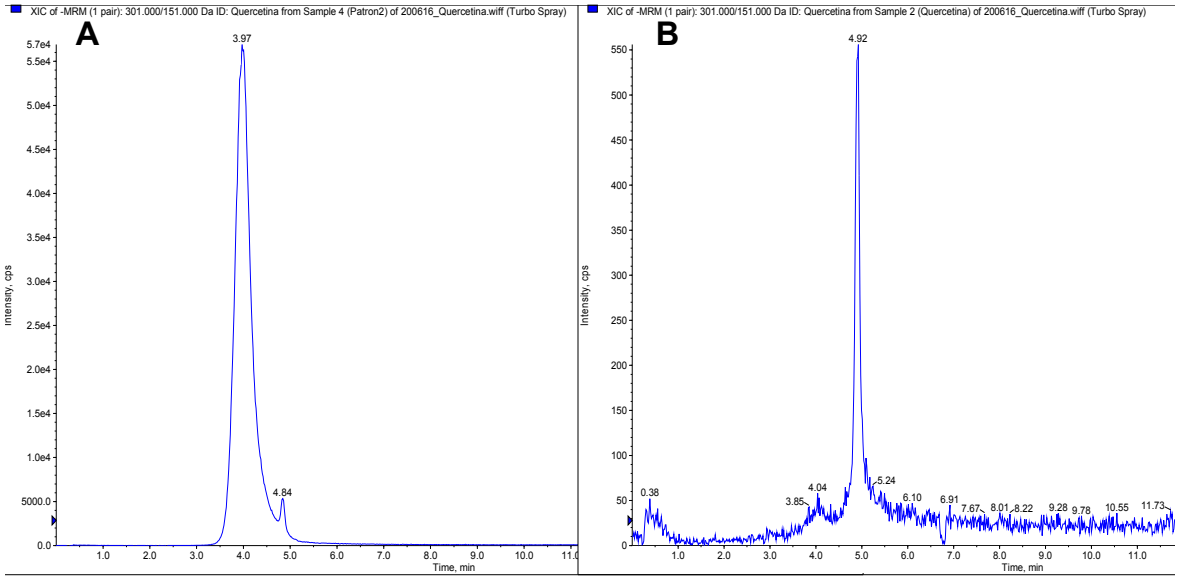

Figure 4.73 Q identification by HPLC-MS
A. Extracted-ion chromatogram of Q standard (**A**) and Q extracted from G90V 9CR-Q (**B**), and mass spectrum of Q standard (**C**) and Q extracted from G90V 9CR-Q (**D**)

In the sample, a presence of a peak at one minute displaced compared to the retention time of Q was observed. To ensure that this peak corresponds to Q, a product ion scan of both the sample and the standard was done (Figure 4.74). In this experiment the ions characteristics of Q could be found in the sample. The concentration detected was 0.0035 ppm (0.0115 µM).

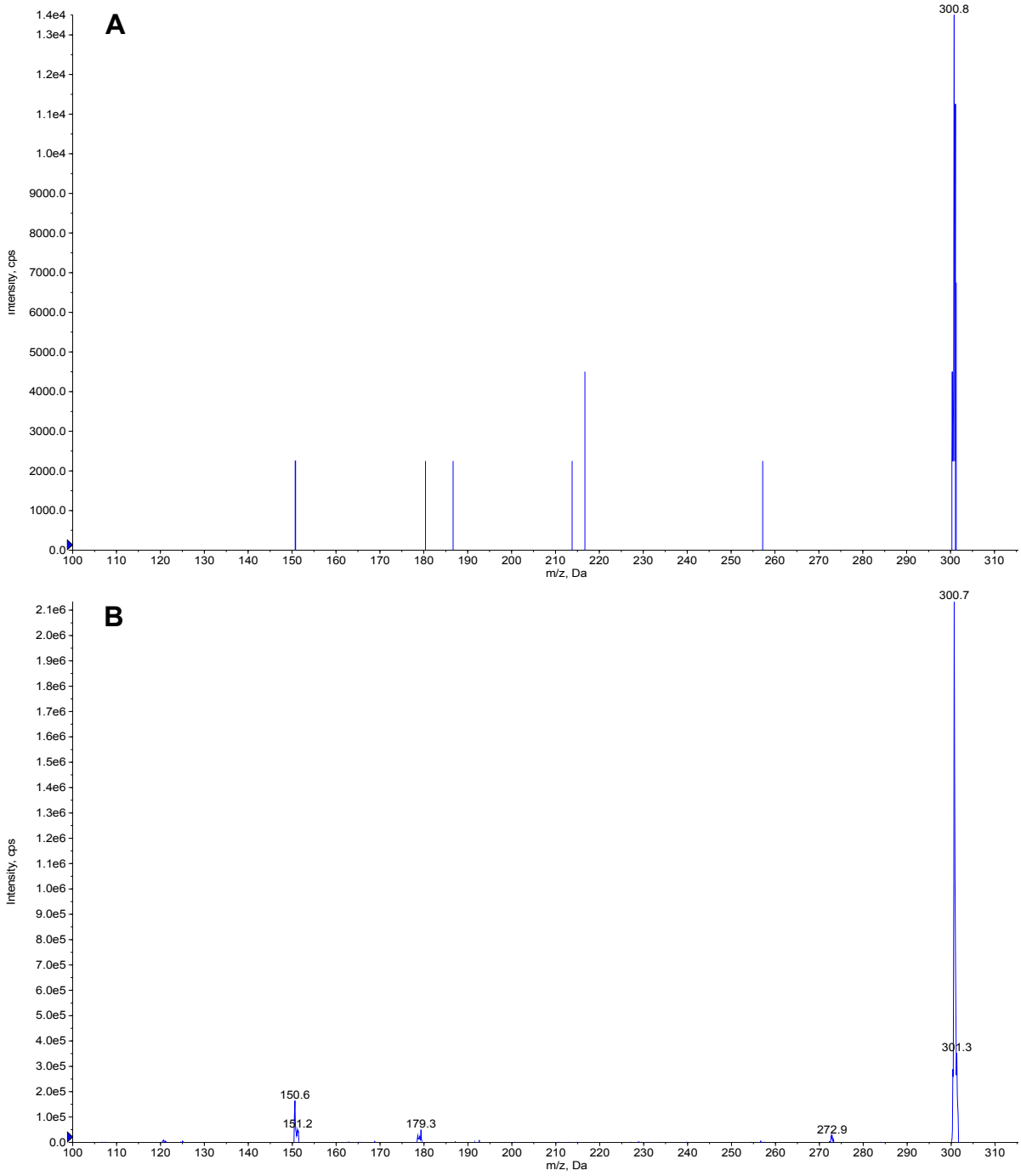

Figure 4.74 Product ion scan of both Q standard and Q extracted from the sample **A,** mass spectrum of Q standard. **B**. Q extracted from G90V-9CR-Q

The displacement in the retention time that has been observed in the sample could be due to the presence of remaining detergent still present in the sample, since a complete scan of the sample detected a mass of 509 that coincides with the mass of DM detergent (Figure 4.75)

.

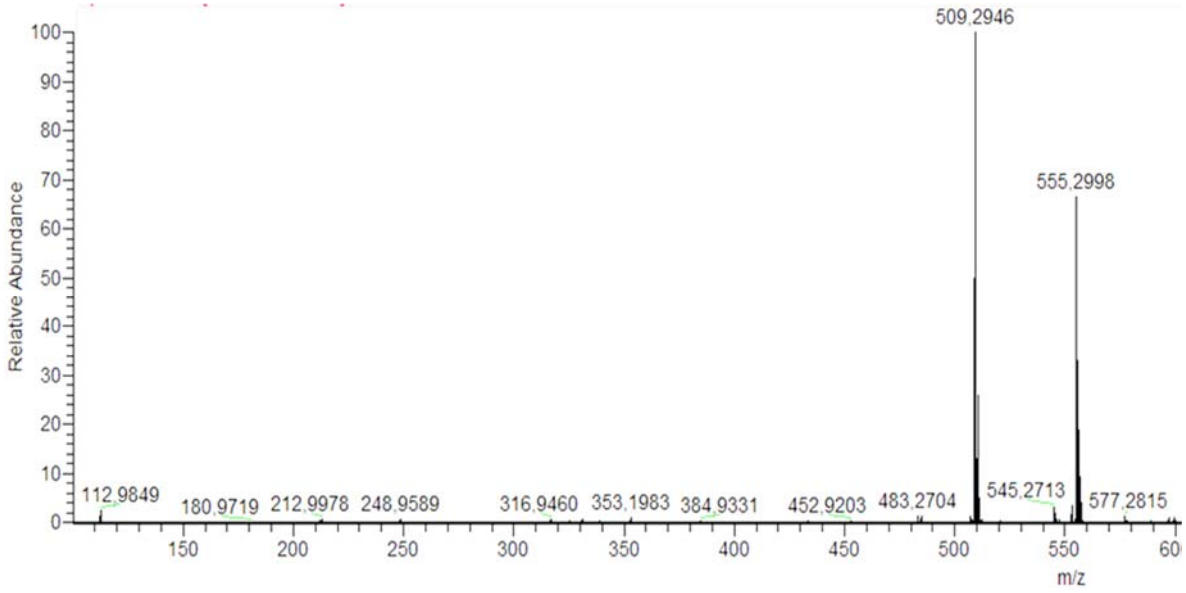

Figure 4.75 Extracted-ion chromatogram that could correspond to DM detergent.

9CR is the most studied analog of Rho in addition to the native 11CR containing protein. Several properties have been attributed to this analog such as being a potential therapeutic agent for type 2 Leber congenital amaurosis (Koenekoop et al., 2014) as well as certain forms of RP (Toledo et al., 2011). In addition, 9-cis retinoids may bind more freely with the opsin apoprotein than the native 11-cis retinoid (Srinivasan et al., 2014).

The results found in this research show the specific binding properties of 9CR, especially in the case of the G90V mutant in which its percentage and rate of regeneration were higher with this analog than with 11CR. This could be attributed to the stronger interaction energy acquired by the C-13-methyl group from Y268 and W265, favoring the entry into the retinal binding site (Srinivasan et al., 2014). In addition, its chemical stability also increases after regeneration with the retinal analog and that reflects an improvement of the structural compaction in the SB environment. Our results indicate a synergistic effect of the combination of 9CR and Q in improving some of the properties of RP mutations. Thus, besides the known pharmaceutical application of retinoids to address visual dysfunctions, other small molecules have also been investigated for their properties as pharmacological chaperones (Bernier et al., 2004; Krebs et al., 2004; Sawkar et al., 2006). Many of these molecules acting as pharmacologic chaperones would bind and stabilize mutant proteins thus improving folding problems (Noorwez et al., 2008).

In this regard, Q improved the partial misfolding problem of G90V RP mutant. In this case the A_{280}/A_{max} ratio was more similar to the WT reducing in about 15% the misfolding problems that are common for RP mutants (Opefi et al., 2013). Previous research suggested that flavonoids (the group to which Q belongs) may be involved in in vision physiology and eye health (Kalt et al., 2010).

4.5. Computational studies on Rho and its interaction with polyphenols

The computational analysis carried out in this investigation had the objective to study the binding preferences of the polyphenols studied here. Structures of these compounds (Figure 4.76) were downloaded from the PubChem website and prepared (generating energy minimized 3D structures, sampling diverse ring conformation, stereoisomers etc.) using LigPrep tool also from Schrodinger.

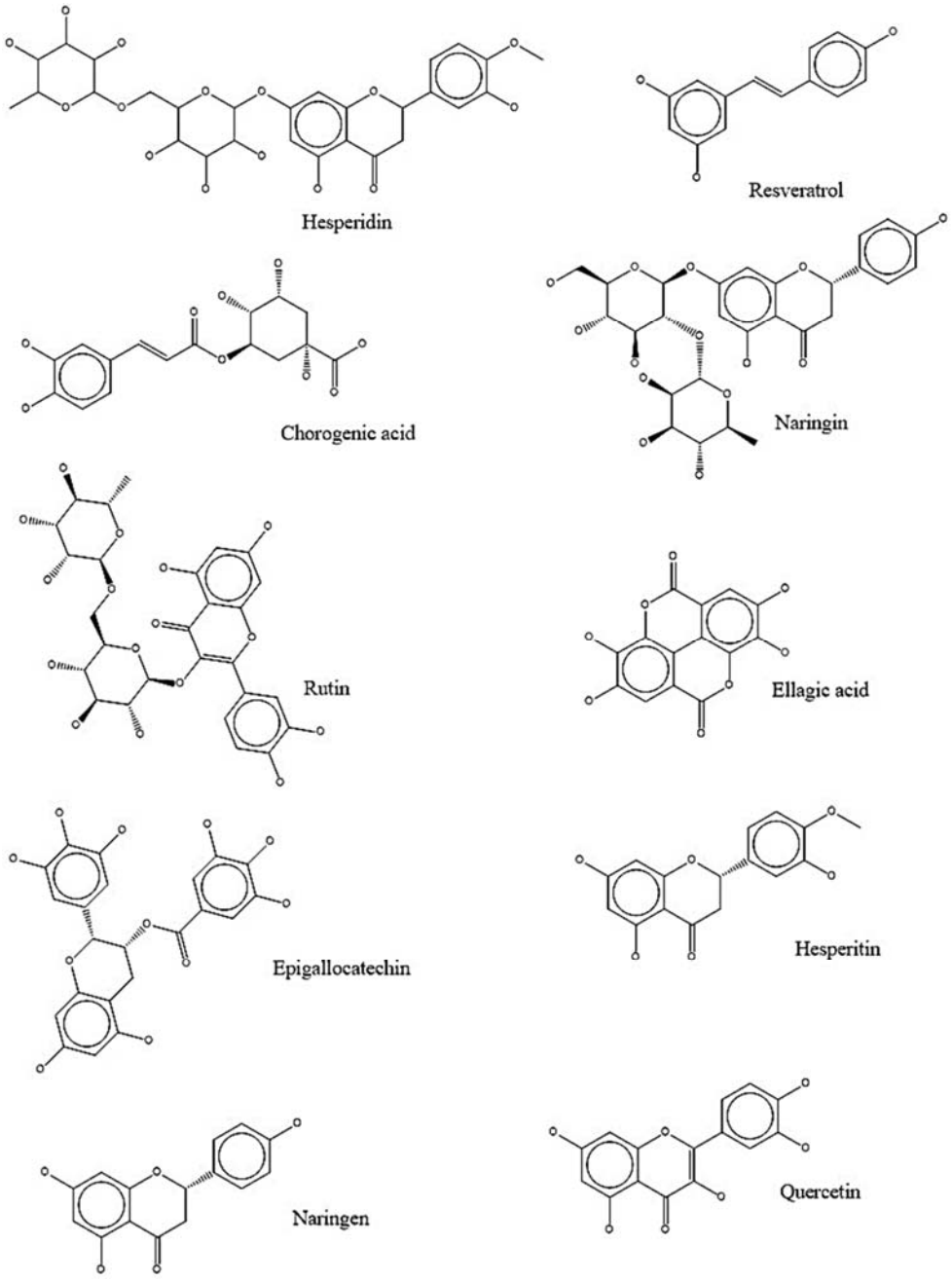

Figure 4.76 Polyphenols structures used prepared using LigPrep

4.5.1 Binding site identification

Prior to molecular docking studies, the receptors were examined in order to identify energetically favorable sites for ligands to bind. For this purpose, we used the Schrodinger site recognition software SiteMap, which locates binding sites which size, functionality, and extent of solvent exposure are suitable for occupancy by hydrophobic groups or by ligand hydrogen-bond donors, acceptors, or metal-binding functionality. The sites are assessed for their inclination to ligand binding, then accurately ranked in order to eliminate those not likely to be suitable for ligand occupancy. The crystallographic structures: 2PED (9-*cis*-Rho), 1GZM (11-*cis*-Rho) and 3CAP (opsin) were obtained from the protein data bank. These structures were prepared (optimization of hydrogen bonds, protonation states etc.) using the protein preparation wizard tool of the Schrodinger software.

In opsin, the results from SiteMap (Figure 4.77) showed 5 possible binding sites for a ligand to occupy. The first annotated as **1** in the figure is the orthosteric site found inside the helices just below the extracellular region of the receptor. Due to the fact that the second extracellular loop (ECL2) of opsin goes a bit deeper in the receptor that in most crystallized class A GPCRs, this pocket seems a little smaller than in other crystallized class A GPCRs. The site is characterized to be both hydrophobic and with hydrogen bond donor and acceptor characteristics. Binding site number **2** is found just along the orthosteric site **1** but on the outside of the helixes (TM1 and TM2). This is very small site in comparison to site **1** and is mostly hydrophobic.

Site **3** is found on the extracellular region of the receptor and involves some residues in the ECL2 and some of N-terminal residues. The site pocket has very little hydrophobic character, and is majorly hydrogen bond acceptor and donor pocket. Like site **2**, site **4** is found on the sides of helices. In this case, site **4** is found just above the intracellular region, on the side between TM3, TM4 and TM5. Lastly, site 5 is majorly located in the intracellular region of the receptor and it is the biggest site with both hydrophobic character and hydrogen bond acceptor and donor characteristics. Along with site 2, site 4 and 5, were not considered to be relevant because it was considered that the membrane bilayer would impair ligand binding to these sites.

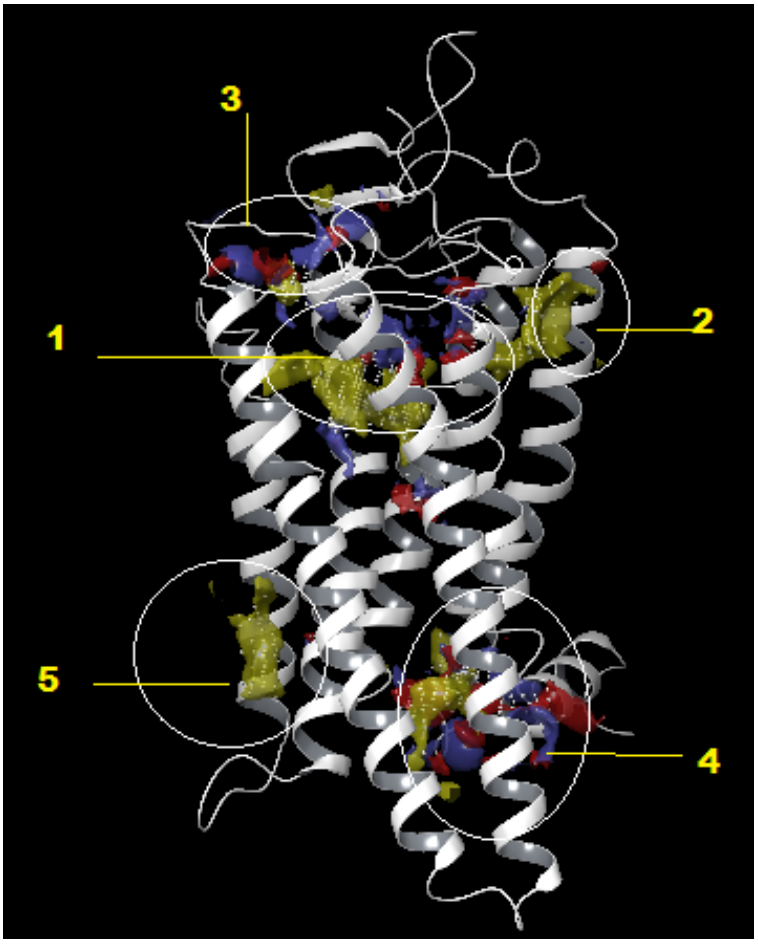

Figure 4.77 Pictorial view of the putative binding sites identified using SiteMap in opsin.

For Rho (Figure 4.78A) and isoRho (Figure 4.78B), in general, the identified sites are similar to those found in native opsin with the major difference being that not all the sites in opsins are found in the Rho neither in isoRho. With site 1 already occupied by the respective retinal, each Rho contains 3 binding sites. 9-*cis*-Rho, only site 3 site 4 and site 5 are identified, while in 11-*cis*-Rho, only site 2, site 4 and site 5 are identified. Along with site 2, site 4 and 5 are not considered as possible binding sites due to the assumption that the membrane bilayer would impair the ligand entering these sites.

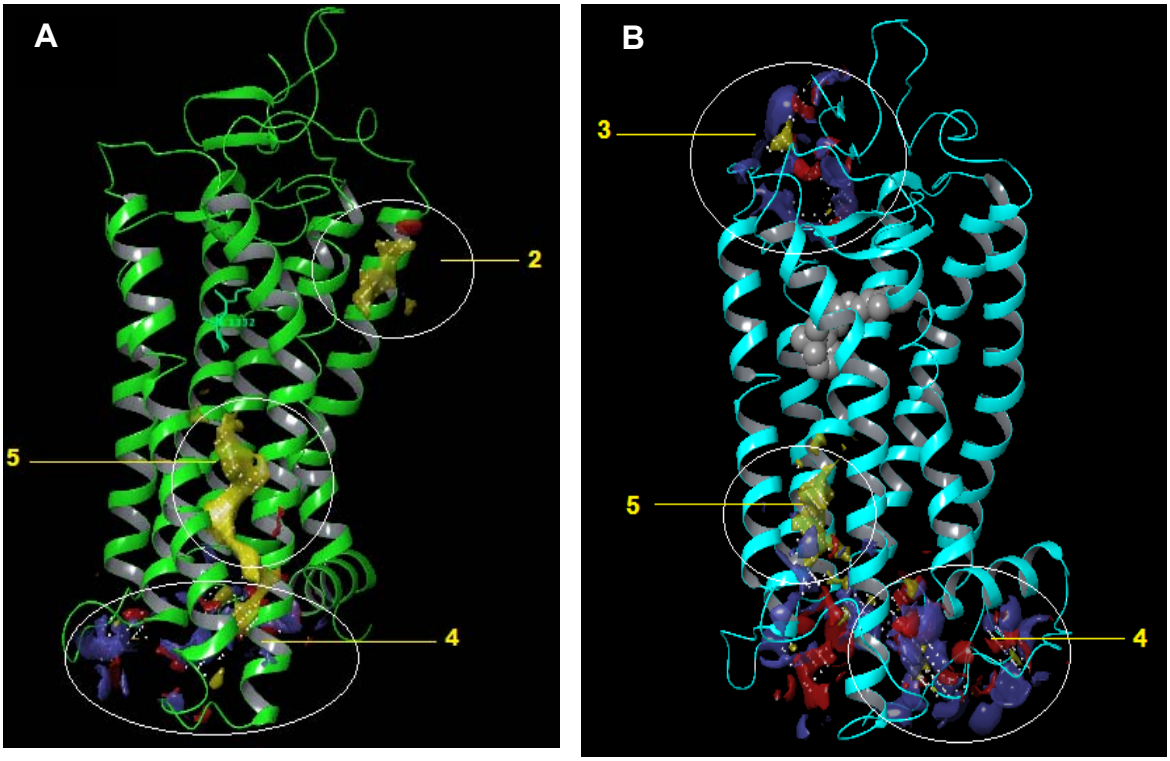

Figure 4.78 Putative binding sites identified by SiteMap in rhodopsin (11CR) and isorhodopsin (9CR) **A** Rho with 11CR in green sticks. **B**. 9 *cis*-Rho with 9CR in gray space filling balls.

4.5.2 Molecular docking

Site 1

This is the binding site of retinal and consequently, it is only available in opsin. Out of the 10 ligands, only R, chorogenic acid, ellagic acid, hesperitin, naringen and Q bind to it. Considering the size of hesperidin, naringin, rutin and EGCG with respect to the size of the orthosteric site 1, it can be concluded that they are unable to bind at this pocket because they are too big for the pocket. The prospective bound conformation shows the ligands sitting on the hydrophobic pocket interacting with Glu181. Only chorogenic acid and ellagic acid show an additional interaction with Lys296.

Site 2 and Site 5

Due to their characteristics, being shallow hydrophobic pockets none of the 10 polyphenols were found to bind to these sites.

Site 3 and Site 4

All ten compounds are found to bind to these two sites. As previously stated, site 3 is only available to 9-cis-Rho. Figure 4.79 shows the prospective bound conformation of the diverse ligands to the site. In contrast, site 4 which is at the cytoplasmic side is available to all three crystallographic structures and all the compounds were found to dock there nicely.

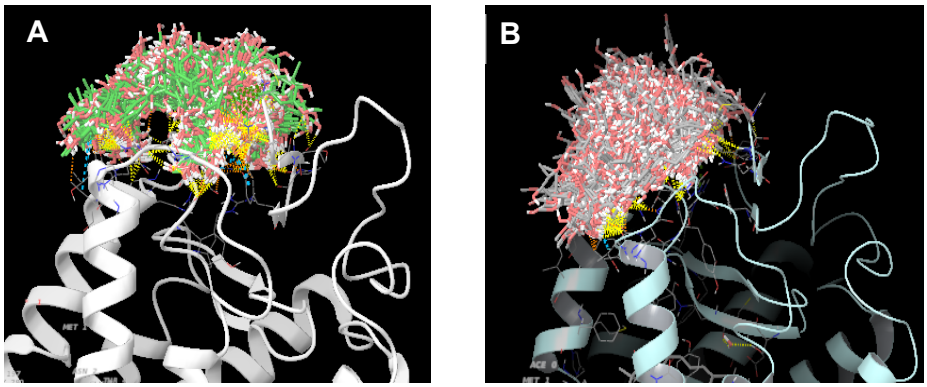

Figure 4.79 Polyphenol compounds as they are bound to opsin (**A**) and isoRho (**B**) in site 3.

4.5.2 Comparison of Rho and 9-cis-Rho and Q molecular docking

Due to these differences found in the binding sites of Rho and isoRho, a comparison of the two structures was performed. It was found that although the ligands do not change significantly the TM region (Figure 4.80A), the two structures show differences in EC2 (Figure 4.80B).

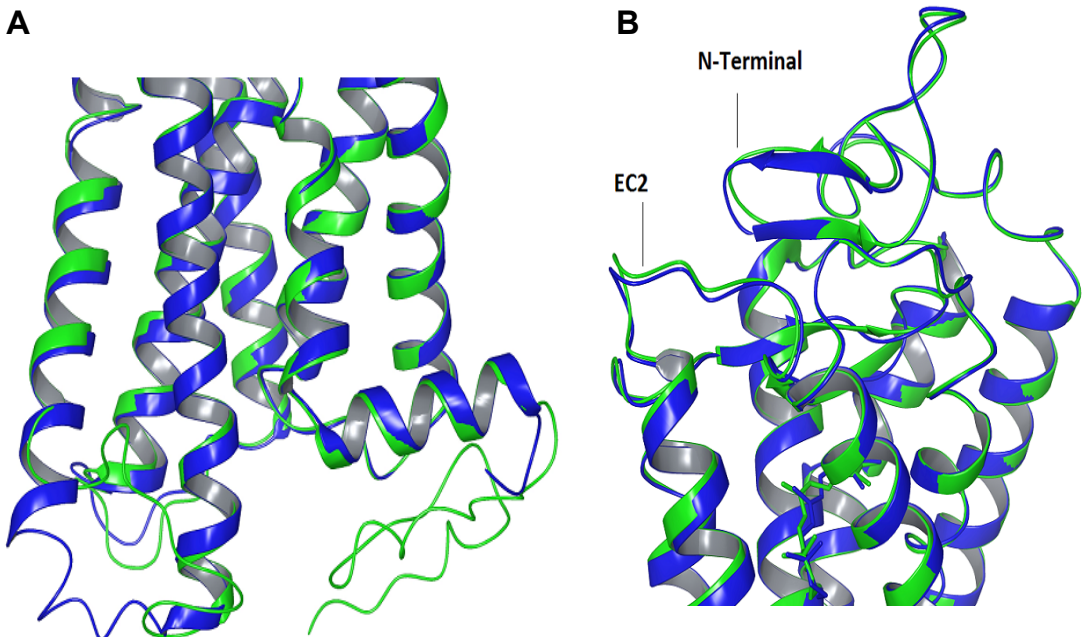

Figure 4.80 Overlapping of the structures of Rho (in blue) and isoRho (in green) showing a structural difference at ECL 2.

The results of the docking study reveal that Q binds differentially to both structures. Specially, it binds to a site involving the extracellular loop EC2 in the 9-*cis*-Rho that is not found on the corresponding Rho (Figure 4.81).

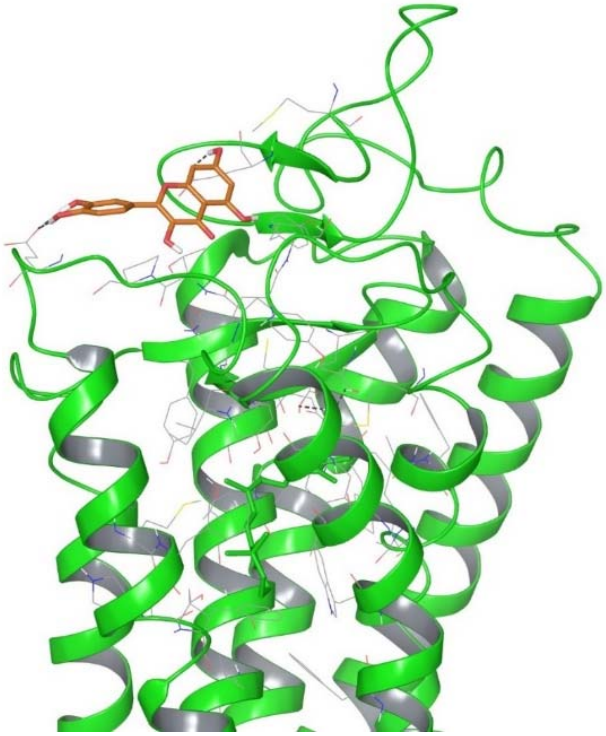

Figure 4.81 Structure of Q (orange) bound to the 9CR (green).

In *silico* studies demonstrate that the potential ligand binding sites are different when the orthosteric ligand is 11CR or 9CR. The molecular docking results reveal that the binding site 3, which is not found in Rho, is the site where Q can bind. This site involves the ECL2 in which a slight difference was observed by superimposing the structures of Rho and isoRho, difference that also was observed in the N-terminus. The ECL2 in particular has been the target of a number of functional studies indicating its role in GPCRs activation that bind either small molecules or large peptide ligands (Klco et al., 2005; Scarselli et al., 2007).

It has been shown that all the phenolic compounds studied here can bind to the 3 and 4 putative binding sites, but the binding site 3 only occurs when the orthosteric ligand is 9CR. In our case, the experiments performed at different concentrations of Q, R and EGCG for the WT and G90V, Y102H and I30YN mutants were done with the native 11CR and therefore no significant differences were observed. This opens an interesting avenue for future research aimed at elucidating the action mechanism of these phenolic compounds as allosteric modulators but using 9CR as the orthosteric ligand.

5. GENERAL DISCUSSION

Our results suggest that Q may act as an allosteric modulator of Rho and G90V mutant when their orthosteric ligand is 9CR. In *silico* studies demonstrate that the potential ligand binding sites are different when the orthosteric ligand is 11CR or 9CR. The molecular docking results reveal that the binding site 3, which is not found in Rho, would be the site where Q could bind. This site involves the ECL2 in which a slight difference was observed by superimposing the structures of Rho and isoRho, difference that was also observed in the N-terminus. The second extracellular loop in particular has been the target of a number of functional studies indicating its role in GPCRs activation that bind either small molecules or large peptide ligands (Klco et al., 2005; Scarselli et al., 2007). In Rho, ECL 2 is part of the retinal plug (Janz et al., 2003), and forms a cap over the binding site of its photoreactive chromophore. A well-defined H-bonded network stabilizes the ECL2 structure which is formed by a number of polar residues, at the center of this network is Glu181 which is H-bonded to Try192 and Try 268, and is connected to Glu113 the counterion to the retinal PSB. Computational studies identified ECL2 as part of the stable folding core of inactive Rho (Rader et al., 2004). In its active conformation (Meta II) it has been reported the displacement of ECL2 from the retinal binding site and a rearrangement in the hydrogen-bonding networks connecting ECL2 with the extracellular ends of TM4, TM5 and TM6. Furthermore, NMR measurements reveal that structural changes in ECL2 are coupled to the motion of helix TM5 and breaking of the ionic lock that regulates activation (Ahuja et al., 2009).

Given the characteristics of the ECL2, it is probable that, because the Q is bound there, it gives more stability and compaction in the retinal binding pocket environment which is reflected in the chemical stability presented by WT 9CR-Q and G90V-9CR-Q. In addition, this more compact structure also affects the retinal release after the hydrolysis of Meta II which was increased to almost double in the G90V 9CR-Q mutant. This great difference in the Meta II decay for this mutant (with Q that would be bound at ECL2) could be due to the replacement of glycine by valine, increase the required space of valine side chain which affects the C2 constriction within of the channel through which the retinal is uptake through opening A and the release of all-trans-retinal through opening B. It is important to note that along almost its full length, the floor of the channel is provided by ECL2 (Hildebrand et al., 2009).

In the Gt activation assays, very marked changes in the activation kinetics were observed again in the samples WT 9CR-Q and G90V 9CR-Q, and in the case of G90V 9CR-Q the Gt activation was lower than in the mutant without treatment. These results suggest that when Q is bound to ECL2, the activation process is affected because the presence of Q prevents the rearrangement in the hydrogen-bonding networks connecting ECL2 with the extracellular ends of TM5 impairing the breaking of the ionic lock that regulates activation (Ahuja et al., 2009).

In this study, using various techniques of molecular biology and analytical methods coupled with *in silico* computational studies, Q has been shown to act as an allosteric modulator of 9-cis-Rho and more importantly, that property has an effect on the stability of G90V 9CR mutant associated with RP. The results presented here demonstrate that the same allosteric modulator (Q) can act as an orthosteric ligand enhancer (because it increases the regeneration rate) and at the same time decrease Gt activation. This modulated response that presents Q like an allosteric modulator of Rho mutants can be exploited in drug design and the development of novel pharmacological approaches for RP treatment. This opens the possibility of exploring other flavonoids and phenolic compounds that could have an effect similar to those found for Q. However, further studies are still needed to provide more detailed information on the effects reported here.

6. CONCLUSIONS

- The levels of WT opsin expression, at the level of mRNA, increased significantly as the concentration of Q increased.

- Q, R and EGCG affected the expression of the WT and mutants studied here, decreasing the protein yield possibly due to overcrowding effects in the cytosol of the cell.
- No significant differences were observed in the physical and functional properties of pigments regenerated with 11CR (11CR) treated with Q or R at concentrations of 1 μM and 10 μM.
- The *in silico* studies suggest that the potential ligand binding sites are different when the orthosteric ligand is 11CR or 9CR, and the docking study reveals that Q binds to a site involving the extracellular loop 2 (ECL2) in the 9-cis-Rho which is not found on Rho.
- Molecular modeling analysis also indicated that the flavonoids Q, rutin, hesperidin, EGCG, naringin, hesperitin and naringenin, the stilbene R, and the phenolic acids chorogenic and ellagic, can bind to different sites in the case of 9-*cis*-Rho and in the case of Rho (regenerated with 11CR).

- The presence of Q during the WT 9CR and G90V 9CR mutant expression increases the thermal and chemical stability of the purified photoreceptor proteins.
- The kinetics change in Gt activation, in the Q-treated samples, clearly indicates a cooperative effect between Q and 9CR.
- The identification of Q by HPLC-MS in the purified samples together with the other results reported, suggests that Q could be acting as an allosteric modulator of WT Rho and G90V Rho mutant Associated with retinitis pigmentosa

- Overall, our studies using various experimental techniques going from molecular biology to analytical methods, coupled with *in silico* computational studies, have shown that Q can potentially act as an allosteric modulator of 9-cis-Rho and more importantly, that property has an effect on the stability of G90V-9CR mutant associated with RP.
- These results open new possibilities to use natural polyphenolic compounds, in combination with specific retinoids like 9CR, for the treatment of retinal degeneration associated with RP. This approach will help in preventing potential immunogenic problems with the use of microbial opsins in optogenetic methods. It may also elude the potential toxic effects of photochromic ligands recently proposed as therapeutical strategies in optopharmacological innovations.

7. BIBLIOGRAPHY

Adler, A. J., & Edwards, R. B. (2000). Human interphotoreceptor matrix contains serum albumin and retinol-binding protein. *Experimental Eye Research*, *70*(2), 227–34.

Adler, A. J., & Evans, C. D. (1985). Some functional characteristics of purified bovine interphotoreceptor retinol-binding protein. *Investigative Ophthalmology & Visual Science*, *26*(3), 273–82.

Adler, A. J., & Spencer, S. A. (1991). Effect of light on endogenous ligands carried by interphotoreceptor retinoid-binding protein. *Experimental Eye*

Aguilà, M., Toledo, D., Morillo, M., Dominguez, M., Vaz, B., Alvarez, R., … Garriga, P. Structural coupling of 11-cis-7-methyl-retinal and amino acids at the ligand binding pocket of rhodopsin. *Photochemistry and Photobiology*, *85*(2), 485–93.

Ahuja, S., Hornak, V., Yan, E. C. Y., Syrett, N., Goncalves, J. A., Hirshfeld, A., … Eilers, M. (2009). Helix movement is coupled to displacement of the second extracellular loop in rhodopsin activation. *Nature Structural & Molecular Biology*, *16*(2), 168–75.

Alexander, S. P. H., Benson, H. E., Faccenda, E., Pawson, A. J., Sharman, J. L., Spedding, M., … Harmar, A. J. (2013). The Concise Guide to PHARMACOLOGY 2013/14: G protein-coupled receptors. *British Journal of Pharmacology*, *170*(8), 1459–581.

Anekonda, T. S., & Adamus, G. (2008). Resveratrol prevents antibody-induced apoptotic death of retinal cells through upregulation of Sirt1 and Ku70. *BMC Research Notes*, *1*, 122.

Batista, A. N. L., Batista, J. M., Bolzani, V. S., Furlan, M., & Blanch, E. W. (2013). Selective DMSO-induced conformational changes in proteins from Raman optical activity. *Physical Chemistry Chemical Physics : PCCP*, *15*(46), 20147–52.

Becker, O. M., Shacham, S., Marantz, Y., & Noiman, S. (2003). Modeling the 3D structure of GPCRs: advances and application to drug discovery. *Current Opinion in Drug Discovery & Development*, *6*(3), 353–61.

Beharry, S., Zhong, M., & Molday, R. S. (2004). N-retinylidene-phosphatidylethanolamine is the preferred retinoid substrate for the photoreceptor-specific ABC transporter ABCA4 (ABCR). *The Journal of Biological Chemistry*, *279*(52), 53972–9.

Bermudez, M., & Wolber, G. (2015). Structure versus function-The impact of computational methods on the discovery of specific GPCR-ligands. *Bioorganic & Medicinal Chemistry*, *23*(14), 3907–12.

Bernier, V., Bichet, D. G., & Bouvier, M. (2004). Pharmacological chaperone action on G-protein-coupled receptors. *Current Opinion in Pharmacology*, *4*(5), 528–33.

Berson, E. L. (1993). Retinitis pigmentosa. The Friedenwald Lecture. *Investigative Ophthalmology & Visual Science*, *34*(5), 1659–76.

Bosch, L., Iarriccio, L., & Garriga, P. (2005). New prospects for drug discovery from structural studies of rhodopsin. *Current Pharmaceutical Design*, *11*(17), 2243–56.

Bourne, H. R., & Meng, E. C. (2000). Structure. Rhodopsin sees the light. *Science (New York, N.Y.)*, *289*(5480), 733–4.

Budzynski, E., Gross, A. K., McAlear, S. D., Peachey, N. S., Shukla, M., He, F., … Nishina, P. M. (2010). Mutations of the opsin gene (Y102H and I307N) lead to light-induced degeneration of photoreceptors and constitutive activation of phototransduction in mice. *The Journal of Biological Chemistry*, *285*(19), 14521–33.

Chang, V. T., Crispin, M., Aricescu, A. R., Harvey, D. J., Nettleship, J. E., Fennelly, J. A., … Davis, S. J. (2007). Glycoprotein structural genomics: solving the glycosylation problem. *Structure (London, England : 1993)*, *15*(3), 267–73.

Chapple, J. P., & Cheetham, M. E. (2003). The chaperone environment at the cytoplasmic face of the endoplasmic reticulum can modulate rhodopsin processing and inclusion formation. *The Journal of Biological Chemistry*, *278*(21), 19087–94.

Chey, S., Claus, C., & Liebert, U. G. (2010). Validation and application of normalization factors for gene expression studies in rubella virus-infected cell lines with quantitative real-time PCR. *Journal of Cellular Biochemistry*, *110*(1), 118–28.

Choe, H.-W., Kim, Y. J., Park, J. H., Morizumi, T., Pai, E. F., Krauss, N., … Ernst, O. P. (2011). Crystal structure of metarhodopsin II. *Nature*, *471*(7340), 651–5.

Cideciyan, A. V, Hood, D. C., Huang, Y., Banin, E., Li, Z. Y., Stone, E. M., … Jacobson, S. G. (1998). Disease sequence from mutant rhodopsin allele to rod and cone photoreceptor degeneration in man. *Proceedings of the National Academy of Sciences of the United States of America*, *95*(12), 7103–8.

Cideciyan, A. V, Jacobson, S. G., Aleman, T. S., Gu, D., Pearce-Kelling, S. E., Sumaroka, A., … Aguirre, G. D. (2005). In vivo dynamics of retinal injury and repair in the rhodopsin mutant dog model of human retinitis pigmentosa. *Proceedings of the National Academy of Sciences of the United States of America*, *102*(14), 5233–8.

Croft, K. D. (2016). Dietary polyphenols: Antioxidants or not? *Archives of Biochemistry and Biophysics*, *595*, 120–4.

Crouch, R. K., Chader, G. J., Wiggert, B., & Pepperberg, D. R. (1996). Retinoids and the visual process. *Photochemistry and Photobiology*, *64*(4), 613–21.

Crouch, R. K., Hazard, E. S., Lind, T., Wiggert, B., Chader, G., & Corson, D. W. (1992). Interphotoreceptor retinoid-binding protein and alpha-tocopherol preserve the isomeric and oxidation state of retinol. *Photochemistry and Photobiology*, *56*(2), 251–5.

Crozier, A., Jaganath, I. B., & Clifford, M. N. (2009). Dietary phenolics: chemistry, bioavailability and effects on health. *Natural Product Reports*, *26*(8), 1001–43.

Culhane, K. J., Liu, Y., Cai, Y., & Yan, E. C. Y. (2015). Transmembrane signal transduction by peptide hormones via family B G protein-coupled receptors. *Frontiers in Pharmacology*, *6*, 264.

Cvijic, M. E., Sum, C. S., Alt, A., & Zhang, L. (2015). GPCR profiling: from hits to leads and from genotype to phenotype. *Drug Discovery Today. Technologies*, *18*, 30–7.

D'Andrea, G. (2015). Quercetin: A flavonol with multifaceted therapeutic applications? *Fitoterapia*, *106*, 256–71.

Day, A. J., Bao, Y., Morgan, M. R., & Williamson, G. (2000). Conjugation position of quercetin glucuronides and effect on biological activity. *Free Radical Biology & Medicine*, *29*(12), 1234–43.

Deretic, D., Williams, A. H., Ransom, N., Morel, V., Hargrave, P. A., & Arendt, A. (2005). Rhodopsin C terminus, the site of mutations causing retinal disease, regulates trafficking by binding to ADP-ribosylation factor 4 (ARF4). *Proceedings of the National Academy of Sciences of the United States of America*, *102*(9), 3301–6.

Dong, X., Ramon, E., Herrera-Hernández, M. G., & Garriga, P. (2015). Phospholipid Bicelles Improve the Conformational Stability of Rhodopsin Mutants Associated with Retinitis Pigmentosa. *Biochemistry*, *54*(31), 4795–4804.

Edwards, R. B., & Adler, A. J. (1994). Exchange of retinol between IRBP and CRBP. *Experimental*

Eye Research, *59*(2), 161–70.

Farrar, G. J., Kenna, P. F., & Humphries, P. (2002). On the genetics of retinitis pigmentosa and on mutation-independent approaches to therapeutic intervention. *The EMBO Journal*, *21*(5), 857–64.

Farrens, D. L., & Khorana, H. G. (1995). Structure and function in rhodopsin. Measurement of the rate of metarhodopsin II decay by fluorescence spectroscopy. *The Journal of Biological Chemistry*, *270*(10), 5073–6.

Fernández-Sampedro, M. A., Invergo, B. M., Ramon, E., Bertranpetit, J., & Garriga, P. (2016). Functional role of positively selected amino acid substitutions in mammalian rhodopsin evolution. *Scientific Reports*, *6*, 21570.

Fleige, S., & Pfaffl, M. W. (2006). RNA integrity and the effect on the real-time qRT-PCR performance. *Molecular Aspects of Medicine*, *27*, 126–139.

Flock, T., Ravarani, C. N. J., Sun, D., Venkatakrishnan, A. J., Kayikci, M., Tate, C. G., … Babu, M. M. (2015). Universal allosteric mechanism for Gα activation by GPCRs. *Nature*, *524*(7564), 173–9.

Franco, R., Martínez-Pinilla, E., Lanciego, J. L., & Navarro, G. (2016). Basic Pharmacological and Structural Evidence for Class A G-Protein-Coupled Receptor Heteromerization. *Frontiers in Pharmacology*, *7*, 76.

Frederick, J. M., Krasnoperova, N. V, Hoffmann, K., Church-Kopish, J., Rüther, K., Howes, K., … Baehr, W. (2001). Mutant rhodopsin transgene expression on a null background. *Investigative Ophthalmology & Visual Science*, *42*(3), 826–33.

Fredriksson, R., Lagerström, M. C., Lundin, L.-G., & Schiöth, H. B. (2003). The G-protein-coupled receptors in the human genome form five main families. Phylogenetic analysis, paralogon groups, and fingerprints. *Molecular Pharmacology*, *63*(6), 1256–72.

Fukada, Y., Matsuda, T., Kokame, K., Takao, T., Shimonishi, Y., Akino, T., & Yoshizawa, T. (1994). Effects of carboxyl methylation of photoreceptor G protein gamma-subunit in visual transduction. *The Journal of Biological Chemistry*, *269*(7), 5163–70.

Garriga, P., & Manyosa, J. (2002). The eye photoreceptor protein rhodopsin. Structural implications for retinal disease. *FEBS Letters*, *528*(1–3), 17–22.

Garwin, G. G., & Saari, J. C. (2000). High-performance liquid chromatography analysis of visual cycle retinoids. *Methods in Enzymology*, *316*, 313–24.

Graf, B. A., Milbury, P. E., & Blumberg, J. B. (2005). Flavonols, flavones, flavanones, and human health: epidemiological evidence. *Journal of Medicinal Food*, *8*(3), 281–90.

Guo, D., Hillger, J. M., IJzerman, A. P., & Heitman, L. H. (2014). Drug-target residence time--a case for G protein-coupled receptors. *Medicinal Research Reviews*, *34*(4), 856–92.

Hanneken, A., Lin, F.-F., Johnson, J., & Maher, P. (2006). Flavonoids protect human retinal pigment epithelial cells from oxidative-stress-induced death. *Investigative Ophthalmology & Visual Science*, *47*(7), 3164–77.

Harbison, G. S., Smith, S. O., Pardoen, J. A., Winkel, C., Lugtenburg, J., Herzfeld, J., … Griffin, R. G. (1984). Dark-adapted bacteriorhodopsin contains 13-cis, 15-syn and all-trans, 15-anti retinal Schiff bases. *Proceedings of the National Academy of Sciences of the United States of America*, *81*(6), 1706–9.

Hartl, F. U., & Hayer-Hartl, M. (2002). Molecular chaperones in the cytosol: from nascent chain to folded protein. *Science (New York, N.Y.)*, *295*(5561), 1852–8.

Hartman, R. E., Shah, A., Fagan, A. M., Schwetye, K. E., Parsadanian, M., Schulman, R. N., …

Holtzman, D. M. (2006). Pomegranate juice decreases amyloid load and improves behavior in a mouse model of Alzheimer's disease. *Neurobiology of Disease*, *24*(3), 506–15.

Heitzmann, H. (1972). Rhodopsin is the predominant protein of rod outer segment membranes. *Nature: New Biology*, *235*(56), 114.

Herrera-Hernández, M. (2015). Molecular Mechanisms of Retinal Toxicity Induced by Light and Chemical Damage. *Advances in Molecular …*, *9*, 215–258.

Hildebrand, P. W., Scheerer, P., Park, J. H., Choe, H.-W., Piechnick, R., Ernst, O. P., … Heck, M. (2009). A ligand channel through the G protein coupled receptor opsin. *PloS One*, *4*(2), e4382.

Hiller, C., Kühhorn, J., & Gmeiner, P. (2013). Class A G-protein-coupled receptor (GPCR) dimers and bivalent ligands. *Journal of Medicinal Chemistry*, *56*(17), 6542–59.

Hillger, J. M., Schoop, J., Boomsma, D. I., Slagboom, P. E., IJzerman, A. P., & Heitman, L. H. (2015). Whole-cell biosensor for label-free detection of GPCR-mediated drug responses in personal cell lines. *Biosensors & Bioelectronics*, *74*, 233–42.

Hofmann, K. P., Scheerer, P., Hildebrand, P. W., Choe, H.-W., Park, J. H., Heck, M., & Ernst, O. P. (2009). A G protein-coupled receptor at work: the rhodopsin model. *Trends in Biochemical Sciences*, *34*(11), 540–52.

Hou, Z., Sang, S., You, H., Lee, M.-J., Hong, J., Chin, K.-V., & Yang, C. S. (2005). Mechanism of action of (-)-epigallocatechin-3-gallate: auto-oxidation-dependent inactivation of epidermal growth factor receptor and direct effects on growth inhibition in human esophageal cancer KYSE 150 cells. *Cancer Research*, *65*(17), 8049–56.

HUBBARD, R. (1954). The molecular weight of rhodopsin and the nature of the rhodopsin-digitonin complex. *The Journal of General Physiology*, *37*(3), 381–99. Retrieved from http://www.pubmedcentral.nih.gov/articlerender.fcgi?artid=2147455&tool=pmcentrez&rendertype=abstract

Hubbard, R., & Kropf, A. (1958). THE ACTION OF LIGHT ON RHODOPSIN. *Proceedings of the National Academy of Sciences of the United States of America*, *44*(2), 130–9.

Iannaccone, A., Man, D., Waseem, N., Jennings, B. J., Ganapathiraju, M., Gallaher, K., … Klein-Seetharaman, J. (2006). Retinitis pigmentosa associated with rhodopsin mutations: Correlation between phenotypic variability and molecular effects. *Vision Research*, *46*(27), 4556–67.

Jackson, M., & Mantsch, H. H. (1991). Beware of proteins in DMSO. *Biochimica et Biophysica Acta*, *1078*(2), 231–5.

Janz, J. M., & Farrens, D. L. (2003). Assessing structural elements that influence Schiff base stability: mutants E113Q and D190N destabilize rhodopsin through different mechanisms. *Vision Research*, *43*(28), 2991–3002.

Janz, J. M., Fay, J. F., & Farrens, D. L. (2003). Stability of dark state rhodopsin is mediated by a conserved ion pair in intradiscal loop E-2. *The Journal of Biological Chemistry*, *278*(19), 16982–91.

Jastrzebska, B., Palczewski, K., & Golczak, M. (2011). Role of bulk water in hydrolysis of the rhodopsin chromophore. *The Journal of Biological Chemistry*, *286*(21), 18930–7.

Jin, M., Li, S., Moghrabi, W. N., Sun, H., & Travis, G. H. (2005). Rpe65 is the retinoid isomerase in bovine retinal pigment epithelium. *Cell*, *122*(3), 449–59.

Johnson, J., Maher, P., & Hanneken, A. (2009). The flavonoid, eriodictyol, induces long-term protection in ARPE-19 cells through its effects on Nrf2 activation and phase 2 gene expression. *Investigative Ophthalmology & Visual Science*, *50*(5), 2398–406.

Jurasekova, Z., Domingo, C., Garcia-Ramos, J. V, & Sanchez-Cortes, S. (2014). Effect of pH on the chemical modification of quercetin and structurally related flavonoids characterized by optical (UV-visible and Raman) spectroscopy. *Physical Chemistry Chemical Physics : PCCP*, *16*(25), 12802–11.

Kalt, W., Hanneken, A., Milbury, P., & Tremblay, F. (2010). Recent research on polyphenolics in vision and eye health. *Journal of Agricultural and Food Chemistry*, *58*(7), 4001–7.

Kanwal, S., Nishat, S., & Khan, M. I. (2012). Docking of human rhodopsin mutant (Gly90→Asp) with beta-arrestin and cyanidin 3-rutinoside to cure night blindness. *Bioinformation*, *8*(3), 128–33.

Kapetanovic, I. M. (2008). Computer-aided drug discovery and development (CADDD): in silico-chemico-biological approach. *Chemico-Biological Interactions*, *171*(2), 165–76.

Katritch, V., Cherezov, V., & Stevens, R. C. (2012). Diversity and modularity of G protein-coupled receptor structures. *Trends in Pharmacological Sciences*, *33*(1), 17–27.

Khoury, E., Clément, S., & Laporte, S. A. (2014). Allosteric and biased g protein-coupled receptor signaling regulation: potentials for new therapeutics. *Frontiers in Endocrinology*, *5*, 68.

Kim, H. S., Byun, S. H., & Lee, B. M. (2005). Effects of chemical carcinogens and physicochemical factors on the UV spectrophotometric determination of DNA. *Journal of Toxicology and Environmental Health. Part A*, *68*(23–24), 2081–95.

Kimura, A., Namekata, K., Guo, X., Noro, T., Harada, C., & Harada, T. (2015). Valproic acid prevents NMDA-induced retinal ganglion cell death via stimulation of neuronal TrkB receptor signaling. *The American Journal of Pathology*, *185*(3), 756–64.

King, R. E., Kent, K. D., & Bomser, J. A. (2005). Resveratrol reduces oxidation and proliferation of human retinal pigment epithelial cells via extracellular signal-regulated kinase inhibition. *Chemico-Biological Interactions*, *151*(2), 143–9.

Kiser, P. D., Golczak, M., & Palczewski, K. (2014). Chemistry of the Retinoid (Visual) Cycle. *Chemical Reviews*, *114*(1), 194–232.

Klco, J. M., Wiegand, C. B., Narzinski, K., & Baranski, T. J. (2005). Essential role for the second extracellular loop in C5a receptor activation. *Nature Structural & Molecular Biology*, *12*(4), 320–6.

Kobayashi, T. (2016). Structural Life Science towards the Regulation of Selective GPCR Signaling. *Yakugaku Zasshi : Journal of the Pharmaceutical Society of Japan*, *136*(2), 179–84.

Koenekoop, R. K., Sui, R., Sallum, J., van den Born, L. I., Ajlan, R., Khan, A., … Saperstein, D. A. (2014). Oral 9-cis retinoid for childhood blindness due to Leber congenital amaurosis caused by RPE65 or LRAT mutations: an open-label phase 1b trial. *Lancet (London, England)*, *384*(9953), 1513–20.

Kook, D., Wolf, A. H., Yu, A. L., Neubauer, A. S., Priglinger, S. G., Kampik, A., & Welge-Lüssen, U. C. (2008). The protective effect of quercetin against oxidative stress in the human RPE in vitro. *Investigative Ophthalmology & Visual Science*, *49*(4), 1712–20.

Krebs, M. P., Holden, D. C., Joshi, P., Clark, C. L., Lee, A. H., & Kaushal, S. (2010). Molecular mechanisms of rhodopsin retinitis pigmentosa and the efficacy of pharmacological rescue. *Journal of Molecular Biology*, *395*(5), 1063–78.

Krebs, M. P., Noorwez, S. M., Malhotra, R., & Kaushal, S. (2004). Quality control of integral membrane proteins. *Trends in Biochemical Sciences*, *29*(12), 648–55.

Kubota, S., Kurihara, T., Ebinuma, M., Kubota, M., Yuki, K., Sasaki, M., … Tsubota, K. (2010). Resveratrol prevents light-induced retinal degeneration via suppressing activator protein-1

activation. *The American Journal of Pathology*, *177*(4), 1725–31.

Lamb, T. D., & Pugh, E. N. (2006). Phototransduction, dark adaptation, and rhodopsin regeneration the proctor lecture. *Investigative Ophthalmology & Visual Science*, *47*(12), 5137–52.

Lane, J. R., Abdul-Ridha, A., & Canals, M. (2013). Regulation of G protein-coupled receptors by allosteric ligands. *ACS Chemical Neuroscience*, *4*(4), 527–34.

Lavecchia, A., & Di Giovanni, C. (2013). Virtual screening strategies in drug discovery: a critical review. *Current Medicinal Chemistry*, *20*(23), 2839–60.

Li, C.-P., Yao, J., Tao, Z.-F., Li, X.-M., Jiang, Q., & Yan, B. (2013). Epigallocatechin-gallate (EGCG) regulates autophagy in human retinal pigment epithelial cells: a potential role for reducing UVB light-induced retinal damage. *Biochemical and Biophysical Research Communications*, *438*(4), 739–45.

Lin, Z. S., Fong, S. L., & Bridges, C. D. (1989). Retinoids bound to interstitial retinol-binding protein during light and dark-adaptation. *Vision Research*, *29*(12), 1699–709.

Lindsley, C. W., Emmitte, K. A., Hopkins, C. R., Bridges, T. M., Gregory, K. J., Niswender, C. M., & Conn, P. J. (2016). Practical Strategies and Concepts in GPCR Allosteric Modulator Discovery: Recent Advances with Metabotropic Glutamate Receptors. *Chemical Reviews*.

Liu, M. Y., Liu, J., Mehrotra, D., Liu, Y., Guo, Y., Baldera-Aguayo, P. A., … Yan, E. C. Y. (2013). Thermal stability of rhodopsin and progression of retinitis pigmentosa: comparison of S186W and D190N rhodopsin mutants. *The Journal of Biological Chemistry*, *288*(24), 17698–712.

Liu, W., & Guo, R. (2006). Interaction between flavonoid, quercetin and surfactant aggregates with different charges. *Journal of Colloid and Interface Science*, *302*(2), 625–32.

Liu, X., Garriga, P., & Khorana, H. G. (1996). Structure and function in rhodopsin: correct folding and misfolding in two point mutants in the intradiscal domain of rhodopsin identified in retinitis pigmentosa. *Proceedings of the National Academy of Sciences of the United States of America*, *93*(10), 4554–9.

Longo, P. A., Kavran, J. M., Kim, M.-S., & Leahy, D. J. (2013). Transient mammalian cell transfection with polyethylenimine (PEI). *Methods in Enzymology*, *529*, 227–40.

Maeda, A., Maeda, T., Golczak, M., Chou, S., Desai, A., Hoppel, C. L., … Palczewski, K. (2009). Involvement of all-trans-retinal in acute light-induced retinopathy of mice. *The Journal of Biological Chemistry*, *284*(22), 15173–83.

Maeda, A., Maeda, T., Sun, W., Zhang, H., Baehr, W., & Palczewski, K. (2007). Redundant and unique roles of retinol dehydrogenases in the mouse retina. *Proceedings of the National Academy of Sciences of the United States of America*, *104*(49), 19565–70.

Maeda, T., Dong, Z., Jin, H., Sawada, O., Gao, S., Utkhede, D., … Palczewski, K. (2013). QLT091001, a 9-cis-retinal analog, is well-tolerated by retinas of mice with impaired visual cycles. *Investigative Ophthalmology & Visual Science*, *54*(1), 455–66.

Maeda, T., Maeda, A., Matosky, M., Okano, K., Roos, S., Tang, J., & Palczewski, K. (2009). Evaluation of potential therapies for a mouse model of human age-related macular degeneration caused by delayed all-trans-retinal clearance. *Investigative Ophthalmology & Visual Science*, *50*(10), 4917–25.

Maher, P., & Hanneken, A. (2005). Flavonoids protect retinal ganglion cells from oxidative stress-induced death. *Investigative Ophthalmology & Visual Science*, *46*(12), 4796–803.

Mansoor, S., Gupta, N., Patil, A. J., Estrago-Franco, M. F., Ramirez, C., Migon, R., … Kenney, M. C. (2010). Inhibition of apoptosis in human retinal pigment epithelial cells treated with benzo(e)pyrene, a toxic component of cigarette smoke. *Investigative Ophthalmology &*

Visual Science, *51*(5), 2601–7.

Martí-Solano, M., Schmidt, D., Kolb, P., & Selent, J. (2016). Drugging specific conformational states of GPCRs: challenges and opportunities for computational chemistry. *Drug Discovery Today*, *21*(4), 625–31.

Matsumoto, H., Nakamura, Y., Tachibanaki, S., Kawamura, S., & Hirayama, M. (2003). Stimulatory effect of cyanidin 3-glycosides on the regeneration of rhodopsin. *Journal of Agricultural and Food Chemistry*, *51*(12), 3560–3.

McBee, J. K., Palczewski, K., Baehr, W., & Pepperberg, D. R. (2001). Confronting complexity: the interlink of phototransduction and retinoid metabolism in the vertebrate retina. *Progress in Retinal and Eye Research*, *20*(4), 469–529.

McConnell, D. G., Dangler, C. A., Eadie, D. M., & Litman, B. J. (1981). The effect of detergent selection on retinal outer segment A280/A500 ratios. *The Journal of Biological Chemistry*, *256*(10), 4913–8.

Mendes, H. F., van der Spuy, J., Chapple, J. P., & Cheetham, M. E. (2005). Mechanisms of cell death in rhodopsin retinitis pigmentosa: implications for therapy. *Trends in Molecular Medicine*, *11*(4), 177–85.

Metodiewa, D., Jaiswal, A. K., Cenas, N., Dickancaité, E., & Segura-Aguilar, J. (1999). Quercetin may act as a cytotoxic prooxidant after its metabolic activation to semiquinone and quinoidal product. *Free Radical Biology & Medicine*, *26*(1–2), 107–16.

Moiseyev, G., Chen, Y., Takahashi, Y., Wu, B. X., & Ma, J.-X. (2005). RPE65 is the isomerohydrolase in the retinoid visual cycle. *Proceedings of the National Academy of Sciences of the United States of America*, *102*(35), 12413–8.

Molday, R. S. (2007). ATP-binding cassette transporter ABCA4: molecular properties and role in vision and macular degeneration. *Journal of Bioenergetics and Biomembranes*, *39*(5–6), 507–17.

Munishkina, L. A., & Fink, A. L. (2007). Fluorescence as a method to reveal structures and membrane-interactions of amyloidogenic proteins. *Biochimica et Biophysica Acta*, *1768*(8), 1862–85.

Murgueitio, M. S., Bermudez, M., Mortier, J., & Wolber, G. (2012). In silico virtual screening approaches for anti-viral drug discovery. *Drug Discovery Today. Technologies*, *9*(3), e175-226.

Nakamichi, H., & Okada, T. (2007). X-ray crystallographic analysis of 9-cis-rhodopsin, a model analogue visual pigment. *Photochemistry and Photobiology*, *83*(2), 232–5.

Naseem, B., Shah, S. W. H., Hasan, A., & Sakhawat Shah, S. (2010). Interaction of flavonoids, the naturally occurring antioxidants with different media: a UV-visible spectroscopic study. *Spectrochimica Acta. Part A, Molecular and Biomolecular Spectroscopy*, *75*(4), 1341–6.

Neidhardt, J., Barthelmes, D., Farahmand, F., Fleischhauer, J. C., & Berger, W. (2006). Different Amino Acid Substitutions at the Same Position in Rhodopsin Lead to Distinct Phenotypes. *Investigative Opthalmology & Visual Science*, *47*(4), 1630.

Nickell, S., Park, P. S.-H., Baumeister, W., & Palczewski, K. (2007). Three-dimensional architecture of murine rod outer segments determined by cryoelectron tomography. *The Journal of Cell Biology*, *177*(5), 917–25.

Noorwez, S. M., Ostrov, D. A., McDowell, J. H., Krebs, M. P., & Kaushal, S. (2008). A high-throughput screening method for small-molecule pharmacologic chaperones of misfolded rhodopsin. *Investigative Ophthalmology & Visual Science*, *49*(7), 3224–30.

Opefi, C. A., South, K., Reynolds, C. A., Smith, S. O., & Reeves, P. J. (2013). Retinitis pigmentosa

mutants provide insight into the role of the N-terminal cap in rhodopsin folding, structure, and function. *The Journal of Biological Chemistry*, *288*(47), 33912–26.

Oprian, D. D., Molday, R. S., Kaufman, R. J., & Khorana, H. G. (1987). Expression of a synthetic bovine rhodopsin gene in monkey kidney cells. *Proceedings of the National Academy of Sciences of the United States of America*, *84*(24), 8874–8.

Palczewski, K. (2006). G protein-coupled receptor rhodopsin. *Annual Review of Biochemistry*, *75*, 743–67.

Palczewski, K., Kumasaka, T., Hori, T., Behnke, C. A., Motoshima, H., Fox, B. A., … Miyano, M. (2000). Crystal structure of rhodopsin: A G protein-coupled receptor. *Science (New York, N.Y.)*, *289*(5480), 739–45.

Park, J. H., Scheerer, P., Hofmann, K. P., Choe, H.-W., & Ernst, O. P. (2008). Crystal structure of the ligand-free G-protein-coupled receptor opsin. *Nature*, *454*(7201), 183–7.

Parker, R. O., & Crouch, R. K. (2010). Retinol dehydrogenases (RDHs) in the visual cycle. *Experimental Eye Research*, *91*(6), 788–92.

Pepperberg, D. R., Okajima, T. L., Wiggert, B., Ripps, H., Crouch, R. K., & Chader, G. J. (1993). Interphotoreceptor retinoid-binding protein (IRBP). Molecular biology and physiological role in the visual cycle of rhodopsin. *Molecular Neurobiology*, *7*(1), 61–85.

Piechnick, R., Ritter, E., Hildebrand, P. W., Ernst, O. P., Scheerer, P., Hofmann, K. P., & Heck, M. (2012). Effect of channel mutations on the uptake and release of the retinal ligand in opsin. *Proceedings of the National Academy of Sciences of the United States of America*, *109*(14), 5247–52.

Polat, N., Ciftci, O., Cetin, A., & Yılmaz, T. (2015). Toxic effects of systemic cisplatin on rat eyes and the protective effect of hesperidin against this toxicity. *Cutaneous and Ocular Toxicology*, 1–7.

Pupo, A. S., Duarte, D. A., Lima, V., Teixeira, L. B., Parreiras-E-Silva, L. T., & Costa-Neto, C. M. (2016). Recent updates on GPCR biased agonism. *Pharmacological Research*.

Rader, A. J., Anderson, G., Isin, B., Khorana, H. G., Bahar, I., & Klein-Seetharaman, J. (2004). Identification of core amino acids stabilizing rhodopsin. *Proceedings of the National Academy of Sciences of the United States of America*, *101*(19), 7246–51.

Rakoczy, E. P., Kiel, C., McKeone, R., Stricher, F., & Serrano, L. (2011). Analysis of disease-linked rhodopsin mutations based on structure, function, and protein stability calculations. *Journal of Molecular Biology*, *405*(2), 584–606.

Ramon, E., Cordomí, A., Aguilà, M., Srinivasan, S., Dong, X., Moore, A. T., … Garriga, P. (2014). Differential light-induced responses in sectorial inherited retinal degeneration. *The Journal of Biological Chemistry*, *289*(52), 35918–28.

Ramon, E., del Valle, L. J., & Garriga, P. (2003). Unusual thermal and conformational properties of the rhodopsin congenital night blindness mutant Thr-94 --> Ile. *The Journal of Biological Chemistry*, *278*(8), 6427–32.

Ramon, E., Marron, J., del Valle, L., Bosch, L., Andrés, A., Manyosa, J., & Garriga, P. (2003). Effect of dodecyl maltoside detergent on rhodopsin stability and function. *Vision Research*, *43*(28), 3055–61.

Rask-Andersen, M., Almén, M. S., & Schiöth, H. B. (2011). Trends in the exploitation of novel drug targets. *Nature Reviews. Drug Discovery*, *10*(8), 579–90.

Rhone, M., & Basu, A. (2008). Phytochemicals and age-related eye diseases. *Nutrition Reviews*, *66*(8), 465–72.

Ridge, K. D., Abdulaev, N. G., Sousa, M., & Palczewski, K. (2003). Phototransduction: crystal clear. *Trends in Biochemical Sciences*, *28*(9), 479–87.

Saari, J. C. (2000). Biochemistry of visual pigment regeneration: the Friedenwald lecture. *Investigative Ophthalmology & Visual Science*, *41*(2), 337–48.

Sakmar, T. P., Franke, R. R., & Khorana, H. G. (1989). Glutamic acid-113 serves as the retinylidene Schiff base counterion in bovine rhodopsin. *Proceedings of the National Academy of Sciences of the United States of America*, *86*(21), 8309–13.

Salesse, C., Boucher, F., & Leblanc, R. M. (1984). An evaluation of purity criteria for bovine rod outer segment membranes. *Analytical Biochemistry*, *142*(2), 258–66.

Saliba, R. S., Munro, P. M. G., Luthert, P. J., & Cheetham, M. E. (2002). The cellular fate of mutant rhodopsin: quality control, degradation and aggresome formation. *Journal of Cell Science*, *115*(Pt 14), 2907–18.

Sasaki, M., Yuki, K., Kurihara, T., Miyake, S., Noda, K., Kobayashi, S., … Ozawa, Y. (2012). Biological role of lutein in the light-induced retinal degeneration. *The Journal of Nutritional Biochemistry*, *23*(5), 423–9.

Sato, J., Makita, N., & Iiri, T. (2016). Inverse agonism: the classic concept of GPCRs revisited. *Endocrine Journal*.

Sawkar, A. R., D'Haeze, W., & Kelly, J. W. (2006). Therapeutic strategies to ameliorate lysosomal storage disorders--a focus on Gaucher disease. *Cellular and Molecular Life Sciences : CMLS*, *63*(10), 1179–92.

Scarselli, M., Li, B., Kim, S.-K., & Wess, J. (2007). Multiple residues in the second extracellular loop are critical for M3 muscarinic acetylcholine receptor activation. *The Journal of Biological Chemistry*, *282*(10), 7385–96.

Sekharan, S., & Morokuma, K. (2011). Why 11-cis-retinal? Why not 7-cis-, 9-cis-, or 13-cis-retinal in the eye? *Journal of the American Chemical Society*, *133*(47), 19052–5.

Shoichet, B. K., & Kobilka, B. K. (2012). Structure-based drug screening for G-protein-coupled receptors. *Trends in Pharmacological Sciences*, *33*(5), 268–72.

Srinivasan, S., Ramon, E., Cordomí, A., & Garriga, P. (2014). Binding specificity of retinal analogs to photoactivated visual pigments suggest mechanism for fine-tuning GPCR-ligand interactions. *Chemistry & Biology*, *21*(3), 369–78.

Standfuss, J., Xie, G., Edwards, P. C., Burghammer, M., Oprian, D. D., & Schertler, G. F. X. (2007). Crystal structure of a thermally stable rhodopsin mutant. *Journal of Molecular Biology*, *372*(5), 1179–88.

Stevens, R. C., Cherezov, V., Katritch, V., Abagyan, R., Kuhn, P., Rosen, H., & Wüthrich, K. (2013). The GPCR Network: a large-scale collaboration to determine human GPCR structure and function. *Nature Reviews. Drug Discovery*, *12*(1), 25–34.

Stevenson, D. E., & Hurst, R. D. (2007). Polyphenolic phytochemicals--just antioxidants or much more? *Cellular and Molecular Life Sciences : CMLS*, *64*(22), 2900–16.

Sun, H., Molday, R. S., & Nathans, J. (1999). Retinal stimulates ATP hydrolysis by purified and reconstituted ABCR, the photoreceptor-specific ATP-binding cassette transporter responsible for Stargardt disease. *The Journal of Biological Chemistry*, *274*(12), 8269–81.

Sun, H., & Nathans, J. (2001). ABCR, the ATP-binding cassette transporter responsible for Stargardt macular dystrophy, is an efficient target of all-trans-retinal-mediated photooxidative damage in vitro. Implications for retinal disease. *The Journal of Biological Chemistry*, *276*(15), 11766–74.

Tam, B. M., & Moritz, O. L. (2007). Dark rearing rescues P23H rhodopsin-induced retinal degeneration in a transgenic Xenopus laevis model of retinitis pigmentosa: a chromophore-dependent mechanism characterized by production of N-terminally truncated mutant rhodopsin. *The Journal of Neuroscience : The Official Journal of the Society for Neuroscience*, *27*(34), 9043–53.

Tehan, B. G., Bortolato, A., Blaney, F. E., Weir, M. P., & Mason, J. S. (2014). Unifying family A GPCR theories of activation. *Pharmacology & Therapeutics*, *143*(1), 51–60.

Terstappen, G. C., & Reggiani, A. (2001). In silico research in drug discovery. *Trends in Pharmacological Sciences*, *22*(1), 23–6. Retrieved from http://www.ncbi.nlm.nih.gov/pubmed/11165668

Tirupula, K. C., Balem, F., Yanamala, N., & Klein-Seetharaman, J. (2009). pH-dependent interaction of rhodopsin with cyanidin-3-glucoside. 2. Functional aspects. *Photochemistry and Photobiology*, *85*(2), 463–70.

Toledo, D., Ramon, E., Aguilà, M., Cordomí, A., Pérez, J. J., Mendes, H. F., … Garriga, P. (2011). Molecular mechanisms of disease for mutations at Gly-90 in rhodopsin. *The Journal of Biological Chemistry*, *286*(46), 39993–40001.

Travis, G. H. (1998). Mechanisms of cell death in the inherited retinal degenerations. *American Journal of Human Genetics*, *62*(3), 503–8.

Travis, G. H., Golczak, M., Moise, A. R., & Palczewski, K. (2007). Diseases caused by defects in the visual cycle: retinoids as potential therapeutic agents. *Annual Review of Pharmacology and Toxicology*, *47*, 469–512.

Tsao, R. (2010). Chemistry and biochemistry of dietary polyphenols. *Nutrients*, *2*(12), 1231–46.

Tsuchiya, H. (2010). Structure-dependent membrane interaction of flavonoids associated with their bioactivity. *Food Chemistry*, *120*(4), 1089–1096.

Unger, V. M., Hargrave, P. A., Baldwin, J. M., & Schertler, G. F. (1997). Arrangement of rhodopsin transmembrane alpha-helices. *Nature*, *389*(6647), 203–6.

van den Berg, R., Haenen, G. R. M. M., van den Berg, H., & Bast, A. (1999). Applicability of an improved Trolox equivalent antioxidant capacity (TEAC) assay for evaluation of antioxidant capacity measurements of mixtures. *Food Chemistry*, *66*(4), 511–517.

Van Hooser, J. P., Liang, Y., Maeda, T., Kuksa, V., Jang, G.-F., He, Y.-G., … Palczewski, K. (2002). Recovery of visual functions in a mouse model of Leber congenital amaurosis. *The Journal of Biological Chemistry*, *277*(21), 19173–82.

Vandesompele, J., De Preter, K., Pattyn, F., Poppe, B., Van Roy, N., De Paepe, A., & Speleman, F. (2002). Accurate normalization of real-time quantitative RT-PCR data by geometric averaging of multiple internal control genes. *Genome Biology*, *3*(7), RESEARCH0034.

Veleri, S., Lazar, C. H., Chang, B., Sieving, P. A., Banin, E., & Swaroop, A. (2015). Biology and therapy of inherited retinal degenerative disease: insights from mouse models. *Disease Models & Mechanisms*, *8*(2), 109–129.

Venkatakrishnan, A. J., Deupi, X., Lebon, G., Heydenreich, F. M., Flock, T., Miljus, T., … Babu, M. M. (2016). Diverse activation pathways in class A GPCRs converge near the G-protein-coupling region. *Nature*, *536*(7617), 484–7.

Volikakis, G. J., & Efstathiou, C. E. (2000). Determination of rutin and other flavonoids by flow-injection/adsorptive stripping voltammetry using nujol-graphite and diphenylether-graphite paste electrodes. *Talanta*, *51*(4), 775–85. Retrieved from http://www.ncbi.nlm.nih.gov/pubmed/18967910

Weng, J., Mata, N. L., Azarian, S. M., Tzekov, R. T., Birch, D. G., & Travis, G. H. (1999). Insights

into the function of Rim protein in photoreceptors and etiology of Stargardt's disease from the phenotype in abcr knockout mice. *Cell*, *98*(1), 13–23.

Winer, J., Jung, C. K., Shackel, I., & Williams, P. M. (1999). Development and validation of real-time quantitative reverse transcriptase-polymerase chain reaction for monitoring gene expression in cardiac myocytes in vitro. *Analytical Biochemistry*, *270*(1), 41–9.

Xu, G.-R., & Kim, S. (2006). Selective Determination of Quercetin Using Carbon Nanotube-Modified Electrodes. *Electroanalysis*, *18*(18), 1786–1792.

Xu, G., In, M., Yuan, Y., Lee, J., & Kim, S. (2007). In situ spectroelectrochemical study of quercetin oxidation and complexation with metal ions in acidic solutions. *BULLETIN-KOREAN CHEMICAL SOCIETY*, *28*(5), 889–892.

Yanamala, N., Tirupula, K. C., Balem, F., & Klein-Seetharaman, J. (2009). pH-dependent interaction of rhodopsin with cyanidin-3-glucoside. 1. Structural aspects. *Photochemistry and Photobiology*, *85*(2), 454–62.

Zalewska, M., Siara, M., & Sajewicz, W. (2014). G protein-coupled receptors: abnormalities in signal transmission, disease states and pharmacotherapy. *Acta Poloniae Pharmaceutica*, *71*(2), 229–43.

Zhang, D., Zhao, Q., & Wu, B. (2015). Structural Studies of G Protein-Coupled Receptors. *Molecules and Cells*, *38*(10), 836–42.

Zhong, M., Kawaguchi, R., Kassai, M., & Sun, H. (2012). Retina, retinol, retinal and the natural history of vitamin A as a light sensor. *Nutrients*, *4*(12), 2069–96.

Zhou, A., Kikandi, S., & Sadik, O. A. (2007). Electrochemical degradation of quercetin: Isolation and structural elucidation of the degradation products. *Electrochemistry Communications*, *9*(9), 2246–2255.

8. ACKNOWLEDGEMENTS

I would like to express my gratitude to Prof. Pere Garriga who has been very kind since the day I arrived to his lab. I am very much thankful for his constant support, guidance, and encouragement throughout the project.

My sincere thanks also goes to Dra. Eva Ramon who has been a mentor to me. Her dedication towards since enhanced muy perseverance an in a way motivated to do a better research. I also thank for her relentless support, guidance, discussions and encouragements throughout muy research

I wish to thank Dr. Juan Jesus Perez and Dra Cecylia Lupala who have made models I have used in this thesis. I also thank for the discussions we had, which helped me to visualize the conformational changes observed from my studies.

And I would like to thank all people from GBMI group, and my friends whose mede this thesis possible an unforgettable experience for me.

I wish to thank my fellowship from Consejo Nacional de Ciencia y Tecnología (CONACYT) which were financially supporting my stay.

Finally, I would like to thank to my family My housband, my parents and siblings, you are always ther for me.

9. ANNEXES

Annex A

Sequence of synthetic bovine opsin gene

```
aattcatgaacggtaccgaaggcccaaacttctacgttcctttctccaacaagacgggcgtg
  F  M  N  G  T  E  G  P  N  F  Y  V  P  F  S  N  K  T  G  V
gtgcgcagcccgttcgaggctccgcagtactacctggcggagccctggcagttctccatg
V  R  S  P  F  E  A  P  Q  Y  Y  L  A  E  P  W  Q  F  S  M
ctggccgcctacatgttcctgctgatcatgcttggcttcccgatcaacttcctcacgctg
L  A  A  Y  M  F  L  L  I  M  L  G  F  P  I  N  F  L  T  L
tacgtcacagtccagcacaagaagcttcgcacaccgctcaactacatcctgctcaacctg
Y  V  T  V  Q  H  K  K  L  R  T  P  L  N  Y  I  L  L  N  L
gccgtggcagatctcttcatggtcttcggtggcttcaccaccaccctctacacctctctc
A  V  A  D  L  F  M  V  F  G  G  F  T  T  T  L  Y  T  S  L
catgggtacttcgtctttgggccgacgggctgcaacctcgagggcttctttgccaccctg
H  G  Y  F  V  F  G  P  T  G  C  N  L  E  G  F  F  A  T  L
ggcggtgaaattgcactgtggtctctggtagtactggcgatcgagcggtacgtggtggtg
G  G  E  I  A  L  W  S  L  V  V  L  A  I  E  R  Y  V  V  V
tgcaagcccatgagcaacttccgcttcggtgagaaccacgccatcatgggcgtcgccttc
C  K  P  M  S  N  F  R  F  G  E  N  H  A  I  M  G  V  A  F
acctgggtcatggctctggcctgtgcggccccgccgctcgtcggctggtctagatacatc
T  W  V  M  A  L  A  C  A  A  P  P  L  V  G  W  S  R  Y  I
ccggagggcatgcagtgctcgtgcgggatcgattactacacgccgcacgaggagaccaac
P  E  G  M  Q  C  S  C  G  I  D  Y  Y  T  P  H  E  E  T  N
aatgagtcgttcgtcatctacatgttcgtggtccacttcatcatcccgctgattgtcatc
N  E  S  F  V  I  Y  M  F  V  V  H  F  I  I  P  L  I  V  I
ttcttctgctatggccagctggtgttcaccgtcaaggaggctgcagcccagcagcaggag
F  F  C  Y  G  Q  L  V  F  T  V  K  E  A  A  A  Q  Q  Q  E
agcgccaccactcagaaggccgagaaggaggtcacgcgtatggttatcatcatggtcatc
S  A  T  T  Q  K  A  E  K  E  V  T  R  M  V  I  I  M  V  I
gctttcctaatctgctggctgccatatgctggtgtggcgttctacatcttcacccatcag
A  F  L  I  C  W  L  P  Y  A  G  V  A  F  Y  I  F  T  H  Q
ggctctgactttgggcccatcttcatgaccatcccggctttctttgccaagacgtctgcc
G  S  D  F  G  P  I  F  M  T  I  P  A  F  F  A  K  T  S  A
gtctacaacccggtcatctacatcatgatgaacaagcagttccggaactgcatggtcacc
V  Y  N  P  V  I  Y  I  M  M  N  K  Q  F  R  N  C  M  V  T
actctctgctgtggcaagaacccgctgggtgacgacgaggcgtcgaccaccgtctccaag
T  L  C  C  G  K  N  P  L  G  D  D  E  A  S  T  T  V  S  K
acagagaccagccaagtggcgcctgcctaag
T  E  T  S  Q  V  A  P  A  -
```

Annex B

Competent cells protocol

The whole procedure is performed under sterile conditions. All materials and solutions used must be autoclaved and work near the flame to avoid any contamination.

1. Incubate one colony of E coli DH5α in a falcon tube containing 50 ml of LB media at 37°C and 230 rpm ON.
2. Transfer 1 ml of this culture to 100 ml of LB media and incubate 37°C , 230 rpm until A_{600} =0.6 (normally between 3-4 h).
3. Obtained the absorbance, keep the culture 25 min on ice. Centrifuge 10 min at 4000 rpm, 4°C and discard the SN.
4. Manually or with pipette resuspend very gentle the cells with CaCl2 100 mM and keep on ice for 30 min and then centrifugue 10 min, 4000 rpm and 4°C. Discard the SN.
5. Resuspend the cells with 2 ml solution of CaCl2 100 mM and 20% of glycerol. Divide in aliquots of 50 ul and store at -80°C.
6.- To verify the correct functioning of the cells prepared, make a transformation with 100 ng of DNA.

Annex C

Miniprep procedure using QIAprep Spin Miniprep Kit

1 Resuspend pelleted bacterial cells in 250 µl Buffer P1 and transfer to a microcentrifuge tube.
2 Add 250 µl Buffer P2 and mix thoroughly by inverting the tube until the solution becomes clear. Do not allow the lysis reaction to proceed for more than 5 min.
3. Add 350 µl buffer N3 and mix immediately and thoroughly by inverting the tube.
4. Centrifuge for 15 min at 14,000 rpm
5. Apply the supernatant from step 4 to the QIAprep spin column by decanting. Centrifuge for 60 s and discard the flow-through
6. Wash the QIAprep spin column by adding 0.75 ml buffer PE. Centrifuge for 60 s and discard the flow through.
7. Centrifuge 1 min to remove residual wash buffer
8. Place the QIAprep column in a clear 1.5 ml microcentrifuge tube. To elute DNA add 30 µl of dd water to the center of the QIAprep spin column. Let stand for 15 min and centrifuge for 1 min.

Annex D

Maxiprep procedure using PureLinkTM HiPure Plasmid filter Purification form Invitrogen.

1.- Add 10 mL resuspension buffer (R3) with RNase A to each pellet (one pellet per each 500 ml of culture), resuspend the bacteria until homogeneous.

2.- Add 10 ml lysis buffer (L7). Mix gently by inverting the capped tube until the lysate mixture is thoroughly homogeneous. Do not vortex. Incubate at room temperature for 5 min (Do not allow lysis to proceed for more than 5 min.

3.- Add 10 ml precipitation buffer (N3) and mix immediately by inverting the tube until the mixture is thoroughly homogeneous (Do not vortex).

4. Transfer the precipitated lysate from above into a previously equilibrated (30 ml equilibration buffer (EQ1) HiPure filter maxi column. Let the lysate run through the filter by gravity flow until the flow stops. Discard the flow through.

5.- Wash the residual bacterial lysate in the HiPure filter maxi column with 10 ml wash buffer (W8). Again, let the buffer flow through the column until the flow stops.

6. Immediatley after, remove the inner filtration cartridge from the column (discard it) and wash the column with 50mL of wash buffer (W8). Allow the solution in the column to drain by gravity flow. Discard the flow-through

7.- Place a sterile 50-ml tube (elution tube) under the column and add 15 ml elution buffer (E4) into the Maxi column to elute the DNA. Allow the solution to drain by gravity flow. Do not force out any remaining solution. The elution tube contains the purified DNA.

8.- Add 10.5 ml isopropanol to the elution tube. Mix well and centrifuge the tube at 18 000 rpm for 50 min at 4°C. Carefully remove and discard the SN.

9.- Add 5 ml 70% ethanol to resuspend the DNA pellet and centrifuge 14 000 rpm for 15 min at 4°C. Carefully remove and discard the SN.

10. Resuspen the DNA pellet in 500 µl TE buffer (TE) or water and proceeds to quantify.

Annex E

Coupling the antibody Rho-1D4 to the CNBr-activated Sepharose 4B

1.- Measure a dilution (1:10) of Rho-1D4 antibody in the spectrophotometer at 280 nm. Get the concentration by Beer-Lambert law using ε= 1383

2. According to the final amount of gel to be prepared and based on the concentration of antibody, make appropriate calculations. It is considered that 1 gram of lyophilized sepharose gives about 3.5 ml final volume of gel, and are needed 5-10 mg antibody per ml gel.

3.-Dissolve the Rho-1D4 antibody in coupling buffer (0.1M) $NaHCO_3$ pH 8.3 containing 0.5M NaCl. Use about 5 ml coupling solution /g lyophilized powder.

4.- Weigh out the required amount of powder of CNBr-activated Sepharose 4B and suspend it in 10 ml 1mM HCl. Let it dissolve for 15 min until all the lumps are completely dissolved. If it is necessary, stir with a glass bar.

5.- Wash the sheparose using a glass filter (porosity G3) connected to a vacuum pump. Use approximately 200 ml 1mM HCl per gram of powder (add it in several aliquots). Do it slowly, in a time of 30 min.

6.- Wash again with 2 gel volumes of coupling buffer and transfer by using a spatul into a tube containing the antibody previously dissolved in the coupling buffer. Agitate overnight at 4°C.

7.- Wash away excess of antibody at least 5 (gel) volumes of coupling buffer.

8.- Block any remaining active groups. Transfer the gel to 0.1M Tris-HCl buffer, pH 8.0. Let it stand for 2 hours agitating at room temperature.

9.- Remove the Tris-HCl by filtering at least three cycles of alternating pH buffers, 0.01M acetic acid/sodium acetate, pH 4 containing 0.5M NaCl followed b a a wash with 0.1M Tris-HCl, pH 8. Wash with 5 gel volume of each buffer.

10. Transfer the treated sheparosa couples into a 15 ml falcon tube containing 6 mL buffer PBS 1x and 0.004% AzNa. Allow to settle and adjust the buffer volume (1:1 gel: buffer). Storage at 4°C

11.- Determine the capacity binding

Annex F

Regeneration protocol CNBr-activated Sepharose 4B coupled to Rho-1D4

Once used Sepharose-Rho1D4, can be reused a second or third time after a regeneration.

1.- Put 3 ml used Sepharose-Rho1D4 in a 10 ml syringe with filter and wash with 4x3ml and 2x5ml Glycine buffer (100 mM glycine, 100 mM NaCl , 0.2% DM pH 2.2)
2.- Wash again with 4x3ml and 3x10ml PBS 1x buffer containing 0.004% NaAz pH 7.4. Check that pH of the last wash is around 7.
3.- Transfer the regenerated Sepharose-Rho1D into a 15 ml falcon tube containing 6 mL buffer PBS 1x and 0.004% AzNa. Allow to settle and adjust the buffer volume (1:1 gel: buffer). Storage at 4°C
4.- Determine the capacity binding

Annex G

Buffers, culture media and solutions used

Elution buffer	Buffer (PBS 1x or HEPES or SP) containing 0.05% of DM, pH 7.4 or 6 (for SP)
2YT medium	1.6 g Tryptone, 1.0 g yeast extract, 0.5 g NaCl.
Buffer A	20 mM Tris, pH 7.4, 1mM CaCl2, 2 mM DTT, 0.1 mM PMSF (DTT and PMSF are added just before use)
Buffer C	10 mM Tris, pH 7.4, 100mM NaCl, 5 mM $MgCl_2$, 2 mM DTT, 0.1 mM PMSF (DTT and PMSF are added just before use)
Buffer D	10 mM Tris, pH 7.4, 0.1mM EDTA, 2 mM DTT, 0.1 mM PMSF (DTT and PMSF are added just before use)
Buffer E	20 mM Tris, pH 7.4, 100mM NaCl, 50% grlycerol 5 mM $MgCl_2$, 2 mM DTT, 0.1 mM PMSF (DTT and PMSF are added just before use
COS-1 culture media	500 ml DMEM media, 50 ml FBS, 5 ml L-glutamine 200mM and 5 ml of penicillin-streptomycin solution (5,000 units penicillin and 5mg streptomycin/mL)
Gt buffer 10X	0. 25 M Tris, pH 7.5, 50 mM MgCl2 and 1 M NaCl
HEK Gnti culture media	500 ml DMEM F12 media, 50 ml FBS, 5 ml L-glutamine 200mM and 5 ml of penicillin-streptomycin solution (5,000 units penicillin and 5mg streptomycin/mL)
LB agar	LB media and Agar 3%
PBS 1X	137mM NaCl, 2.7mM KCl, 10mM Na_2HPO_4 and 1.8mM KH_2PO_4
Protein loading buffer 4X	Tris 0.0625 M, 2% SDS, 10% glycerol, 0.4M DTT and 0.1% Blue Bromophenol.
TBS buffer	8g NaCl, 1.121g Tris, 0.4 ml HCl in 1 L ddH_2O, pH 8.0

TGS	3g Tris, 14.4 g Glycine, 1 g SDS, pH 8.3 up to 1 L with ddH_2O.
Trypsin solution	4.5ml of PBS 1X and 0.5ml of Trypsin-EDTA 10X (0.5% trypsin, 0.2% EDTA)
TTBS buffer	Tween 20 (1 ml) dissolved in 1L TBS solution

Annex H

Amino acids

A	alanine (Ala)
C	cysteine (Cys)
D	aspartate (Asp)
E	glutamate (Glu)
F	phenylalanine (Phe)
G	glycine (Gly)
H	histidine (His)
I	isoleucine (Ile)
K	lysine (Lys)
L	leucine (Leu)
M	methionine (Met)
N	asparagine (Asn)
P	proline (Pro)
Q	glutamine (Gln)
R	arginine (Arg)
S	serine (Ser)
T	threonine (Thr)
V	valine (Val)
W	tryptophan (Trp)
Y	tyrosine (Tyr)